Interference Management in 5G Cellular Networks

HUU MINH TAM HO

THIS DISSERTATION IS SUBMITTED
FOR THE REQUIREMENT OF DOCTOR OF PHILOSOPHY TO
FACULTY OF ENGINEERING & INFORMATION TECHNOLOGY
UNIVERSITY OF TECHNOLOGY SYDNEY

September 2016

Acknowledgments

My special thanks are given to my principal supervisor, Professor Tuan Hoang, for his dedication and patience. Without his constant supervision and generous support, my PhD study would not have been completed.

I am also deeply grateful to Doctor Duy Ngo of The University of Newcastle, Australia, for his productive research collaboration, valuable advice and continuous encouragement over the years. As well, I would like to thank Doctor Ali Arshad Nasir, who is now at King Fahd University of Petroleum and Minerals (KFUPM), KSA, for his cooperative reviews and comments on my research. Furthermore, I am grateful to Prof Ha Nguyen (University of Saskatchewan, Saskatoon, SK, Canada), Prof. Trung Q. Duong (Queen's University Belfast, UK) and Prof. Vincent Poor (Princeton University, USA) for their time and input in my work.

Special thanks are extended to my friends and colleagues in Prof. Tuan Hoang's research group at the University of Technology Sydney for making my PhD study joyful and memorable. Particularly, I appreciate Ye Shi, Zhichao Sheng, Johann Begua and Enlong Che for sharing their PhD candidature with me. I would like to express my gratitude to my best friends, Phien Ho and Bao Truong, for their understanding and encouragement that help me overcome the most challenging periods of my PhD candidature.

Finally, my deepest gratitude goes out to my family for their unconditional love and endless encouragement. They have always given me so much support and hope for the very best of myself.

Certificate of Authorship

I certify that the work in this dissertation has not previously been submitted for a degree nor has it been submitted as part of the requirements for a degree except as fully acknowledged within the text.

I also certify that the dissertation has been written by me. Any help that I have received in my research work and the preparation of the dissertation itself has been acknowledged. In addition, I certify that all information sources and literature used are indicated in the dissertation.

Signature _____

Name HUU MINH TAM HO

Contents

Abstract

This dissertation is concerned with the nonconvex optimization problems of interference management under the consideration of new disruptive technologies in the fifth-generation cellular networks. These problems are the key to the successful roll-out of these new technologies but have remained unsolved due to their mathematical challenge. Therefore, this dissertation provides novel minorants/majorants of the nonconvex functions which are then used for the successive convex approximation framework.

The first considered technology is heterogeneous networks (HetNet) in which base stations (BSs) of various sizes and types are densely deployed in the same area. Although HetNet provides a significant improvement in spectral efficiency and offloading, designing an optimal power transmission and association control policy is challenging, especially when both quality-of-service (QoS) and backhaul capacity are considered. Maximizing the total network throughput or the fairness among users in HetNet are challenging mixed integer nonconvex optimization problems. Iterative algorithms based on alternating descent and successive convex programming are proposed to address such problems.

Next, we consider a full-duplex multi-user multiple-input multiple-output (FD MU-MIMO) multicell network in which base stations simultaneously serve both downlink (DL) users and uplink (UL) users on the same frequency band via multiple antennas to potentially double the spectral efficiency. Since the use of FD radios introduces additional self-interference (SI) and cross interference of UL between DL transmissions, the

minimum cell throughput maximization and the sum network throughput maximization with QoS guarantee are nonconvex challenging problems. To solve such challenging optimization problems, we develop path-following algorithms based on successive convex quadratic programming framework. As a byproduct, the proposed algorithms can be extended to the optimal precoding matrix design in a half-duplex MU-MIMO multicell network with the Han-Kobayashi transmission strategy.

Finally, the last research work stems from the need of prolonging user equipments' battery life in power-limited networks. Toward this end, we consider the optimal design of precoding matrices in the emerging energy-harvesting-enabled (EH-enabled) MU-MIMO networks in which BSs can transfer information and energy to UEs on the same channel using either power splitting (PS) or time switching (TS) mechanisms. The total network throughput maximization problem under QoS constraints and EH constraints with either PS or TS in FD networks is computationally difficult due to nonconcave objective function and nonconvex constraints. We propose new inner approximations of these problems based on which a successive convex programming framework is applied to address them.

List of Figures

List of Tables

Abbreviations

1G	First generation
3GPP	Third Generation Partnership Project
5G	Fifth generation
BS	Base station
CDMA	Code division multiple access
CoMP	Coordinated multipoint transmission/reception
CPU	Central processing unit
CR	Cognitive radio
CSI	Channel state information
d.c.	Difference of convex functions
DCD	Dual Coordinate Descent
DCI	Difference-of-convex iterations
DL	Downlink
DLU	Downlink user equipment
DPC	Dirty paper coding
DSL	Digital Subscriber Line
EH	Energy harvesting
FBS	Femto base station
FD	Full-duplex
HD	Half-duplex
HetNet	Heterogeneous network
H-K	Han-Kobayashi
IA	Interference aware
IC	Interference coordination
ID	Information decoding
IN	Interference network
JP	Joint signal processing
KKT	Karush-Kuhn-Tucker

LOS	Line-of-sight
LTE	Long Term Evolution
MBS	Macro base station
MIMO	Multiple-input multiple-output
MISO	Multiple-input single-output
MMSE-SIC	Minimum mean square error - Successive interference cancellation
MU	Multi-user
NOMA	Non-orthogonal multiple access
NP-hard	Non-deterministic polynomial-time hard
PBS	Pico base station
PoP	Point of Presence
PS	Power splitting
QCQP	Quadratically constrained quadratic program
QoS	Quality-of-Servive
QPI	Quadratic programming iterations
RF	Radio frequency
RHS	Right hand side
s.t.	Subject to
SCQP	Successive convex quadratic programming
SDN	Software-defined networking
SDP	Semi-definite programming
SI	Self-interference
SINR	Signal-to-interference-plus-noise ratio
SISO	Single-input single-output
SNR	Signal-to-noise ratio
SOCP	Second-order-cone programming
SU	Single-user
SVD	Singular value decomposition
TS	Time switching
UE	User equipment
UL	Uplink
ULU	Uplink user equipment

Notations

$\mathbb{R}$	Set of real numbers
$\mathbb{R}^+$	Set of positive real numbers
$\mathbb{C}$	Set of complex numbers
$\emptyset$	Empty set
$\|\mathcal{S}\|$	Cardinality of set $\mathcal{S}$
$\mathcal{S}_1 \setminus \mathcal{S}_2$	Elements of set $\mathcal{S}_2$ are excluded for set $\mathcal{S}_1$
x	Vector of constants
$\mathbf{x}$	Vector of variables
X	Matrix of constants
$\mathbf{X}$	Matrix of variables
I_n	Identity matrix of size $n \times n$
$1_{n\times m}$	All-one matrix of size $n \times m$
X^H	Hermitian transpose of a matrix X
X^T	Transpose of a matrix X
$\|x\|$	Absolute value of a complex scalar x
$\|A\|$	Determinant of a square matrix A
$\langle A \rangle$	Trace of a matrix A
$\langle X, Y \rangle = \langle X^H Y \rangle$	Inner product of X and Y
$\|x\|$	Norm of a vector x
$\|X\|$	Frobenius norm of a matrix X
$\|X\|^2 = \langle X X^H \rangle$	Frobenius squared norm of a matrix X
$A \succeq B$	$A - B$ is a positive semidefinite matrix
$\mathbb{E}[.]$	Expectation operator
$\mathrm{Re}\{.\}$	Real part of a complex number
$(x)^+$	$\max\{x, 0\}$
∇f	Gradient of a scalar function f
X^*	Optimal solution of an optimization program

$\forall$ for all
$\mathcal{O}$ Big O notation

Author's Publications

The contents of this dissertation are based on the following papers that have been published, accepted, or submitted to peer-reviewed journals and conferences.

Journal Papers:

1. **H. H. M. Tam**, H. D. Tuan, and D. T. Ngo, "Successive convex quadratic programming for quality-of-service management in full-duplex MU-MIMO multicell networks," *IEEE Transaction on Communication*, vol. 64, no. 6, pp. 2340-2353, June 2016.

2. E. Che, H. D. Tuan, **H. H. M. Tam**, and H. H. Nguyen, "Successive interference mitigation in multiuser MIMO interference channels," *IEEE Transaction on Communications*, vol. 63, no. 6, pp. 2185-2199, June 2015.

3. **H. H. M. Tam**, H. D. Tuan, D. T. Ngo, T. Q. Duong and H. V. Poor, "Joint load balancing and interference management for small-cell heterogeneous networks with limited backhaul capacity," *IEEE Transaction on Wireless Communications*, vol. 16, no. 2, pp. 872-884, February 2017.

4. **H. H. M. Tam**, H. D. Tuan, A. A. Nasir, T. Q. Duong and H. V. Poor, "MIMO energy harvesting in full-duplex MU-MIMO networks," *IEEE Transactions on Wireless Communication*, 2017.

5. **H. H. M. Tam**, H. D. Tuan, D. T. Ngo, and H. H. Nguyen, "Precoding design for Han-Kobayashis signal splitting in MIMO interference networks," *IEICE Transactions on Communication*, December 2016.

6. Zhichao Sheng, H. D. Tuan, **H. H. M. Tam**, and Ha H. Nguyen, "Energy-Efficient precoding in multicell networks with full-duplex base stations," *EURASIP Journal on Wireless Communications and Networking*, March 2017.

7. H. D. Tuan, D. T. Ngo, and **H. H. M. Tam**, "Joint power allocation for MIMO-OFDM full-duplex relaying communications," *EURASIP Journal on Wireless Communications and Networking*, January 2017.

Conference Papers:

1. **H. H. M. Tam**, E. Che and H. D. Tuan, "Optimized linear precoder in MIMO interference channel using D.C. programming," in *Proc. 7th International Conference on Signal Processing and Communication Systems (ICSPCS)*, pp. 1-5, December 2013.

2. H. H. Kha, H. D. Tuan, H. H. Nguyen and **H. H. M. Tam**, "Joint design of user power allocation and relay beamforming in two-way MIMO relay networks," in *Proc. 7th International Conference on Signal Processing and Communication Systems (ICSPCS)*, pp. 1-6, December 2013.

3. **H. H. M. Tam**, H. D. Tuan and E. Che, "Coordinated downlink beamforming in multicell wireless network," in *Proc. 2014 IEEE Fifth International Conference on Communications and Electronics (ICCE)*, pp. 83-86, July 2014.

4. **H. H. M. Tam**, H. D. Tuan and E. Che, "Power minimization in MU-MIMO cellular network under rate constraints," in *Proc. 2014 IEEE Global Conference on Signal and Information Processing (GlobalSIP)*, pp. 113-117, December 2014.

5. E. Che, H. D. Tuan, **H. H. M. Tam** and H. H. Nguyen, "Maximisation of sum rate in cognitive multi-cell wireless networks with QoS constraints," in *Proc. 8th International Conference on Signal Processing and Communication Systems (ICSPCS)*, pp. 1-4, December 2014.

6. **H. H. M. Tam**, H. D. Tuan, D. T. Ngo and E. Che, "User Pairing and Precoder Design with Han-Kobayashi Transmission Strategy in MU-MIMO Multicell Networks," in *Proc. 2015 IEEE Global Communications Conference (GLOBECOM)*, pp. 1-6, December 2015.

7. **H. H. M. Tam**, H. D. Tuan and D. T. Ngo, "User association in small cell heterogeneous network with downlink sum rate," in *Proc. 2015 IEEE Global Conference on Signal and Information Processing (GlobalSIP)*, pp. 123-127, December 2015.

8. Z. Sheng, H. D. Tuan, Y. Fang, **H. H. M. Tam** and Y. Sun, "Data rate maximization based power allocation for OFDM System in a high-speed train environment," in *Proc. 2015 IEEE Global Conference on Signal and Information Processing (GlobalSIP)*, pp. 265-269, December 2015.

9. Y. Shi, H. D. Tuan, S. W. Su and **H. H. M. Tam**, "Nonsmooth optimization for optimal power flow over transmission networks," in *Proc. 2015 IEEE Global Conference on Signal and Information Processing (GlobalSIP)*, pp. 1141-1144, December 2015.

10. H. D. Tuan, D. T. Ngo and **H. H. M. Tam**, "Joint power allocation for MIMO-OFDM communication with full-duplex relaying," to appear in *Proc. 10th International Conference on Signal Processing and Communication Systems (ICSPCS)*, pp. 1-5, December 2016.

Chapter 1

Introduction

Since the introduction of the first generation (1G) cellular networks in the 1980s, humanity has witnessed its dynamic evolution. From being a substitute for landlines, mobiles phones have become increasingly popular, with more than seven billion mobile subscriptions worldwide in 2015 [ITU, 2015]. In addition, more than ever wireless devices are used to stream and download various types of media and data. Fig. 1.1 shows the prediction of Cisco of the significant global data growth from 2015 to 2020 with traffic growing about 53% each year in which smartphones, tablets, and video streaming are the main driving forces [Cisco, 2016]. With the exponential growth rate of both data consumption and the number of subscriptions, a series of workshops has been organized around the globe to identify the framework and overall objectives of the fifth generation (5G) of the cellular networks [Alexiou, 2013]. The expectations of 5G communication technologies are to serve 100 times more devices, to offer 1000 times more aggregated throughput and to prolong battery life by 10 times [Metis, 2013].

Simultaneously meeting these expectations is very challenging and may not be practical since different applications have different performance requirements. For instance, high-definition video stream application such as Netflix require a very high data rate with relaxed latency, whereas driverless cars require up to one-millisecond latency but low data rate. On the other hand, prolonging the battery life of the sensors is a top priority

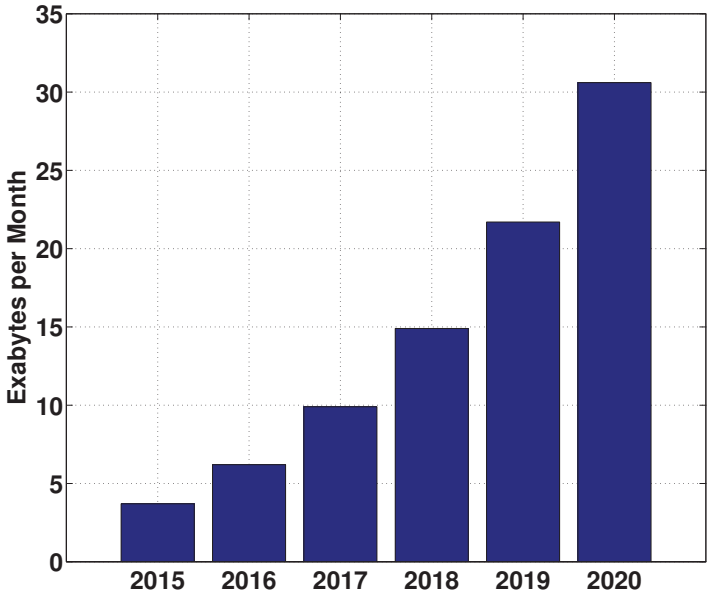

Figure 1.1: The predicted growth of global data use [Cisco, 2016].

in a wireless sensor network.

To realize the expectations, there are many revolutionary technologies under consideration including non-orthogonal multiple access (NOMA) [Ding et al., 2014; Benjebbour et al., 2015], large-scale antenna systems (massive MIMO) [Rusek et al., 2013; Larsson et al., 2014], full-duplex (FD) radio [Hong et al., 2014; Duarte et al., 2014], millimeter wave communications [Li et al., 2014; Rappaport et al., 2013], heterogeneous networks (HetNets) [Andrews, 2013], cognitive radio (CR) [Kim and Giannakis, 2011; Wang et al., 2013], simultaneous information decoding (ID) and energy harvesting (EH) networks [Lu, Niyato, Wang and Kim, 2015; Lu et al., 2016] and software-defined networking (SDN) [Sezer et al., 2013]. Therefore, numerous problems and designs must be addressed before 5G comes into practice. The research of this dissertation examines three disruptive technologies that not only provide significant performance improvement but also change the architecture of the current network, i.e.,

- HetNets in which cells of different types are densely deployed to serve a large

number of user equipments (UEs);

- FD networks in which transmitters can send and receive simultaneously on the same frequency band to boost the network throughput;
- EH technology that enables ID and EH from the received radio frequency signal on the same frequency band to prolong devices' battery life.

To provide better understanding of the benefits and difficulties of these three investigated technologies, a general review of them is provided as the following sections.

1.1 Heterogeneous Networks (HetNet)

Traditionally, macro cells are designed to serve a large area (i.e., 1-30 km in cell radius). Consequently, UEs at cell edges cannot be served with high throughput since the signal strength attenuates quickly with distance. Moreover, there are isolated areas (e.g., residential and office areas) that the radio signals cannot penetrate due to walls and obstacles. In addition, the macro cell can be easily overloaded in areas with high population of UEs (e.g., shopping malls or concerts) in which each UE is served with a small amount of resources (i.e., time slots or frequency bands) despite receiving signals with a high signal-to-noise (SNR) ratio.

To address these issues, heterogeneous networks (HetNet) in which numerous low-power small cell base stations (BSs) overlapping with a macro cell area as depicted in Fig. 1.2 have been introduced to serve the massive number of UEs in the next generation cellular network. [Andrews, 2013] has considered HetNet as a cellular paradigm shift as well as the only scalable way to address the high demand of throughput of numerous UEs since it offers the following benefits [Chandrasekhar et al., 2008]:

- *Better coverage*: UEs in the isolated areas can now be served by newly deployed small cells. Moreover, the signal reception quality or SNR is enhanced thanks to

the shortened BS-UE distance.

- *Better spectral efficiency*: Since small cells transmit with much smaller power than the macro cells, they can opportunistically transmit in the same resource blocks with the macro cells without creating much interference to the macrocell's UEs. Consequently, HetNet provides a more efficient area spectral efficiency (i.e., total number of UEs served per Hz per unit area).

- *Macrocell offload*: The traffic that is traditionally concentrated at macro cells can be offloaded to smaller cells where the resources (i.e., spectrum and time slots) are more available. Consequently, UEs' quality-of-service (QoS) is improved thanks to less competition for radio resources.

- *Cost effectiveness*: In comparison to macrocells, the deployment cost of the microcells and picocells can be reduced thanks to smaller deployment sizes and flexible backhaul solutions (e.g., DSL links, optical cables or wireless links). Moreover, femto cells are deployed mainly by an end user in a plug-and-play manner which eliminates the expense of site survey and network planning process.

However, small-cells' BSs are generally equipped with low capacity backhaul for economic benefits [Andrews, Buzzi, Choi, Hanly, Lozano, Soong and Zhang, 2014]. If these BSs serve too many high throughput-demanding UEs, there will be a potentially unacceptable level of delay/jitter at the UEs due to the bottleneck in transporting data through their non-ideal backhaul links. Backhaul capacity constraints are necessary when designing the BS-UE association rules (i.e., deciding which UEs are served by which BS). Moreover, since small-cells's BSs can be closely located to each other, intercell interference in HetNet becomes much more acute in comparison to traditional networks [Lopez-Perez et al., 2011]. Given established BS-UE associations, the interference can be effectively managed via power control. Nevertheless, the once presumably optimal BS-UE associations might be no longer optimal after the power control strategy

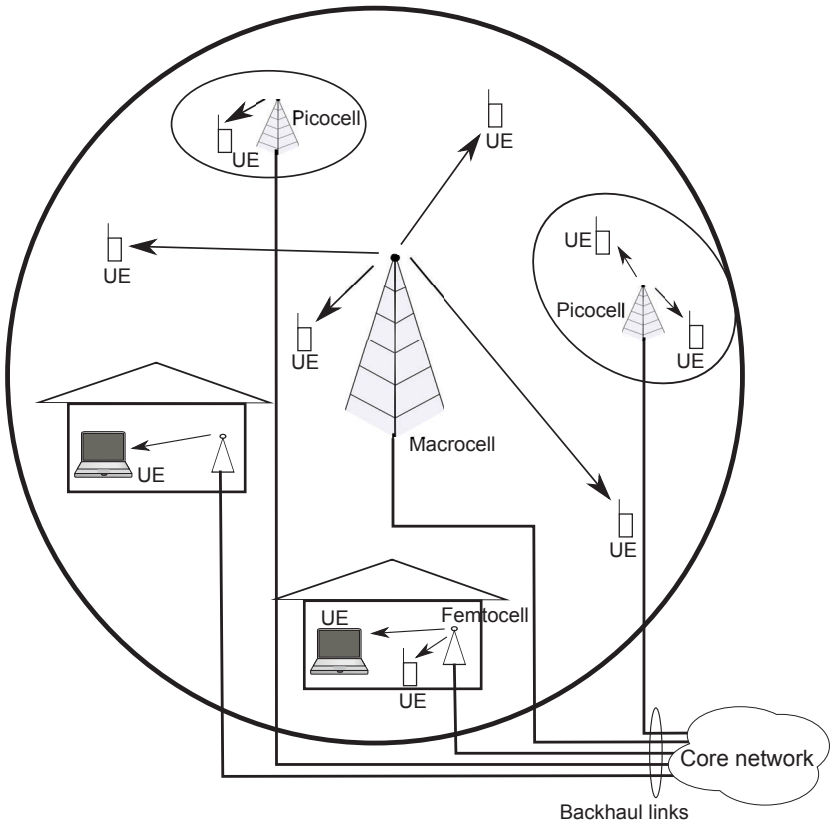

Figure 1.2: An example of HetNet.

is updated. Therefore, jointly optimal designs of both traffic offloading and interference management are crucial to achieve high network performance.

However, the joint design problems belong to the difficult class of mixed integer nonconvex optimization since the BS-UE association variables and the transmit power variables are binary and continuous, respectively. In addition, the backhaul constraints are nonconvex even under fixed BS-UE association variables. Furthermore, the throughput function is coupled by both BS-UE association variables and the transmit power variables, making the problem even more challenging. Despite the high complexity of the joint problems, the promising benefits for HetNet motivate the research of this dissertation to develop novel solution frameworks.

1.2 FD Networks

It has long been believed to be impossible to simultaneously transmit and receive signals on the same frequency band due to the severe self-interference (SI) from the transmit antenna of a transmitter toward its receive antenna [Goldsmith, 2005]. Since transmit antennas and receive antennas are closely co-located, the incurred SI is many times (100 dB+) stronger than the background noise, which creates a significant degradation of the network performance. Every traditional radio transmits and receives on either a different frequency or time slot to avoid the SI.

Until recently, SI can be suppressed to a sustainable level for FD communication thanks to the breakthroughs in hardware design [Duarte et al., 2012; Everett et al., 2014; Duarte et al., 2014; Anttila et al, 2014; Heino et al, 2015]. DUPLO project [DUPLO project, 2015] also provides a proof-of-concept that validates the feasibility of FD radios. This breakthrough enables numerous new network designs allowing in-band full duplex transmissions. In particular, the spectrum dedicated for downlink (DL) transmission can now be used for uplink (UL) transmissions as well. With the new implementation of FD radios in Long Term Evolution (LTE) networks, spectrum licence holders immediately double their spectrum assets that are worth billions of dollars.

Still, the state-of-the-art SI canceller cannot perfectly eliminate all the SI. The residual SI, albeit being reduced, still has a substantial impact on the network performance. In addition, since the DL and UL transmission is simultaneously conducted on the same frequency band, there will be cross interference between the UL and the DL transmissions as illustrated in Fig. 1.3. The UL and DL transmission problems can no longer be separated due to the joint dependency of throughput functions on the UL and the DL transmissions.

Moreover, since UL and DL transmissions in FD networks have adverse effects on each other' s performance, it is important to guarantee a minimum QoS for all receivers to

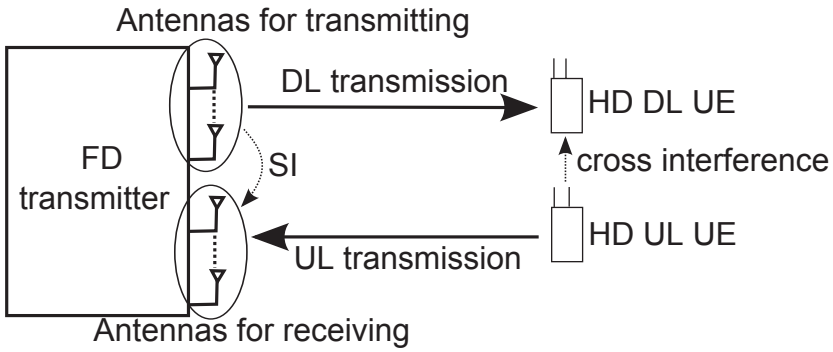

Figure 1.3: An example of interference in a simple FD network with one transmitter, one half-duplex (HD) DL UE and one HD UL UE.

avoid the situations in which one transmission direction is completely shut off for the sake of the other. Nonetheless, QoS guarantee results in difficult nonconvex constraints which have not been efficiently addressed before. Even finding a feasible point to the design is already challenging due to the nonconvexity and disconnectivity of the feasible set. Therefore, it is attractive and useful to analyze the mutual effect of UL and DL transmissions in FD networks by designing of precoding matrices (i.e., matrices that represent antenna transmit patterns) for both UL and DL transmissions to manage the newly generated interference.

1.3 Energy-harvesting-enabled (EH-enabled) Networks

To prolong the battery life of devices, it is appealing to harvest energy from the ambient radio frequency (RF) signals [Lu, Niyato, Wang and Kim, 2015; Lu et al., 2016]. This approach not only enhances the battery life but also opens up an opportunity to eliminate the need of replacing batteries in some power-limited networks via wireless charging. Although it is possible to opportunistically harvest energy from nature sources such as wind and sun, the amount of harvested energy is unpredictable and cannot be controlled. In the next generation cellular networks, small-cells' BS could become dedicated and reliable wireless energy sources that power up distant EH-enabled UEs [Buzzi

et al., 2016]. Taking advantage of the close BS-UE proximity in small cells, battery powered UEs can harvest an adequate amount of RF energy for practical applications [Ding et al., 2015; Lu, Niyato, Wang and Kim, 2015; Lu et al., 2016].

Though RF energy transferring has been used long ago to power devices that are several meters to several kilometers away from the transmitter [Huang and Lau, 2014; Lu, Wang, Niyato and Han, 2015], there is a recently emerging interest in the use of RF signals for both information transferring and energy delivering [Varshney, 2008; Shen et al., 2014]. The transmitter can now behave as both the information source and the energy source to provide efficient and on-demand services for low-power-consumption devices such as sensors as depicted in Fig. 1.4. The advantage of this approach is that it can be implemented on the existing wireless communication networks without hardware modification at the transmitters.

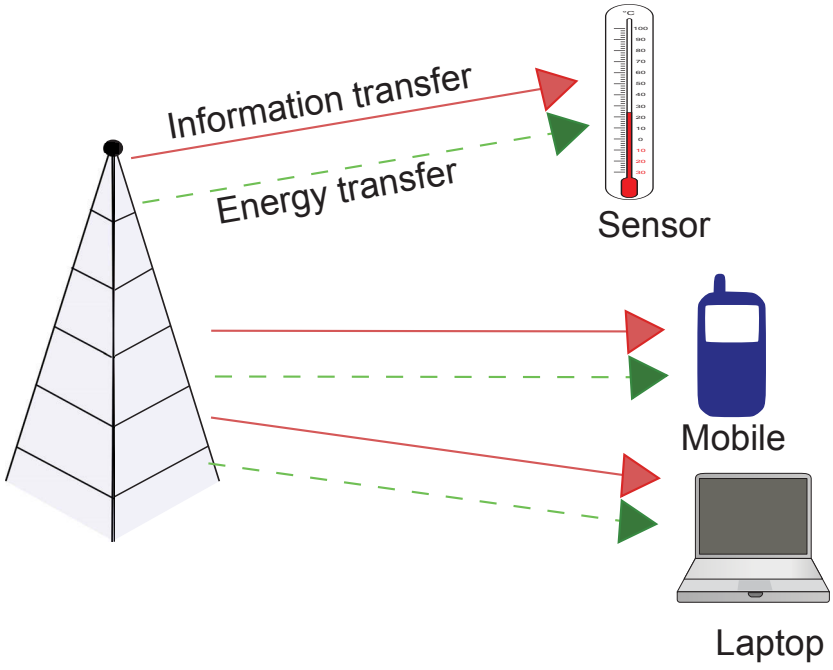

Figure 1.4: An example of interference in an EH-enabled network in which a transmitter sends information and transfers energy on the same channel.

In this approach, there are two typical implementations for wireless EH and ID. The first is by splitting the received signal into two portions for decoding information and

harvesting energy separately, namely receive power splitting (PS). The second is named transmit time switching (TS) in which the receiver harvests energy for a portion of a time frame and decodes information for the rest of the time. The receiver architecture designs of these two implementations are depicted in Fig. 1.5.

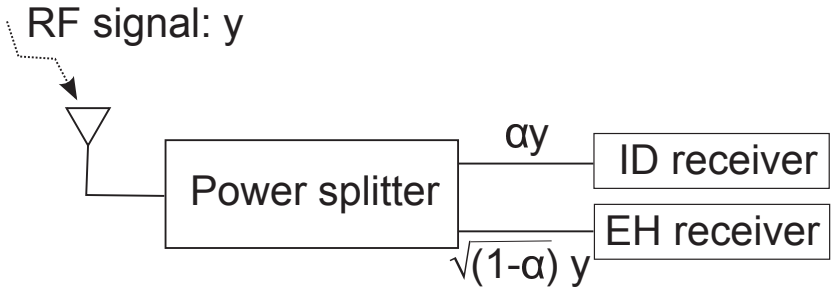

(a) Power splitting architecture

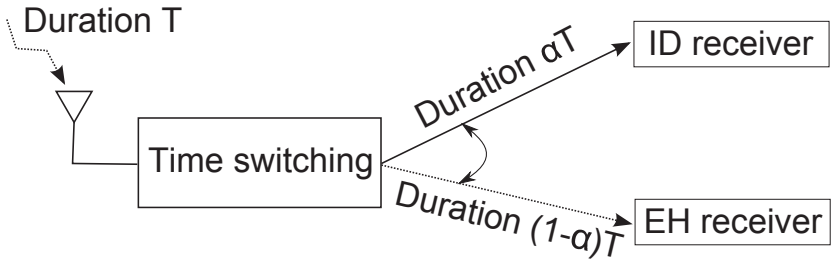

(b) Time switching architecture

Figure 1.5: Receiver architecture designs for EH-enabled receiver.

However, it is not possible to maximize the total network throughput and the total harvested energy at the same time since the received signal is split for ID and EH. The tradeoff between ID and EH in the EH-enabled system has been investigated in point-to-point communications or in an interference channel (i.e., there are many point-to-point pairs of transceivers communicating at the same time). However, the rate-energy trade-off is still unknown for a general network such as a multicell multi-user MIMO network. In addition, the EH-enabled UEs can opportunistically harvest even more energy from UL transmissions in the FD network. Although the relationship between ID and EH becomes even more complicated in FD communications, the potential for better spectral efficiency and higher harvested energy motivates the research of this dissertation to design the optimal splitting factors and precoding matrices for either PS

or TS.

1.4 Objectives and Contributions

The key common factor that hinders the practicality of these three technologies investigated in this dissertation is the generated interference which can significantly degrade the network performance. To mitigate the interference, it is crucial to properly manage the resources in the wireless cellular network. These resources can be categorized into two groups. In the first group, resources can be represented as continuous variables such as transmit power, antenna transmit patterns, or transmit/receive durations. Resources in the second group are discrete in nature such as time slots, subcarriers, devices or logical links. The variables that represent this group are either binary or integer and restricted in a finite set. Proper allocation of these resources is the key to mitigating the interference and maximizing the network performance while satisfying physical/design limitations as well as network/application requirements. However, since a universal frequency reuse approach[1] will be applied in the next generation wireless network for better spectral utilization [Lopez-Perez et al., 2009; 3GPP, 2010], this task is nontrivial due to the intricate relationship between resource allocation and network performance in wireless networks. For instance, the increase in transmit power of a BS can enhance the throughput of its serving UEs but degrade the reception quality of other nearby UEs due to the incurred interference. On the order hand, letting a UE be served by a BS that provides the largest signal strength may not be the optimal solution if that BS is currently serving a large number of UEs. Consequently, most of interference management problems are open and challenging nonconvex optimization problems, especially when new technologies are adopted in 5G.

The main objective of this dissertation is to develop numerically tractable algorithms

[1] The practice of universal frequency reuse in a network means that all transmitters and receivers in that network are operating on the same frequency band

to find optimal solutions of various NP-hard nonconvex optimization problems in the next generation cellular networks. With the newly developed inner approximations, these problems can be addressed via a successive convex approximation framework. The resulting optimal resource management strategies will provide insights into the achievable performance of the wireless cellular network when the new technologies are applied. In particular, the objectives and contributions of research in this dissertation include the followings:

- To study a joint design of BS-UE associations and transmit power control to maximize network total throughput or to provide fairness among UEs in the downlink of a HetNet. The effect of imperfect backhaul links is also considered. Both problems belong to the difficult class of mixed-integer nonconvex optimization. Algorithms based on an exact penalty method combined with successive convex programming are proposed to address these problems.

- To investigate a joint design of UL and DL linear precoders in a MU-MIMO multicell network to maximize the total network throughput or the UE's fairness. The effects of self-interference (SI) and the cross interference from UL to DL transmissions on the network throughput are also studied. The problem is nonconvex and will be addressed by the proposed successive convex quadratic programming.

- To analyze a joint design of precoding matrices for the sum throughput maximization in an EH-enabled FD MU-MIMO network. Both throughput constraints and EH constraints are considered to guarantee the QoS requirements. The total harvested energy maximization problem is also studied. All these problems will be addressed by the newly proposed path-following algorithms.

1.5 Dissertation Outline

The outline of the dissertation is as follows:

Chapter 1

This chapter presents the motivation and objectives of this PhD research. The overview of each problem and its challenges are introduced.

Chapter 2

An overview of optimization theory with an emphasis on successive convex approximation framework are firstly provided. Then, a brief review of some fundamental concepts of wireless communication channels and transmission techniques that are frequently used throughout this dissertation is introduced.

Chapter 3

New strategies are devised for joint load balancing and interference management in the downlink of a heterogeneous network, where small cells are densely deployed within the coverage area of a traditional macrocell. Unlike existing work, the limited backhaul capacity at each BS is taken into account. The objective here is either (i) to maximize the network sum rate subject to minimum throughput requirements at individual UEs, or (ii) to maximize the minimum UE throughput. The inherently binary BS-UE association variables are strongly coupled with the transmit power variables. New iterative algorithms are developed based on an exact penalty method combined with successive convex programming, where we deal with the binary BS-UE association problem and the nonconvex power allocation problem one at a time. Numerical results demonstrate the efficiency of the proposed algorithms in both traffic offloading and interference mitigation.

The work in this chapter has been published in:

- **H. H. M. Tam**, H. D. Tuan, D. T. Ngo, T. Q. Duong and H. V. Poor, "Joint load balancing and interference management for small-cell heterogeneous networks with limited backhaul capacity," *IEEE Transaction on Wireless Communications*,

vol. 16, no. 2, pp. 872-884, February 2017.

Chapter 4

The designs for jointly optimal linear precoders for both BSs and users in a FD MU-MIMO multicell network are studied. The BSs are full-duplexing transceivers while uplink users and downlink users (DLUs) are equipped with multiple antennas. Here, the network QoS requirement is expressed in terms of the minimum throughput at the BSs and DLUs. The problems of either QoS-constrained sum throughput maximization or minimum cell throughput maximization are considered. The first problem has a nonconcave objective and a nonconvex feasible set, whereas the second problem has a nonconcave and nonsmooth objective. To solve such challenging optimization problems, iterative low-complexity algorithms that only invoke one simple convex quadratic program at each iteration are developed. Numerical results demonstrate the advantages of our successive convex quadratic programming framework over existing solutions.

Moreover, the proposed approach can also be extended for the optimal precoding matrices design in an HD MU-MIMO multicell network with the Han-Kobayashi (H-K) transmission strategy [Han and Kobayashi, 1981]. The key benefit of H-K strategy is that it gives the largest known achievable capacity region [Etkin et al., 2008; Karmakar and Varanasi, 2013]. However, the throughput function is a highly nonlinear and nonsmooth function in the precoding matrix variables, which renders existing approaches unable to address the difficult sum network throughput maximization problem. For the first time, the optimal precoding matrices under H-K strategy are found via a successive convex quadratic programming algorithm that generates a sequence of improved points. Numerical results confirm the advantages of our proposed algorithm over conventional coordinated precoding approaches where the intercell interference is treated as noise.

The work in this chapter has been published in:

- **H. H. M. Tam**, H. D. Tuan, and D. T. Ngo, "Successive convex quadratic programming for quality-of-service management in full-duplex MU-MIMO multicell networks," *IEEE Transaction on Communication*, vol. 64, no. 6, pp. 2340-2353, June 2016.

- **H. H. M. Tam**, H. D. Tuan, D. T. Ngo, and H. H. Nguyen, "Precoding design for Han-Kobayashis signal splitting in MIMO interference networks," *IEICE Transactions on Communication*, December 2016.

Chapter 5

An efficient design of precoding matrices for the sum throughput maximization under throughput QoS constraints and EH constraints for energy-constrained devices for a FD MU-MIMO network is investigated in this chapter. Both TS and PS are considered to ensure practical EH and ID. The considered practical problems are quite complex due to the highly nonconvex objective and constraints. Especially, with TS, which is implementation-wise quite simple, the problem is even more challenging because the time splitting variable is not only coupled with the DL throughput function but also coupled with the SI in the UL throughput function. New path-following algorithms which require a convex quadratic program for each iteration are developed for the solutions of these problems. In the end, the merits of the proposed algorithms are illustrated through extensive simulations.

The work in this chapter has been published in:

- **H. H. M. Tam**, H. D. Tuan, A. A. Nasir, T. Q. Duong and H. V. Poor, "MIMO energy harvesting in full-duplex MU-MIMO networks," *IEEE Transactions on Wireless Communication*, 2017.

Chapter 6

This chapter firstly summarizes the studies and contributions of this PhD dissertation.

The potential future research developments are then presented.

Chapter 2

Background

In this chapter, the general introduction of some optimization concepts and techniques that are frequently used to address the challenging mathematical problems in this dissertation will be provided. Then, an overview of MIMO transmission techniques that will be used throughout this dissertation is presented. The focus of this overview is on DL transmissions since the BSs are equipped with much better hardware capabilities than UEs and thus can implement complex processing algorithms. In particular, the benefits of MIMO system are briefly discussed. Then the system model and the achievable capacity of a single-user MIMO network and a multi-user MIMO network are presented. In the context of multicell networks, coordinated multipoint transmission/reception techniques will be introduced as a key technology to mitigate the intercell interference.

2.1 Optimization Background

2.1.1 Convex Optimization

Fundamental definitions in convex optimization are given as follows

Definition 2.1. *[Tuy, 1998] A set $\mathcal{S}$ is convex if for any $\mathbf{x}$ and $\mathbf{y}$ in $\mathcal{S}$ and $\alpha \in [0,1]$, it is true that $\alpha\mathbf{x} + (1-\alpha)\mathbf{y}$ also belongs to $\mathbf{S}$.*

Definition 2.2. *[Tuy, 1998] A function $f(\mathbf{x})$ is convex in $\mathbf{x}$ on a convex domain $\mathcal{S}$ if for any $\mathbf{x}$ and $\mathbf{y}$ in $\mathcal{S}$ and $\alpha \in [0,1]$, it is true that*

$$f(\alpha\mathbf{x} + (1-\alpha)\mathbf{y}) \leq \alpha f(\mathbf{x}) + (1-\alpha)f(\mathbf{y}).$$

Definition 2.3. *[Tuy, 1998] A function $f(\mathbf{x})$ is concave in $\mathbf{x}$ on a convex domain $\mathcal{S}$ if for any $\mathbf{x}$ and $\mathbf{y}$ in $\mathcal{S}$ and $\alpha \in [0,1]$, it is true that*

$$f(\alpha\mathbf{x} + (1-\alpha)\mathbf{y}) \geq \alpha f(\mathbf{x}) + (1-\alpha)f(\mathbf{y}).$$

Definition 2.4. *[Tuy, 1998] For a convex function $f : \mathbb{R}^n \to \mathbb{R}$ or $f : \mathbb{C}^n \to \mathbb{R}$, the constraint $f(\mathbf{x}) \leq 0$ is called convex whereas the constraint $f(\mathbf{x}) \geq 0$ is called reverse convex.*

Definition 2.5. *[Tuy, 1998] An optimization problem $\min_{\mathbf{x}} f(\mathbf{x})$ s.t. $\mathbf{x} \in \mathcal{S}$ is said to be convex if $f(\mathbf{x})$ is a convex function in $\mathbf{x}$ and $\mathcal{S}$ is a convex set.*

Note that maximizing a concave function over a convex set is the same as minimizing of a convex function over a convex set and thus is a convex program.

Definition 2.6. *[Tuy, 1998] $\mathbf{x}^* \in \mathcal{S}$ is a global minimizer of a function f over a set $\mathcal{S}$ if and only if $f(\mathbf{x}^*) \leq f(\mathbf{x}), \forall \mathbf{x} \in \mathcal{S}$. Then $f(\mathbf{x}^*)$ is called the global minimum of f over $\mathbf{S}$.*

Definition 2.7. *[Horst and Tuy, 1996] Let $\epsilon > 0$ be a real number. An ϵ-neighbourhood of a point $\mathbf{x}^* \in \mathcal{S}$ is defined as:*

$$N(\mathbf{x}^*, \epsilon) := \{\mathbf{x} \in \mathcal{S} : ||\mathbf{x} - \mathbf{x}^*|| \leq \epsilon\}.$$

A point $\mathbf{x}^*$ is called a local minimizer of a function f over $\mathcal{S}$ if and only if there exists $\epsilon > 0$ such that $f(\mathbf{x}^*) \leq f(\mathbf{x})$ for all $\mathbf{x} \in N(\mathbf{x}^*, \epsilon)$.

Convex programming is inarguably one of the most popular classes of optimization problems and finds its use in various application areas such as signal processing, control and finance. The most fundamental property of convex programming is that any found local minimizers are also the global minimizer. Nevertheless, many problems in wireless communications, especially in the 5G cellular network, are nonconvex. In some particular cases, these seemingly nonconvex problems can be transformed to convex optimization problems via mathematical manipulation. On the other hand, a nonconvex problem is typically addressed by its convex approximmated/relaxed problem whose global minimum can be served as the upper bound of the original problem. In addition, iterative optimization frameworks such as alternating optimization [Bertsekas, 1999], block coordinate descent[Bertsekas, 1999] and successive convex approximation [Marks and Wright, 1978] can be applied to find local minimizers. Under these frameworks, a simple convex problem is solved for each iteration. Therefore, convex programming is still an essential tool to solve the challenging nonconvex problems in the modern communication systems.

Semi-definite programming (SDP) is an important class of convex optimization [Boyd and Vandenberghe, 2004] that is frequently encountered in the wireless communication problems. Typically, an SDP has the following form:

$$\begin{aligned} \min_{\mathbf{Q}} \quad & \langle C\mathbf{Q} \rangle \\ \text{s.t.} \quad & \langle A_i\mathbf{Q} \rangle = b_i, \forall i = 1, \ldots, p \\ & \mathbf{Q} \succeq 0, \end{aligned} \tag{2.1}$$

where $C \in \mathbb{C}^{n\times n}, A_i \in \mathbb{C}^{n\times n}, i = 1, \ldots, p$ are known symmetric matrices and $\mathbf{Q} \succeq 0$ means that $\mathbf{Q}$ is a positive semidefinite matrix.

Second-order cone programming (SOCP) is another special class of convex programming that is closely related to quadratic programming [Boyd and Vandenberghe, 2004]. An

SOCP has the following form:

$$\begin{aligned} \min_{\mathbf{x}} \quad & c^T\mathbf{x} \\ \text{s.t.} \quad & \|A_i\mathbf{x}+b_i\| \leq c_i^T\mathbf{x}+d_i, \forall i=1,\ldots,p \\ & M\mathbf{x}=m, \end{aligned} \tag{2.2}$$

where $c \in \mathbb{R}^n, A_i \in \mathbb{R}^{n_i \times n}, b_i \in \mathbb{R}_i^n, c_i \in \mathbb{R}^n, d_i \in \mathbb{R}, M \in \mathbb{R}^{l \times n}$ and $m \in \mathbb{R}^l$. The constraint

$$\|A_i\mathbf{x}+b_i\| \leq c_i^T\mathbf{x}+d_i$$

is called second-order cone constraint. With $A_i = 0,\ \forall i$, an SOCP becomes an LP whereas a SOCP is a quadratically constrained quadratic program programming (QCQP) if $c_i = 0,\ \forall i$. Also, an SOCP can be equivalently represented as an SDP by applying the Schur complement on the second-order cone constraints. The advantage of SOCP over SDP is that the former has lower computational complexity than the latter of the same SDP size [Alizadeh and Goldfarb, 2001]. For other classes of convex programming, the reader can refer to [Boyd and Vandenberghe, 2004] for more details.

2.1.2 A Generic Successive Convex Approximation Framework for Nonconvex Programming

The main aim of this dissertation is to investigate the network performance in terms of total network throughput or UE's fairness under the consideration of new technologies in 5G. Unfortunately, all of considered problems are nonconvex or even nonsmooth. The main approach in this dissertation is to apply the successive convex approximation framework [Gao and Sherali, 2009] in which the challenging original problem is addressed by successively solving its convex approximation.

Consider the following nonconvex problem:

$$\begin{aligned} \min_{\mathbf{x}} \quad & f_0(\mathbf{x}) \\ \text{s.t.} \quad & f_i(\mathbf{x}) \leq a_i, i=1,\ldots,p, \end{aligned} \tag{2.3}$$

where $f_i(\mathbf{x})$ are nonconvex functions. Many nonconvex problems are NP-hard and it is thus very complicated to locate its global minimizer in this case. Instead, finding a local minimizer is more tractable and computationally efficient. By using the convex approximations $\bar{f}_i^{(\kappa)}(\mathbf{x}) \approx f_i(\mathbf{x})$, one has the approximated problem of (2.3) at the κ-iteration:

$$\begin{aligned} \min_{\mathbf{x}} \quad & \bar{f}_0^{(\kappa)}(\mathbf{x}) \\ \text{s.t.} \quad & \bar{f}_i^{(\kappa)}(\mathbf{x}) \leq a_i, i = 1, \ldots, p, \end{aligned} \tag{2.4}$$

whose global minimizer is $\bar{x}^{(\kappa+1)}$.

The following concepts of function approximations [Tuy, 1998] play an important role in the subsequent development.

Definition 2.8. *A function $\bar{f}$ is called a (global) majorant of function a f at a point $\bar{x}$ in the definition domain of f if $\bar{f}(\bar{x}) = f(\bar{x})$ and $f(\mathbf{x}) \leq \bar{f}(\mathbf{x})\ \forall\ \mathbf{x}$.*

Definition 2.9. *A function $\bar{f}$ is called a (global) minorant of function a f at a point $\bar{x}$ in the definition domain of f if $\bar{f}(\bar{x}) = f(\bar{x})$ and $f(\mathbf{x}) \geq \bar{f}(\mathbf{x})\ \forall\ \mathbf{x}$.*

Based on these definitions, if $\bar{f}_i^{(\kappa)}(\mathbf{x})$ is a majorant of $f_i(\mathbf{x})$ at $\bar{x}^{(\kappa)}$ and $\nabla \bar{f}_i^{(\kappa)}(\bar{x}^{(\kappa)}) = \nabla f_i(\bar{x}^{(\kappa)})$, [Marks and Wright, 1978; Grover, 1997] show that the following procedure will converge to a point that satisfies Karush-Kuhn-Tucker (KKT) conditions of the original problem (2.3):

- Choose the initial point $x^{(0)}$ that is feasible to (2.3).
- κ-iteration: Solve problem (2.4) and obtain its global minimizer $\bar{x}^{(\kappa+1)}$. Set $\kappa := \kappa + 1$. Repeat this step until convergence.

An important property of this procedure is that it generates a sequence of feasible and improved solution $\{\bar{x}^{(\kappa)}\}$ such that

$$f_0(\bar{x}^{(\kappa+1)}) \leq \bar{f}_0^{(\kappa)}(\bar{x}^{(\kappa+1)}) \leq \bar{f}_0^{(\kappa)}(\bar{x}^{(\kappa)}) = f_0(\bar{x}^{(\kappa)}).$$

The idea of this procedure is illustrated in Fig. 2.1. However, finding a majorant of a nonconvex function is not always an easy task and it requires an understanding of some advanced mathematical tools. In the followings, two techniques frequently applied in this dissertation are introduced.

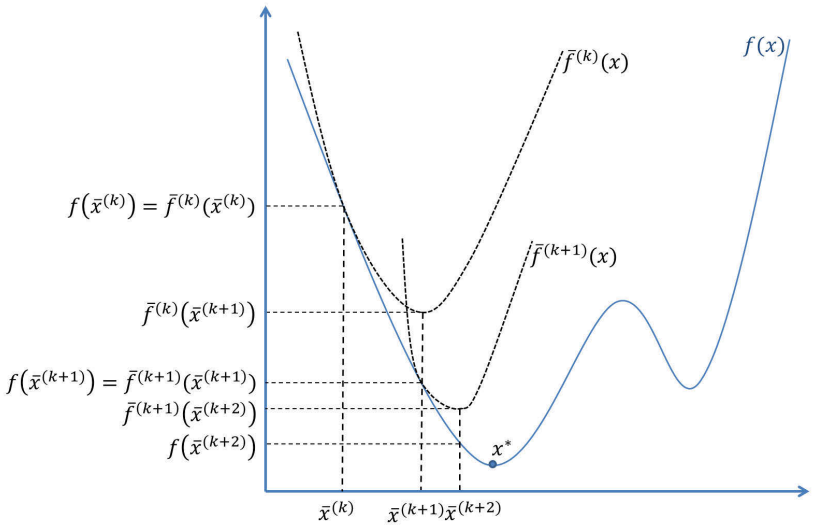

Figure 2.1: An illustration of successive convex approximation.

Firstly, one has the following property of a convex function.

Theorem 2.1. *[Tuy, 1998] If $f(\mathbf{x})$ is a convex function in $\mathbf{x}$ over a convex set $\mathcal{S}$, the first-order approximation $\bar{f}(\mathbf{x})$ of $f(\mathbf{x})$ at $\bar{x}$ is also its minorant as:*

$$\bar{f}(\mathbf{x}) := f(\bar{x}) + \langle \nabla f(\bar{x}), \mathbf{x} - \bar{x} \rangle \leq f(\mathbf{x}),$$

where $\nabla f(\bar{x})$ is a gradient of $f(\mathbf{x})$ at $\bar{x}$.

This property is very useful when a nonconvex function $f(\mathbf{x})$ is a difference of two convex functions (d.c.):

$$f(\mathbf{x}) = g(\mathbf{x}) - h(\mathbf{x}),$$

where $g(\mathbf{x})$ and $h(\mathbf{x})$ are convex in $\mathbf{x}$. Then, the majorant of $f(\mathbf{x})$ at $\bar{x}$ is given as

$$g(\mathbf{x}) - h(\bar{x}) - \langle \nabla h(\bar{x}), \mathbf{x} - \bar{x} \rangle \geq f(\mathbf{x}).$$

since

$$h(\bar{x}) - \langle \nabla h(\bar{x}), \mathbf{x} - \bar{x} \rangle \leq h(\mathbf{x}).$$

For instance, the following functions are d.c. functions [Horst and Tuy, 1996] :

- $f(\mathbf{x}) = -g(\mathbf{x})$, where $g(\mathbf{x})$ is a convex function.
- $f(x) = -\log(x) + \log(1 + x)$.
- $\max_i f_i(\mathbf{x})$, where $f_i(\mathbf{x})$ are d.c. functions.

Unfortunately, recognizing the d.c. form of a nonconvex function $f(\mathbf{x})$ is not always easy. On some occasions, although $f(\mathbf{x})$ is nonconvex in $\mathbf{x}$, $h(g(\mathbf{x})) := f(\mathbf{x})$ is convex in $g(\mathbf{x})$. In this case, the minorant of $f(\mathbf{x})$ is found as:

$$f(\mathbf{x}) \geq f(\bar{x}) + \langle \nabla_{g(\mathbf{x})} h(g(\bar{x})), g(\mathbf{x}) - g(\bar{x}) \rangle,$$

where $\nabla_{g(\mathbf{x})} h(g(\bar{x}))$ is a gradient of $h(g(\mathbf{x}))$ at $g(\bar{x})$. For example, for any x and y in $\mathbb{R}^+$, $f(x, y) := -xy$ is a nonconvex bilinear function but $h(g(x), g(y)) := -\sqrt{g(x)g(y)} = f(x, y)$ where $g(x) := x^2 \geq 0$ is a convex geometric mean in $g(x)$ and $g(y)$. The minorant of $f(x, y)$ at $(\bar{x}, \bar{y})$ is thus

$$-\bar{x}\bar{y} - \frac{\bar{y}}{2\bar{x}}(\mathbf{x}^2 - \bar{x}^2) - \frac{\bar{x}}{2\bar{y}}(\mathbf{y}^2 - \bar{y}^2) \leq f(x, y), \forall\ x \in \mathbb{R}^+, \forall\ y \in \mathbb{R}^+.$$

It should be noted that a nonconvex function $f(\mathbf{x})$ can have multiple minorants and not all minorants are convex. In this dissertation, one of the main contributions is to propose convex minorants of many nonconvex and complicated functions which are then used in the successive convex approximation framework.

2.2 Multiuser MIMO Systems

Initial work of point-to-point MIMO systems (i.e., single-user MIMO systems) [Winters, 1987; Foschini, 1996; Telatar, 1999] has shown a significant enhancement of spectral

efficiency and reliability compared to single-antenna networks. In practice, single-user MIMO (SU-MIMO) has been considered as a key technology to boost spectral efficiency in LTE [Liu et al., 2012]. Furthermore, a BS equipped with multiple antennas can simultaneously serve different UEs on the same frequency band by spatially multiplexing different data streams. The advantages of MIMO systems are provided by the following gains:

- Diversity gain: In MIMO systems, a symbol is sent and received via by multiple antennas. The UE receives multiple independently faded replicas of the same symbol, resulting in a reduction in the probability that all replicas are badly faded at the same time. The reliability of data transmission is thus improved. For a MIMO system with N_t transmit antennas and N_r receive antennas, the maximum diversity order is $N_t \times N_r$ [Sanayei and Nosratinia, 2004].

- Array gain or beamforming gain: This is the enhancement in the quality of signal reception by coherently combining the replicated symbols from multiple antennas. In practice, the radiation beam can be focused to the desired UE by applying proper precoding matrices prior to transmission. The radiation beam can also be directed away from the undesired UEs to reduce the undue interference, resulting in better signal reception at these UEs.

- Spatial multiplexing gain: By exploiting the multiple antennas, multiple data streams can be multiplexed into the same frequency band and transmitted at the same time. In other words, different symbols are simultaneously sent via different faded paths to a receiver or multiple receivers. In the high signal-to-noise (SNR) ratio region, it is shown in [Foschini, 1996] that the capacity of a point-to-point MIMO channel is linearly proportional to the spatial multiplexing gain as

$$C(SNR) = \min\{N_t, N_r\} \log(SNR) + \mathcal{O}(\log(SNR)). \tag{2.5}$$

  where $\min\{N_t, N_r\}$ is the spatial multiplexing gain. However, some of these streams may suffer from weak SNRs, reducing the reliability of the reception

of symbols tranmitting on these stream. This is a fundamental tradeoff between diversity gain and spatial multiplexing gain [Zheng and Tse, 2003].

In the followings, the capacity of the SU-MIMO communication and MU-MIMO communication will be introduced. The concepts and techniques that are introduced in the section can also be interchangably applied for both uplink and downlink transmission. Throughout this dissertation, the channel state information (CSI) is always assumed to be known at a central processing unit.

2.2.1 SU-MIMO Communications

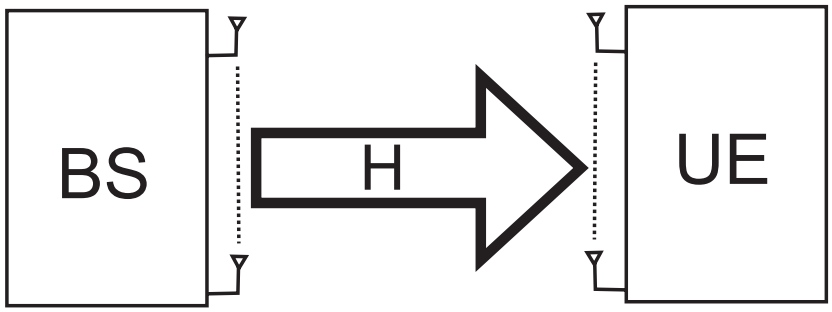

Figure 2.2: An example of an SU-MIMO network.

A typical SU-MIMO includes one BS and one UE as depicted in Fig. 2.2. The MIMO transmission channel is represented by a matrix $H \in \mathbb{C}^{N_r \times N_t}$ where N_t and N_r are the number of BS transmit antennas and receive antennas, respectively. Denote a vector of symbols intended to the UE as $s \in \mathbb{C}^{d \times 1}$ where $d \leq \min\{N_t, N_r\}$ is a number of symbols. The BS processes these symbols via a precoding matrix $\mathbf{V} \in \mathbb{C}^{N_t \times d}$ before transmission. Upon defining the transmit covariance matrix as $\mathbf{Q} = \mathbf{V}s(\mathbf{V}s)^H$, the achievable throughput at the UE is

$$R(\mathbf{Q}) = \log_2 \left| I_{N_r} + \frac{1}{\sigma^2} H\mathbf{Q}H^H \right|, \tag{2.6}$$

where σ^2 is the noise power at the UE and I_{N_r} is the identical matrix of size N_r. To find the optimal $\mathbf{Q}$ that maximizes the throughput, the following optimization problem

is addressed:

$$\max_{Q \succeq 0} R(\mathbf{Q}) \ : \ \langle \mathbf{Q} \rangle \leq P, \ \text{rank}(\mathbf{Q}) = d, \tag{2.7}$$

where P is the maximum transmit power of the BS. Assuming $d = N_t$, the difficult rank constraint $\text{rank}(\mathbf{Q}) = d$ can be neglected and (2.7) reduces to a convex program. [Telatar, 1999] shows that each symbol in s can be transmitted through a parallel subchannel. In particular, one has $H = U\Sigma V^H$ via singular value decomposition (SVD) where $U \in \mathbb{C}^{N_r \times N_r}$ and $V \in \mathbb{C}^{N_t \times N_t}$ are unitary matrices. Σ is an $N_t \times N_t$ diagonal matrix with the singular value λ_i for $i = 1, \ldots, N_{\min}$ where $N_{\min} = \min\{N_t, N_r\}$. Then, the received signal y at the UE can be represented as

$$y = Hs + n = U\Sigma V^H s + n \tag{2.8}$$

$$\Leftrightarrow U^H \mathbf{y} = \Sigma(V^H s) + U^H n \tag{2.9}$$

$$\Leftrightarrow \bar{y} = \Sigma \bar{s} + \bar{n}, \tag{2.10}$$

where $\bar{y} = U^H y$, $\bar{s} = V^H s$ and $\bar{n} = U^H n$. U^H and V^H can be understood as the receive filter and transmit precoding matrices, respectively. Because U is an unitary matrix, $\bar{n}$ has the same mean and variance as n. As shown in (2.10), the i-th symbol s_i in s is transmitted through a SISO subchannel with a channel gain of λ_i. The throughput of each symbol is $\log(1 + \lambda_i^2 P_i / \sigma^2)$ where P_i is the transmit power of symbol s_i and $\sum_i P_i \leq P$. A water-filling algorithm [Chuah et al., 2002] can be applied to find the optimal transmit power P_i^* as

$$P_i^* = \left(\mu - \frac{\sigma^2}{\lambda_i^2} \right)^+, \tag{2.11}$$

where μ is chosen such that $\sum_i P_i = P$. As shown in (2.10), each symbol in s_i is transmitted with power P_i^* through a parallel subchannel whose channel gain is λ_i. If the subchannel power λ_i is small in comparison to σ^2 for some i, the reliability of the reception of s_i is low. This illustrates the tradeoff between the multiplexing gain and the diversity gain.

2.2.2 MU-MIMO Communications

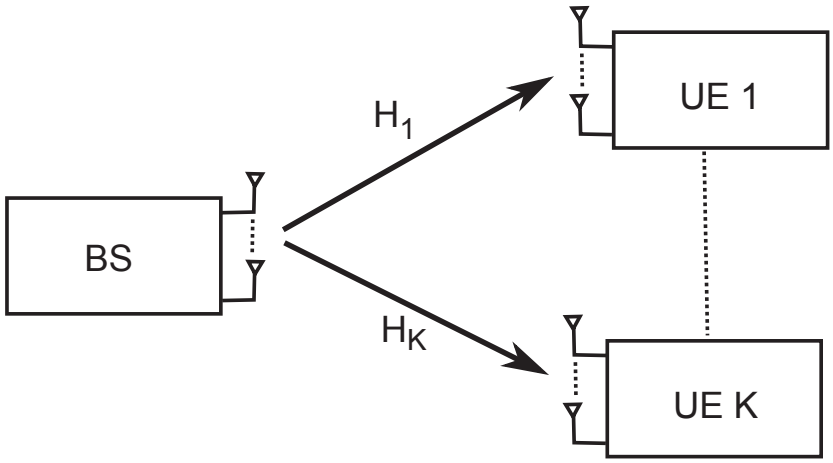

Figure 2.3: An example of an MU-MIMO network.

A typical MU-MIMO includes one BS equipped with N_t antennas and K UEs equipped with N_r antennas as depicted in Fig. 2.3. Denote $H_i \in \mathbb{C}^{N_r \times N_t}$ as the channel matrix from BS to UE i. The BS transmits the vector of symbols $s_i \in \mathbb{C}^{d\times 1}, \mathbb{E}\{\mathbf{s}_i\mathbf{s}_i^H\} = I_d$ to UE i where d is the number of concurrent symbols and $d \leq \min\{N_r, N_t\}$ [1]. The symbol vector s_i is precoded by the matrix $\mathbf{V}_i \in \mathbb{C}^{N_t \times d}$. The received signal at UE i is

$$y_i = H_i\mathbf{V}_i s_i + \sum_{j=1, j\neq i}^{K} H_j\mathbf{V}_j s_j + n_i, \tag{2.12}$$

where n_i is the additive white circularly symmetric complex Gaussian noise with variance σ. Notice that UE i receives not only its desired symbols s_i but also the symbols intended to other UEs. Without proper network designs, these unwanted signals will significantly degrade the network performance due to interference.

In the literature, the Dirty paper coding (DPC) technique of [Costa, 1983] is shown to be optimal for maximizing the network throughput in MU-MIMO communications where there is only one transmitter. By constructing the codeword for each UE in such a way that the UEs with higher order do not see the interference from the signals

[1] The transmit power of each symbol will be included in the design of precoding matrices.

intended for lower order UEs, the throughput at UE i is

$$R_i(\mathbf{Q}) = \log_2 \left| I_{Nr} + H_i \mathbf{Q}_i H_i^H \left(\sum_{j>i} H_j \mathbf{Q}_j H_j^H + \sigma^2 I_{N_r} \right)^{-1} \right|, \tag{2.13}$$

where $\mathbf{Q}_i = \mathbf{V}_i \mathbf{V}_i^H \succeq 0$ is the transmit covariance of UE i and $\mathbf{Q} = [\mathbf{Q}_i]_{i=1,\ldots,K}$. Although $R_i(\mathbf{Q})$ is a nonconvex function in $\mathbf{Q}$, the total throughput

$$\sum_{i=1}^{K} R_i(\mathbf{Q}) = \log_2 |I_{Nr} + \sum_{i=1}^{K} H_i \mathbf{Q}_i H_i^H| - \log_2 |\sigma^2 I_{N_r}| \tag{2.14}$$

is actually a concave function in $\mathbf{Q}$. Consequently, the total throughput maximization problem

$$\max_{\mathbf{Q}} \sum_{i=1}^{K} R_i(\mathbf{Q}) \ : \ \sum_{i=1}^{K} \langle \mathbf{Q}_i \rangle \leq P \tag{2.15}$$

is a convex problem. However, this approach is impractical since DPC requires the non-causal knowledge of the channels as well as a complicated successive encoding process [Caire and Shamai, 2003; Yu and Cioffi, 2004].

A practical approach is to decode the desired signal only and consider the others as white noise. Thus, a natural design of precoding matrices is to minimize the incurred interference. Block diagonalization [Spencer et al., 2004] is a design of $\mathbf{V}_i$ in which the interference toward all other UEs due to the transmission of s_i is zero. In particular, one defines $\overline{H}_i = [H_1^T \ldots H_{i-1}^T \ H_{i+1}^T \ldots H_K^T]^T$ as a collection of channels to all UEs except that to UE i. The zero interference constraint is expressed as

$$\overline{H}_i \mathbf{V}_i = \mathbf{0}, \tag{2.16}$$

where $\mathbf{0}$ is a matrix of all zeros with a proper size. The SVD of $\overline{H}_i$ is given as $\overline{H}_i = \overline{\mathbf{U}}_i \overline{\Sigma}_i \left[(\overline{\mathbf{V}}_i^1)^T (\overline{\mathbf{V}}_i^0)^T \right]^T$ where $\overline{\mathbf{V}}_i^0$ contains all singular vectors corresponding to the zero singular values in $\overline{\Sigma}_i$. By letting each $\mathbf{V}_i$ to be some columns in $\overline{\mathbf{V}}_i^0$, the constraint (2.16) is automatically satisfied since $\overline{\mathbf{V}}_i^0$ belongs to the null space of $\overline{H}_i$. Therefore, the reception of s_i at UE i is interference-free. The condition for this approach to be feasible is $N_t \geq K N_r$ so that the null space of $\overline{H}_i$ is not empty. However, forcing the

interference to be zero results in a degradation of network throughput. On the other hand, if the block diagonalization is not applied, the throughput function at the UE i is

$$R_i(\mathbf{V}) = \log_2 \left| I_{Nr} + H_i \mathbf{V}_i \mathbf{V}_i^H H_i^H \left(\sum_{j \neq i} H_j \mathbf{V}_j \mathbf{V}_j^H H_j^H + \sigma^2 I_{N_r} \right)^{-1} \right|, \tag{2.17}$$

where $\mathbf{V} = [\mathbf{V}_i]_{i=1,\ldots,K}$. Unlike (2.13), the total network throughput based on (2.17) is a nonconvex function and maximizing the network throughput is thus a difficult optimization problem.

In a multi-user system, it is also essential to guarantee that each UE is served with a minimum throughput. In literature, this constraint is actually a linear constraint in an MU-SISO network as

$$\log_2 \left(1 + g_i \mathbf{p}_i \left(\sum_{j \neq i} g_j \mathbf{p}_j + \sigma^2 \right)^{-1} \right) \geq r, \tag{2.18}$$

$$\Leftrightarrow g_i \mathbf{p}_i \geq (2^r - 1) \left(\sum_{j \neq i} g_j \mathbf{p}_j + \sigma^2 \right), \tag{2.19}$$

where $\mathbf{p}_i$ is the transmit power of UE i, g_i is the channel gain from BS to UE i, and r is the guaranteed minimum throughput. In an MU-MISO network, both the channel matrix H_i and the precoding matrix $\mathbf{V}_i$ are vectors and the throughput constraint can be recast as a convex second-order-cone constraint [Wiesel et al., 2006] as

$$\log_2 \left(1 + |H_i^T \mathbf{V}_i|^2 \left(\sum_{j \neq i} |H_j^T \mathbf{V}_j|^2 + \sigma^2 \right)^{-1} \right) \geq r, \tag{2.20}$$

$$\Leftrightarrow |H_i^T \mathbf{V}_i|^2 \geq (2^r - 1) \left(\sum_{j \neq i} |H_j^T \mathbf{V}_j|^2 + \sigma^2 \right), \tag{2.21}$$

$$\Leftrightarrow \mathrm{Re}\{H_i^T \mathbf{V}_i\} \geq \sqrt{2^r - 1} \|X\|, \tag{2.22}$$

where $X = [H_1^T \mathbf{V}_1 \ldots H_K^T \mathbf{V}_K \ \sigma]$. However, there is no convex representation of the throughput constraint in an MU-MIMO network since the throughput function (2.17) now involves with the determinant operation of a matrix. Consequently, the sum network throughput maximization with throughput guarantee for each UE is still an open

problem. Motivated by this shortcoming, an effective method to handle problems involved with the challenging throughput constraint is proposed in Chapters 4 and 5.

2.2.3 Coordinated Multipoint Transmission/Reception (CoMP)

To enhance the spectrum efficiency, multiple BSs are allowed to operate on the same time slots and on the same frequency band (i.e., universal/fractional frequency reuse) [Damnjanovic et al., 2011; Andrews, Buzzi, Choi, Hanly, Lozano, Soong and Zhang, 2014]. This results in extra intercell interference from one BS towards the UEs served by other BSs as depicted in Fig. 2.4. Therefore, it is necessary to have some forms of coordination among the BSs to mitigate the generated intercell interference. CoMP [Gesbert et al., 2010; Lee, Kim, Lee, Ng, Mazzarese, Liu, Xiao and Zhou, 2012] has been supported by LTE and LTE-Advanced standards as a key technology to improve coverage and spectral efficiency by providing a common feedback and signaling framework among the BSs. Based on the extent of the coordination, there are three modes of CoMP: Interference Aware (IA), Interference Coordination (IC) and Joint Signal Processing (JP).

In the IA mode, there is no exchange of UE's data and control information (e.g. channel information, transmit precoding matrices) among the BSs. A BS selfishly adjusts its transmission beam to maximize the performance of its own UEs based on feedback of those UEs on the measured interference. There is no intention of reducing intercell interference in the IA mode. Therefore, IA forms a non-cooperative game among BSs with an aim to find a Nash equilibrium (NE) point. Although an NE point can be far away from the optimal point, the IA mode can serve as a baseline for other coordination techniques thanks to its simplicity.

In the IC mode, there is also no data exchange among the BSs, which means that a UE only receives its desired data stream from its serving BS. To mitigate the intercell interference, the control information among the BSs is shared to enable the precoding

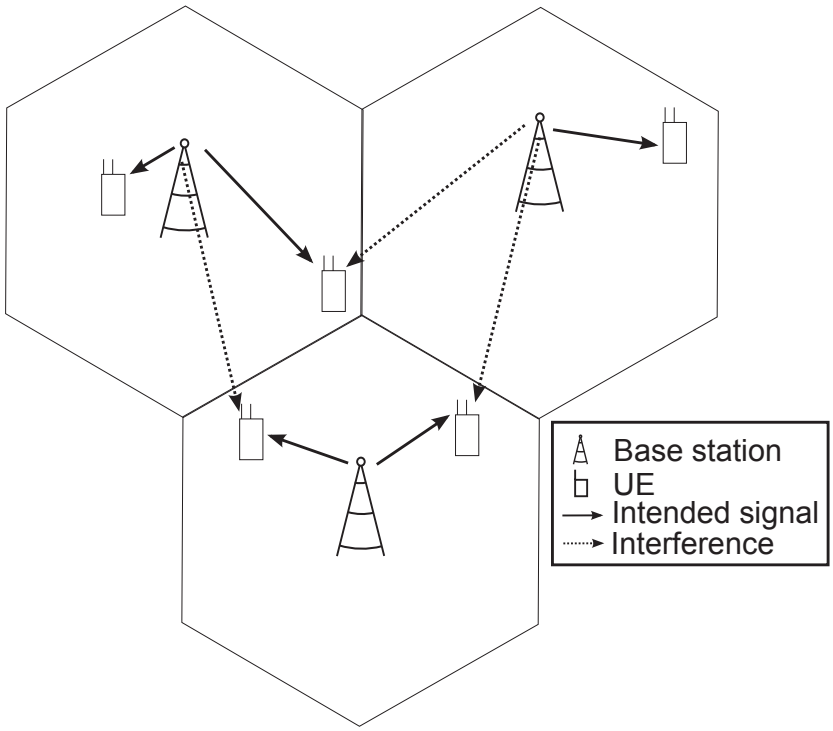

Figure 2.4: An example of a multicell MU-MIMO network applying IA or IC. Unintended signals are treated as white noise.

designs that exploit the antenna gain to steer the radiation beam away from the undesired UEs while focusing the desired UEs. Even in SISO networks where there is no antenna gain, the exchange information is helpful in determining a proper transmit power of each BS.

In the JP mode, both UE's data and control information are shared among BSs. A UE can receive its desired data streams from multiple BSs as depicted in Fig. 2.5. The multicell network can now be considered as a single-cell network in which only one transmitter whose antennas are geographically separated. Although this mode allows the best exploitation of the antenna gain and the spatial multiplexing gain in comparison to the other two modes, the high amount of exchanged information puts a stringent requirement on the backhaul links of BSs . This feature limits the practical use of the JP mode.

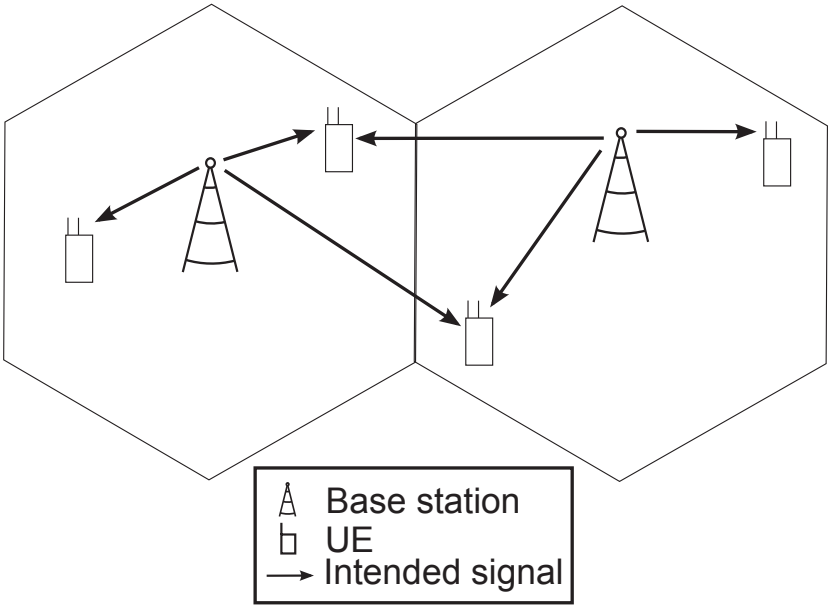

Figure 2.5: An example of a multicell MU-MIMO network applying JP. UEs can receive desired data streams from multiple BSs.

In practice, the IC mode is more popular because it can efficiently mitigate the interference without putting a large burden of signaling on the backhaul links. For this reason, this dissertation will assume the IC mode whenever CoMP techniques are employed.

Chapter 3

Joint Load Balancing and Interference Management for Small-Cell Heterogeneous Networks with Limited Backhaul Capacity

3.1 Introduction

Cell densification is currently the best hope to meet the unprecedented data increase (the 1000× data challenge) in the 5G wireless networks [Andrews, 2013; Hossain et al., 2014; Li et al., 2014]. By densely deploying cells of different types and sizes (e.g., macro, micro, pico, femto), the resulting HetNet can offer a substantial growth in area spectral efficiency and full network coverage in regions traditionally difficult to penetrate. Another key benefit of HetNet is data offloading, where traffic otherwise transported via the traditional macrocell is directed to the newly deployed small cells.

Traditionally, a UE is associated with the BS that offers the maximum signal-to-interference-plus noise ratio (SINR), i.e., the max-SINR rule (see, e.g., [Dhillon et al., 2012]). As a result, a 'hotspot' BS with advantageous link conditions and/or high transmit power would potentially be inundated with too many UEs while other BSs only serve a few UEs. Range expansion is a heuristic method that may help balance

the traffic load among different BSs, in which the SINR is regulated through a positive bias level [Damnjanovic et al., 2011; Jo et al., 2012]. Still, it is challenging to determine optimal bias levels for multiple cells. Other related BS-UE association rules proposed in the literature are based on maximizing the estimated throughput [Lee, Son, Gong and Yi, 2012] and sum logarithmic throughput [Ye et al., 2013; Fooladivanda and Rosenberg, 2013; Shen and Yu, 2014]. Using Lagrangian duality decomposition [Low and Lapsley, 1999], the association rule in [Boostanimehr and Bhargava, 2015] aims at maximizing the network sum-rate while satisfying the Quality-of-Service (QoS) constraints. A heuristic adjustment is then proposed to keep the total number of time slots demanded by the UEs below that available at the BSs. In [Corroy and Mathar, 2012; Corroy et al., 2012], a binary relaxation method is proposed to find the optimal association rule for the sum-rate and minimum-rate maximization objectives. However, the proposed method is limited to a two-cell network. An extensive overview of the state-of-the-art in user association for 5G networks can be found in [Liu, Wang, Chen, Elkashlan, Wong, Schober and Hanzo, 2016].

A common assumption in the above existing work is the availability of ideal backhaul links with unlimited capacity. This assumption is not true for HetNets. Here, the low-power BSs of small cells (e.g., pico and femto) connect to the core network via low capacity backhaul (e.g., DSL links) for economic benefits [Andrews, Singh, Ye, Lin and Dhillon, 2014]. If these small-cell BSs must serve too many UEs, their non-ideal backhaul becomes the bottleneck in transporting the required amount of data traffic to the UEs, resulting in a potentially unacceptable level of delay/jitter at the UEs. The study of [Beyranvand et al., 2015] proposes an optimal BS-UE association rule that maximizes the logarithmic utility function while guaranteeing a target delay. Note that one can guarantee certain levels of delay if the demanded throughput at the BSs is kept below their respective backhaul capacity [Ghimire and Rosenberg, 2015]. Instead of maximizing the network sum-rate or the minimum UE's throughput, [Singh and Andrews, 2014] devises a backhaul-aware BS-UE association rule that is based on

biasing, cell size and user distribution.

Interference is a major issue in dense small-cell HetNets, wherein numerous cell boundaries with poorly defined patterns are created. Compared with traditional cellular networks, the effects of the intercell interference are much more acute and unpredictable, especially at the cell edges [Lopez-Perez et al., 2011]. Power control is an effective way to manage the interference, assuming that the BS-UE links have already been established. For a given BS-UE association, [Yu et al., 2014] devises an optimal BS transmit power policy for sum-rate maximization with backhaul capacity constraints by solving the KKT conditions. However, due to the nonconvexity of the considered problem, a KKT point may not even be locally optimal or feasible. In addition, the once presumably optimal BS-UE associations will no longer be optimal when the new transmit power values are used as a result of power control. It is therefore essential to design jointly optimal strategies for both traffic offload and interference management.

For CDMA-based networks, joint optimization of BS-UE association and interference management is considered in [Ha and Le, 2014] for network sum-rate maximization and in [Sun et al., 2015] for minimum UE's SINR maximization. It is not straightforward to apply the results of [Ha and Le, 2014] and [Sun et al., 2015] to networks in which a BS uses orthogonal channels to serve its UEs to eliminate intracell interference. Different from CDMA, each UE here is only assigned with a fraction of the time/frequency slots depending on the current load at its serving BS. Assuming zero intracell interference, [Madan et al., 2010] proposes an iterative procedure for joint BS-UE association and interference management that guarantees a maximum delay not be exceeded. Yet, the convergence of the proposed heuristic method is not proven. Using game theory, [Hong and Garcia, 2012] finds the Nash equilibrium for such joint optimization problem, albeit without considering QoS constraints. It is commonly known that a Nash equilibrium may not be efficient as it could be far away from the actual optimal solution. Notably, the practical issue of imperfect backhaul links is not considered in [Madan et al., 2010] and [Hong and Garcia, 2012], presumably due to the nonconvexity of the backhaul

capacity constraints even when the BS-UE association is fixed.

In this chapter, we formulate new problems for joint traffic offload and interference management in the downlink of a HetNet. Aiming to maximize the network throughput and the minimum UE rate, our formulations accommodate both backhaul capacity constraints and UE QoS requirements. The considered problems belong to the difficult class of mixed integer nonconvex optimization. The binary BS-UE association variables are strongly coupled with the transmit power variables, making the problems even more challenging to solve.

We then develop new iterative algorithms based on alternating descent [Bertsekas, 1999] and successive convex programming for the formulated problems. Alternating descent allows us to decouple the original problem into two subproblems and deal with them one at a time. Even so, each resulting subproblem is still challenging. For a fixed power allocation, the BS-UE association subproblem is combinatorial. And for a fixed BS-UE association, the power allocation subproblem is highly nonconvex. We propose to deal with the binary nature of BS-UE association by relaxation combined with a penalty method. We then employ successive convex programming to solve two subproblems in the same time scale. We prove that our proposed alternating descent algorithms converge, where only two simple convex problems are to be solved in each iteration. Simulation results show that the proposed algorithms enhance the network throughput through better load balancing and interference management.

The rest of this chapter is organized as follows: Sec. 3.2 formulates the problems of joint load balancing and interference management. Sec. 3.3 proposes an alternating descent algorithm to solve the sum-rate maximization problem. Sec. 3.4 extends the devised solution to the case of minimum UE rate maximization. Sec. 3.5 presents numerical results to demonstrate the performance of our proposed algorithms. Finally, Sec. 3.6 concludes the chapter.

3.2 System Model and Problem Formulations

Consider the downlink of a K-cell HetNet in which one macrocell is overlaid with $K-1$ small cells, as depicted in Fig. 3.1. To best exploit the limited radio spectrum, universal frequency reuse is adopted [Ye et al., 2013; Shen and Yu, 2014]. Without loss of generality, we assume that macro base station (MBS) serving the macrocell is indexed as BS 1, and the BS serving small cell k (e.g., a micro/pico/femto BS) is indexed as BS $k \in \{2, 3, \ldots, K\}$. Transmitting at a much lower power than an MBS, the small-cell BSs are deployed densely in order to extend network coverage, increase throughput and offload data traffic from the MBS.

We assume that each BS $k \in \{1, 2, \ldots, K\}$ connects to a backhaul link with limited capacity. The backhaul link of each BS carries the downlink traffic for its serviced UEs from the core network to that BS via a central access point called 'Point of Presence' (PoP) [Beyranvand et al., 2015; Jafari et al., 2015; Zhang et al., 2016]. The PoP is connected to the core network via an optical fiber link whose capacity is much higher than the total capacity of all links from the PoP to all BSs. Therefore, the effect of core network-PoP link capacity is neglected in our model [Zhang et al., 2016]. For simplicity, we also neglect the traffic coming from the control plane [Ghimire and Rosenberg, 2015].

In the considered HetNet, there are N UEs looking for the serving BSs. Similar to the BSs, the UEs are each equipped with one antenna. A snapshot model is adopted where the channels remain unchanged during the optimization process. This channel assumption is well-justified for networks with a low degree of mobility and/or very high throughput. A central processing unit is employed to collect all the channel state information and perform the underlying network optimization.

In this chapter, a UE is allowed to associate with at most one BS, but a BS can serve multiple UEs. Assume that BS $k \in \{1, 2, \ldots, K\}$ has a full buffer and transmits with power $\mathbf{p}_k$. First, consider that only one UE $n \in \{1, 2, \ldots, N\}$ is connected to BS k.

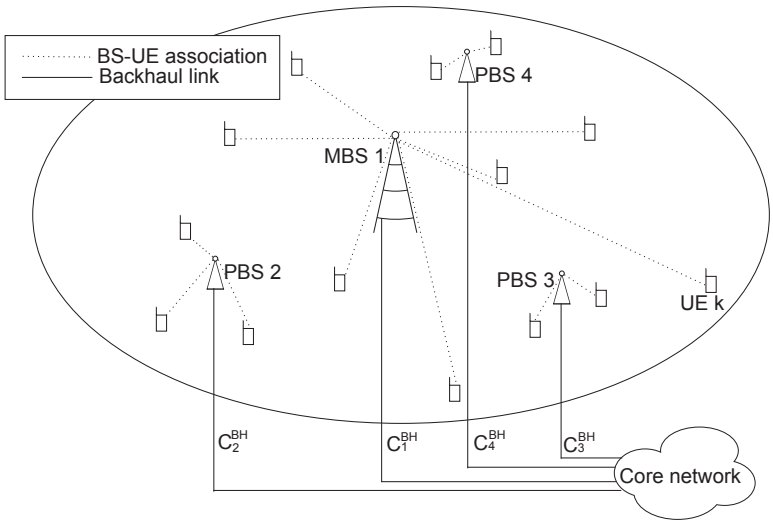

Figure 3.1: A small-cell HetNet with limited-capacity backhaul links. 'MBS', 'PBS' and 'PoP' refer to macro BS, pico BS and Point of Presence, respectively.

The achieved data rate in nats/s/Hz of UE n is expressed as:

$$r_{nk}(\mathbf{p}) \triangleq \ln\left(1 + \frac{g_{nk}\mathbf{p}_k}{\sum_{j\neq k, j=1}^{K} g_{nj}\mathbf{p}_j + \sigma^2}\right), \tag{3.1}$$

where $\mathbf{p} \triangleq (\mathbf{p}_1, \mathbf{p}_2, \ldots, \mathbf{p}_K)^T$, g_{nk} is the channel gain from BS k to UE n, and σ^2 is the power of background additive white Gaussian noise. As seen from (3.1), UE n is subjected to the intercell interference from other BS $j \neq k$.

Next, consider the general case of multiple UEs connecting to a BS. The BS will then divide the total available time into a number of time slots and allocates them to its serviced UEs in a round-robin fashion [Shen and Yu, 2014; Ye et al., 2013]. As such, each connected UE will receive an equal amount of transmission time while there is no intracell interference. Denote $\mathbf{x}_{nk} \in \{0, 1\}$ as the BS-UE association variable, i.e., $\mathbf{x}_{nk} = 1$ if UE n is associated with BS k and $\mathbf{x}_{nk} = 0$ otherwise. Define $\mathbf{x}_k \triangleq [\mathbf{x}_{1k}, \ldots, \mathbf{x}_{Nk}]^T$ and $\mathbf{x} \triangleq \left[\mathbf{x}_1^T, \ldots, \mathbf{x}_K^T\right]^T$. If BS k serves a total of $\langle \mathbf{x}_k \rangle \triangleq \sum_{\hat{n}=1}^{N} \mathbf{x}_{\hat{n}k}$ UEs, then each of these UEs will be allocated $1/\langle \mathbf{x}_k \rangle$ of the total available time. Effectively, data rate perceived by a connected UE n is $r_{nk}(\mathbf{p})/\langle \mathbf{x}_k \rangle$, which will be further reduced as more and more UEs are associated to BS k. To reflect the fact that this rate is only possible if UE n actually connects to BS k, we define the effective data rate given to UE n by

BS k as:

$$r_{nk}^{\text{eff}}(\mathbf{x}_k, \mathbf{p}) \triangleq \frac{\mathbf{x}_{nk} r_{nk}(\mathbf{p})}{\langle \mathbf{x}_k \rangle}. \tag{3.2}$$

It follows that the sum effective data rate of cell k is

$$r_k^{\text{eff}}(\mathbf{x}, \mathbf{p}) \triangleq \sum_{n=1}^{N} r_{nk}^{\text{eff}}(\mathbf{p}) = \sum_{n=1}^{N} \frac{\mathbf{x}_{nk} r_{nk}(\mathbf{p})}{\langle \mathbf{x}_k \rangle}, \tag{3.3}$$

which is required not to exceed the limited backhaul capacity available to BS k [Olmos et al., 2013],[Qian et al., 2013]. The total network throughput across all K cells is then simply

$$\sum_{k=1}^{K} r_k^{\text{eff}}(\mathbf{x}, \mathbf{p}) = \sum_{k=1}^{K} \sum_{n=1}^{N} \frac{\mathbf{x}_{nk} r_{nk}(\mathbf{p})}{\langle \mathbf{x}_k \rangle}. \tag{3.4}$$

This chapter aims to enhance the network throughput by joint optimization of BS-UE association and transmit power allocation. Importantly, our design takes into account both the QoS requirement of each UE and the limited backhaul capacity at each BS. If too many UEs connect a particular BS (e.g., due to favorable channel conditions), then (i) the perceived rate of each UE will decrease and potentially not satisfy the minimum QoS requirement, and (ii) the sum effective rate of the corresponding cell may increase and potentially exceed the backhaul capacity. With a proper BS-UE association, the traffic load will be more balanced among different BSs and the network crowding issue can be alleviated. With adaptive power allocation, the intercell interference can be effectively managed to further improve the throughput. Here, we will consider the

following joint design problem for sum-rate maximization.

$$\max_{\mathbf{p},\,\mathbf{x}_{nk}\in\{0,1\}} \quad \sum_{k=1}^{K}\sum_{n=1}^{N}\frac{\mathbf{x}_{nk}r_{nk}(\mathbf{p})}{\langle\mathbf{x}_k\rangle} \tag{3.5a}$$

$$\text{s.t.} \quad \sum_{k=1}^{K}\mathbf{x}_{nk}=1,\ n=1,\ldots,N \tag{3.5b}$$

$$\langle\mathbf{x}_k\rangle\geq 1,\ k=1,\ldots,K \tag{3.5c}$$

$$\sum_{k=1}^{K}\frac{\mathbf{x}_{nk}r_{nk}(\mathbf{p})}{\langle\mathbf{x}_k\rangle}\geq R_n^{\mathrm{QoS}},\ n=1,\ldots,N \tag{3.5d}$$

$$\sum_{n=1}^{N}\mathbf{x}_{nk}r_{nk}(\mathbf{p})\leq C_k^{\mathrm{BH}}\langle\mathbf{x}_k\rangle,\ k=1,\ldots,K \tag{3.5e}$$

$$0\leq\mathbf{p}_k\leq P_k^{\max},\ k=1,\ldots,K. \tag{3.5f}$$

Constraint (3.5b) ensures each UE be connected with one BS only. Constraint (3.5c) requires each BS serves at least one UE [Shen and Yu, 2014; Fooladivanda and Rosenberg, 2013; Ye et al., 2013; Beyranvand et al., 2015]. In (3.5d) and (3.5e), $R_n^{\mathrm{QoS}}\geq 0$ and $C_k^{\mathrm{BH}}\geq 0$ specify the minimum throughput requirement for UE n and the backhaul capacity for cell k, respectively. Finally, (3.5f) caps the maximum transmit power of each BS k.

We also consider the following problem of maximizing the minimum effective rate among all UEs:

$$\begin{aligned}\max_{\mathbf{p},\,\mathbf{x}_{nk}\in\{0,1\}} \quad & \min_{n=1,\ldots,N}\left\{\sum_{k=1}^{K}\frac{\mathbf{x}_{nk}r_{nk}(\mathbf{p})}{\langle\mathbf{x}_k\rangle}\right\}\\ \text{s.t.} \quad & (3.5\text{b}),(3.5\text{c}),(3.5\text{e}),(3.5\text{f}).\end{aligned} \tag{3.6}$$

In problem (3.6), our aim is to support the most vulnerable UEs, e.g., those at the cell edges.

Both problems (3.5) and (3.6) belong to the difficult class of mixed-integer programming. The strong coupling between the binary variables $\mathbf{x}$ and the continuous variables $\mathbf{p}$ make the problems even more challenging. State-of-the-arts in existing literature typically apply the alternating optimization framework [Kuang et al., 2012; Chitti et al.,

2013; Ha and Le, 2014; Shen and Yu, 2014; Sun et al., 2015]. In this 'divide-and-conquer' approach, instead of dealing with $\mathbf{x}$ and $\mathbf{p}$ simultaneously, one decouples the original problems into subproblems of lower dimensions and resolve one subproblem at a time. Still for our problems (3.5) and (3.6) at hand, the BS-UE association problem for optimization in binary $\mathbf{x}$ scales exponentially with the number of BSs and UEs. It is not practical to try all the possible BS-UE combinations, even for networks of small-to-medium size. Moreover, for a given BS-UE combination, the power allocation for optimization in $\mathbf{p}$ remains highly nonconvex. Specifically, problem (3.5) has a nonconvex objective subject to nonconvex QoS and backhaul constraints, whereas problem (3.6) has a nonsmooth nonconvex objective subject also to a nonconvex set.

In what follows, we will address both problems (3.5) and (3.6) by a novel alternating descent method, which aims at improving the iterative solutions. It is noteworthy that the proposed joint user association and power control algorithms, although designed for single-antenna networks, can serve as a fundamental building block for subsequent development of joint user association and beamforming/precoding in multiple-antenna networks [Shen and Yu, 2014].

3.3 Proposed Alternating Descent Algorithm for Sum-Rate Maximization

3.3.1 BS-UE Association for Fixed Transmit Power

Given a fixed $\mathbf{p} := p$, we aim to solve problem (3.5) in variable $\mathbf{x}$. References [Corroy and Mathar, 2012; Corroy et al., 2012] considered the simplest case with $K = 2$ cells, under which the objective function (3.5a)

$$\frac{\sum_{n=1}^{N} \mathbf{x}_{n1} r_{n1}(p)}{\langle \mathbf{x}_1 \rangle} + \frac{\sum_{n=1}^{N} \mathbf{x}_{n2} r_{n2}(p)}{\langle \mathbf{x}_2 \rangle} = \frac{\sum_{n=1}^{N} \mathbf{x}_{n1} r_{n1}(p) \langle \mathbf{x}_2 \rangle + \sum_{n=1}^{N} \mathbf{x}_{n2} r_{n2}(p) \langle \mathbf{x}_1 \rangle}{\langle \mathbf{x}_1 \rangle \langle \mathbf{x}_2 \rangle}$$

is a fraction of linear functions in the new rank-one constrained matrix variable $\mathbf{X} = \mathbf{x}\mathbf{x}^T$ for $\mathbf{x} = \left[\mathbf{x}_1^T, \mathbf{x}_2^T\right]^T$. By dropping the constraint $\mathsf{rank}(\mathbf{X}) = 1$ and relaxing binary constraints on its entries to real numbers belonging to the interval $[0, 1]$, a bisection search is used in finding the optimal solution of the resultant program. It should be emphasized again that such a relaxation only works if there are two cells in the network. This is because for $K > 2$ the objective function (3.5a) becomes a fraction of nonlinear functions in $\mathbf{X} = \mathbf{x}\mathbf{x}^T$.

Our objective here is to devise a solution that works for a general network with an arbitrary number of cells. To begin with, notice that all the constraints (3.5b), (3.5c) and (3.5e) are linear in $\mathbf{x}$, but not (3.5d). The following proposition allows us to equivalently recast the nonconvex constraint (3.5d) as a system of linear constraints on $\mathbf{x}$.

Proposition 3.1. *Under the constraint (3.5b), the constraint (3.5d) is equivalent to*

$$(M - (M-1)\mathbf{x}_{nk})\, r_{nk}(p) \geq R_n^{QoS}\langle \mathbf{x}_k \rangle,\ n = 1, \ldots, N,\ k = 1, \ldots, K \tag{3.7}$$

for a sufficiently large number M.

Proof. Denote by $(3.5\text{d})_n$ the constraint (3.5d) for n. It is sufficient to show that each $(3.5\text{d})_n$ is equivalent to the following K constraints:

$$(M - (M-1)\mathbf{x}_{nk})\, r_{nk}(p) \geq R_n^{\text{QoS}}\langle \mathbf{x}_k \rangle,\ k = 1, \ldots, K. \tag{3.8}$$

Under the constraint (3.5b), for each n there is k_n such that $\mathbf{x}_{nk_n} = 1$ and $\mathbf{x}_{nk} = 0, \forall k \in \{1, \ldots, K\} \setminus \{k_n\}$. Therefore, (3.8) merely means that

$$r_{nk_n}(p) \geq R_n^{\text{QoS}}\langle \mathbf{x}_{k_n} \rangle, \tag{3.9}$$

and

$$M r_{nk}(p) \geq R_n^{\text{QoS}}\langle \mathbf{x}_k \rangle, k \neq k_n. \tag{3.10}$$

Note that (3.9) is $(3.5\text{d})_n$, showing the implication (3.8) $\Rightarrow (3.5d)_n$.

On the other hand, (3.10) holds true for $0 < M < +\infty$ because its right hand side is obviously bounded while the factor $r_{nk}(p)$ on the left hand side is strictly positive. The inverse implication $(3.5d)_n \Rightarrow (3.8)$ thus follows, yielding the equivalence between (3.8) and $(3.5\text{d})_n$. ■

Next, we deal with the binary nature of $\mathbf{x}$. For $\mathbf{x}_{\hat{n}k} \in \{0,1\}$, one has $\mathbf{x}_{\hat{n}k} = \mathbf{x}_{\hat{n}k}^2$ and thus $\langle \mathbf{x}_k \rangle = \langle \mathbf{x}_k^2 \rangle \triangleq \sum_{\hat{n}=1}^{N} \mathbf{x}_{\hat{n}k}^2$. The objective function (3.5a) is then expressed as

$$\sum_{k=1}^{K} \sum_{n=1}^{N} \frac{\mathbf{x}_{nk}^2 r_{nk}(p)}{\langle \mathbf{x}_k^2 \rangle}. \tag{3.11}$$

On the one hand, it is straightforward to see that $\mathbf{x}_{nk} \in \{0,1\}$ is equivalent to $\mathbf{x}_{nk}^2 = \mathbf{x}_{nk},\ \mathbf{x}_{nk} \in [0,1]$. On the other hand, it holds true that $\mathbf{x}_{nk}^2 \leq \mathbf{x}_{nk}$ for $\mathbf{x}_{nk} \in [0,1]$. Following [Che et al., 2014], we relax binary $\mathbf{x}_{nk}$ to $\mathbf{x}_{nk} \in [0,1]$ and introduce a penalty term in the objective function (3.11) to enforce $\mathbf{x}_{nk}^2 = \mathbf{x}_{nk}$, thus making $\mathbf{x}_{nk}$ binary. This leads to the following problem:

$$\begin{aligned} \max_{\mathbf{x}_k \in [0,1]^N} \quad & \mathcal{P}_1(\mathbf{x}, p) \triangleq \sum_{k=1}^{K} \sum_{n=1}^{N} \frac{\mathbf{x}_{nk}^2 r_{nk}(p)}{\langle \mathbf{x}_k^2 \rangle} + \lambda \sum_{k=1}^{K} \sum_{n=1}^{N} \left(\mathbf{x}_{nk}^2 - \mathbf{x}_{nk} \right) \\ \text{s.t.} \quad & (3.5\text{b}) - (3.5\text{e}), \end{aligned} \tag{3.12}$$

where $\lambda \geq 0$ is a constant penalty factor. Parameter λ signifies the relative importance of recovering binary values for $\mathbf{x}$ over throughput maximization. In (3.12), the term $\sum_{k=1}^{K} \sum_{n=1}^{N} (\mathbf{x}_{nk} - \mathbf{x}_{nk}^2)$ is always nonnegative and can therefore be used to measure the degree of satisfaction of the binary constraints $\mathbf{x}_{nk} \in \{0,1\},\ \forall n,k$. Without squaring such a term, the above penalization is exact, meaning that the constraints $\mathbf{x} \in \{0,1\},\ \forall n,k$ can be satisfied by a maximizer of (3.12) with a finite value of λ (see, e.g., [Bonnans et al., 2006, Ch. 16]). This nice property makes such exact penalization attractive.

With Proposition 3.1, problem (3.12) becomes

$$\begin{aligned} \max_{\mathbf{x}_k \in [0,1]^N} \quad & \mathcal{P}_1(\mathbf{x}, p) \\ \text{s.t.} \quad & (3.5\text{b}), (3.5\text{c}), (3.5\text{e}), (3.7). \end{aligned} \tag{3.13}$$

3.3 Proposed Alternating Descent Algorithm for Sum-Rate Maximization

With an appropriate choice of λ, problems (3.13) and (3.5) are equivalent in the sense that they share the same optimal solution [Che et al., 2014, Sec. II]. Since problem (3.13) is still nonconvex, we now employ successive convex programming to solve it.

Proposition 3.2. *For a given point $(x^{(\kappa)}, p)$, the following convex problem is a global lower bound maximization for* (3.13)*:*

$$\begin{aligned} \max_{\mathbf{x}_k \in [0,1]^N} \quad & \tilde{\mathcal{P}}_1^{(\kappa)}(\mathbf{x}, p) \triangleq \sum_{k=1}^{K} \sum_{n=1}^{N} \alpha_{nk}^{(\kappa)}(\mathbf{x}, p) + \lambda \sum_{k=1}^{K} \sum_{n=1}^{N} \gamma_{nk}^{(\kappa)}(\mathbf{x}) \\ \textit{s.t.} \quad & (3.5\text{b}), (3.5\text{c}), (3.5\text{e}), (3.7), \end{aligned} \tag{3.14}$$

where we define

$$\alpha_{nk}^{(\kappa)}(\mathbf{x}, p) \triangleq \frac{(x_{nk}^{(\kappa)})^2 r_{nk}(p)}{\langle (x_k^{(\kappa)})^2 \rangle} + \frac{2x_{nk}^{(\kappa)} \left(\mathbf{x}_{nk} - x_{nk}^{(\kappa)} \right) r_{nk}(p)}{\langle (x_k^{(\kappa)})^2 \rangle} - \frac{(x_{nk}^{(\kappa)})^2 r_{nk}(p)}{\left(\langle (x_k^{(\kappa)})^2 \rangle \right)^2} \left(\langle \mathbf{x}_k^2 \rangle - \langle (x_k^{(\kappa)})^2 \rangle \right), \tag{3.15a}$$

$$\gamma_{nk}^{(\kappa)}(\mathbf{x}) \triangleq (x_{nk}^{(\kappa)})^2 - x_{nk}^{(\kappa)} + (2x_{nk}^{(\kappa)} - 1) \left(\mathbf{x}_{nk} - x_{nk}^{(\kappa)} \right). \tag{3.15b}$$

Proof. See Appendix A, where we show that the objective $\tilde{\mathcal{P}}_1^{(\kappa)}(., p)$ in (3.14) is a global lower bound of the objective $\mathcal{P}_1(\mathbf{x}, p)$ in (3.13), i.e.

$$\mathcal{P}_1(\mathbf{x}, p) \geq \tilde{\mathcal{P}}_1^{(\kappa)}(\mathbf{x}, p), \ \forall \mathbf{x} \quad \text{and} \quad \mathcal{P}_1(x^{(\kappa)}, p) = \tilde{\mathcal{P}}_1^{(\kappa)}(x^{(\kappa)}, p). \tag{3.16}$$

■

The nonconvex problem (3.13) can then be addressed by instead solving its global lower bound maximization (3.14) in a sequential manner as follows: After initializing from a feasible point $x^{(0)}$ of problem (3.13), we iteratively solve problem (3.14) to generate a sequence $\{x^{(\kappa)}\}$, $\kappa = 1, 2, \ldots$ of feasible and improved points toward the optimal solution of (3.13). More specifically, at iteration κ we use $x^{(\kappa-1)}$ as a feasible point to solve (3.14) and obtain $x^{(\kappa)}$.

Theorem 3.1. *Initialized from a feasible point $x^{(0)}$, the sequence $\{x^{(\kappa)}\}$ obtained by iteratively solving* (3.14) *is a sequence of improved points of* (3.13)*, which converges to a KKT point.*

Proof. Note that $x^{(\kappa)}$ and $x^{(\kappa+1)}$ are a feasible point and the optimal solution of (3.14), respectively. By using (3.16),

$$\mathcal{P}_1(x^{(\kappa+1)}, p) \geq \tilde{\mathcal{P}}_1^{(\kappa)}(x^{(\kappa+1)}, p) \geq \tilde{\mathcal{P}}_1^{(\kappa)}(x^{(\kappa)}, p) = \mathcal{P}_1(x^{(\kappa)}, p), \tag{3.17}$$

i.e. $x^{(\kappa+1)}$ is a better point of (3.13) than $x^{(\kappa)}$. Since the sequence $\{x^{(\kappa)}\}$ is bounded, by Cauchy's theorem there is a convergent subsequence $\{x^{(\kappa_\nu)}\}$ with a limit point $\bar{x}$, i.e.

$$\lim_{\nu \to +\infty} [\mathcal{P}_1(x^{(\kappa_\nu)}, p) - \mathcal{P}_1(\bar{x}, p)] = 0.$$

For every κ there is ν such that $\kappa_\nu \leq \kappa \leq \kappa_{\nu+1}$ so

$$\begin{aligned} 0 &= \lim_{\nu \to +\infty} [\mathcal{P}_1(x^{(\kappa_\nu)}, p) - \mathcal{P}_1(\bar{x}, p)] \\ &\leq \lim_{\nu \to +\infty} [\mathcal{P}_1(x^{\kappa)}, p) - \mathcal{P}_1(\bar{x}, p)] \\ &\leq \lim_{\nu \to +\infty} [\mathcal{P}_1(x^{\kappa_{\nu+1})}, p) - \mathcal{P}_1(\bar{x}, p)] \\ &= 0, \end{aligned}$$

showing that $\lim_{\kappa \to +\infty} \mathcal{P}_1(x^{\kappa)}, p) = \mathcal{P}_1(\bar{x}, p)$. Then, each accumulation point $\bar{x}$ of the sequence $\{x^{(\kappa)}\}$ is a KKT-point according to [Marks and Wright, 1978, Theorem 1]. The proof of Theorem 3.1 is thus complete. ■

3.3.2 Power Allocation for Fixed BS-UE Association

Given $\mathbf{x} := x$, we proceed to solving problem (3.5) in the variable $\mathbf{p}$. Although the difference-of-convex iterations (DCI) approach of [Kha et al., 2012] can be applied in the absence of backhaul constraints (3.5e), the required log-determinant optimization is computationally expensive even for commercialized convex solvers. This drawback is particularly severe in HetNets which consist of a large number of densely deployed BSs and UEs. Reference [Yu et al., 2014] proposes solving the KKT conditions, followed by applying the gradient descent method to update Lagrangian multipliers in order to satisfy (3.5e). Nevertheless, a solution derived from the KKT conditions of a nonconvex problem may not be locally optimal or even feasible.

3.3 Proposed Alternating Descent Algorithm for Sum-Rate Maximization

Our aim here is to devise an efficient and optimal power allocation solution. Using Proposition 3.1 and simple algebraic manipulations, (3.5d) is expressed as the following linear constraints:

$$g_{nk}\mathbf{p}_k \geq \left[\exp\left(\frac{R_n^{\mathrm{QoS}}\langle x_k\rangle}{M-(M-1)x_{nk}}\right)-1\right]\left(\sum_{j\neq k,j=1}^{K} g_{nj}\mathbf{p}_j+\sigma^2\right), \quad n=1,\ldots,N,\ k=1,\ldots,K. \tag{3.18}$$

Problem (3.5) is then reduced to

$$\max_{\mathbf{p}} \mathcal{P}_1(x,\mathbf{p}) \triangleq \sum_{k=1}^{K}\sum_{n=1}^{N}\frac{(x_{nk})^2}{\langle x_k^2\rangle} r_{nk}(\mathbf{p}) \tag{3.19a}$$

$$\text{s.t.} \quad \sum_{n=1}^{N} x_{nk} r_{nk}(\mathbf{p}) \leq C_k^{\mathrm{BH}}\langle x_k\rangle,\ k=1,\ldots,K \tag{3.19b}$$

$$(3.5\text{f}), (3.18).$$

Because (3.19a) and (3.19b) are still nonconvex in $\mathbf{p}$, we instead consider their convex bounds as given in the following result.

Proposition 3.3. *The rate function $r_{nk}(\mathbf{p})$ in (3.1) admits*

$$r_{nk}(\mathbf{p}) \leq \theta_{nk}^{(\kappa)}(\mathbf{p}) \triangleq r_{nk}(p^{(\kappa)}) + \frac{1}{\sum\limits_{j\neq k,j=1}^{K} g_{nj}p_j^{(\kappa)}+\sigma^2}\sum_{j\neq k,j=1}^{K}(g_{nj}p_j^{(\kappa)})^2\left(\frac{1}{g_{nj}\mathbf{p}_j}-\frac{1}{g_{nj}p_j^{(\kappa)}}\right) + \frac{1}{\sum_{j=1}^{K} g_{nj}p_j^{(\kappa)}+\sigma^2}\sum_{j=1}^{K} g_{nj}(\mathbf{p}_j - p_j^{(\kappa)}) \tag{3.20}$$

as its upper bound, and

$$r_{nk}(\mathbf{p}) \geq \beta_{nk}^{(\kappa)}(\mathbf{p}) \triangleq r_{nk}(p^{(\kappa)}) - \frac{1}{\sum\limits_{j=1}^{K} g_{nj}p_j^{(\kappa)}+\sigma^2}\sum_{j=1}^{K}(g_{nj}p_j^{(\kappa)})^2\left(\frac{1}{g_{nj}\mathbf{p}_j}-\frac{1}{g_{nj}p_j^{(\kappa)}}\right) - \frac{1}{\sum_{j\neq k,j=1}^{K} g_{nj}p_j^{(\kappa)}+\sigma^2}\sum_{j\neq k,j=1}^{K} g_{nj}(\mathbf{p}_j - p_j^{(\kappa)}) \tag{3.21}$$

as its lower bound.

Proof. See Appendix B. ■

3.3 Proposed Alternating Descent Algorithm for Sum-Rate Maximization

With the bounds in (3.20) and (3.21), we now address the nonconvex problem (3.19) by successive convex programming. Specifically, after initializing a feasible point $p^{(0)}$ of problem (3.19), we iteratively solve the following global lower bound maximization of (3.19):

$$\max_{\mathbf{p}} \ \bar{\mathcal{P}}_1^{(\kappa)}(x, \mathbf{p}) \triangleq \sum_{k=1}^{K} \sum_{n=1}^{N} \frac{(x_{nk})^2}{\langle x_k^2 \rangle} \beta_{nk}^{(\kappa)}(\mathbf{p}) \tag{3.22a}$$

$$\text{s.t.} \quad \sum_{n=1}^{N} x_{nk} \theta_{nk}(\mathbf{p}) \leq C_k^{\mathrm{BH}} \langle x_k \rangle, \ k = 1, \ldots, K \tag{3.22b}$$

$$(3.5\text{f}), (3.18)$$

to generate a sequence $\{p^{(\kappa)}\}$, $\kappa = 1, 2, \ldots$ of feasible and improved points toward the solution of (3.19). At iteration κ, we use $p^{(\kappa-1)}$ as a feasible point to solve (3.22) and obtain $p^{(\kappa)}$. Similarly to Theorem 3.1, we can prove the following result.

Theorem 3.2. *Initialized from a feasible point $p^{(0)}$, the sequence $\{p^{(\kappa)}\}$ obtained by iteratively solving* (3.22) *is a sequence of improved points, which converges to a KKT point of* (3.19).

3.3.3 Joint Optimization of BS-UE Association and Power Allocation

The alternating optimization framework requires solving a series of convex problems (3.14) [cf. Section 3.3.1] followed by solving a series of convex problems (3.22) [cf. Section 3.3.2] and repeating until convergence. Realizing that solving one instant of (3.14) and (3.22) alone already provides a better point, we use them as an alternating descent to achieve a much faster convergence speed. The proposed joint optimization of BS-UE association and power allocation for sum-rate maximization is summarized in Algorithm 1. Our alternating descent approach gives flexibility in executing user association and power control in the same time slot (as in Algorithm 1) or different time slots (by selectively deactivating Step 3 or 4 of Algorithm 1).

Algorithm 1 Joint BS-UE Association and Power Allocation for Sum-Rate Maximization

1: Initialize $x_{nk}^{(0)} := \frac{1}{KN},\ n = 1, \ldots, N,\ k = 1, \ldots, K$ and $p_k^{(0)} := P_k^{\max},\ k = 1, \ldots, K$. Set $\kappa := 0$.
2: **repeat**
3: Solve convex program (3.14) with $p := p^{(\kappa)}$ to find optimal solution $x^\star$.
4: Solve convex program (3.22) with $x := x^*$ to find optimal solution $p^\star$.
5: Set $(x^{(\kappa+1)}, p^{(\kappa+1)}) := (x^\star, p^\star)$ and $\kappa := \kappa + 1$.
6: **until** $\left|\left(\mathcal{P}_1(x^{(\kappa)}, p^{(\kappa)}) - \mathcal{P}_1(x^{(\kappa-1)}, p^{(\kappa-1)})\right) / \mathcal{P}_1(x^{(\kappa-1)}, p^{(\kappa-1)})\right| < \epsilon$

At each iteration of Algorithm 1, the computational complexity of solving convex problems (3.14) and (3.22) is only polynomial in the number of variables and constraints. To see this, (3.14) can be equivalently reformulated as an optimization problem with $a \triangleq (NK + 1)$ real-valued scalar decision variables, a linear objective, $b \triangleq (N + 2K + NK)$ linear constraints and one quadratic constraint. Similarly, (3.22) can be equivalently reformulated as a semidefinite program with $(2K+1)$ scalar variables, a linear objective and a system of linear matrix inequalities. The complexity required to solve (3.14) and (3.22) is thus $\mathcal{O}\left((1 + a + b)a^2\sqrt{b + 1}\right)$ and

$$\mathcal{O}\left(\left[(2K + 1)^2(K + 1)^3 + (2K + 1)^2 NK^3\right]\sqrt{3K + NK + 1}\right),$$

respectively [Nemirovski, 2004].

Theorem 3.3. *Initialized from a feasible point $(x^{(0)}, p^{(0)})$, Algorithm 1 converges to a solution of problem* (3.5) *after a finite number of iterations for a given error tolerance $\epsilon > 0$.*

Proof. The BS-UE association problem (3.13) and the power allocation problem (3.19) have the same objective function $\mathcal{P}_1(\mathbf{x}, \mathbf{p})$. From (3.17), (3.20) and (3.21), we have the following relations:

$$\begin{aligned}\mathcal{P}_1(x^{(\kappa+1)}, p^{(\kappa+1)}) &\geq \bar{\mathcal{P}}_1^{(\kappa)}(x^{(\kappa+1)}, p^{(\kappa+1)}) \geq \bar{\mathcal{P}}_1^{(\kappa)}(x^{(\kappa+1)}, p^{(\kappa)}) \\ &= \mathcal{P}_1(x^{(\kappa+1)}, p^{(\kappa)}) \geq \tilde{\mathcal{P}}_1^{(\kappa)}(x^{(\kappa+1)}, p^{(\kappa)}) \\ &\geq \tilde{\mathcal{P}}_1^{(\kappa)}(x^{(\kappa)}, p^{(\kappa)}) = \mathcal{P}_1(x^{(\kappa)}, p^{(\kappa)}). \end{aligned} \tag{3.23}$$

It means that alternatingly solving their respective convex minorants (3.14) and (3.22) always improves $\mathcal{P}_1(\mathbf{x}, \mathbf{p})$ in each iteration. As such, once initialized from a feasible point $(x^{(0)}, p^{(0)})$ that satisfies (3.5b), (3.5c) and (3.5f), Algorithm 1 generates a sequence $\{(x^{(\kappa)}, p^{(\kappa)})\}$ of feasible and improved points which eventually converges to a solution $(\bar{x}, \bar{p})$ of (3.5). Note that $\bar{x}$ is a KKT point of (3.13) for $p = \bar{p}$ while $\bar{p}$ is a KKT of (3.19) for $x = \bar{x}$. Under the stopping criterion

$$\left|\left(\mathcal{P}_1(x^{(\kappa+1)}, p^{(\kappa+1)}) - \mathcal{P}_1(x^{(\kappa)}, p^{(\kappa)})\right) / \mathcal{P}_1(x^{(\kappa)}, p^{(\kappa)})\right| < \epsilon, \tag{3.24}$$

Algorithm 1 terminates after a finite number of iterations for a given $\epsilon > 0$. ■

3.4 Proposed Alternating Descent Algorithm for Minimum UE Rate Maximization

The above developed Algorithm 1 is readily extendable to solve the max-min problem (3.6). In this case, we consider the following objective function.

$$\mathcal{P}_2(\mathbf{x}, \mathbf{p}) \triangleq \min_{n=1,\ldots,N} \left\{ \sum_{k=1}^{K} \frac{\mathbf{x}_{nk}^2 r_{nk}(\mathbf{p})}{\langle \mathbf{x}_k^2 \rangle} \right\} + \lambda \sum_{k=1}^{K} \sum_{n=1}^{N} \left(\mathbf{x}_{nk}^2 - \mathbf{x}_{nk} \right), \tag{3.25}$$

where $\mathbf{x}_{nk} \in [0, 1],\ n = 1, \ldots, N,\ k = 1, \ldots, K$ and $\lambda \geq 0$ is a constant penalty factor. The BS-UE association problem for a fixed power allocation $\mathbf{p} := p$ is now

$$\begin{aligned} \max_{\mathbf{x}_k \in [0,1]^N} \quad & \mathcal{P}_2(\mathbf{x}, p) \\ \text{s.t.} \quad & (3.5\text{b}), (3.5\text{c}), (3.5\text{e}). \end{aligned} \tag{3.26}$$

Although the constraint set of (3.26) is convex, its objective is nonsmooth and nonconvex. Similar to Proposition 3.2, it can be shown that the following convex problem is a global lower bound maximization of (3.26):

$$\begin{aligned} \max_{\mathbf{x}_k \in [0,1]^N} \quad & \tilde{\mathcal{P}}_2(\mathbf{x}, p) \triangleq \min_{n=1,\ldots,N} \left\{ \sum_{k=1}^{K} \alpha_{nk}^{(\kappa)}(\mathbf{x}, p) \right\} + \lambda \sum_{k=1}^{K} \sum_{n=1}^{N} w_{nk} \gamma_{nk}^{(\kappa)}(\mathbf{x}), \\ \text{s.t.} \quad & (3.5\text{b}), (3.5\text{c}), (3.5\text{e}), \end{aligned} \tag{3.27}$$

where $\alpha_{nk}^{(\kappa)}(\mathbf{x}, p)$ and $\gamma_{nk}^{(\kappa)}(\mathbf{x})$ have previously been defined in (3.15).

Next, the power allocation problem for a fixed $\mathbf{x} := x$ is

$$\begin{aligned} \max_{\mathbf{p}} \quad & \mathcal{P}_2(x, \mathbf{p}) \triangleq \min_{k=1,\ldots,K} \left\{ \sum_{n=1}^{N} \frac{x_{nk}^2}{\langle x_k^2 \rangle} r_{nk}(\mathbf{p}) \right\} \\ \text{s.t.} \quad & (3.5\text{e}), (3.5\text{f}), \end{aligned} \tag{3.28}$$

which has a nonsmooth nonconvex objective function and a nonconvex set. Similar to Proposition 3.3, it can be shown that the following convex problem is a global lower bound maximization of (3.28):

$$\begin{aligned} \max_{\mathbf{p}} \quad & \bar{\mathcal{P}}_2^{(\kappa)}(x, \mathbf{p}) \triangleq \min_{k=1,\ldots,K} \left\{ \sum_{n=1}^{N} \frac{x_{nk}^2}{\langle x_k^2 \rangle} \beta_{nk}(\mathbf{p}) \right\} \\ \text{s.t.} \quad & (3.22\text{b}), (3.5\text{f}), \end{aligned} \tag{3.29}$$

where $\beta_{nk}(\mathbf{p})$ has previously been defined in (3.21).

To solve problem (3.6) in *both* $\mathbf{x}$ and $\mathbf{p}$, we modify Algorithm 1 as follows. In Step 3, we solve convex problem (3.27) instead of (3.14). In Step 4, we solve convex problem (3.29) instead of (3.22). And because the objective function is now $\mathcal{P}_2(x, \mathbf{p})$, the proposed algorithm for problem (3.6) terminates when

$$\left| \left(\mathcal{P}_2(x^{(\kappa)}, p^{(\kappa)}) - \mathcal{P}_2(x^{(\kappa-1)}, p^{(\kappa-1)}) \right) / \mathcal{P}_2(x^{(\kappa-1)}, p^{(\kappa-1)}) \right| < \epsilon.$$

We shall refer to this modified algorithm as Algorithm 2.

In each iteration of Algorithm 2, the computational complexity of solving problem (3.27) is $\mathcal{O}\left((N + a + d)c^2\sqrt{c + N}\right)$, because (3.27) can be equivalently reformulated as an optimization problem with $a = (NK + 1)$ scalar real decision variables, a linear objective, $c \triangleq (N + K)$ linear constraints and N quadratic constraints [Nemirovski, 2004]. Similarly, the complexity of solving problem (3.29) is

$$\mathcal{O}\left(\left[cd^2(K+1)^2 + d^2NK^3 \right] \sqrt{3K + NK + N} \right),$$

because (3.29) can be reformulated as a semidefinite program with $d \triangleq (2K + 1)$ scalar variables, a linear objective and a system of linear matrix inequalities. Finally, similar

to Theorem 3.3, it can be proved that once initialized from a feasible point $(x^{(0)}, p^{(0)})$ that satisfies (3.5b), (3.5c) and (3.5f), Algorithm 2 converges after a finite number of iterations for a given error tolerance ϵ.

3.5 Illustrative Examples

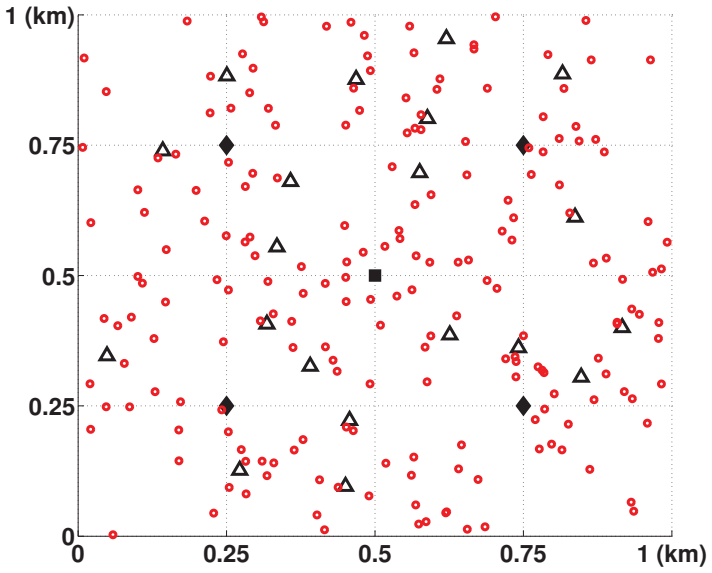

Figure 3.2: A three-tier network with one fixed MBS (black square), four fixed PBSs (black diamonds), twenty random FBSs (black triangles) and 200 random UEs (red circles).

Consider a three-tier HetNet where four pico BSs (PBSs) and twenty femto BSs (FBSs) are deployed within a macrocell of size $1,000\text{m} \times 1,000\text{m}$. The locations of MBS and PBSs are fixed whereas those of FBSs are random, as shown in Fig. 3.2. We assume there are $N = 200$ UEs randomly distributed over the macrocell coverage area. The network topology is then fixed during the optimization process. Without loss of generality, we only consider the effect of pathloss when generating the channel gains. The fading channel is not considered in this work to provide a clear and simple illustration of the BSs' footprint. The proposed algorithms can be applied for the fading channel without

modifications. To illustrate the impact of imperfect backhaul links, we assume that the MBS, PBSs, and FBSs are each equipped with a backhaul link of capacity $C^{\mathrm{BH}}, C^{\mathrm{BH}}/3$ and $C^{\mathrm{BH}}/10$, respectively. Following [Tipmongkolsilp et al., 2011], we choose $C^{\mathrm{BH}} \in \{100, 150, 200, \infty\}$ Mbps where $C^{\mathrm{BH}} = \infty$ represents the ideal backhaul. For simplicity, we set the required minimum UE throughput as $R_n^{\mathrm{QoS}} = R^{\mathrm{QoS}},\ n = 1, \ldots, N$. The error tolerance for the algorithms is set as $\epsilon = 10^{-4}$. Other 3GPP LTE parameters used to setup our simulations are listed in Table 3.1 [3GPP TS 36.814 V9.0.0, 2010]. Note that we divide the obtained rate results by $\ln(2)$ to arrive at the unit of bps/Hz.

Table 3.1: Simulation parameters used in all numerical examples

Parameter	**Value**
Minimum distance between MBS-UE	35m
Minimum distance between PBS/FBS-UE	10m
Path loss model for MBS-UE links	$128.1 + 37.6 \ln_{10}(d)$, d is in km
Path loss model for PBS-UE links and FBS-UE links	$140.7 + 36.7 \ln_{10}(d)$, d is in km
Maximum MBS transmit power	43dBm
Maximum PBS transmit power	24dBm
Maximum FBS transmit power	20dBm
Background noise power	-104dBm
System bandwidth	10MHz
Frequency reuse factor	1

First, we compare the sum-rate performance of the joint design in Algorithm 1 to that of Algorithm 1 but with full BS transmit power (i.e., no power control). We use the heuristic BS-UE association schemes, namely, max-SINR and DCD [Shen and Yu, 2014] as benchmarks where full BS transmit power is also assumed. As both benchmark schemes assume ideal backhaul, we set $C^{\mathrm{BH}} = \infty$ here for a fair comparison. And since the max-SINR and DCD schemes do not include the minimum UE throughput constraint, we first assume $R^{\mathrm{QoS}} = 0$ in these two schemes to find their BS-UE associations, followed by calculating their achieved sum-rates and minimum UE rates. Fig. 3.3 shows that joint design of load balancing and interference management in Algorithm 1 gives much higher network throughput over load balancing alone. This can be explained by noting that the joint design has an extra dimension of BS transmit power to optimize to

further enhance the sum-rate performance. When comparing Algorithm 1 with full BS transmit power to the max-SINR and DCD schemes, the former offers more flexibility in setting the desired minimum R^{QoS}. Furthermore, for the same values of R^{QoS} that are achieved by the max-SINR and DCD schemes, the sole BS-UE design by Algorithm 1 gives a slightly better sum-rate performance as can be observed from Fig. 3.3.

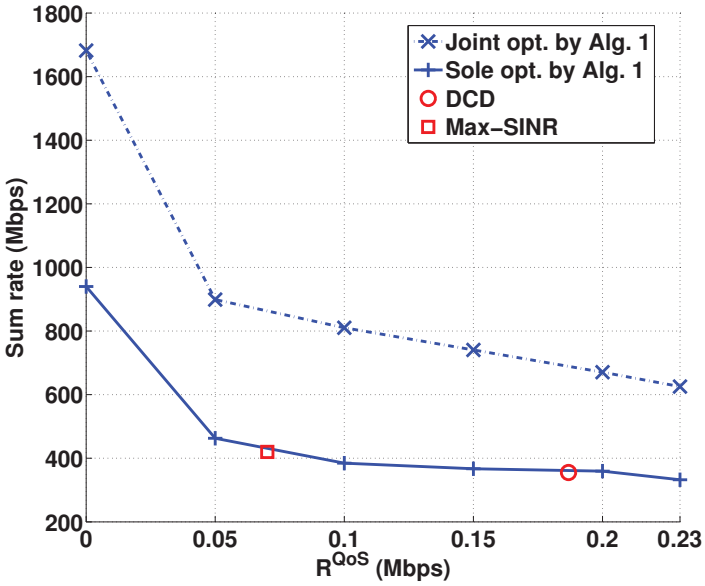

Figure 3.3: Sum-rate performance of Algorithm 1 under ideal backhaul links.

Next, we evaluate the effects of QoS constraints and limited backhaul capacity in the joint design of Algorithm 1. Fig. 3.4 shows that as we move away from the assumption of ideal backhaul, the total throughput is gradually degraded. This observation is as expected because the feasible region of problem (3.5) becomes more restricted. For each value of C^{BH}, Fig. 3.4 also shows that lowering the UE throughput requirement R^{QoS} actually increases the total throughput. However, while such an throughput improvement is pronounced for the ideal backhaul, it is not much so for limited backhaul capacity cases where reducing R^{QoS} beyond 0.2Mbps only marginally improves the sum-rate. Our numerical analysis reveals that most of the PBSs and FBSs have fully utilized their respective limited backhaul capacities of $C^{\mathrm{BH}}/3$ and $C^{\mathrm{BH}}/10$, leaving no room for further throughput improvement at these small cells even if R^{QoS} is small. Such an

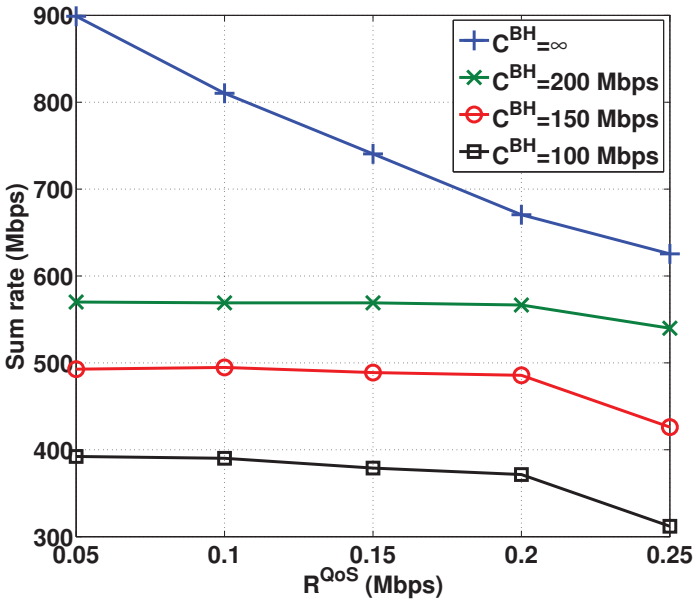

Figure 3.4: Effects of QoS constraints and limited backhaul capacity on the sum-rate performance of Algorithm 1.

observation again verifies that backhaul capacity is in fact a bottleneck for network performance.

Fig. 3.5 further demonstrates that for a given R^{QoS}, switching from ideal backhaul ($C^{\text{BH}} = \infty$) to non-ideal backhaul ($C^{\text{BH}} = 100$Mbps) may limit the offloading capability of small cells. Indeed, many UEs will be transferred from the small cells back to the macrocell. This observation can be explained as follows. The small cells are more easily overloaded in the non-ideal backhaul case as their backhaul capacity is much smaller than that of the macrocell. To meet their backhaul limitations, small-cell BSs decrease their transmit power to shrink their cell size and serve fewer UEs with lower cell throughput. With 19dB-23dB higher in power budget compared to that available to small-cell BSs, the MBS then increases its transmit power (and effectively its coverage area) to take over the UEs pushed out by the small cells. And with 3-10 times more backhaul capacity, the MBS is still able to accommodate the incoming traffic. This can be best observed in Fig. 3.6(b) [cf. Fig. 3.6(a)] and Fig. 3.6(d) [cf. Fig. 3.6(c)], where

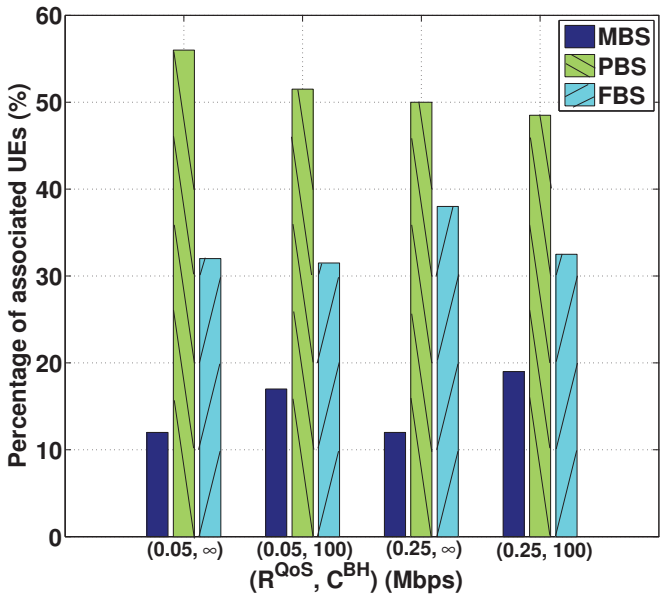

Figure 3.5: Effects of QoS constraints and limited backhaul capacity on the load distribution by Algorithm 1.

the MBS serves more distant UEs for $C^{\mathrm{BH}} = 100$Mbps.

Fig. 3.7 demonstrates the fairness given by Algorithm 2 for max-min UE rates. Here, we compare against Algorithm 1 for sum-rate maximization where $R^{\mathrm{QoS}} = 0.05$Mbps is assumed. As seen from the figure, Algorithm 2 improves the minimum UE rate as the cost of reduced total throughput. Furthermore, for $C^{\mathrm{BH}} \geq 150$ Mbps, reducing backhaul capacity does not affect much the minimum UE rate and sum-rate performance of Algorithm 2 because the ample backhaul capacity at each cell can still accommodate more data traffic. However, for $C^{\mathrm{BH}} \leq 100$ Mbps, the minimum UE rate by Algorithm 2 starts to fall dramatically. And at $C^{\mathrm{BH}} = 50$Mbps, the achieved minimum UE rate drops by more than 4.5 times compared to that in the ideal backhaul case. At this point, a significantly larger number of UEs turns to the MBS for service as shown Fig. 3.8. This is because the MBS still has available backhaul capacity while the PBSs and FBSs are more likely to be overloaded.

Finally, we examine the convergence of the proposed algorithms. It is sufficient to

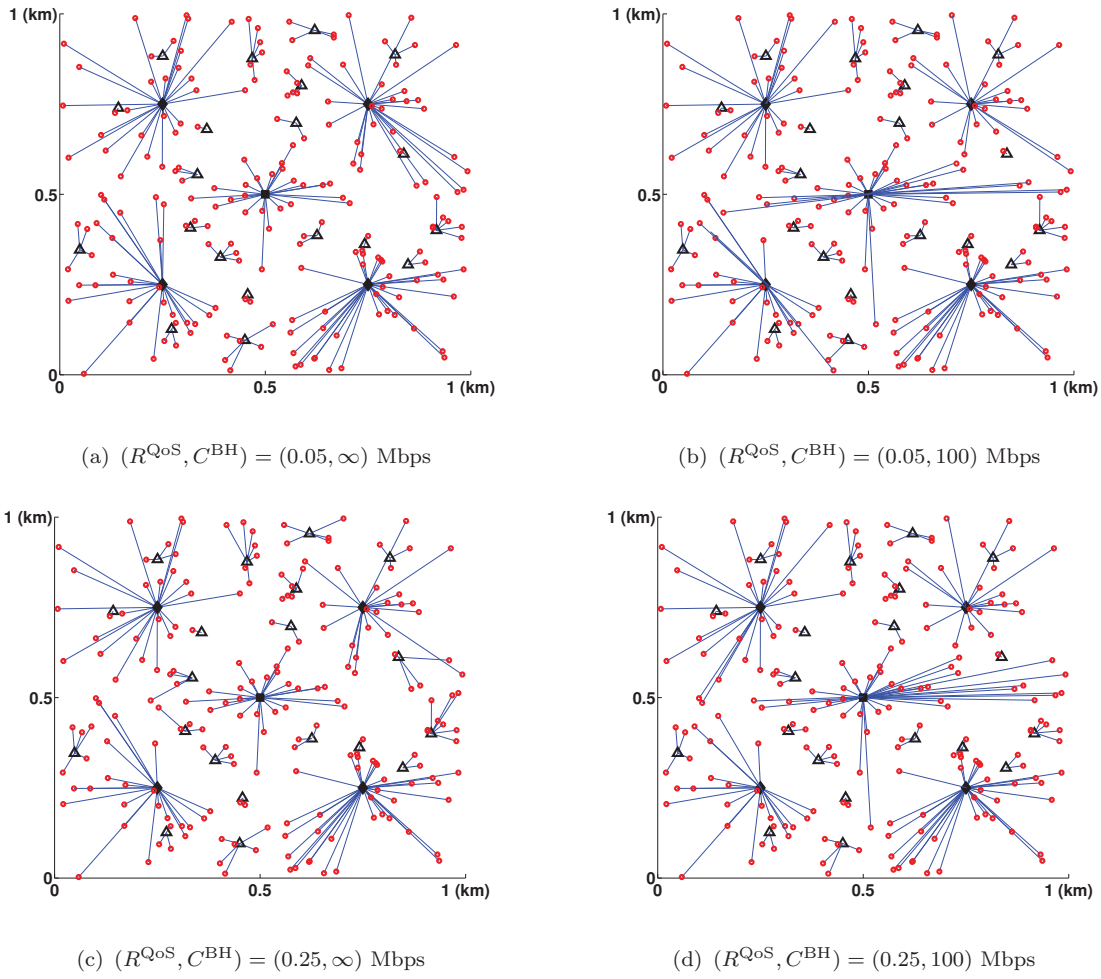

(a) $(R^{\mathrm{QoS}}, C^{\mathrm{BH}}) = (0.05, \infty)$ Mbps

(b) $(R^{\mathrm{QoS}}, C^{\mathrm{BH}}) = (0.05, 100)$ Mbps

(c) $(R^{\mathrm{QoS}}, C^{\mathrm{BH}}) = (0.25, \infty)$ Mbps

(d) $(R^{\mathrm{QoS}}, C^{\mathrm{BH}}) = (0.25, 100)$ Mbps

Figure 3.6: Changes in BS-UE associations by Algorithm 1 under various choices of UE QoS requirements and backhaul capacity.

choose a large value of the penalty factor λ in the exact penalty method. To improve the convergence speed of Algorithms 1 and 2, our implementation starts with $\lambda = 10^3$ and fine-tunes λ through a bisection search until the objective functions no longer change and binary values of $\mathbf{x}$ are found. For brevity, only the case of $C^{\mathrm{BH}} = 100$Mbps is presented for illustration. Fig. 3.9(a) plots the convergence of the objective function (3.19) by Algorithm 1 for $R^{\mathrm{QoS}} = 0.1$Mbps. Fig. 3.9(b) plots the convergence of the objective function (3.25) by Algorithm 2. In these plots, the system bandwidth is normalized to unit to ensure the compatibility of the utility function and the penalty

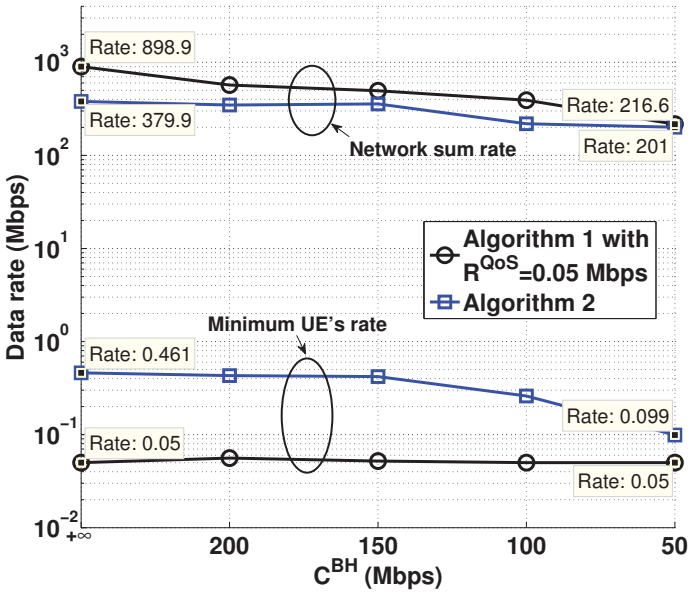

Figure 3.7: Fairness by Algorithm 2 and effects of limited backhaul capacity on the minimum UE rate.

term in (3.19) and (3.25). The number of iterations in each plot corresponds to the presented values of λ. As can be seen from Fig. 3.9, the proposed algorithms only require at most ten iterations to converge. It is worth noting that each iteration of our algorithms involves solving only two easy convex problems, each with polynomial complexity.

3.6 Conclusions

In this chapter, we have proposed new joint BS-UE association and power control schemes for HetNets. Specifically, we have addressed two difficult mixed-integer optimization problems: (i) sum-throughput maximization under QoS constraints and (ii) maximization of minimum UE throughput. Our problem formulations also include the practical constraint of limited backhaul capacity. Our developed alternative descent algorithms are based on an exact penalty method combined with successive convex

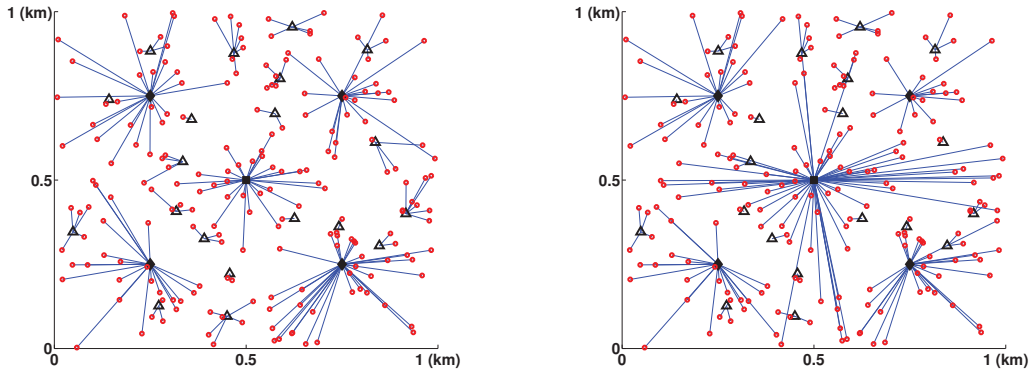

(a) $C^{\mathrm{BH}} = \infty$ (b) $C^{\mathrm{BH}} = 50$ Mbps

Figure 3.8: More UEs switch to MBS when backhaul capacity is limited in Algorithm 2.

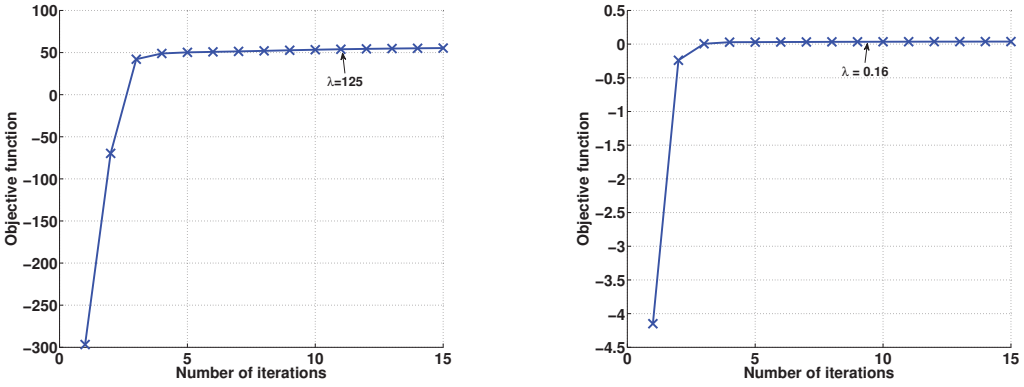

(a) Algorithm 1 (b) Algorithm 2

Figure 3.9: Convergence of Algorithms 1 and 2 for $\epsilon = 10^{-4}$.

programming, where we address the binary BS-UE association problem and the non-convex power allocation problem separately. At each iteration, only two simple convex problems are solved in the same time scale. Our algorithms improve the objective functions in each iteration and converge eventually. Simulation results have demonstrated the usefulness of our devised algorithms in both traffic offloading and interference management. The simulated data rate indeed does not meet the expectation of 5G. However, the main purpose of this Section is to proposed a method to optimize the power

allocation and BS-UE association in HetNet. Future researches will investigate the implement of MIMO transmission and OFMD system which can much further enhance the performance of the network.

Chapter 4

Successive Convex Quadratic Programming for Interference Management in MU-MIMO Multicell Networks

In this chapter, the main focus is on developing path-following algorithms based on successive convex quadratic programming for QoS management in the FD MU-MIMO multicell networks. Then the proposed algorithms are extended to address the optimal precoding matrices design in the half-duplex MU-MIMO multicell networks with H-K transmission strategy [Han and Kobayashi, 1981]. Though H-K strategy is not a part of 5G technologies, the significant enhancement in the capacity region that this strategy provides is the driving force of this investigation.

4.1 Precoding Design for QoS Management in Full-Duplex MU-MIMO Multicell Networks

4.1.1 Introduction

Full-duplexing is recently proposed as one of the key transceiving techniques for the 5G networks with the potential of doubling the capacity of wireless links [Choi and Shirani-Mehr, 2013; Sabharwal et al, 2014; Heino et al, 2015]. Different from the conventional

time-division and frequency-division duplexing, FD allows simultaneous transmissions to multiple DLUs and multiple reception from multiple ULUs in the same time slot and on the same frequency. Such bidirectional communication on the same radio resources is traditionally assumed impractical, due to the huge SI between transmit and receive antennas on the same device. Only recently, advances in hardware design have allowed the SI to be suppressed to a level potentially suitable for FD communications [Everett et al., 2014; Duarte et al., 2014; Anttila et al, 2014; Heino et al, 2015].

Under FD, the interference situation in a multicell network is further complicated not only by the residual SI but also the cross interference between the uplink and the downlink transmissions. In the uplink, the additional interference includes the SI from the same BS and the downlink interference from other BSs, which further degrades the QoS of the ULUs. In the downlink, the QoS of the DLUs is adversely affected by the additional interference from the ULUs. Note that one of the most common figure-of-merit for network QoS is the achievable data throughput. With these new forms of interference, it is not straightforward to extend the available signal precoding designs that manage interference in the traditional half-duplexing (HD) networks [Ng and Huang, 2010; Shi et al., 2011; Wang et al., 2012; Song et al., 2007; Cai et al., 2012; Huang et al., 2013] to the new FD settings. In the FD cases, both uplink and downlink throughput functions jointly depend on the uplink and the downlink precoders. Most importantly, FD destroys the computationally tractable structure of the throughput functions. For instance, while the uplink throughput function can be made concave with respect to the signal covariances of the ULUs in a single-cell network (e.g., by implementing the successive interference cancellation receiver at the BS), it is not concave in the signal covariances of the DLUs.

While guaranteeing a minimum QoS for all users is essential, it should be emphasized that existing works for HD and FD MU-MIMO networks [Ng and Huang, 2010; Shi et al., 2011; Wang et al., 2012; Song et al., 2007; Cai et al., 2012; Huang et al., 2013; Huberman and Le-Ngoc, 2015; Nguyen et al., 2014; Xu and Wang, 2012] at best can

only apply to the problem of total throughput maximization without rate constraints. Such problem formulations generally result in an unfair allocation of the available radio resources. Users with favorable link conditions get most of the throughput, whereas the remaining users achieve low (or even zero) throughput. Unfortunately, any throughput guarantee leads to the inherently difficult nonconvex throughput constraints. In this case, even finding a feasible point is already a challenging task because the feasible set is nonconvex and disconnected.

In this section, we consider a general MU-MIMO multicell network. The BSs are equipped with multiple antennas and operate in the FD mode. There are two separate groups of multi-antenna UEs in each cell—the ULUs and the DLUs—both operate in the HD mode. In the uplink, the receiver of a BS suffers from (i) the uplink interference from all ULUs in other cells, (ii) the downlink interference from other BSs, and (iii) the SI from its own downlink transmission. In the downlink, the receiver of a DLU is subject to (i) the downlink interference from all BSs including its serving BS and (ii) the uplink interference from all ULUs in the same cell. Note that while we restrict to the above cases for the clarity of analysis and presentation, our proposed approach in this section can be straightforwardly extended to the case that the uplink interference is generated by all ULUs in all cells.

Our objective is to develop jointly optimal linear precoders for both BSs and ULUs in order to manage all the aforementioned types of interference. Specifically, we consider the following two problems which aim to optimally and fairly share the radio resources among the cells.

- Problem (P1): Maximizing the total network throughput subject to data rate constraints at each cell. This problem involves a nonconvex objective function and nonconvex constraints.
- Problem (P2): Maximizing the minimum throughput among all cells. The objective function of this problem is not only nonconvex but also nonsmooth.

In (P1), it is difficult to even find a feasible point from the nonconvex feasible set. In (P2), the nonsmoothness of the objective function presents an extra dimension of technical difficulty.

To the authors' best knowledge, existing works can only address some specific single-cell cases of Problem (P1) without the nonconvex throughput constraints. Indeed, the nonconvex constraints have never been effectively dealt with. Since the publication of [Kha et al., 2012], it has been known that the uplink and downlink throughput functions are d.c. (difference of two convex functions) [Tuy, 1998] in the signal covariance variables. Their maximization over (convex) power constraints can thus be computationally solved by the so-called d.c. iteration (DCI) algorithm of [Kha et al., 2012]. Reference [Huberman and Le-Ngoc, 2015] follows the approach in [Kha et al., 2012] to address the problem of power-constrained single-cell throughput maximization via the signal covariance design. Reference [Nguyen et al., 2014] also considers the problem of single-cell throughput maximization where downlink beamformers and uplink transmit powers are jointly optimized. Here, the BS is equipped with multiple antennas whereas each DLU/ULU only has a single antenna. The difficult nonconvex rank-one matrix constraints on the outer products of the beamforming vectors are dropped to arrive at a d.c. optimization formulation, for which DCI [Kha et al., 2012] can be applied. To find a feasible rank-one matrix point from which the beamforming vector can be recovered, [Nguyen et al., 2014] resorts to the randomization techniques which are shown inefficient by [Phan et al., 2012].

For the problems that we presently consider, the throughput functions are very complicated in the precoding matrix variables, resulting in complex d.c. optimizations (see [Kha et al., 2012; Che and Tuan, 2013*b*; Tam et al., 2013; Che and Tuan, 2014]). The DCI algorithm of [Kha et al., 2012] may not be efficiently applied to Problem (P1) even when there is no data rate constraint. Each iteration of the DCI algorithm involves a difficult convex program—a challenge for existing convex solvers to efficiently compute for optimal solutions. Optimizing the QoS via minimal cell throughput maximization

in Problem (P2) is similarly difficult. We also note that the optimization of nonsmooth and nonconvex objective functions such as that in Problem (P2) has never been appropriately addressed in any previous works.

The aim of this chpater is to develop novel solutions that directly tackle the nonconvexity of the formulated problems. Specifically, we solve both problems (P1) and (P2) by successive convex quadratic programming (SCQP), where each iteration (referred to as QPI) involves a simple convex quadratic program. Once initialized from a feasible point, the proposed SCQP algorithms generate a sequence of feasible and improved points, which monotonically converges to an optimum of (P1) or (P2). Moreover, the QPI admits a closed-form optimal solution when the rate constraints in (P1) are not required.

While successive convex programming is a natural approach to solving nonconvex optimization problems (see, e.g., [Marks and Wright, 1978]), it does not quite instruct how to develop the specific algorithms to resolve the problems at hand. In this section, we specifically construct the SCQP algorithms to serve as a new computationally tractable framework for many difficult nonconvex interference management problems in both HD and FD network settings. Therefore, our SCQP approach is novel even from the optimization-theoretical perspective. The proposed algorithms lend themselves to practical solutions for large-scale MU-MIMO networks. The complexity per iteration is low since only one simple quadratic program needs to be solved. Here we completely avoid the log det operation, a major bottleneck for fast computation in the available commercial convex solvers. Furthermore, the devised algorithms do not face any convergence issue at all. Given any initial feasible point, our path-following algorithms are guaranteed to always converge to an optimal solution.

The rest of this section is organized as follows: Section 4.1.2 presents the system model and formulates the QoS management problems. Section 4.1.3 proposes the SCQP approach to solve problem (P1). Section 4.1.4 extends the proposed SCQP framework to

solve problem (P2). Section 4.1.5 evaluates the performance of our devised solutions by numerical examples. Finally, Section 4.1.6 concludes the section.

4.1.2 System Model and Optimization Problem Formulations

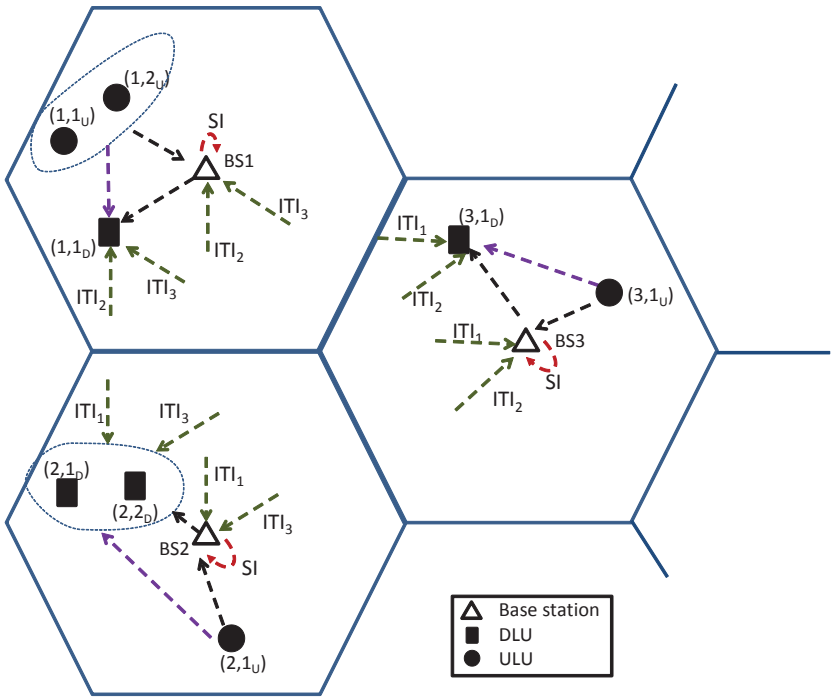

Figure 4.1: Interference scenario in an FD multicell network, where SI denotes the self-interference and ITI_i denotes the interference from the BS and ULUs of cell i.

We consider an MU-MIMO network consisting of I cells. As illustrated in Fig. 4.1, the BS of cell $i \in \{1, \ldots, I\}$ serves a group of D DLUs in the downlink (DL) channel and a group of U ULUs in uplink (UL) channel. Each BS operates in the FD mode and is equipped with $N \triangleq N_1 + N_2$ antennas, where N_1 antennas are used to transmit and the remaining N_2 antennas to receive signals. In cell i, DLU (i, j_{D}) and ULU (i, j_{U}) operate in the HD mode and each is equipped with N_r antennas. In the DL, let a complex-valued vector $s_{i,j_{\mathsf{D}}} \in \mathbb{C}^{d_1}$ denote the symbols intended for DLU (i, j_{D}), where $\mathbb{E}\left[s_{i,j_{\mathsf{D}}}(s_{i,j_{\mathsf{D}}})^H\right] = I_{d_1}$, d_1 is the number of concurrent data streams and $d_1 \leq \min\{N_1, N_r\}$. We also denote the complex-valued precoding matrix for DLU (i, j_{D}) as

$\mathbf{V}_{i,j_\mathsf{D}} \in \mathbb{C}^{N_1 \times d_1}$. Similarly, in the UL, let $s_{i,j_\mathsf{U}} \in \mathbb{C}^{d_2}$ denote the symbols sent by ULU (i, j_U), where $\mathbb{E}\left[s_{i,j_\mathsf{U}}(s_{i,j_\mathsf{U}})^H\right] = I_{d_2}$, d_2 is the number of concurrent data streams and $d_2 \leq \min\{N_2, N_r\}$. The precoding matrix of ULU (i, j_U) is denoted as $\mathbf{V}_{i,j_\mathsf{U}} \in \mathbb{C}^{N_r \times d_2}$. For notational convenience, let us define

$$\mathcal{I} \triangleq \{1, 2, \ldots, I\}; \quad \mathcal{D} \triangleq \{1_\mathsf{D}, 2_\mathsf{D}, \ldots, D_\mathsf{D}\}; \quad \mathcal{U} \triangleq \{1_\mathsf{U}, 2_\mathsf{U}, \ldots, U_\mathsf{U}\};$$
$$\mathcal{S}_1 \triangleq \mathcal{I} \times \mathcal{D}; \quad \mathcal{S}_2 \triangleq \mathcal{I} \times \mathcal{U}; \quad \mathbf{V} \triangleq [\mathbf{V}_{i,j}]_{(i,j)\in\mathcal{S}_1 \cup \mathcal{S}_2}.$$

In the DL channel, the received signal at DLU (i, j_D) is expressed as:

$$y_{i,j_\mathsf{D}} \triangleq \underbrace{H_{i,i,j_\mathsf{D}}\mathbf{V}_{i,j_\mathsf{D}}s_{i,j_\mathsf{D}}}_{\text{desired signal}} + \underbrace{\sum_{(m,\ell_\mathsf{D})\in\mathcal{S}_1\setminus(i,j_\mathsf{D})} H_{m,i,j_\mathsf{D}}\mathbf{V}_{m,\ell_\mathsf{D}}s_{m,\ell_\mathsf{D}}}_{\text{DL interference}} + \underbrace{\sum_{\ell_\mathsf{U}\in\mathcal{U}} H_{i,i_\mathsf{D},\ell_\mathsf{U}}\mathbf{V}_{i,\ell_\mathsf{U}}s_{i,\ell_\mathsf{U}}}_{\text{UL intracell interference}} + n_{i,j_\mathsf{D}}, \tag{4.1}$$

where $H_{m,i,j_\mathsf{D}} \in \mathbb{C}^{N_r \times N_1}$ and $H_{i,i_\mathsf{D},\ell_\mathsf{U}} \in \mathbb{C}^{N_r \times N_r}$ are the channel matrices from BS m to DLU (i, j_D) and from ULU (i, ℓ_U) to DLU (i, j_D), respectively. Also, n_{i,j_D} is the additive white circularly symmetric complex Gaussian noise with variance σ^2_D. The DLU decodes its own message while treating all other messages as noise. The downlink throughput at DLU (i, j_D) is then given as:

$$f_{i,j_\mathsf{D}}(\mathbf{V}) \triangleq \ln\left|I_{N_r} + \mathcal{L}_{i,j_\mathsf{D}}(\mathbf{V}_{i,j_\mathsf{D}})\mathcal{L}^H_{i,j_\mathsf{D}}(\mathbf{V}_{i,j_\mathsf{D}})\Psi^{-1}_{i,j_\mathsf{D}}(\mathbf{V})\right|, \tag{4.2}$$

where

$$\mathcal{L}_{i,j_\mathsf{D}}(\mathbf{V}_{i,j_\mathsf{D}}) \triangleq H_{i,i,j_\mathsf{D}}\mathbf{V}_{i,j_\mathsf{D}}, \tag{4.3}$$

which means that

$$\mathcal{L}_{i,j_\mathsf{D}}(\mathbf{V}_{i,j_\mathsf{D}})\mathcal{L}^H_{i,j_\mathsf{D}}(\mathbf{V}_{i,j_\mathsf{D}}) = H_{i,i,j_\mathsf{D}}\mathbf{V}_{i,j_\mathsf{D}}\mathbf{V}^H_{i,j_\mathsf{D}}H^H_{i,i,j_\mathsf{D}}, \tag{4.4}$$

and

$$\Psi_{i,j_\mathsf{D}}(\mathbf{V}) \triangleq \sum_{(m,\ell_\mathsf{D})\in\mathcal{S}_1\setminus(i,j_\mathsf{D})} H_{m,i,j_\mathsf{D}}\mathbf{V}_{m,\ell_\mathsf{D}}\mathbf{V}^H_{m,\ell_\mathsf{D}}H^H_{m,i,j_\mathsf{D}} + \sum_{\ell_\mathsf{U}\in\mathcal{U}} H_{i,i_\mathsf{D},\ell_\mathsf{U}}\mathbf{V}_{i,\ell_\mathsf{U}}\mathbf{V}^H_{i,\ell_\mathsf{U}}H^H_{i,i_\mathsf{D},\ell_\mathsf{U}} + \sigma^2_\mathsf{D}I_{N_r}. \tag{4.5}$$

In the UL channel, the received signal at BS i is expressed as

$$y_i \triangleq \underbrace{\sum_{\ell_{\mathsf{U}}\in\mathcal{U}} H_{i,\ell_{\mathsf{U}},i}\mathbf{V}_{i,\ell_{\mathsf{U}}}s_{i,\ell_{\mathsf{U}}}}_{\text{desired signal}} + \underbrace{\sum_{m\in\mathcal{I}\setminus\{i\}}\sum_{\ell_{\mathsf{U}}\in\mathcal{U}} H_{m,\ell_{\mathsf{U}},i}\mathbf{V}_{m,\ell_{\mathsf{U}}}s_{m,\ell_{\mathsf{U}}}}_{\text{UL interference}} + \underbrace{H_i^{\mathcal{SI}}\sum_{\ell_{\mathsf{D}}\in\mathcal{D}}\mathbf{V}_{i,\ell_{\mathsf{D}}}\tilde{s}_{i,\ell_{\mathsf{D}}}}_{\text{residual SI}}$$
$$+ \underbrace{\sum_{m\in\mathcal{I}\setminus\{i\}} H_{m,i}^{\mathcal{B}}\sum_{j_{\mathsf{D}}\in\mathcal{D}}\mathbf{V}_{m,j_{\mathsf{D}}}s_{m,s_{\mathsf{D}}}}_{\text{DL intercell interference}} + n_i, \tag{4.6}$$

where $H_{m,\ell_{\mathsf{U}},i}\in\mathbb{C}^{N_2\times N_r}$ and $H_{m,i}^{\mathcal{B}}\in\mathbb{C}^{N_2\times N_1}$ are the channel matrices from ULU (m,ℓ_{U}) to BS i and from BS m to BS i, respectively; n_i is the additive white circularly symmetric complex Gaussian noise with variance σ_{U}^2; $H_i^{\mathcal{SI}}\in\mathbb{C}^{N_2\times N_1}$ is the residual self-loop channel from the transmit antennas to the receive antennas at BS i after all real-time cancelation in both analog and digital domains [Duarte et al., 2012, 2014]; $\tilde{s}_{i,\ell_{\mathsf{D}}}$ is the additive Gaussian noise with $\mathbb{E}\left[\tilde{s}_{i,j_{\mathsf{D}}}(\tilde{s}_{i,j_{\mathsf{D}}})^H\right]=\sigma_{SI}^2 I_{d_1}$ that models the effect of analog circuit non-ideality and the limited dynamic range of the analog-to-digital converter (ADC) [Korpi et al, 2014; Sabharwal et al, 2014; Duarte et al., 2012; Anttila et al, 2014]; and the SI level σ_{SI}^2 is the ratio of the average SI powers before and after the SI cancelation process. Upon applying the Minimum mean square error - Successive interference cancellation (MMSE-SIC) decoder, the achievable uplink throughput at BS i is given as [Tse and Viswanath, 2005]

$$f_i(\mathbf{V}) \triangleq \ln\left|I_{N_2}+\mathcal{L}_i(\mathbf{V}_{\mathsf{U}i})\mathcal{L}_i^H(\mathbf{V}_{\mathsf{U}i})\Psi_i^{-1}(\mathbf{V})\right|, \tag{4.7}$$

where $\mathbf{V}_{\mathsf{U}i}\triangleq(\mathbf{V}_{i,\ell_{\mathsf{U}}})_{\ell_{\mathsf{U}}\in\mathcal{U}}$ and

$$\mathcal{L}_i(\mathbf{V}_{\mathsf{U}i}) \triangleq \left[H_{i,1_{\mathsf{U}},i}\mathbf{V}_{i,1_{\mathsf{U}}}, H_{i,2_{\mathsf{U}},i}\mathbf{V}_{i,2_{\mathsf{U}}},\ldots,H_{i,U_{\mathsf{U}},i}\mathbf{V}_{i,U_{\mathsf{U}}}\right], \tag{4.8}$$

which means that

$$\mathcal{L}_i(\mathbf{V}_{\mathsf{U}i})\mathcal{L}_i^H(\mathbf{V}_{\mathsf{U}i}) = \sum_{\ell=1}^{U} H_{i,\ell_{\mathsf{U}},i}\mathbf{V}_{i,\ell_{\mathsf{U}}}\mathbf{V}_{i,\ell_{\mathsf{U}}}^H H_{i,\ell_{\mathsf{U}},i}^H, \tag{4.9}$$

and

$$\Psi_i(\mathbf{V}) \triangleq \sum_{m\in\mathcal{I}\setminus\{i\}}\sum_{\ell_{\mathsf{U}}\in\mathcal{U}} H_{m,\ell_{\mathsf{U}},i}\mathbf{V}_{m,\ell_{\mathsf{U}}}\mathbf{V}_{m,\ell_{\mathsf{U}}}^H H_{m,\ell_{\mathsf{U}},i}^H + \sigma_{SI}^2 H_i^{\mathcal{SI}}\left(\sum_{\ell_{\mathsf{D}}\in\mathcal{D}}\mathbf{V}_{i,\ell_{\mathsf{D}}}\mathbf{V}_{i,\ell_{\mathsf{D}}}^H\right)(H_i^{\mathcal{SI}})^H + \sum_{m\in\mathcal{I}\setminus\{i\}} H_{m,i}^{\mathcal{B}}\left(\sum_{j_{\mathsf{D}}\in\mathcal{D}}\mathbf{V}_{m,j_{\mathsf{D}}}\mathbf{V}_{m,j_{\mathsf{D}}}^H\right)(H_{m,i}^{\mathcal{B}})^H + \sigma_{\mathsf{U}}^2 I_{N_2}. \tag{4.10}$$

In this section, we consider two precoding design problems for QoS management in the MU-MIMO FD multicell network. The first problem is the following QoS-constrained sum throughput maximization:

$$\max_{\mathbf{V}}\ \mathcal{P}_1(\mathbf{V}) \triangleq \left[\sum_{(i,j_{\mathsf{D}})\in\mathcal{S}_1} f_{i,j_{\mathsf{D}}}(\mathbf{V}) + \sum_{i\in\mathcal{I}} f_i(\mathbf{V})\right] \quad \text{s.t.} \tag{4.11a}$$

$$\sum_{j_{\mathsf{D}}\in\mathcal{D}}\langle\mathbf{V}_{i,j_{\mathsf{D}}}\mathbf{V}_{i,j_{\mathsf{D}}}^H\rangle \le P_{\mathrm{BS}}^{\max},\ i\in\mathcal{I};\quad \langle\mathbf{V}_{i,j_{\mathsf{U}}}\mathbf{V}_{i,j_{\mathsf{U}})}^H\rangle \le P_{\mathrm{UE}}^{\max},\ (i,j_{\mathsf{U}})\in\mathcal{S}_2, \tag{4.11b}$$

$$f_{i,j_{\mathsf{D}}}(\mathbf{V}) \ge r_{i,j_{\mathsf{D}}}^{\min},\ (i,j_{\mathsf{D}})\in\mathcal{S}_1;\quad f_i(\mathbf{V}) \ge r_i^{\mathsf{U},\min},\ i\in\mathcal{I}. \tag{4.11c}$$

The objective function in (4.11a) is nonconcave. The convex constraints (4.11b) specify the maximum transmit power available at the BSs and the ULUs. The highly nonconvex constraints (4.11c) represent the QoS guarantee, where $r_{i,j_{\mathsf{D}}}^{\min}$ and $r_i^{\mathsf{U},\min}$ are the minimum data rates required by DLU (i,j_{D}) and BS i, respectively. It should be emphasized that the approach in this section also works for the sum downlink throughput constraints of all DLUs in a cell and the uplink throughput constraints of individual ULUs. For clarity of presentation, we do not include those constraints here.

The second problem of interest is the following QoS maximin problem:

$$\max_{\mathbf{V}}\ \mathcal{P}_2(\mathbf{V}) \triangleq \min_{i\in\mathcal{I}}\left[\sum_{j_{\mathsf{D}}\in\mathcal{D}} f_{i,j_{\mathsf{D}}}(\mathbf{V}) + f_i(\mathbf{V})\right] \quad \text{s.t.} \quad (4.11b), \tag{4.12}$$

where the minimal cell throughput is maximized. This problem has a nonconcave and nonsmooth objective function and is subject to convex power constraints.

As in all previous works on precoding and interference suppression in multi-cell MIMO cooperative networks (see, e.g., [Ng and Huang, 2010; Shi et al., 2011; Wang et al.,

2012; Song et al., 2007; Cai et al., 2012; Huang et al., 2013; Huberman and Le-Ngoc, 2015; Nguyen et al., 2014, 2013] and references therein), the conventional assumption here is that full channel state information (CSI) is available to a central processing site [Gesbert et al., 2010; Lee, Kim, Lee, Ng, Mazzarese, Liu, Xiao and Zhou, 2012], which solves the optimization of problems (4.11) and (4.12) in coordinating the network transmission. This assumption is practical if there are high-performing channel estimation mechanisms in place and a central processing unit available to collect and disseminate the relevant CSI. More importantly, the full CSI assumption together with our proposed optimal algorithms helps provide the best performance that can be achieved by FD MIMO precoding. Such benchmark performance is crucial in evaluating the potential of FD systems and future technical developments such as robust schemes against the imperfect channel estimation and distributed implementations.

Remark 4.1. Upon introducing the new variable

$$\mathbf{W}_{i,j} \triangleq \mathbf{V}_{i,j}\mathbf{V}_{i,j}^H \succeq 0, \tag{4.13}$$

which must satisfy the following rank constraints

$$\text{rank}(\mathbf{W}_{i,j_\text{D}}) \leq d_1;\ \text{rank}(\mathbf{W}_{i,j_\text{U}}) \leq d_2, \tag{4.14}$$

it is seen that (4.5) and (4.10) are linear in $\mathbf{W} \triangleq [\mathbf{W}_{i,j}]_{(i,j)\in\mathcal{S}_1\cup\mathcal{S}_2}$. Accordingly, the throughput expressions (4.2) and (4.7) are d.c. functions in $\mathbf{W}$.

If we further assume that $\mathbf{W}_{i,j}$ is the covariance of the signal $s_{i,j}$, the rank constraints (4.14) are dropped. In the new variable $\mathbf{W}$ and without (4.14), problems (4.11) and (4.12) are reduced to the special case of covariance design. Such simplified problems belong to the class of d.c. programming [Kha et al., 2012], and their solutions provide the upper bounds to the original problems (4.11) and (4.12). The works of [Huberman and Le-Ngoc, 2015] and [Nguyen et al., 2014] use the DCI technique in [Kha et al., 2012] to address the single-cell sum throughput maximization similar to (4.11), albeit by covariance design and without rate constraints. Even with these simplifications,

each iteration of DCI still involves a mixed semidefinite log det optimization problem, which is convex but cannot be efficiently solved by existing convex solvers. Reference [Nguyen et al., 2013] also employs DCI [Kha et al., 2012] to tackle a similar single-cell sum throughput maximization problem without rate constraints. Yet to facilitate their solution, [Nguyen et al., 2013] ignores the UL interference and requires other strict conditions of interference alignment for the DL interference cancelation.

In what follows, we will solve (4.11) and (4.12) via a sequence of convex quadratic programs in $\mathbf{V}$; hence, constraints (4.14) will be automatically satisfied. The approach developed here applies to a general multicell network setting with QoS constraints and it treats the covariance design as a special case, even bypassing the semidefinite constraint (4.13).

4.1.3 QoS-Constrained Sum Throughput Maximization

Considering the sum throughput maximization problem (4.11), the key difficulty is how to handle the highly nonconcave functions $f_{i,j_{\mathsf{D}}}(\mathbf{V})$ and $f_i(\mathbf{V})$ there. First, using the identity $\ln|I+AB^{-1}| = -\ln|I-A(A+B)^{-1}|,\ \forall\ A\succeq 0, B\succ 0$, we rewrite $f_{i,j_{\mathsf{D}}}(\mathbf{V})$ in (4.2) and $f_i(\mathbf{V})$ in (4.7) as:

$$f_{i,j_{\mathsf{D}}}(\mathbf{V}) = -\ln\left|I_{N_r} - \mathcal{L}_{i,j_{\mathsf{D}}}(\mathbf{V}_{i,j_{\mathsf{D}}})\mathcal{L}_{i,j_{\mathsf{D}}}^{H}(\mathbf{V}_{i,j_{\mathsf{D}}})\mathcal{M}_{i,j_{\mathsf{D}}}^{-1}(\mathbf{V})\right|, \tag{4.15}$$

$$f_i(\mathbf{V}) = -\ln\left|I_{N_2} - \mathcal{L}_i(\mathbf{V}_{\mathsf{U}i})\mathcal{L}_i^{H}(\mathbf{V}_{\mathsf{U}i})\mathcal{M}_i^{-1}(\mathbf{V})\right|, \tag{4.16}$$

where

$$\mathcal{M}_{i,j_{\mathsf{D}}}(\mathbf{V}) \triangleq \mathcal{L}_{i,j_{\mathsf{D}}}(\mathbf{V}_{i,j_{\mathsf{D}}})\mathcal{L}_{i,j_{\mathsf{D}}}^{H}(\mathbf{V}_{i,j_{\mathsf{D}}}) + \Psi_{i,j_{\mathsf{D}}}(\mathbf{V}) \tag{4.17}$$

$$\succeq \Psi_{i,j_{\mathsf{D}}}(\mathbf{V}), \tag{4.18}$$

$$\mathcal{M}_i(\mathbf{V}) \triangleq \mathcal{L}_i(\mathbf{V}_{\mathsf{U}i})\mathcal{L}_i^{H}(\mathbf{V}_{\mathsf{U}i}) + \Psi(\mathbf{V}_i) \tag{4.19}$$

$$\succeq \Psi(\mathbf{V}_i), \tag{4.20}$$

which are concretized by (3.1) and (3.2) in Appendix C.

At $V^{(\kappa)} \triangleq [V_{i,j}^{(\kappa)}]_{(i,j)\in\mathcal{S}_1\cup\mathcal{S}_2}$, we define the following quadratic functions in $\mathbf{V}$:

$$\Theta_{i,j_{\mathsf{D}}}^{(\kappa)}(\mathbf{V}) \triangleq f_{i,j_{\mathsf{D}}}(V^{(\kappa)}) + 2\,\mathrm{Re}\left\{\langle \Psi_{i,j_{\mathsf{D}}}^{-1}(V^{(\kappa)})\mathcal{L}_{i,j_{\mathsf{D}}}(V_{i,j_{\mathsf{D}}}^{(\kappa)}), \mathcal{L}_{i,j_{\mathsf{D}}}(\mathbf{V}_{i,j_{\mathsf{D}}}) - \mathcal{L}_{i,j_{\mathsf{D}}}(V_{i,j_{\mathsf{D}}}^{(\kappa)})\rangle\right\}$$
$$- \langle \Psi_{i,j_{\mathsf{D}}}^{-1}(V^{(\kappa)}) - \mathcal{M}_{i,j_{\mathsf{D}}}^{-1}(V^{(\kappa)}), \mathcal{M}_{i,j_{\mathsf{D}}}(\mathbf{V}) - \mathcal{M}_{i,j_{\mathsf{D}}}(V^{(\kappa)})\rangle, \tag{4.21}$$

$$\Theta_{i}^{(\kappa)}(\mathbf{V}) \triangleq f_{i}(V^{(\kappa)}) + 2\,\mathrm{Re}\left\{\langle \Psi_{i}^{-1}(V^{(\kappa)})\mathcal{L}_{i}(V_{\mathsf{U}i}^{(\kappa)}), \mathcal{L}_{i}(\mathbf{V}_{\mathsf{U}i}) - \mathcal{L}_{i}(V_{\mathsf{U}i}^{(\kappa)})\rangle\right\}$$
$$- \langle \Psi_{i}^{-1}(V^{(\kappa)}) - \mathcal{M}_{i}^{-1}(V^{(\kappa)}), \mathcal{M}_{i}(\mathbf{V}) - \mathcal{M}_{i}(V^{(\kappa)})\rangle, \tag{4.22}$$

which are also concretized by (3.3) and (3.6) in Appendix C. It follows from (4.18) and (4.20) that

$$\Psi_{i,j_{\mathsf{D}}}^{-1}(V^{(\kappa)}) - \mathcal{M}_{i,j_{\mathsf{D}}}^{-1}(V^{(\kappa)}) \succeq 0,$$
$$\Psi_{i}^{-1}(V^{(\kappa)}) - \mathcal{M}_{i}^{-1}(V^{(\kappa)}) \succeq 0$$

in (4.21) and (4.22). Therefore, the functions $\Theta_{i,j_{\mathsf{D}}}^{(\kappa)}(\mathbf{V})$ and $\Theta_{i}^{(\kappa)}(\mathbf{V})$ are concave.

The following result shows that the highly nonlinear and nonconcave functions $f_{i,j_{\mathsf{D}}}(\cdot)$ and $f_i(\cdot)$ in problem (4.11) can be globally and locally approximated by concave quadratic functions.

Theorem 4.1. *It is true that*

$$f_{i,j_{\mathsf{D}}}(V^{(\kappa)}) = \Theta_{i,j_{\mathsf{D}}}^{(\kappa)}(V^{(\kappa)}) \quad \textit{and} \quad f_{i,j_{\mathsf{D}}}(\mathbf{V}) \geq \Theta_{i,j_{\mathsf{D}}}^{(\kappa)}(\mathbf{V}) \quad \forall\ \mathbf{V}, \tag{4.23}$$

$$f_{i}(V^{(\kappa)}) = \Theta_{i}^{(\kappa)}(V^{(\kappa)}) \quad \textit{and} \quad f_{i}(\mathbf{V}) \geq \Theta_{i}^{(\kappa)}(\mathbf{V}) \quad \forall\ \mathbf{V}. \tag{4.24}$$

Proof. See Appendix D. ■

We now address the nonconvex problem (4.11) by successively solving the following convex quadratic program (QP):

$$\max_{\mathbf{V}}\ \mathcal{P}_1^{(\kappa)}(\mathbf{V}) \triangleq \left[\sum_{(i,j_{\mathsf{D}})\in\mathcal{S}_1} \Theta_{i,j_{\mathsf{D}}}^{(\kappa)}(\mathbf{V}) + \sum_{i\in\mathcal{I}} \Theta_{i}^{(\kappa)}(\mathbf{V})\right]\ :\ (4.11b), \tag{4.25a}$$

$$\Theta_{i,j_{\mathsf{D}}}^{(\kappa)}(\mathbf{V}) \geq r_{i,j_{\mathsf{D}}}^{\min},\ (i,j_{\mathsf{D}})\in\mathcal{S}_1; \quad \Theta_{i}^{(\kappa)}(\mathbf{V}) \geq r_{i}^{\mathsf{U},\min},\ i\in\mathcal{I}. \tag{4.25b}$$

Note that (4.25) involves $n = 2(N_1d_1ID + N_rd_2IU)$ scalar real decision variables and $m = ID + 2I + IU$ quadratic constraints so its computational complexity is $\mathcal{O}(n^2m^{2.5} + m^{3.5})$.

Proposition 4.1. *Let $V^{(\kappa)}$ be a feasible point to (4.11). The optimal solution $V^{(\kappa+1)}$ of convex program (4.25) is feasible to the nonconvex program (4.11) and it is better than $V^{(\kappa)}$, i.e.,*

$$\mathcal{P}_1(V^{(\kappa+1)}) \geq \mathcal{P}_1(V^{(\kappa)}). \tag{4.26}$$

Consequently, once initialized from a feasible point $V^{(0)}$ to (4.11), the κ-th QP iteration (4.25) generates a sequence $\{V^{(\kappa)}\}$ of feasible and improved points toward the nonconvex program (4.11), which converges to an optimal solution of (4.11). Under the stopping criterion

$$\left|\left(\mathcal{P}_1(V^{(\kappa+1)}) - \mathcal{P}_1(V^{(\kappa)})\right)/\mathcal{P}_1(V^{(\kappa)})\right| \leq \epsilon$$

for a given tolerance $\epsilon > 0$, the QP iterations will terminate after finitely many iterations.

Proof. See Appendix E. ■

Algorithm 3 Proposed SCQP for QoS-constrained sum throughput maximization

Initialization: Set $\kappa := 0$, and choose a feasible point $V^{(0)}$ that satisfies (4.11b)-(4.11c).
κ-th iteration: Solve (4.25) for an optimal solution V^* and set $\kappa := \kappa + 1$, $V^{(\kappa)} := V^*$ and calculate $\mathcal{P}_1(V^{(\kappa)})$. Stop if $\left|\left(\mathcal{P}_1(V^{(\kappa)}) - \mathcal{P}_1(V^{(\kappa-1)})\right)/\mathcal{P}_1(V^{(\kappa-1)})\right| \leq \epsilon$.

The proposed SCQP that solves problem (4.11) is summarized in Algorithm 3. It should be emphasized that finding a feasible initial point $V^{(0)}$ to meet nonconvex throughput constraint (4.11c) is difficult. To this end, let us consider the following problem:

$$\max_{\mathbf{V}} \mathcal{P}_3(\mathbf{V}) \triangleq \min_{(i,j_{\mathsf{D}})\in\mathcal{S}_1} \left\{ \frac{f_{i,j_{\mathsf{D}}}(\mathbf{V})}{r_{i,j_{\mathsf{D}}}^{\min}}, \frac{f_i(\mathbf{V})}{r_i^{\mathsf{U},\min}} \right\} \ : \ (4.11b). \tag{4.27}$$

It is observed that problems (4.27) and (4.12) have a similar form. Therefore, they can be solved by Algorithm 4 developed in the next section, which terminates as soon as

$$f_{i,j_{\mathsf{D}}}(V^{(\kappa)})/r_{i,j_{\mathsf{D}}}^{\min} \geq 1 \text{ and } f_i(V^{(\kappa)})/r_i^{\mathsf{U},\min} \geq 1, \ \forall (i,j_{\mathsf{D}}) \in \mathcal{S}_1. \tag{4.28}$$

The found solution $V^{(\kappa)}$ is feasible to (4.11c) and thus is used as the initial solution $V^{(0)}$ in Algorithm 3.

In the absence of QoS constraints (4.11c), QP (4.25) can be further decomposed into I convex quadratic subprograms in the DL precoders $\mathbf{V}_{\mathsf{D}i} \triangleq (\mathbf{V}_{i,1_\mathsf{D}}, \ldots, \mathbf{V}_{i,D_\mathsf{D}})$ as:

$$\max_{\mathbf{V}_{i,j_\mathsf{D}}, j_\mathsf{D}\in\mathcal{D}} \left[\sum_{j_\mathsf{D}\in\mathcal{D}} 2\,\mathrm{Re}\left\{ \langle \tilde{\mathcal{A}}_{i,j_\mathsf{D}}^{(\kappa)}, \mathbf{V}_{i,j_\mathsf{D}} \rangle \right\} - \sum_{j_\mathsf{D}\in\mathcal{D}} \sum_{(m,\ell_\mathsf{D})\in\mathcal{S}_1} \langle (\mathbf{V}_{i,j_\mathsf{D}})^H \tilde{\mathcal{B}}_{m,\ell_\mathsf{D}}^{(\kappa)}(i) \mathbf{V}_{i,j_\mathsf{D}} \rangle \right.$$
$$\left. -\sigma_{SI}^2 \sum_{j_\mathsf{D}\in\mathcal{D}} \langle (\mathbf{V}_{i,j_\mathsf{D}})^H \tilde{\mathcal{F}}_i^{(\kappa)} \mathbf{V}_{i,j_\mathsf{D}} \rangle - \sum_{m\in\mathcal{I}\setminus\{i\}} \sum_{j_\mathsf{D}\in\mathcal{D}} \langle (\mathbf{V}_{i,j_\mathsf{D}})^H \tilde{\mathcal{G}}_m^{(\kappa)}(i) \mathbf{V}_{m,j_\mathsf{D}} \rangle \right] :$$
$$\sum_{j_\mathsf{D}\in\mathcal{D}} ||\mathbf{V}_{i,j_\mathsf{D}}||^2 \leq P_{\mathrm{BS}}^{\max}, \quad (4.29)$$

and I convex quadratic subprograms in the UL precoders $\mathbf{V}_{\mathsf{U}i} = (\mathbf{V}_{i,1_\mathsf{U}}, \ldots, \mathbf{V}_{i,U_\mathsf{U}})$ as:

$$\max_{\mathbf{V}_{i,\ell_\mathsf{U}}, \ell_\mathsf{U}\in\mathcal{U}} \left[2 \sum_{\ell_\mathsf{U}\in\mathcal{U}} \mathrm{Re}\left\{ \langle \tilde{\mathcal{D}}_i^{(\kappa)}(\ell_\mathsf{U}), \mathbf{V}_{i,\ell_\mathsf{U}} \rangle \right\} - \sum_{j_\mathsf{D}\in\mathcal{D}} \sum_{\ell_\mathsf{U}\in\mathcal{U}} \langle (\mathbf{V}_{i,\ell_\mathsf{U}})^H \tilde{\mathcal{C}}_{i,j_\mathsf{D}}^{(\kappa)}(\ell_\mathsf{U}) \mathbf{V}_{i,\ell_\mathsf{U}} \rangle \right.$$
$$\left. - \sum_{(m,\ell_\mathsf{U})\in\mathcal{S}_2} \langle (\mathbf{V}_{i,\ell_\mathsf{U}})^H \tilde{\mathcal{E}}_m^{(\kappa)}(i,\ell_\mathsf{U}) \mathbf{V}_{i,\ell_\mathsf{U}} \rangle \right] : \sum_{j_\mathsf{U}\in\mathcal{U}} ||\mathbf{V}_{i,j_\mathsf{U}}||^2 \leq P_{\mathrm{UE}}^{\max}. \quad (4.30)$$

Here, all matrices in (4.29) and (4.30) are defined by (3.4), (3.5) and (3.7) in Appendix C.

If we define

$$\mathcal{R}_{i,j_\mathsf{D}}^{(\kappa)} \triangleq \sum_{(i,j_\mathsf{D})\in\mathcal{S}_1} \tilde{\mathcal{B}}_{i,j_\mathsf{D}}^{(\kappa)}(i) + \tilde{\mathcal{F}}_i^{(\kappa)} + \sum_{m\in\mathcal{I}\setminus\{i\}} \tilde{\mathcal{G}}_m^{(\kappa)}(i), \quad (4.31)$$

the closed-form optimal solution of (4.29) is derived from the Karush-Kuhn-Tucker (KKT) conditions as:

$$V_{i,j_\mathsf{D}}^{(\kappa+1)} = \begin{cases} \left(\mathcal{R}_{i,j_\mathsf{D}}^{(\kappa)}\right)^{-1} \tilde{\mathcal{A}}_{i,j_\mathsf{D}}^{(\kappa)}, & \text{if } \sum_{j_\mathsf{D}\in\mathcal{D}} \left\| (\mathcal{R}_{i,j_\mathsf{D}}^{(\kappa)})^{-1} \tilde{\mathcal{A}}_{i,j_\mathsf{D}}^{(\kappa)} \right\|^2 \leq P_{\mathrm{BS}}^{\max} \\ \left(\mathcal{R}_{i,j_\mathsf{D}}^{(\kappa)} + \mu_{i,j_\mathsf{D}} I_{N_r}\right)^{-1} \tilde{\mathcal{A}}_{i,j_\mathsf{D}}^{(\kappa)}, & \text{otherwise} \end{cases} \quad (4.32)$$

where $\mu_{i,j_\mathsf{D}} > 0$ is chosen such that $\sum_{j_\mathsf{D}\in\mathcal{D}} \left\| \left(\mathcal{R}_{i,j_\mathsf{D}}^{(\kappa)} + \mu_{i,j_\mathsf{D}} I_{N_r}\right)^{-1} \tilde{\mathcal{A}}_{i,j_\mathsf{D}}^{(\kappa)} \right\|^2 = P_{\mathrm{BS}}^{\max}$.

Similarly, if we define

$$\mathcal{Q}_{i,\ell_\mathsf{U}}^{(\kappa)} \triangleq \sum_{j_\mathsf{D}\in\mathcal{D}} \tilde{\mathcal{C}}_{i,j_\mathsf{D}}^{(\kappa)}(\ell_\mathsf{U}) + \sum_{m\in\mathcal{I}} \tilde{\mathcal{E}}_m^{(\kappa)}(i,\ell_\mathsf{U}), \quad (4.33)$$

the closed-form optimal solution of (4.30) is derived from the KKT conditions as:

$$V_{i,\ell_{\mathsf{U}}}^{(\kappa+1)} = \begin{cases} \left(\mathcal{Q}_{i,\ell_{\mathsf{U}}}^{(\kappa)}\right)^{-1} \tilde{\mathcal{D}}_i^{(\kappa)}(\ell_u), & \text{if } \sum\limits_{\ell_{\mathsf{U}}\in\mathcal{U}} \left\| (\mathcal{Q}_{i,\ell_{\mathsf{U}}}^{(\kappa)})^{-1} \tilde{\mathcal{D}}_i^{(\kappa)}(\ell_u) \right\|^2 \le P_{\mathrm{UE}}^{\max} \\ \left(\mathcal{Q}_{i,\ell_{\mathsf{U}}}^{(\kappa)} + \mu_{i,\ell_{\mathsf{U}}} I_{N_2}\right)^{-1} \tilde{\mathcal{D}}_i^{(\kappa)}(\ell_u), & \text{otherwise} \end{cases} \tag{4.34}$$

where $\mu_{i,\ell_{\mathsf{U}}} > 0$ is chosen such that $\sum\limits_{\ell_{\mathsf{U}}\in\mathcal{U}} \left\| (\mathcal{Q}_{i,\ell_{\mathsf{U}}}^{(\kappa)} + \mu_{i,\ell_{\mathsf{U}}} I_{N_r})^{-1} \tilde{\mathcal{D}}_i^{(\kappa)}(\ell_u) \right\|^2 = P_{\mathrm{UE}}^{\max}$.

4.1.4 Maximization of Minimum Cell Throughput

Initialized by a feasible point $V^{(0)}$ to (4.12), an iterative point $V^{(\kappa+1)}$ for $\kappa = 0, 1, \ldots$ is generated as the optimal solution of the following convex quadratic maximin problem:

$$\max_{\mathbf{V}} \ \mathcal{P}_2^{(\kappa)}(\mathbf{V}) \triangleq \min_{i\in\mathcal{I}} \left[\sum_{j_{\mathsf{D}}\in\mathcal{D}} \Theta_{i,j_{\mathsf{D}}}^{(\kappa)}(\mathbf{V}) + \Theta_i^{(\kappa)}(\mathbf{V}) \right] \ : \ (4.11b), \tag{4.35}$$

under the definitions (4.21)/(3.3) and (4.22)/(3.6) of $\Theta_{i,j_{\mathsf{D}}}^{(\kappa)}(\mathbf{V})$ and $\Theta_i^{(\kappa)}(\mathbf{V})$. Problem (4.35) involves $n = 2(N_1 d_1 ID + N_r d_2 IU) + 1$ scalar real decision variables and $m = ID + 3I + IU$ quadratic constraints, so its computational complexity is $\mathcal{O}(n^2 m^{2.5} + m^{3.5})$.

By Theorem 4.1, program (4.35) is a minorant maximization of the maximin problem (4.12). Each incumbent $V^{(\kappa)}$ of (4.35) is feasible to (4.12). Therefore, analogously to Proposition 4.1 the following result holds.

Proposition 4.2. *Let $V^{(\kappa)}$ be a feasible point to (4.12). The optimal solution $V^{(\kappa+1)}$ of convex quadratic maximin problem (4.35) is feasible to the nonconvex program (4.12) and is better than $V^{(\kappa)}$, i.e.,*

$$\mathcal{P}_2(V^{(\kappa+1)}) \ge \mathcal{P}_2(V^{(\kappa)}). \tag{4.36}$$

Consequently, initialized from a feasible point $(V^{(0)})$ of (4.12), the κ-th QP iteration (4.35) generates a sequence $\{V^{(\kappa)}\}$ of feasible and improved points toward the nonconvex program (4.12), which converges to an optimal solution of (4.12). Under the stopping criterion

$$\left| \left(\mathcal{P}_2(V^{(\kappa+1)}) - \mathcal{P}_2(V^{(\kappa)}) \right) / \mathcal{P}_2(V^{(\kappa)}) \right| \le \epsilon$$

for a given tolerance $\epsilon > 0$, the QP iterations will terminate after finitely many iterations.

Algorithm 4 Proposed SCQP for minimum cell throughput maximization

Initialization: Set $\kappa := 0$, and choose a feasible point $V^{(0)}$ that satisfies (4.11b).
κ-th iteration: Solve (4.35) for an optimal solution V^* and set $\kappa := \kappa + 1$, $V^{(\kappa)} := V^*$ and calculate $\mathcal{P}_2(V^{(\kappa)})$. Stop if $\left|\left(\mathcal{P}_2(V^{(\kappa)}) - \mathcal{P}_2(V^{(\kappa-1)})\right)/\mathcal{P}_2(V^{(\kappa-1)})\right| \leq \epsilon$.

The SCQP that solves problem (4.12) is summarized in Algorithm 4. Recall that because problem (4.11) has nonconvex constraints, finding an initial feasible point $V^{(0)}$ to (4.11) is not straightforward at all. In contrast, problem (4.12) has simple convex constraints and its feasible point can be easily determined for use in Algorithm 4. The initial equi-power points $V_{i,j_{\mathrm{D}}}^{(0)} = \sqrt{P_{\mathrm{BS}}^{\max}/N_1 d_1 ID}\mathbf{1}_{N_1\times d_1}$ and $V_{i,j_{\mathrm{U}}}^{(0)} = \sqrt{P_{\mathrm{UE}}^{\max}/N_r d_2}\mathbf{1}_{N_r\times d_2}$ are used in our numerical examples.

Remark 4.2. The DL throughput can be improved by dirty-paper coding (DPC) [Costa, 1983] in the DL channel. As such, the throughput $f_{i,j_{\mathrm{D}}}$ in (4.2) will be improved to

$$\hat{f}_{i,j_{\mathrm{D}}}(\mathbf{V}) \triangleq \ln\left|I_{N_r} + H_{i,i,j_{\mathrm{D}}}\mathbf{V}_{i,j_{\mathrm{D}}}\mathbf{V}_{i,j_{\mathrm{D}}}^H H_{i,i,j_{\mathrm{D}}}^H \hat{\Psi}_{i,j_{\mathrm{D}}}^{-1}(\mathbf{V})\right|, \tag{4.37}$$

where

$$\begin{aligned}\hat{\Psi}_{i,j_{\mathrm{D}}}(\mathbf{V}) &\triangleq \Psi_{i,j_{\mathrm{D}}}(\mathbf{V}) - \sum_{\ell=j+1}^{D} H_{i,i,j_{\mathrm{D}}}\mathbf{V}_{i,\ell_{\mathrm{D}}}\mathbf{V}_{i,\ell_{\mathrm{D}}}^H H_{i,i,j_{\mathrm{D}}}^H \\ &\preceq \Psi_{i,j_{\mathrm{D}}}(\mathbf{V}).\end{aligned} \tag{4.38}$$

In this case, it is straightforward to adjust Algorithms 3 and 4 to solve problems (4.11) and (4.12) with $f_{i,j_{\mathrm{D}}}$ replaced by $\hat{f}_{i,j_{\mathrm{D}}}$. Implementation of DPC requires significant complexity at both transmitter and receiver and there are no practical dirty paper codes close to the capacity limit [Erez and ten Brink, 2005]. Coordinated linear precoding as considered above is a low complexity, which is able to transmit the same number of data streams as a DPC-based system and thus achieves the same multiplexing gain as DPC.

Remark 4.3. The FD BSs can be reconfigured to operate in the HD mode. Here, all antennas $N = N_1 + N_2$ at each BS are used to serve all the DLUs in the downlink and all the ULUs in the uplink, albeit in two separate resource blocks (e.g., time or frequency). Suppose the achieved sum throughput for the downlink and the uplink are r_{D} and r_{U}, respectively. The effective HD throughput per resource block is calculated as $r_{\mathrm{HD}} = \frac{1}{2}(r_{\mathsf{D}} + r_{\mathsf{U}})$. In this case, the proposed Algorithm 3 also provides a new computational solution that achieves r_{D} and r_{U}. In the next section, we will compare the sum throughput performance under the FD mode with the optimized r_{HD}.

4.1.5 Numerical Results

Table 4.1: Simulation parameters used in all numerical examples

Parameter	**Value**
Carrier frequency	2GHz
System bandwidth	10MHz
Maximum BS transmit power, $P_{\mathrm{BS}}^{\max}$	26dBm
Maximum user transmit power, $P_{\mathrm{UE}}^{\max}$	23dBm
Noise power density	-174dBm/Hz
Noise figure at a DLU receiver	9dB
Noise figure at a BS receiver	5dB

We use numerical examples to evaluate the performance of our proposed SCQP algorithms. As will be described later, we consider several network scenarios to study different aspects of the proposed algorithms. In all the considered scenarios, we generate the channel matrix between a BS and a user at a distance d according to the path loss model for line-of-sight (LOS) communications as $10^{-PL_{LOS}/20}\tilde{H}$. Here, $PL_{LOS} = 103.8 + 20.9\log_{10} d$ and each entry of $\tilde{H}$ is an independent circularly-symmetric Gaussian random variable with zero mean and unit variance (denoted as $\mathcal{CN}(0,1)$) [3GPP TS 36.814 V9.0.0, 2010]. We assume that the channel matrix from a ULU to a DLU at a distance d follows the non-line-of-sight (NLOS) path loss model as $10^{-PL_{NLOS}/20}\tilde{H}$,

where $PL_{NLOS} = 145.4 + 37.5 \log_{10} d$ [3GPP TS 36.814 V9.0.0, 2010]. We also model the residual self-loop channel $H_i^{\mathcal{SI}}$ as a complex Gaussian matrix random variable with mean $\sqrt{K/(K+1)}\tilde{H}_{SI}$ and covariance $(1/(K+1))\, I_{N_1 N_2}$, where K is the Rician factor, $\tilde{H}_{SI}$ is a deterministic matrix. For simplicity, we assume $K = 1$ and $\tilde{H}_{SI} = \mathbf{1}_{N_2 \times N_1}$.

Unless stated otherwise, the number of transmit antennas and the number of receive antennas at a BS are set as $N_1 = 4$ and $N_2 = 2$, respectively. Except simulation scenario 4, we assume the numbers of concurrent downlink and uplink data streams are equal to the number of antennas at a DLU/ULU, i.e., $d_1 = d_2 = N_r$. In other words, the precoding matrices $\mathbf{V}_{i,j_{\mathsf{D}}}$ and $\mathbf{V}_{i,j_{\mathsf{U}}}$ in (4.1) and (4.6) are of dimension $N_1 \times N_r$ and $N_r \times N_r$, respectively. To arrive at the final figures, we run each simulation 100 times and average the result. For the ease of reference, we list in Table 4.1 other 3GPP LTE network parameters that we use in all simulations [3GPP TS 36.814 V9.0.0, 2010].

4.1.5.1 Simulation Scenario 1

In this simulation study, we consider the sum throughput maximization problem (4.11a)-(4.11b) (i.e., problem (4.11) without the rate constraint (4.11c)) so that the closed-form solutions in (4.32) and (4.34) apply. We use the example network in Fig. 4.2 to study the sum throughput performance of Algorithm 3 in the presence of SI. By considering a single-cell network with fixed-location users, we can focus on the effect of SI while isolating those of the intracell and intercell interferences.

For both $N_r = 1$ and $N_r = 2$, Fig. 4.3 shows that the performance of the proposed Algorithm 3 almost coincides with its upper bound, which is the result of solving (4.11) (without the rate constraint (4.11c)) in the rank-free covariance variables $\mathbf{W}_{i,j}$ [see (4.13)]. This observation is significant because it means that our QPI solution approaches the global optimum of problem (4.11a)-(4.11b) over all the considered SI values. As mentioned at the end of Section 4.1.3, this 'upper bound' problem has been addressed in [Huberman and Le-Ngoc, 2015] by using the DCI algorithm of [Kha

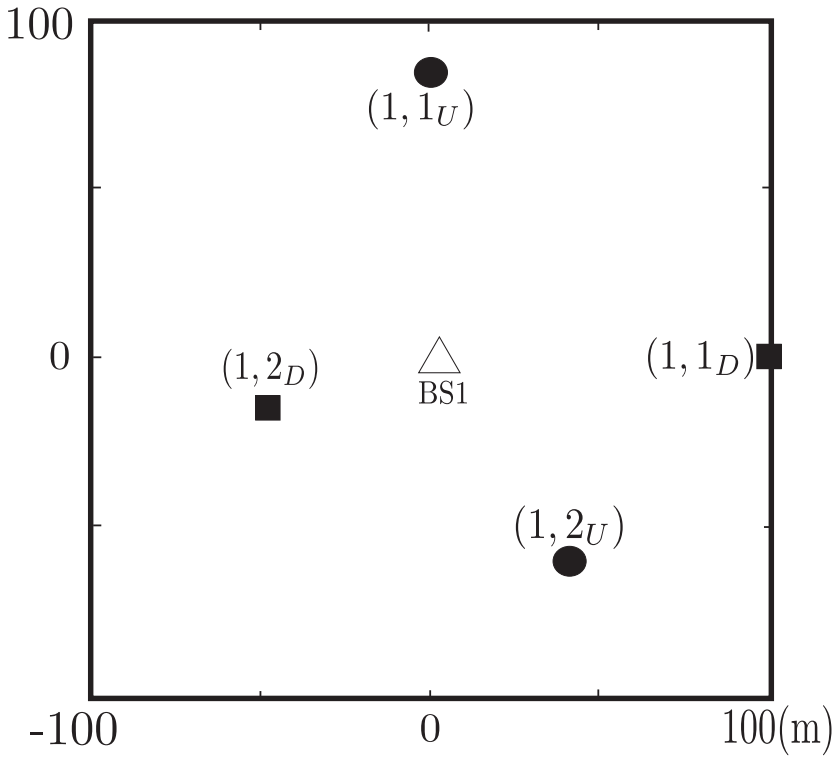

Figure 4.2: Scenario 1: A single-cell network with 2 DLUs and 2 ULUs. The user locations are fixed.

et al., 2012]. The specific case of $N_r = 1$ corresponds to the joint design of uplink power allocation at ULUs and BS downlink beamforming towards DLUs, which has been studied in [Nguyen et al., 2014] by using the DCI algorithm of [Kha et al., 2012] to solve (4.11) (without the rate constraint (4.11c)) in the rank-free covariance variables $\mathbf{W}_{i,j_\mathsf{D}}$ and scalar variables $\mathbf{W}_{i,j_\mathsf{U}}$ and then by employing randomization techniques to find rank-one $\mathbf{W}_{i,j_\mathsf{D}}$ for satisfying (4.14). Fig. 4.3(a) shows that our QPI solution handles the SI much better than that by [Nguyen et al., 2014]. An improvement of almost 4 bps/Hz is achieved in the practical range of $\sigma_{SI}^2 \geq -80$dB.

Fig. 4.4 further illustrates how Algorithm 3 distributes the total throughput into the downlink and uplink channels. An important observation is that when the ratio σ_{SI}^2 increases, the BS consistently decreases the throughput in the downlink so as to reduce the effect of SI to the uplink channel. Because the improvement in the uplink throughput sufficiently compensates the reduction in the downlink throughput, the

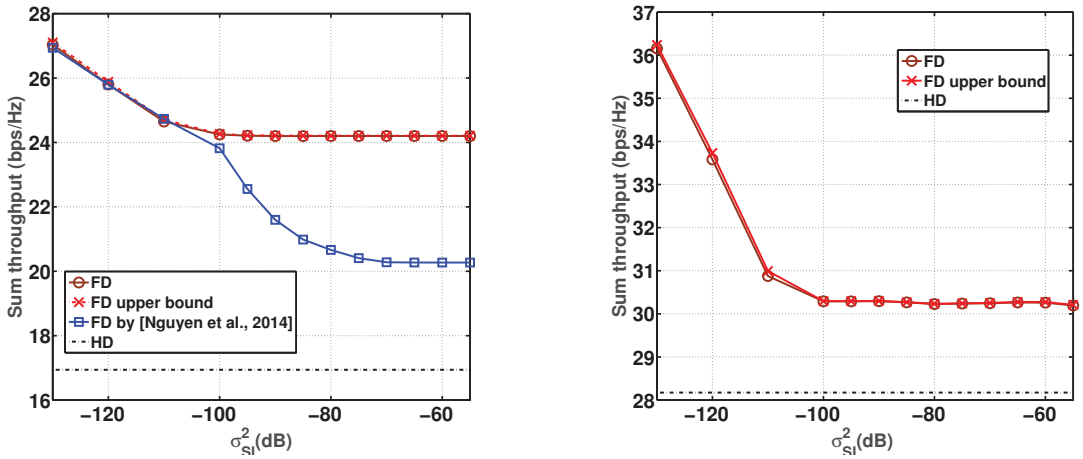

(a) $N_r = 1$ (b) $N_r = 2$

Figure 4.3: Effect of SI on the sum throughput performance of Algorithm 3.

overall FD throughput still outperforms the average HD throughput. As presented in Fig. 4.3, although the achieved FD sum throughput does not double the effective HD sum throughput, significant gains of up to 60% and 40% are offered by Algorithm 3 for $N_r = 1$ and $N_r = 2$, respectively. When the residual SI becomes the dominant interference in (4.6), we have found that the BS optimal precoder matrices $\mathbf{V}_{i,\ell_{\mathsf{D}}}$ effectively null out such SI. This explains why the performance of FD appears insensitive to the increase of σ_{SI}^2 when σ_{SI}^2 is greater than -100dB for $N_r = 1$ and -90dB for $N_r = 2$.

On the other hand, whenever the entries of the self-loop channel $H_i^{\mathcal{SI}}$ in (4.6) are treated as independent circularly symmetric complex Gaussian random variables with zero mean and unit variance, the residual SI in (4.10) becomes

$$\sigma_{SI}^2 \mathbb{E}\left\{ H_i^{\mathcal{SI}} \left(\sum_{\ell_D \in \mathsf{D}} \mathbf{V}_{i,\ell_D} \mathbf{V}_{i,\ell_D}^H \right) (H_i^{SI})^H \right\} = \sigma_{SI}^2 \Big\langle \sum_{\ell_D \in \mathsf{D}} \mathbf{V}_{i,\ell_D} \mathbf{V}_{i,\ell_D}^H \Big\rangle I_{N_r}.$$

Such residual SI only depends on the BS transmit power and it cannot be mitigated by precoder matrices $\mathbf{V}_{i,\ell_{\mathsf{D}}}$. To avoid channel deactivation due to excessive SI σ_{SI}^2, in the simulation we impose the uplink and downlink QoS constraints as $f_i(\mathbf{V}) \geq 5$bps/Hz and $\sum_{j_{\mathsf{D}}} f_{i,j_{\mathsf{D}}}(\mathbf{V}) \geq 5$bps/Hz, respectively. For the network configuration in Fig. 4.2 where $N_r = 2$, $d_1 = d_2 = 1$, Fig. 4.5(a) shows that the FD sum throughput is always

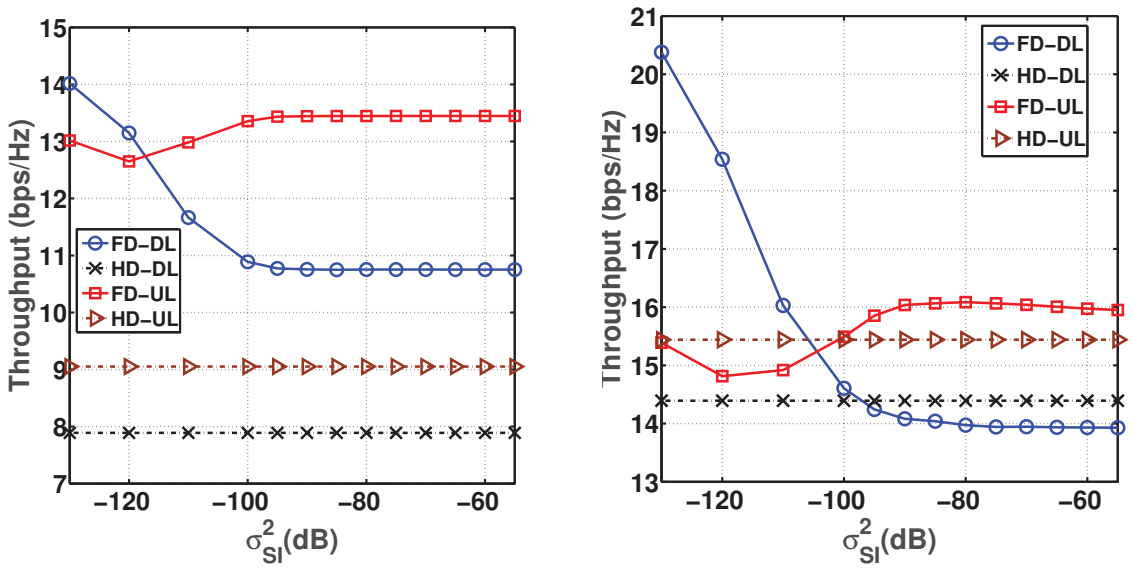

(a) $N_r = 1$ (b) $N_r = 2$

Figure 4.4: Effect of SI on the DL and UL throughput performance of Algorithm 3.

degraded as σ^2_{SI} increases. Still, whenever $\sigma^2_{SI} \leq -120$dB it is higher than the HD sum throughput. Fig. 4.5(b) further shows that the FD DL throughput is on the decreasing trend when $\sigma^2_{SI} \leq -110$dB so as to avoid the excessive SI toward the UL receiver. After $\sigma^2_{SI} = -110$dB, it levels off due to the imposed downlink QoS constraint.

4.1.5.2 Simulation Scenario 2

In this simulation study, we use the example network in Fig. 4.6 to study the sum throughput performance of Algorithm 3 in problem (4.11a)-(4.11b) when the intracell interference changes. Here, we fix $\sigma^2_{SI} = -80$dB and use a single-cell network to isolate the effects of SI and intercell interference. To vary the intracell interference, we fix the location of the DLU at a point B and change the location of the ULU. For each position of the ULU at a point A on the circle of radius of 90m, we find the corresponding throughput. Because we keep the small-scale fading parameter unchanged, a small angle $\widehat{AOB}$ in Fig. 4.6 means a small path loss and accordingly a large intracell interference level.

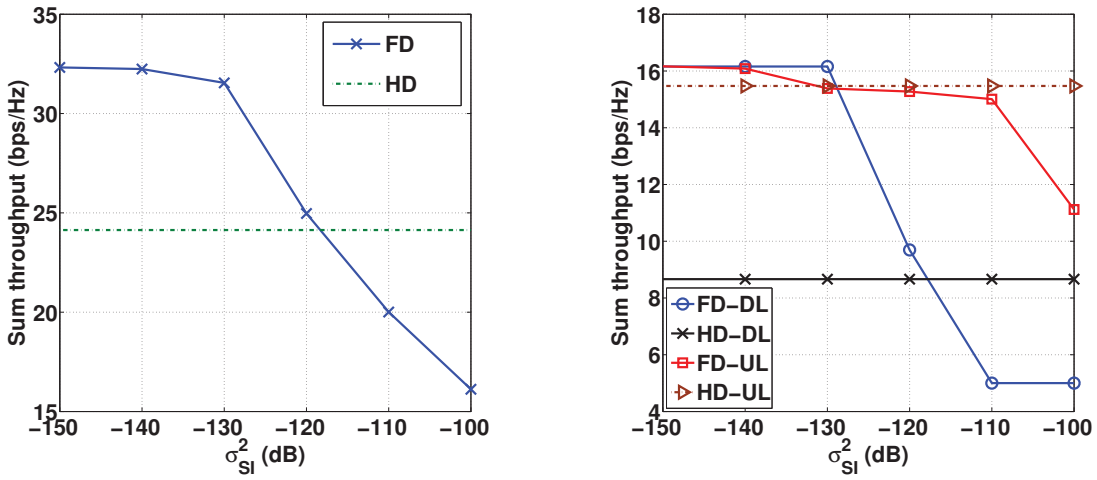

(a) Sum throughput

(b) UL/DL throughput

Figure 4.5: Effect of SI on the network throughput when SI is treated as white noise.

The results in Fig. 4.7 confirm that the proposed Algorithm 3 approaches the upper bound in all the cases that we consider. For $N_r = 1$, our proposed solution also outperforms the solution of [Nguyen et al., 2014] by around 1 bps/Hz as shown in Fig. 4.7(a). It can also be observed from Fig. 4.7 that the FD transmission is always more beneficial than the HD counterpart if the intracell interference is sufficiently small. The most pronounced FD throughput gains of 75% and 65% are respectively achieved by Algorithm 3 for $N_r = 1$ and $N_r = 2$ when the ULU-DLU distance is maximum (i.e., $\widehat{AOB} = \pi$), in which case the intracell interference is smallest.

4.1.5.3 Simulation Scenario 3

In this simulation study, we compare the throughput performance of Algorithm 3 in problem (4.11a)-(4.11b) with that of Algorithm 4 in problem (4.12). Since a multicell network is required in this case to realize the max-min solution in (4.12), we use the 3-cell network in Fig. 4.8. In each cell, we fix the positions of the ULU and the DLU at a distance of $2r/3 = 66.67$m and $r/2 = 50$m from their serving BS, respectively. In terms of sum throughput, Fig. 4.9(a) shows that Algorithm 3 always outperforms

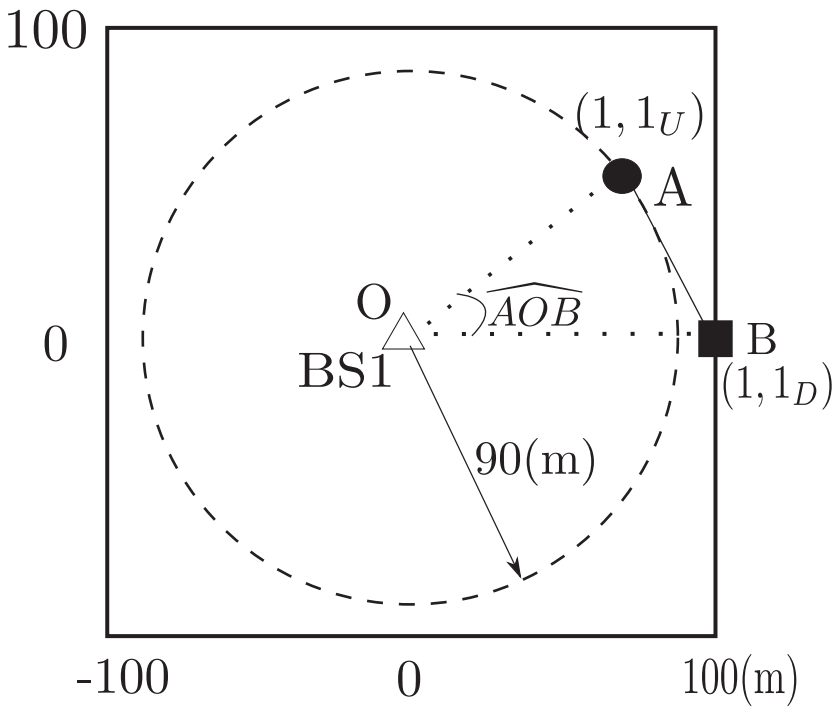

Figure 4.6: Scenario 2: A single-cell network with one DLU and one ULU. The DLU location is fixed at a point B, whereas the ULU is located at any point A on the circle of radius of 90m.

Algorithm 4 by at least 5 bps/Hz. This is because Algorithm 3 is specifically designed to maximize total network throughput. In doing so, it however allocates the available radio resources to the cells with favorable link conditions, leaving the remaining cells with a much lower throughput. From Table 4.2, the number of instances that a DLU in the downlink or a BS in the uplink receives a zero data rate can be as high as 100 over 100 simulation runs. The max-min fairness Algorithm 4 resolves this issue, albeit at the cost of a reduced total network throughput. Fig. 4.9(b) confirms that Algorithm 4 improves the throughput of the cell with the worst link conditions by up to 5 bps/Hz.

Table 4.2: The number of times that at least a DLU or a BS receives a zero data rate in 100 simulation runs

σ^2_{SI}(dB)	-130	-110	-90	-70
$d = 1$	96	98	100	100
$d = 2$	33	42	44	72

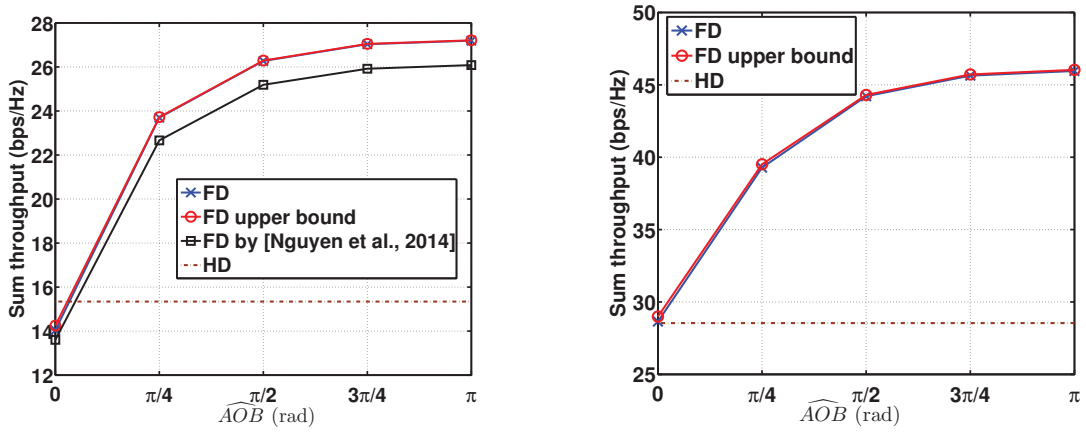

(a) $N_r = 1$ (b) $N_r = 2$

Figure 4.7: Effect of ULU-DLU distance (hence, intracell interference) on the sum throughput performance of Algorithm 3.

4.1.5.4 Simulation Scenario 4

In this simulation study, we evaluate the performance of Algorithm 3 for the rate-constraint problem (4.11a)-(4.11c) where the closed-form solutions in (4.32) and (4.34) no longer apply. Here we examine the impacts of the required minimum rates and the number of cells on the throughput performance. To this end, we fix the total number of users as 12 and consider one-cell, two-cell and three-cell networks. By (I, D, U), we mean there are I cells with radius of 100m in the network, each of which has D DLUs and U ULUs randomly placed according to the uniform distribution within the cell area. Fig. 4.10 presents a realization of such random user deployments. For simplicity, we set $d_1 = d_2 = 1$, $N_r = 2$ and $\sigma_{SI}^2 = -80$dB. In this case, the precoding matrices $\mathbf{V}_{i,j_\mathrm{D}}$ and $\mathbf{V}_{i,j_\mathrm{U}}$ in (4.1) and (4.6) reduce to beamforming vectors of dimension N_1 and 2, respectively. To the best of our knowledge, such FD beamforming optimization problems have not been previously addressed. The approaches in [Nguyen et al., 2014; Che and Tuan, 2014] do not apply because the rank of their optimal covariance matrices is often two while a rank-one solution is strictly required here. To find the sum throughput subject to the rate constraints, we initialize Algorithm 3 with the optimal solution of

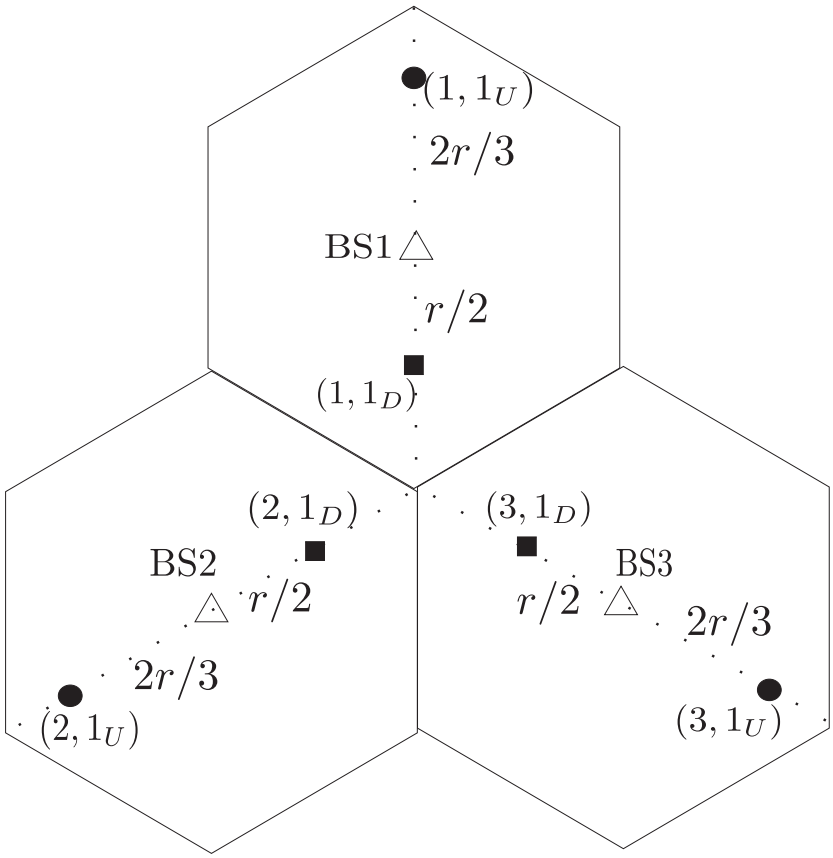

Figure 4.8: Scenario 3: A three-cell network with 1 DLU and 1 ULU. The cell radius is $r = 100$m and the user locations are fixed.

the maximin problem (4.27).

To ensure the feasibility of problem (4.11a)-(4.11c), we first set the minimum rates according to $r_{i,\mathsf{jD}}^{\min} = r_i^{\mathsf{U},\min}/U = \alpha\, r_{\max,\min}$, where $\alpha \in (0,1)$ and $r_{\max,\min}$ is the optimal value of problem (4.27) given by Algorithm 4. As seen from Fig. 4.11, to achieve a higher minimum rate, both the total throughput and the per-cell throughput by Algorithm 3 drop since the feasible set gets more restricted. It is also clear from Fig. 4.11(a) that by deploying more cells to serve the same number of users, a higher total throughput is achieved because the network load per cell is reduced. However, the per-cell throughput of such multicell deployment can be compromised due to the growing intercell interference, as evident from Fig. 4.11(b).

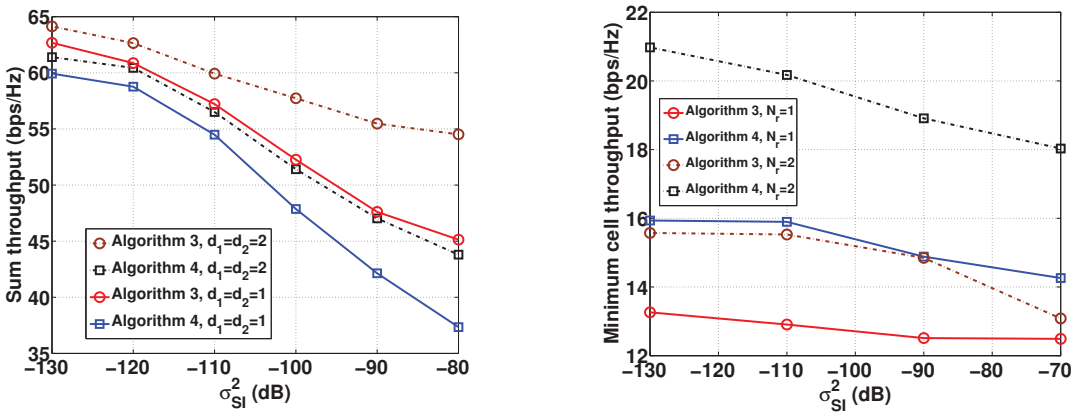

(a) Sum throughput

(b) Minimum cell throughput

Figure 4.9: Comparing the throughput performance of Algorithms 3 and 4.

Finally, we demonstrate the convergence behavior of the proposed algorithms in Fig. 4.12, where the error tolerance for convergence is set as $\epsilon = 10^{-3}$. Fig. 4.12(a) plots the convergence of Algorithm 3 that solves problem (4.11) for $\alpha = 0.8$, whereas Fig. 4.12(b) is for Algorithm 4 that solves problem (4.27). It is observed that the proposed algorithms monotonically improve the objective value after every iteration. Fig. 4.12 also confirms that at least 95% of the final optimal throughput value is reached within 20 iterations. Furthermore, Table 4.3 shows that while the convergence typically occurs well within 50 iterations, it can be as few as 15 iterations on average in one case. Note also that the per-iteration computational complexity of our algorithms is low. Each iteration only involves one simple convex QP, which is solved very efficiently by any available convex solvers. In all the simulations, we resort to CVX, a package for specifying and solving convex programs [Grant and Boyd, 2014].

Table 4.3: The average number of iterations required by Algorithms 3 and 4

(I, D, U)	$(1, 6, 6)$	$(2, 3, 3)$	$(3, 2, 2)$
Algorithm 3	24.77	31.66	37.90
Algorithm 4	14.60	45.40	45.90

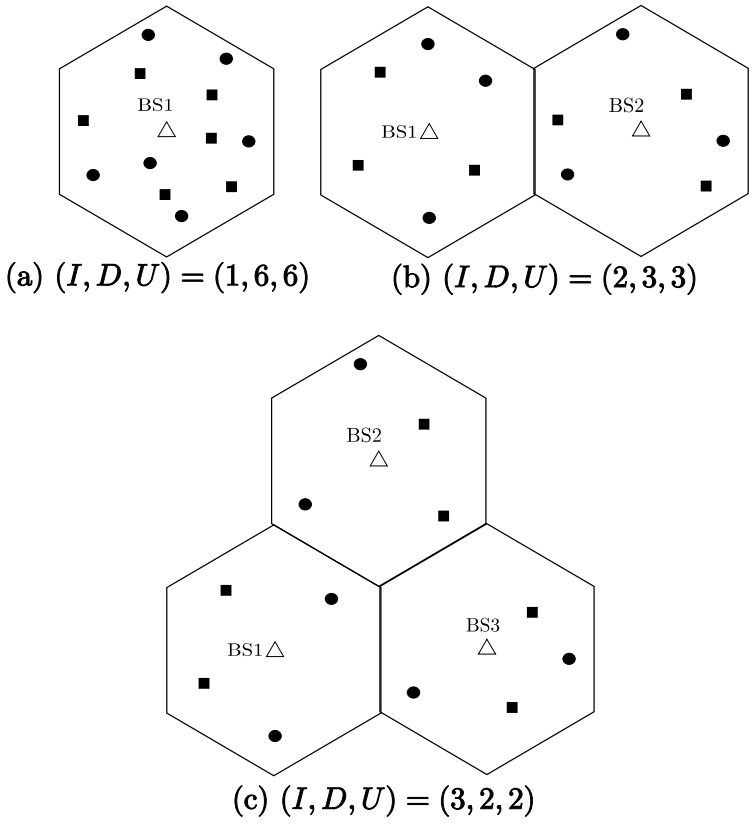

(a) $(I, D, U) = (1, 6, 6)$ (b) $(I, D, U) = (2, 3, 3)$

(c) $(I, D, U) = (3, 2, 2)$

Figure 4.10: Scenario 4: Three cellular network topologies that serve 12 users in total. The cell radius is $r = 100$m and the users are placed randomly according to the uniform distribution.

4.1.6 Conclusions

In this section, we have designed new linear precoders for large-scale MIMO multicell networks, in which FD BSs simultaneously transmit to and receive from their HD users. Specifically, we have considered two difficult nonconvex optimization problems: (i) sum throughput maximization under rate constraints and (ii) maximization of minimum cell throughput. We have proposed iterative low-complexity SCQP algorithms that require solving only one simple convex quadratic program at each iteration. We have proved that our path-following algorithms are guaranteed to monotonically converge to at least a local optimum. Simulation results have been presented in various network scenarios to demonstrate the advantages of our proposed SCQP solutions.

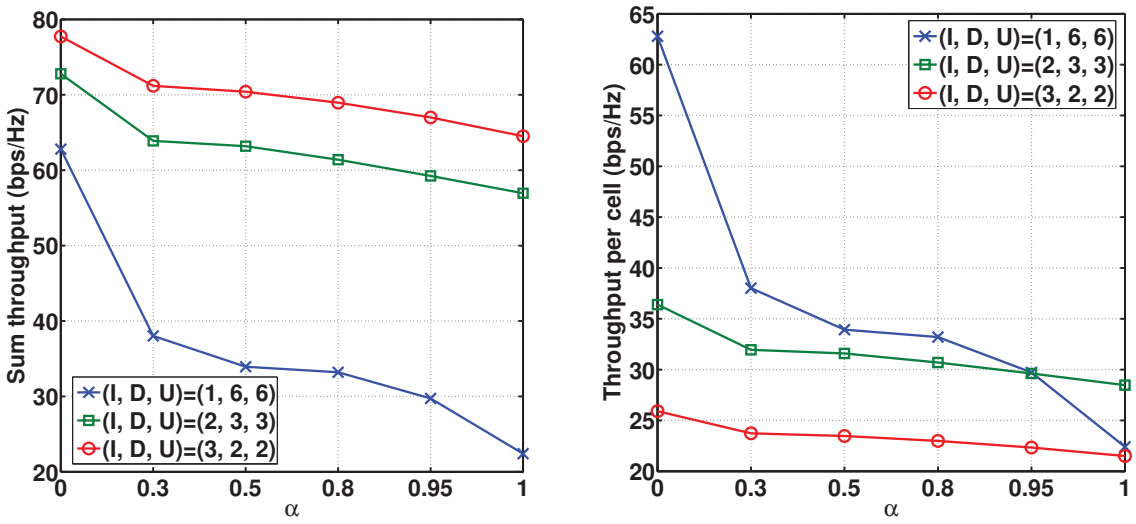

(a) Sum throughput

(b) Per-cell throughput

Figure 4.11: Impact of the required minimum rates and the number of cells on throughput performance of Algorithm 3.

4.2 Precoding Design for Han-Kobayashi's Signal Splitting in MIMO Interference Networks

4.2.1 Introduction

The interference management problem in the FD MU-MIMO multicell networks has been investigated in the previous section. Based on the assumption that interference is treated as white noise, the optimal precoding matrices designs has been proposed to mitigate the interference and maximize the network utilities. Nevertheless, the network performance based on this assumption will be significantly degraded if the interference power is much larger than the power of desired signal (e.g. the interference source is too close to the receiver). This section will investigate a H-K transmission strategy [Han and Kobayashi, 1981] in which the most impactful interferer's signal can be decoded and then subtracted from the received signal to reduce the generated interference. The algorithms to design optimal precoding matrices in the previous section will be adapted

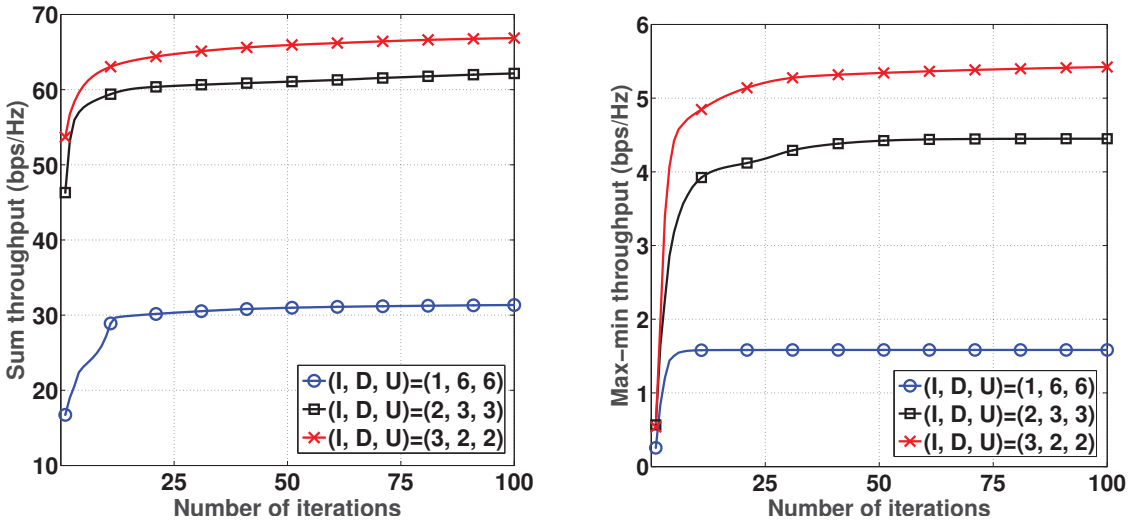

(a) Algorithm 3 (b) Algorithm 4

Figure 4.12: Convergence of Algorithms 3 and 4 for $\epsilon = 10^{-3}$ and $\alpha = 0.8$.

for the designs under H-K transmission. To facilitate the analysis, this section only considers HD transmission.

In literature, if the residual interference is treated as noise, the network capacity is achieved only at low interference regime (see [Annapureddy and Veeravalli, 2011] and references therein) for a general multi-user interference network (IN) or at certain sufficient conditions in terms of matrix equations for two-user INs [Shang and Poor, 2013]. For a two-user two-cell IN (i.e., one user per cell), the H-K strategy [Han and Kobayashi, 1981] is known to give the best achievable rate region [Etkin et al., 2008; Karmakar and Varanasi, 2013]. With the H-K strategy, the transmitted data information of both users is split into two parts: a private message to be decoded at the intended receiver and a common message that can be decoded at both receivers. A part of the interference is thus cancelled off by decoding the common message, while the remaining private message from the other user is treated as noise. Accordingly, it is challenging to perform constructive optimization over such an achievable rate region to realize the potential of H-K strategy [Shang et al., 2006; Etkin et al., 2008].

Jointly beamforming common and private messages to maximize the achievable rate

across MU-MISO INs is first considered in [Dahrouj and Yu, 2011]. At discrete points of the joint space of common and private rates, an ad-hoc intensive search is carried by rank-one constrained SDP for the beamformer vectors. Still, the optimal rate is not achieved. Furthermore, the search proposed by [Dahrouj and Yu, 2011] is not suitable for the problem of sum-rate maximization, which is a more popular metric for INs. Inspired by [Dahrouj and Yu, 2011], the works of [Che and Tuan, 2013*a*; Che et al., 2015] design covariance matrices of the common and private messages in MU-MIMO multicell INs and beamformers for such messages in MU-MISO multicell INs to maximize either the sum-rate or the achievable rate across the networks.

This section aims to find optimal precoder matrices for the common and private messages of independent data streams. The objective is to maximize the sum-rate of an MU-MIMO multicell network. The available solution approaches are not applicable, e.g., [Christensen et al., 2008] for coordinated precoding private messages only and [Che et al., 2015; Che and Tuan, 2013*a*] for covariance design. We propose a successive optimization algorithm in which each iteration only solves a simple convex quadratic program of low computational complexity. Once initialized from a feasible point, our algorithm generates a sequence of monotonically improved points, which eventually converge to at least a local maximum of the formulated nonconvex and nonsmooth problem.

The rest of this section is organized as follows: Section 4.2.2 presents the system model and formulates the precoder design problem. Section 4.2.3 proposes the successive quadratic programming algorithm for solution. Section 4.2.4 verifies the advantages of our devised solution by numerical examples.

4.2.2 System Model and Problem Formulation

Consider the downlink transmissions in a network consisting of N cells, where the base station (BS) of each cell is equipped with N_t antennas and it serves K UEs within its

cell. Each UE is equipped with N_r antennas. Upon denoting $\mathcal{I} \triangleq \{1, 2, \ldots, N\}$ and $\mathcal{J} \triangleq \{1, 2, \ldots, K\}$, the j-th UE in the i-th cell is referred as UE $(i, j) \in \mathcal{S} \triangleq \mathcal{I} \times \mathcal{J}$. Signals are precoded at the BSs prior to transmitting to the UEs. To implement the H-K strategy, where each user decodes the common message of at most one other user, we follow [Dahrouj and Yu, 2011; Che et al., 2015] and introduce the pairing operator $a(i, j)$ to specify which other UE, beside UE (i, j) itself, decodes the common message of UE (i, j). When UE (i, j) has no common message, we let $a(i, j)$ be an empty set. Formally, it is a mapping $a : \mathcal{I} \times \mathcal{J} \to (\mathcal{I} \times \mathcal{J}) \cup \{\emptyset\}$ with the restriction that $a(i, j) = (\tilde{i}, \tilde{j})$ always has $\tilde{i} \neq i$ and $a^{-1}(\tilde{i}, \tilde{j})$ has cardinality of no more than one. With $\emptyset \neq a(i, j) = (\tilde{i}, \tilde{j})$, $\tilde{i} \neq i$, UE (i, j) may split its L ($\leq N_t$) data streams into two parts: the private message $\mathbf{s}^p_{i,j} \in \mathbb{C}^L$ with $\mathbb{E}\{\mathbf{s}^p_{i,j}(\mathbf{s}^p_{i,j})^H\} = \mathbf{I}_L$, and the common message $\mathbf{s}^c_{i,j} \in \mathbb{C}^L$ with $\mathbb{E}\{\mathbf{s}^c_{i,j}(\mathbf{s}^c_{i,j})^H\} = \mathbf{I}_L$. The private and common messages are precoded by matrices $\mathbf{V}^p_{i,j} \in \mathbb{C}^{N_t \times L}$ and $\mathbf{V}^c_{i,j} \in \mathbb{C}^{N_t \times L}$, respectively. The common message $\mathbf{s}^c_{i,j}$ of UE (i, j) is to be decoded by UE (i, j)'s receiver and also by UE $(\tilde{i}, \tilde{j})$'s receiver in a different cell $\tilde{i}$. On the other hand, if $(i, j) = a(\hat{i}, \hat{j})$ for some $\hat{i} \neq i$, the receiver of UE (i, j) also decodes the common message $\mathbf{s}^c_{\hat{i},\hat{j}}$ from UE $(\hat{i}, \hat{j})$ in a different cell $\hat{i} \neq i$.

As in [Dahrouj and Yu, 2011; Che et al., 2015], each UE (i, j) successively decodes the following messages (in the following strict order): (a) its common message $\mathbf{s}^c_{i,j}$ from its own transmitter; (b) the common message $\mathbf{s}^c_{\hat{i},\hat{j}}$ from UE $(\hat{i}, \hat{j})$'s transmitter in the different cell $\hat{i} \neq i$ for which $a(\hat{i}, \hat{j}) = (i, j)$; (c) the private message $\mathbf{s}^p_{i,j}$ from its own transmitter. Note that the decoded messages are also successively subtracted from the received signal for interference mitigation. Intuitively, one's own common message is decoded first to help the decoding of the common information from the other transmitter, while its own private message is decoded last to take advantage of the reduced interference due to common message decoding.

For notational convenience, let us define

$$\mathbf{V}_{i,j} \triangleq [\mathbf{V}^p_{i,j} \quad \mathbf{V}^c_{i,j}], \mathbf{V} \triangleq [\mathbf{V}_{i,j}]_{(i,j)\in\mathcal{S}}, \mathbf{s}_{i,j} \triangleq \begin{bmatrix} \mathbf{s}^p_{i,j} \\ \mathbf{s}^c_{i,j} \end{bmatrix}.$$

The received signal at UE $(i,j) \in \mathcal{S}$ is expressed as:

$$\mathbf{y}_{i,j} = \sum_{(s,l)\in\mathcal{S}} \mathbf{H}_{s,i,j}\mathbf{V}_{s,l}\mathbf{s}_{s,l} + \mathbf{n}_{i,j},$$

where $\mathbf{H}_{s,i,j} \in \mathbb{C}^{N_r \times N_t}$ is the matrix of channel coefficients from BS $s \in \mathcal{I}$ to UE $(i,j) \in \mathcal{S}$. The entries of the additive noise $\mathbf{n}_{i,j} \in \mathbb{C}^{N_r}$ are independent and identically distributed (i.i.d) noise samples with zero mean and variance σ^2. The covariance of $\mathbf{y}_{i,j}$ is thus

$$\mathbf{M}_{i,j}(\mathbf{V}) = \sum_{(s,l)\in\mathcal{S}} \mathbf{H}_{s,i,j}\mathbf{V}_{s,l}\mathbf{V}_{s,l}^H\mathbf{H}_{s,i,j}^H + \sigma^2\mathbf{I}_{N_r}.$$

Under the successive decoding and interference cancellation scheme described above, it follows that:

- UE (i,j) can decode its own common message $\mathbf{s}_{i,j}^c$ with the achievable rate (expressed in nats/s/channel-use):

  $$r_{i,j}^c(\mathbf{V}) = \ln|\mathbf{I}_L + (\mathbf{V}_{i,j}^c)^H\mathbf{H}_{i,i,j}^H\mathbf{M}_{i,j}^c(\mathbf{V})^{-1}\mathbf{H}_{i,i,j}\mathbf{V}_{i,j}^c|,$$

  where $\mathbf{M}_{i,j}^c(\mathbf{V}) \triangleq \mathbf{M}_{i,j}(\mathbf{V}) - \mathbf{H}_{i,i,j}\mathbf{V}_{i,j}^c(\mathbf{V}_{i,j}^c)^H\mathbf{H}_{i,i,j}^H$. Accordingly, $\mathbf{V}_{i,j}^c \equiv \mathbf{0}$, $r_{i,j}^c(\mathbf{V}) \equiv 0$ and $\mathbf{M}_{i,j}^c(\mathbf{V}) \equiv \mathbf{M}_{i,j}(\mathbf{V})$ if $a(i,j) = \emptyset$.

- UE (i,j) can decode the common message $\mathbf{s}_{\hat{i},\hat{j}}^c$ from the interfering user $(\hat{i},\hat{j}) = a^{-1}(i,j)$ with the achievable rate:

  $$r_{i,j}^a(\mathbf{V}) = \ln|\mathbf{I}_L + (\mathbf{V}_{\hat{i},\hat{j}}^c)^H\mathbf{H}_{\hat{i},i,j}^H\mathbf{M}_{i,j}^a(\mathbf{V})^{-1}\mathbf{H}_{\hat{i},i,j}\mathbf{V}_{\hat{i},\hat{j}}^c|,$$

  where $\mathbf{M}_{i,j}^a(\mathbf{V}) \triangleq \mathbf{M}_{i,j}^c(\mathbf{V}) - \mathbf{H}_{\hat{i},i,j}\mathbf{V}_{\hat{i},\hat{j}}^c(\mathbf{V}_{\hat{i},\hat{j}}^c)^H\mathbf{H}_{\hat{i},i,j}^H$. Accordingly, $\mathbf{M}_{i,j}^a(\mathbf{V}) \equiv \mathbf{M}_{i,j}^c(\mathbf{V})$ if $a^{-1}(i,j) = \emptyset$.

- UE (i,j) can decode its own private message $\mathbf{s}_{i,j}^p$ with the achievable rate:

  $$r_{i,j}^p(\mathbf{V}) = \ln|\mathbf{I}_L + (\mathbf{V}_{i,j}^p)^H\mathbf{H}_{i,i,j}^H\mathbf{M}_{i,j}^p(\mathbf{V})^{-1}\mathbf{H}_{i,i,j}\mathbf{V}_{i,j}^p|,$$

  where $\mathbf{M}_{i,j}^p(\mathbf{V}) \triangleq \mathbf{M}_{i,j}^a(\mathbf{V}) - \mathbf{H}_{i,i,j}\mathbf{V}_{i,j}^p(\mathbf{V}_{i,j}^p)^H\mathbf{H}_{i,i,j}^H$.

Similar to [Dahrouj and Yu, 2011, (10)-(12)], the achievable rate region under the successive decoding is given by:

$$\Big\{\boldsymbol{\nu} \triangleq [\nu_{i,j}]_{(i,j)\in\mathcal{I}\times\mathcal{J}} = [\nu^p_{i,j} + \nu^c_{i,j}]_{(i,j)\in\mathcal{I}\times\mathcal{J}} \ : \\ \nu^p_{i,j} \le r^p_{i,j}(\mathbf{V}), \nu^c_{i,j} \le r^c_{i,j}(\mathbf{V}), \nu^c_{i,j} \le r^a_{a(i,j)}(\mathbf{V})\Big\}.$$

As $r^a_{a(i,j)}(\mathbf{V})$ is the achievable rate of decoding the common message $\mathbf{s}^c_{i,j}$ of UE (i,j) by UE $(\tilde{i},\tilde{j}) = a(i,j)$, the constraint $\nu^c_{i,j} \le r^a_{a(i,j)}(\mathbf{V})$ arises only when $a(i,j) \neq \emptyset$. Therefore, by defining the nonsmooth functions

$$r_{i,j}(\mathbf{V}) = r^p_{i,j}(\mathbf{V}) + \min\left\{r^c_{i,j}(\mathbf{V}), r^a_{a(i,j)}(\mathbf{V})\right\}, \tag{4.39}$$

we formulate the problem of sum-rate maximization over the achievable rate region as:

$$\max_{\mathbf{V}} \ \mathcal{P}(\mathbf{V}) \triangleq \sum_{(i,j)\in\mathcal{S}} r_{i,j}(\mathbf{V}) \quad \text{s.t.} \tag{4.40a}$$

$$\sum_{j\in\mathcal{J}} \langle \mathbf{V}_{i,j}\mathbf{V}^H_{i,j}\rangle \le P^{\max}_i, \forall i \in \mathcal{I}, \tag{4.40b}$$

where $P^{\max}_i$ is the maximum transmit power of BS i.

Problem (4.40) is a challenging nonconvex optimization problem because its objective function is nonconvex and even nonsmooth. It should be emphasized that the available sum-rate maximization solutions (see, e.g., [Christensen et al., 2008]) are only suitable for the conventional coordinated precoding approach, which corresponds to $r_{i,j}(\mathbf{V}) \equiv r^p_{i,j}(\mathbf{V})$ and $\mathbf{V} = [\mathbf{V}^p]_{(i,j)\in\mathcal{S}}$ (i.e., there is no split of UE's data). On the other hand, the covariance optimization approach in [Che et al., 2015; Che and Tuan, 2013*a*] is applicable for the case of $L = N_t$ only, i.e., one independent data stream is sent per one transmit antenna. In this particular case, (4.40) can be equivalently transformed to the optimization of a d.c. function in the rank-free outer products $\mathbf{Q}^x_{i,j} = \mathbf{V}^x_{i,j}(\mathbf{V}^x_{i,j})^H \succeq \mathbf{0}$, $x \in \{p,c\}$. The computational complexity of each d.c. iteration in [Che et al., 2015] is high, because it involves the maximization of a logarithmic-determinant function under semi-definite constraints—a difficult convex optimization problem with unknown

polynomial computational complexity. Whenever $L < N_t$, such a variable change leads to the additional difficult rank constraints $\text{rank}(\mathbf{Q}_{i,j}^x) \leq L$ for which there is no available solution method. Indeed, there is no effective d.c. representation of each rate function in (4.39) even for the simplest case of $L = 1$.

In what follows, we will develop an efficient successive optimization algorithm of low computational complexity to solve problem (4.40). Our solution works for both cases of $L = N_t$ and $L < N_t$.

Remark. We adopt the pairing rule proposed in [Dahrouj and Yu, 2011]. At the receiver of each UE, the optimal solution of (4.40) for $\mathbf{V}_{i,j}^c \equiv \mathbf{0}$ is used to identify the interference power from the UEs of other cells. Then, each UE is paired with the UE from a different cell that introduces the strongest interference.

4.2.3 Proposed Precoder Design

Suppose that $\mathbf{V}^{(\kappa)} \triangleq [\mathbf{V}_{i,j}^{p,(\kappa)} \quad \mathbf{V}_{i,j}^{c,(\kappa)}]_{(i,j)\in\mathcal{S}}$ is a feasible point found at $(\kappa-1)$-th iteration. Define the following quadratic functions:

$$\begin{aligned}
r_{i,j}^{c,(\kappa)}(\mathbf{V}) \triangleq\ & r_{i,j}^{c}(\mathbf{V}^{(\kappa)}) + 2\,\text{Re}\{\langle \mathcal{A}_{i,j}^{c,(\kappa)}, \mathbf{V}_{i,j}^{c} - \mathbf{V}_{i,j}^{c,(\kappa)}\rangle\} \\
& - \langle \mathbf{M}_{i,j}^{c}(\mathbf{V}^{(\kappa)})^{-1} - \mathbf{M}_{i,j}(\mathbf{V}^{(\kappa)})^{-1}, \\
& \mathbf{M}_{i,j}(\mathbf{V}) - \mathbf{M}_{i,j}(\mathbf{V}^{(\kappa)})\rangle, \\
r_{i,j}^{a,(\kappa)}(\mathbf{V}) \triangleq\ & r_{i,j}^{a}(\mathbf{V}^{(\kappa)}) + 2\,\text{Re}\{\langle \mathcal{A}_{\hat{i},\hat{j}}^{a,(\kappa)}, \mathbf{V}_{\hat{i},\hat{j}}^{c} - \mathbf{V}_{\hat{i},\hat{j}}^{c,(\kappa)}\rangle\} \\
& - \langle \mathbf{M}_{i,j}^{a}(\mathbf{V}^{(\kappa)})^{-1} - \mathbf{M}_{i,j}^{c}(\mathbf{V}^{(\kappa)})^{-1}, \\
& \mathbf{M}_{i,j}^{c}(\mathbf{V}) - \mathbf{M}_{i,j}^{c}(\mathbf{V}^{(\kappa)})\rangle, \\
r_{i,j}^{p,(\kappa)}(\mathbf{V}) \triangleq\ & r_{i,j}^{p}(\mathbf{V}^{(\kappa)}) + 2\,\text{Re}\{\langle \mathcal{A}_{i,j}^{p,(\kappa)}, \mathbf{V}_{i,j}^{p} - \mathbf{V}_{i,j}^{p,(\kappa)}\rangle\} \\
& - \langle \mathbf{M}_{i,j}^{p}(\mathbf{V}^{(\kappa)})^{-1} - \mathbf{M}_{i,j}^{a}(\mathbf{V}^{(\kappa)})^{-1}, \\
& \mathbf{M}_{i,j}^{a}(\mathbf{V}) - \mathbf{M}_{i,j}^{a}(\mathbf{V}^{(\kappa)})\rangle,
\end{aligned}$$

where

$$\mathcal{A}_{i,j}^{c,(\kappa)} \triangleq \mathbf{H}_{i,i,j}^H \mathbf{M}_{i,j}^c (\mathbf{V}^{(\kappa)})^{-1} \mathbf{H}_{i,i,j} \mathbf{V}_{i,j}^{c,(\kappa)},$$
$$\mathcal{A}_{\hat{i},\hat{j}}^{a,(\kappa)} \triangleq \mathbf{H}_{\hat{i},i,j}^H \mathbf{M}_{i,j}^a (\mathbf{V}^{(\kappa)})^{-1} \mathbf{H}_{\hat{i},i,j} \mathbf{V}_{\hat{i},\hat{j}}^{c,(\kappa)},$$
$$\mathcal{A}_{i,j}^{p,(\kappa)} \triangleq \mathbf{H}_{i,i,j}^H \mathbf{M}_{i,j}^p (\mathbf{V}^{(\kappa)})^{-1} \mathbf{H}_{i,i,j} \mathbf{V}_{i,j}^{p,(\kappa)}.$$

Note that all the above functions are concave in $\mathbf{V}$ because $\mathbf{M}_{i,j}^c (\mathbf{V}^{(\kappa)})^{-1} - \mathbf{M}_{i,j} (\mathbf{V}^{(\kappa)})^{-1} \succeq \mathbf{0}$, $\mathbf{M}_{i,j}^a (\mathbf{V}^{(\kappa)})^{-1} - \mathbf{M}_{i,j}^c (\mathbf{V}^{(\kappa)})^{-1} \succeq \mathbf{0}$, $\mathbf{M}_{i,j}^p (\mathbf{V}^{(\kappa)})^{-1} - \mathbf{M}_{i,j}^a (\mathbf{V}^{(\kappa)})^{-1} \succeq \mathbf{0}$.

The following result shows that the complicated function defined by (4.39) is lower bounded by a concave quadratic function.

Corollary 4.1. *For*

$$r_{i,j}^{(\kappa)}(\mathbf{V}) \triangleq r_{i,j}^{p,(\kappa)}(\mathbf{V}) + \min\{r_{i,j}^{c,(\kappa)}(\mathbf{V}), r_{a(i,j)}^{a,(\kappa)})(\mathbf{V})\},$$

it is true that

$$r_{i,j}(\mathbf{V}^{(\kappa)}) = r_{i,j}^{(\kappa)}(\mathbf{V}^{(\kappa)}) \quad \textit{and} \quad r_{i,j}(\mathbf{V}) \geq r_{i,j}^{(\kappa)}(\mathbf{V}),\ \forall\ \mathbf{V}. \tag{4.41}$$

Proof. The proof is given in Appendix F. ■

In Algorithm 5, we propose a SCQP algorithm to solve problem (4.40). Given a feasible point $\mathbf{V}^{(\kappa)}$, this algorithm iteratively generates a feasible point $\mathbf{V}^{(\kappa+1)}$ as the optimal solution to the following optimization problem at the κ-th iteration:

$$\max_{\mathbf{V}}\ \mathcal{P}^{(\kappa)}(\mathbf{V}) \triangleq \sum_{(i,j)\in\mathcal{S}} r_{i,j}^{(\kappa)}(\mathbf{V}) \quad \text{s.t.} \quad (4.40b). \tag{4.42}$$

Problem (4.42) is a convex quadratic with $m = N + 2KN$ quadratic constraints and $n = 2NKN_tL + KN$ real decision variables. The complexity for computing its optimal solution $\mathbf{V}^{(\kappa+1)}$ is thus $\mathcal{O}(n^2 m^{2.5} + m^{3.5})$. Note that $\mathbf{V}^{(\kappa)}$ is also feasible to (4.42) with $\mathcal{P}(\mathbf{V}^{(\kappa)}) = \mathcal{P}^{(\kappa)}(\mathbf{V}^{(\kappa)})$ by the equality in (4.41). It is then true that $\mathcal{P}^{(\kappa)}(\mathbf{V}^{(\kappa+1)}) > \mathcal{P}^{(\kappa)}(\mathbf{V}^{(\kappa)}) = \mathcal{P}(\mathbf{V}^{(\kappa)})$ whenever $\mathbf{V}^{(\kappa+1)} \neq \mathbf{V}^{(\kappa)}$. Together with $\mathcal{P}(\mathbf{V}^{(\kappa+1)}) \geq \mathcal{P}^{(\kappa)}(\mathbf{V}^{(\kappa)})$

Algorithm 5 Proposed SCQP Algorithm

Initialization: Initialize a feasible point $\mathbf{V}^{(0)}$ that satisfies power constraint (4.40b).
κ-th iteration: Solve convex quadratic program (4.42) to find an optimal solution $\mathbf{V}^*$. If $|(\mathcal{P}(\mathbf{V}^*)-\mathcal{P}(\mathbf{V}^{(\kappa)}))/\mathcal{P}(\mathbf{V}^{(\kappa)})| \leq \epsilon$, terminate. Otherwise, set $\kappa := \kappa+1, \mathbf{V}^{(\kappa)} := \mathbf{V}^*$ and continue.

according to the inequality in (4.41), we have that $\mathcal{P}(\mathbf{V}^{(\kappa+1)}) > \mathcal{P}(\mathbf{V}^{(\kappa)})$, i.e., the optimal solution $\mathbf{V}^{(\kappa+1)}$ of the convex quadratic problem (4.42) is a better point of the nonconvex nonsmooth optimization problem (4.40) than $\mathbf{V}^{(\kappa)}$. Therefore, once initialized from an achievable sum-rate $\mathcal{P}(\mathbf{V}^{(0)})$, the sequence $\{\mathcal{P}(\mathbf{V}^{(\kappa)})\}$ obtained by solving (4.42) is guaranteed to improve at each iteration and it eventually converges to at least a local optimum of (4.40)[Marks and Wright, 1978].

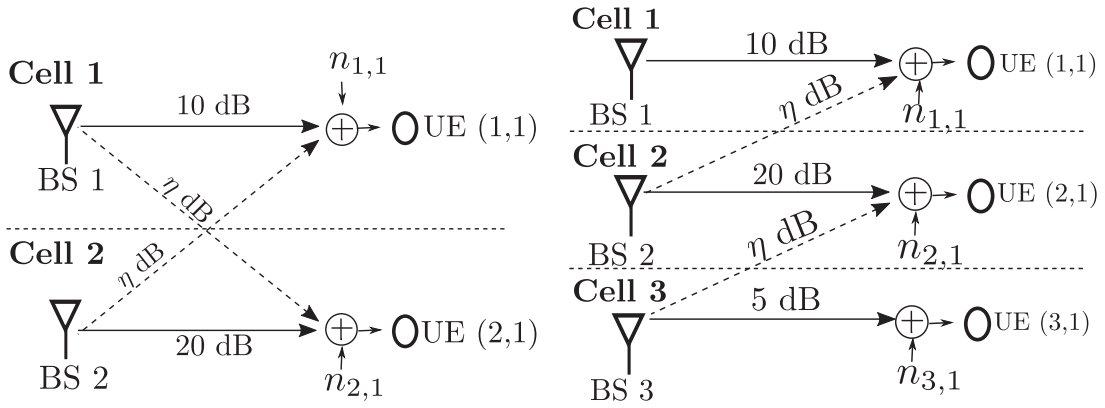

(a) $N = 2, K = 1$ (b) $N = 3, K = 1$

Figure 4.13: Network configurations used in the simulations.

4.2.4 Numerical Results

In our simulations, we assume $\mathbf{H}_{i,s,l} \triangleq \sqrt{\eta_{i,s,l}}\tilde{\mathbf{H}}_{i,s,l}$ where $\tilde{\mathbf{H}}_{i,s,l} \in \mathbb{C}^{N_t \times N_r}$ with $N_t = 4$ and $N_r = 2$ represents the normalized MIMO channel, the entries of which are independent and identically distributed complex Gaussian variables with zero-mean and unit variance. Following [Etkin et al., 2008; Blum, 2003] the direct channel powers $\eta_{i,i,l}$ are fixed, while the interfering channel powers $\eta_{i,j,\ell}$ $(i \neq j)$ are varied to cover all the environment-dependent channel effects, including path loss and shadowing. The

simulation scenarios thus vary from weak MIMO INs to mixed MIMO INs, for which the Han-Kobayashi strategy is advantageous. The notation 'H-K' refers to the Han-Kobayashi strategy whereas 'coordinated' refers to the conventional coordinated precoding approach which only involves private message precoding. It can be seen from (4.40) that the IN sum rate monotonically increases in the number of involved data streams L. Since the covariance optimization approach in [Che et al., 2015] is suitable for $L = N_t = 4$, it is used for performance evaluation in this case. The comparison between the 'H-K' and 'coordinated' schemes is to show the capability of the H-K strategy in mitigating the intercell interferences. Each result in the Monte-Carlo simulation is obtained upon averaging over 100 random network realizations. We set the error tolerance as $\epsilon = 10^{-3}$ and $\sigma^2 = 1$, $P_i^{\max} = 10^3$, $\forall i$ in (4.40). We divide the achieved sum-rate results by ln(2) to arrive at the unit of bps/channel-use for binary communications.

First, we consider the two-cell two-UE MIMO network depicted in Fig. 4.13(a). The values of direct channel gains $\eta_{1,1,1}$ and $\eta_{2,2,1}$ are indicated in the figure, while interference channel gains $\eta_{1,2,1} = \eta_{2,1,1} = \eta$ are varied from -40 dB to 20 dB. In this scenario, UEs do not experience any intracell interference and the only UE pairing possibilities are $a(1,1) = (2,1)$ and $a(2,1) = (1,1)$. Fig. 4.14 also includes the curve of the theoretical lower bound and upper bound by solving the linear inequality [Karmakar and Varanasi, 2013, (52a)-(52i)] and [Karmakar and Varanasi, 2013, (11)-(17)], respectively. As seen, the 'H-K' scheme offers a substantial performance gain over the 'coordinated' counterpart, especially for large interference channel gain η. In particular, an improvement of up to 30% is observed for $L = 1$ and $\eta = 20$ dB. More importantly, the H-K strategy in all considered cases of L is able to achieve better sum rate performance even when the interference channel gain increases. Table 4.4 shows the average number of iterations required for Algorithm 5 to converge, which is similar to the convergence result in [Che et al., 2015, Table IV] for the SDP-based covariance optimization algorithm.

Next, we consider the three-cell three-UE MIMO network depicted in Fig. 4.13(b). The values of direct channel gains are indicated in the figure. Following [Che et al.,

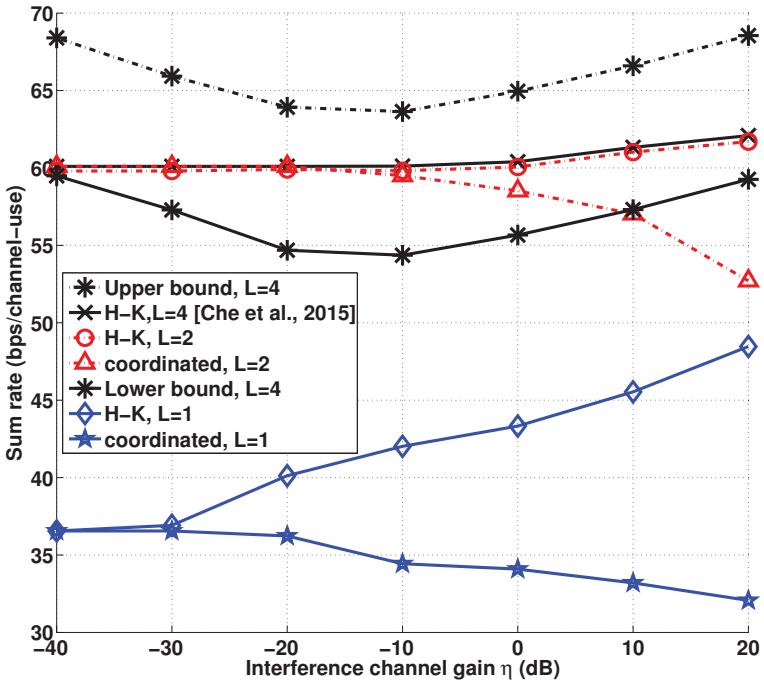

Figure 4.14: Performance results for the network in Fig. 4.13(a).

Table 4.4: Average number of iterations by Algorithm 5 for the network in Fig. 4.13(a).

	η (dB)			
	-10	0	10	20
Coordinated, $L = 1$	5.47	2.515	2	2
H-K, $L = 1$	15.17	20.71	15.62	23.6
Coordinated, $L = 2$	23.88	15.48	10	7.13
H-K, $L = 2$	32.38	16.11	11.91	8.67

2015, Fig. 5(b)], we set $\eta_{1,2,1} = \eta_{2,3,1} = \eta_{3,1,1} = 0$, while varying other interfering channel gains $\eta_{2,1,1} = \eta_{3,2,1} = \eta$ from -40 dB to 30 dB. In this case, the obvious choice for UE pairing is $a(1,1) = (2,1)$, $a(2,1) = (3,1)$. Fig. 4.15 demonstrates the H-K strategy is again able to improve the sum-rate performance under stronger channel interferences for all cases of L. The performance gap between 'H-K' and 'coordinated' curves is widened especially in the high interference region of $\eta \geq 20$ dB.

It is worth noting that in both considered examples, the performances of 'H-K' scheme are not much distinguishable for $L = 2$ and $L = 4$, although the optimal covariance

matrices $\mathbf{Q}_{i,j}^{x} \in \mathbb{C}^{4\times4}$, $x \in \{p, c\}$ are not necessarily of rank $N_r = 2$ [Che et al., 2015]. This result implies that using $L = 2$ data streams gives a performance that is close to the best sum-rate performance. For $L = 1$, an improvement is still observed in the region $\eta \in [-20, -10]$ dB, where the interference per antenna at each UE is at least 14.47 dB and 8.27 dB for the networks in Fig. 4.13(a) and Fig. 4.13(b), respectively. These levels of interference are well above the background noise power of 0 dB. It is sufficient for the low interference regime condition to be satisfied only for the optimal input covariance matrices (those that maximize the achievable sum rate assuming Gaussian inputs and treating interference as noise) if they are full rank [Annapureddy and Veeravalli, 2011].

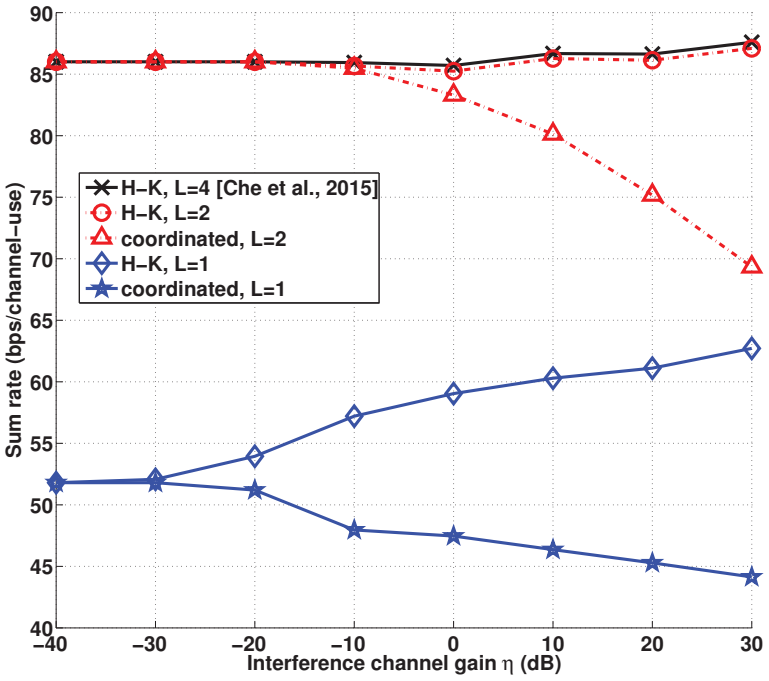

Figure 4.15: Performance results for the network in Fig. 4.13(b).

4.2.5 Conclusions

This section has addressed the problem of precoder design for both common and private messages in MU-MIMO multicell networks under the Han-Kobayashi strategy. Our aim is to find the optimal precoding matrices for network sum-rate maximization. We have

proposed a successive convex quadratic programming algorithm to solve the nonconvex optimization problem in the precoder matrices. Numerical results have confirmed the potential advantages of our proposed approach and also the ability of the Han-Kobayashi to mitigate the intercell interference, which leads to even better sum-rate despite an increase in channel interference.

Chapter 5

Full-Duplex MU-MIMO Networks and MIMO Energy Harvesting

5.1 Introduction

Recently, wireless energy harvesting (i.e. energy constrained devices scavenge energy from the surrounding RF signals) is gaining more and more attraction from both industry and academia [Lu, Niyato, Wang and Kim, 2015; Lu et al., 2016]. Since the amount of energy opportunistically harvested from the ambient/natural energy sources is uncertain and cannot be controlled, BSs in small-cell networks can be configured to become dedicated and reliable wireless energy sources [Buzzi et al., 2016]. The small cell size not only gives the benefit of efficient resource reuse across a geographic area [Andrews, Buzzi, Choi, Hanly, Lozano, Soong and Zhang, 2014] but also provides an adequate amount of RF energy to battery powered UEs for practical applications [Ding et al., 2015; Lu, Niyato, Wang and Kim, 2015; Lu et al., 2016] due to the close BS-UE proximity. In order to transfer both energy and information by the same communication channel, UEs are equipped with both ID receiver and EH receiver. Since the received signal cannot be used for energy harvesting after being decoded, there are two available implementations for wireless energy harvesting and information decoding: (i) PS in which receiver splits the received signal into two streams of different power for

decoding information and harvesting energy separately and (ii) TS to enable the receiver decode information for a portion of a time frame and harvest energy for the rest. Beamforming can be applied to focus the RF signal to EH receiver or enhance throughput at ID receiver [Ding et al., 2015].

Most of previous works (see e.g. [Timotheou et al., 2014; Shi et al., 2014] and references therein) only focus on beamforming power optimization subject to ID throughput and EH constraints with PS in MISO networks. The ID throughput constraints are equivalent to SINR constraints, which are indefinite quadratic in beamforming vectors. The harvested energy constraints are also indefinite quadratic constraints. Thus, [Timotheou et al., 2014; Shi et al., 2014] used semi-definite relaxation (SDR) to relax such indefinite quadratic optimization problems to SDP by dropping the matrix rank-one constraints on the outer products of beamforming vectors. The variable dimension of SDP is explosively large and the beamforming vectors that are recovered based on the matrix solution of SDR perform poorly [Nasir et al., 2015]. Moreover, SDR cannot be applied to throughput or EH maximization as the problems resultant by SDR are still highly nonconvex. Only recently there was an effective development to address these problems [Nasir et al., 2016].

Considering MIMO interference channels, information throughput and harvested energy, i.e., rate-energy (R-E) trade-off was investigated in [Park and Clerckx, 2014] and [Park and Clerckx, 2015], assuming that any UE either acts as an ID receiver or an EH receiver. In case that UEs can operate both as an ID receiver and EH receiver (namely co-located cases), the R-E region of point-to-point MIMO channel was studied in [Zhang and Ho, 2013]. Note that in MIMO networks, the information throughput function is involved with the determinant operation of a matrix and can no longer be expressed in the form of SINR. Consequently, the throughput constraints are always very challenging in precoding signals. [Nguyen et al., 2013; Zong et al., 2016] used zero-forcing or interference-alignment to cancel all interferences, making the throughput functions concave in the signal covariance. The covariance optimization becomes

convex but it is still computationally difficult with no available algorithm of polynomial time. Moreover, there is no known method to recover the precoder matrices from the signal covariance. Only recently, the MIMO throughput function optimization has been successfully addressed for non-EH system in the previous Chapter 4 via a successive convex quadratic programming. The result of Chapter 4 can be adapted to MIMO networks that employ EH by PS approach. However, there is almost no serious research for the systems employing TS in MIMO networks. Though, TS-based system is practically easier to implement, but the related formulated problem is quite complex because the throughput function in such case is coupled with the TS variable that defines the portion of time slot dedicated to EH and ID. This renders the aforementioned precoder design [Nguyen et al., 2013; Zong et al., 2016; Tam et al., 2016] for PS inapplicable. To the best of our knowledge, both the throughput maximization problem and the harvested energy maximization problem with TS are still very open.

All aforementioned works only assume that UEs only harvest energy arriving from BSs' DL transmission. In reality, UEs can also opportunistically harvest energy from other UEs' signals during their UL transmission. Furthermore, by allowing the BSs to simultaneously transmit and receive information, both the spectral efficiency and the amount of transferred energy will be improved. With the recent advances in antenna design and RF circuits in reducing SI [Everett et al., 2014; Duarte et al., 2014; Anttila et al, 2014; Heino et al, 2015], which is the interference from a BS's DL transmission to its UL receiver, the FD technology is recently proposed as one of the key transceiving techniques for the 5G networks [Duarte et al., 2012; Choi and Shirani-Mehr, 2013; Sabharwal et al, 2014; Heino et al, 2015; DUPLO project, 2015]. In this chapter, we are interested in a network in which each FD multi-antenna BS simultaneously serves a group of ULUs and a group of DLUs. In the same time, the BS also transfers energy to DLUs via TS or PS. FD transmission introduces even more interference into the network by adding not only SI but also the interference from ULUs toward DLUs and the interference from DL transmission of other BSs. Consequently, the UL and DL

precoders are coupled in both DL and UL throughput functions, respectively, which makes the optimization problems for UL transmission and DL transmission inseparable.

In literature, [Nguyen et al., 2013; Huberman and Le-Ngoc, 2015; Nguyen et al., 2014] proposed covariance matrices design in (non-EH) FD MU-MIMO networks using D.C. iterations [Kha et al., 2012], which are still very computationally demanding as they require log-determinant function optimizations as mentioned above. Chapter 4 has proposed a framework to directly find the optimal precoding matrices for the sum throughput maximization under throughput constraints in FD MU-MIMO multi-cell networks, which requires only a convex quadratic program of moderate size in each iteration and thus is very computationally efficient.

In this chapter, we propose the design of efficient precoding matrices for the network sum throughput maximization under QoS in terms of MIMO throughput constraints and EH constraints in a FD EH-enabled multicell MU-MIMO network. Both PS and TS are considered for the precoder design and called by PS problem and TS problem, respectively. They are quite challenging computationally due to nonconcave objective function and nonconvex constraints. However, we will see that the PS problem can be efficiently addressed by adapting the algorithm in Chapter 4. On the other hand, the TS problem is much more challenging because the TS variable $\boldsymbol{\alpha}$ is not only coupled with the DL throughput function but also coupled with the SI in the UL throughput function. It is nontrivial to extend algorithms in Chapter 4 to solve the problem for the TS problem. Toward this end, we develop a new inner approximation of the original problem and solve the problem by a path-following algorithm. Finally, we also consider the FD EH maximization problem with throughput QoS constraints with TS. This problem also has a nonconvex objective function and nonconvex constraints and will be addressed by applying an approach similar to that of proposed for the TS problem.

The rest of this chapter is organized as follows: Section II presents the system model the SCP algorithm of the PS problem. The main contribution of the chapter is Section III

and Section IV, which develop algorithms for the TS problem and FD EH maximization problem. Section V evaluates the performance of our devised solutions by numerical examples. Finally, Section VI concludes the chapter.

The following result of Chapter 4 is used.

Theorem 5.1. *For function* $f(\mathbf{V},\mathbf{Y}) = \ln|I_n+\mathbf{V}^H\mathbf{Y}^{-1}\mathbf{V}|$ *in matrix variable* $\mathbf{V}\in\mathbb{C}^{n\times m}$ *and positive definite matrix variable* $\mathbf{Y}\in\mathbb{C}^{m\times m}$*, the following quadratic function is its minorant at* $(\bar{V},\bar{Y})$

$$\tilde{f}(\mathbf{V},\mathbf{Y}) = a + 2\,\mathrm{Re}\{\langle\mathcal{A},\mathbf{V}\rangle\} - \langle\mathcal{B},\mathbf{V}\mathbf{V}^H+\mathbf{Y}\rangle,$$

where $0 > a \triangleq f(\bar{V},\bar{Y}) - \langle\bar{V}^H\bar{Y}^{-1}\bar{V}\rangle$*,* $\mathcal{A} = \bar{Y}^{-1}\bar{V}$ *and* $0 \preceq \mathcal{B} = \bar{Y}^{-1} - (\bar{Y}+\bar{V}\bar{V}^H)^{-1}$.

5.2 EH-enabled FD MU-MIMO Networks

We consider an MU-MIMO EH-enable network consisting of I cells. In cell $i \in \{1,\ldots,I\}$, a group of D DLUs in the DL channel and a group of U ULUs in UL channel are served by a BS i as illustrated in Fig. 5.1. Each BS operates in the FD mode and is equipped with $N \triangleq N_1+N_2$ antennas, where N_1 antennas are used to transmit and the remaining N_2 antennas to receive signals. In cell i, DLU (i,j_{D}) and ULU (i,j_{U}) operate in the HD mode and each is equipped with N_r antennas. In the DL, let $s_{i,j_{\mathsf{D}}}\in\mathbb{C}^{d_1}$ be the symbol intended for DLU (i,j_{D}) where $\mathbb{E}\left[s_{i,j_{\mathsf{D}}}(s_{i,j_{\mathsf{D}}})^H\right] = I_{d_1}$, d_1 is the number of concurrent data streams and $d_1 \le \min\{N_1,N_r\}$. The vector of symbols $s_{i,j_{\mathsf{D}}}$ is precoded and transmitted to DLU (i,j_{D}) through the precoding matrix $\mathbf{V}_{i,j_{\mathsf{D}}}\in\mathbb{C}^{N_1\times d_1}$. Analogously, in the UL, $s_{i,j_{\mathsf{U}}}\in\mathbb{C}^{d_2}$ is the information symbols sent by ULU (i,j_{U}) and is precoded by the precoding matrix $\mathbf{V}_{i,j_{\mathsf{U}}}\in\mathbb{C}^{N_r\times d_2}$, where $\mathbb{E}\left[s_{i,j_{\mathsf{U}}}(s_{i,j_{\mathsf{U}}})^H\right] = I_{d_2}$, d_2 is the number of concurrent data streams and $d_2 \le \min\{N_2,N_r\}$. For notational convenience,

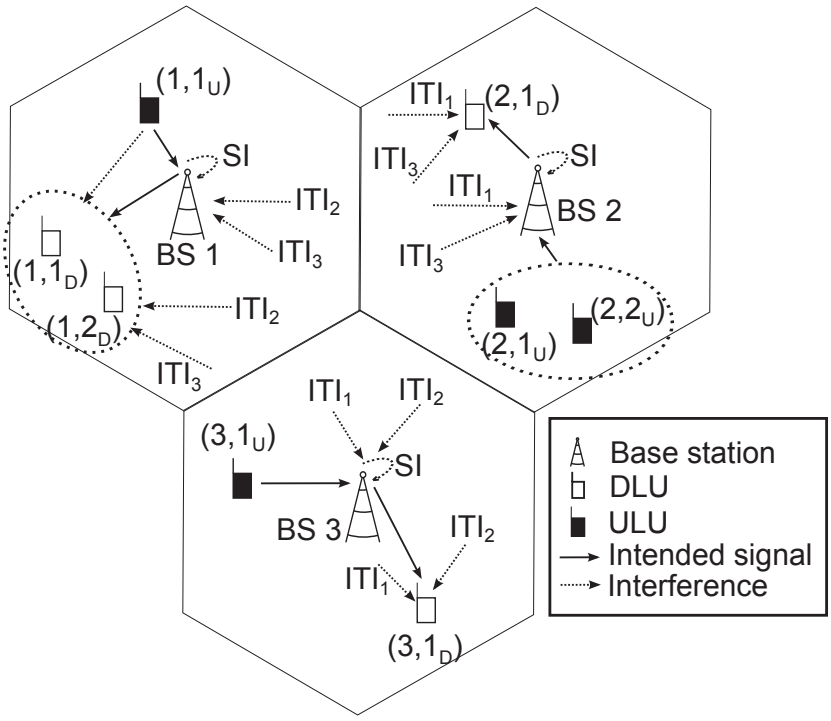

Figure 5.1: Interference scenario in an FD multicell network, where SI denotes the self-interference and ITI_i denotes the interference from the BS and ULUs of cell i.

let us define

$$\mathcal{I} \triangleq \{1, 2, \ldots, I\}; \quad \mathcal{D} \triangleq \{1_{\mathsf{D}}, 2_{\mathsf{D}}, \ldots, D_{\mathsf{D}}\}; \quad \mathcal{U} \triangleq \{1_{\mathsf{U}}, 2_{\mathsf{U}}, \ldots, U_{\mathsf{U}}\};$$
$$\mathcal{S}_1 \triangleq \mathcal{I} \times \mathcal{D}; \quad \mathcal{S}_2 \triangleq \mathcal{I} \times \mathcal{U};$$
$$\mathbf{V}_{\mathsf{D}} = [\mathbf{V}_{i,j_{\mathsf{D}}}]_{(i,j_{\mathsf{D}})\in\mathcal{S}_1}; \mathbf{V}_{\mathsf{U}} = [\mathbf{V}_{i,j_{\mathsf{U}}}]_{(i,j_{\mathsf{U}})\in\mathcal{S}_2}; \mathbf{V} \triangleq [\mathbf{V}_{\mathsf{D}}\ \mathbf{V}_{\mathsf{U}}];$$

In the DL channel, the received signal at DLU (i, j_{D}) is expressed as:

$$y_{i,j_{\mathsf{D}}} \triangleq \underbrace{H_{i,i,j_{\mathsf{D}}}\mathbf{V}_{i,j_{\mathsf{D}}}s_{i,j_{\mathsf{D}}}}_{\text{desired signal}} + \underbrace{\sum_{(m,\ell_{\mathsf{D}})\in\mathcal{S}_1\setminus(i,j_{\mathsf{D}})} H_{m,i,j_{\mathsf{D}}}\mathbf{V}_{m,\ell_{\mathsf{D}}}s_{m,\ell_{\mathsf{D}}}}_{\text{DL interference}} + \underbrace{\sum_{\ell_{\mathsf{U}}\in\mathcal{U}} H_{i,j_{\mathsf{D}},\ell_{\mathsf{U}}}\mathbf{V}_{i,\ell_{\mathsf{U}}}s_{i,\ell_{\mathsf{U}}}}_{\text{UL intracell interference}} + n_{i,j_{\mathsf{D}}}, \tag{5.1}$$

where $H_{m,i,j_{\mathsf{D}}} \in \mathbb{C}^{N_r\times N_1}$ and $H_{i,j_{\mathsf{D}},\ell_{\mathsf{U}}} \in \mathbb{C}^{N_r\times N_r}$ are the channel matrices from BS m to DLU (i, j_{D}) and from ULU (i, ℓ_{U}) to DLU (i, j_{D}), respectively. Also, $n_{i,j_{\mathsf{D}}}$ is the additive white circularly symmetric complex Gaussian noise with variance σ^2_{D}. In this chapter, the UL intercell interference is neglected since it is very small compared to the DL

intercell interference due to the much smaller transmit power of ULUs. Nevertheless, it can be incorporated easily in our formulation.

Assuming that DLUs are equipped by both devices for ID and EH, the power splitting (PS) technique is applied at each DLU to simultaneously conduct information decoding (ID) and energy harvesting (EH). The power splitter divides the received signal y_{i,j_D} into two parts in the proportion of $\boldsymbol{\alpha}_{i,j_\mathsf{D}} : (1-\boldsymbol{\alpha}_{i,j_\mathsf{D}})$ where $\boldsymbol{\alpha}_{i,j_\mathsf{D}} \in (0,1)$ is termed as the PS ratio for DLU (i, j_D). In particular, the signal split to the ID receiver of DLU (i, j_D) is given by

$$\sqrt{\boldsymbol{\alpha}_{i,j_\mathsf{D}}} y_{i,j_\mathsf{D}} + z^c_{i,j_\mathsf{D}}, \tag{5.2}$$

where each r-th element of z^c_{i,j_D} (i.e. $|z^c_{i,j_\mathsf{D},r}|^2 = \sigma_c^2,\ r = 1,..,N_r$) is additional noise introduced by the ID receiver circuity. An EH receiver processes the second part of the split signal $\sqrt{1-\boldsymbol{\alpha}_{i,j_\mathsf{D}}} y_{i,j_\mathsf{D}}$ for the harvested energy

$$\sqrt{\zeta_{i,j_\mathsf{D}}(1-\boldsymbol{\alpha}_{i,j_\mathsf{D}})} y_{i,j_\mathsf{D}},$$

where $\zeta_{i,j_\mathsf{D}} \in (0.4, 0.6)$ is the efficiency of energy conversion. For more complex models of energy harvesting, the reader is refer to [Liu, Zhou, Durrani and Popovski, 2016].

It follows from the receive equation (5.1) and the split equation (5.2) that the downlink information throughput at DLU (i, j_D) is

$$f_{i,j_\mathsf{D}}(\mathbf{V}_\mathsf{D}, \mathbf{V}_\mathsf{U}, \boldsymbol{\alpha}_{i,j_\mathsf{D}}) \triangleq \ln \left| I_{N_r} + (\mathcal{L}_{i,j_\mathsf{D}}(\mathbf{V}_{i,j_\mathsf{D}}))^2 \Psi^{-1}_{i,j_\mathsf{D}}(\mathbf{V}_\mathsf{D}, \mathbf{V}_\mathsf{U}, \boldsymbol{\alpha}_{i,j_\mathsf{D}}) \right|, \tag{5.3}$$

where $\mathcal{L}_{i,j_\mathsf{D}}(\mathbf{V}_{i,j_\mathsf{D}}) \triangleq H_{i,i,j_\mathsf{D}} \mathbf{V}_{i,j_\mathsf{D}}$ and

$$\Psi_{i,j_\mathsf{D}}(\mathbf{V}_\mathsf{D}, \mathbf{V}_\mathsf{U}, \boldsymbol{\alpha}_{i,j_\mathsf{D}}) \triangleq \bar{\Psi}_{i,j_\mathsf{D}}(\mathbf{V}_\mathsf{D}, \mathbf{V}_\mathsf{U}) + (\sigma_c^2/\boldsymbol{\alpha}_{i,j_\mathsf{D}}) I_{N_r} \tag{5.4}$$

with the *downlink interference covariance mapping*

$$\bar{\Psi}_{i,j_\mathsf{D}}(\mathbf{V}_\mathsf{D}, \mathbf{V}_\mathsf{U}) \triangleq \sum_{(m,\ell_\mathsf{D}) \in \mathcal{S}_1 \setminus (i,j_\mathsf{D})} (H_{m,i,j_\mathsf{D}} \mathbf{V}_{m,\ell_\mathsf{D}})^2 + \sum_{\ell_\mathsf{U} \in \mathcal{U}} (H_{i,j_\mathsf{D},\ell_\mathsf{U}} \mathbf{V}_{i,\ell_\mathsf{U}})^2 + \sigma_\mathsf{D} I_{N_r}. \tag{5.5}$$

The harvested energy at UE (i, j_D) is

$$E_{i,j_\mathsf{D}}(\mathbf{V}_\mathsf{D}, \mathbf{V}_\mathsf{U}, \boldsymbol{\alpha}_{i,j_\mathsf{D}}) = \zeta_{i,j_\mathsf{D}}(1-\boldsymbol{\alpha}_{i,j_\mathsf{D}}) \langle \Phi_{i,j_\mathsf{D}}(\mathbf{V}_\mathsf{D}, \mathbf{V}_\mathsf{U}) \rangle, \tag{5.6}$$

with the *downlink signal covariance mapping*

$$\Phi_{i,j_{\mathsf{D}}}(\mathbf{V}_{\mathsf{D}},\mathbf{V}_{\mathsf{U}}) \triangleq \sum_{(m,\ell_{\mathsf{D}})\in\mathcal{S}_1}(H_{m,i,j_{\mathsf{D}}}\mathbf{V}_{m,\ell_{\mathsf{D}}})^2+\sum_{\ell_{\mathsf{U}}\in\mathcal{U}}(H_{i,i_{\mathsf{D}},\ell_{\mathsf{U}}}\mathbf{V}_{i,\ell_{\mathsf{U}}})^2+\sigma_{\mathsf{D}}^2 I_{N_r}. \tag{5.7}$$

In the UL channel, the received signal at BS i is expressed as

$$y_i \triangleq \underbrace{\sum_{\ell_{\mathsf{U}}\in\mathcal{U}} H_{i,\ell_{\mathsf{U}},i}\mathbf{V}_{i,\ell_{\mathsf{U}}}s_{i,\ell_{\mathsf{U}}}}_{\text{desired signal}}+\underbrace{\sum_{m\in\mathcal{I}\setminus\{i\}}\sum_{\ell_{\mathsf{U}}\in\mathcal{U}} H_{m,\ell_{\mathsf{U}},i}\mathbf{V}_{m,\ell_{\mathsf{U}}}s_{m,\ell_{\mathsf{U}}}}_{\text{UL interference}}+\underbrace{\sum_{m\in\mathcal{I}\setminus\{i\}} H_{m,i}^{\mathcal{B}}\sum_{j_{\mathsf{D}}\in\mathcal{D}}\mathbf{V}_{m,j_{\mathsf{D}}}s_{m,s_{\mathsf{D}}}}_{\text{DL intercell interference}}$$
$$+\underbrace{n_i^{SI}}_{\text{residual SI}}+n_i, \tag{5.8}$$

where $H_{m,\ell_{\mathsf{U}},i}\in\mathbb{C}^{N_2\times N_r}$ and $H_{m,i}^{\mathcal{B}}\in\mathbb{C}^{N_2\times N_1}$ are the channel matrices from ULU (m,ℓ_{U}) to BS i and from BS m to BS i, respectively; n_i is the additive white circularly symmetric complex Gaussian noise with variance σ_{U}^2; n_i^{SI} is the residual SI (after self-interference cancellation) at BS i and depends on the transmit power of BS i. Specifically, n_i^{SI} is modelled as the additive white circularly symmetric complex Gaussian noise with variance $\sigma_{SI}^2\sum_{\ell_{\mathsf{D}}\in\mathcal{D}}||\mathbf{V}_{i,\ell_{\mathsf{D}}}||^2$ [Day et al., 2012], where the SI level σ_{SI}^2 is the ratio of the average SI powers after and before the SI cancellation process.

Following [Nguyen et al., 2013, 2014; Tam et al., 2016], the optimal MMSE-SIC decoder is applied at BSs. Therefore, the achievable uplink throughput at BS i is given as [Tse and Viswanath, 2005]

$$f_i(\mathbf{V}_{\mathsf{D}},\mathbf{V}_{\mathsf{U}}) \triangleq \ln\left|I_{N_2}+(\mathcal{L}_i(\mathbf{V}_{\mathsf{U}_i}))^2\Psi_i^{-1}(\mathbf{V}_{\mathsf{D}},\mathbf{V}_{\mathsf{U}})\right|, \tag{5.9}$$

where $\mathbf{V}_{\mathsf{U}_i}\triangleq[\mathbf{V}_{i,\ell_{\mathsf{U}}}]_{\ell_{\mathsf{U}}\in\mathcal{U}}$ and $\mathcal{L}_i(\mathbf{V}_{\mathsf{U}i})\triangleq\left[H_{i,1_{\mathsf{U}},i}\mathbf{V}_{i,1_{\mathsf{U}}},H_{i,2_{\mathsf{U}},i}\mathbf{V}_{i,2_{\mathsf{U}}},\ldots,H_{i,U_{\mathsf{U}},i}\mathbf{V}_{i,U_{\mathsf{U}}}\right]$, which means that $(\mathcal{L}_i(\mathbf{V}_{\mathsf{U}i}))^2=\sum_{\ell=1}^{U}(H_{i,\ell_{\mathsf{U}},i}\mathbf{V}_{i,\ell_{\mathsf{U}}})^2$, and

$$\Psi_i(\mathbf{V}_{\mathsf{D}},\mathbf{V}_{\mathsf{U}}) \triangleq \bar{\Psi}_i^{U}(\mathbf{V}_{\mathsf{U}})+\bar{\Psi}_i^{SI}(\mathbf{V}_{\mathsf{D}}) \tag{5.10}$$

with *uplink interference covariance mapping*

$$\bar{\Psi}_i^{U}(\mathbf{V}_{\mathsf{U}}) \triangleq \sum_{m\in\mathcal{I}\setminus\{i\}}\sum_{\ell_{\mathsf{U}}\in\mathcal{U}}(H_{m,\ell_{\mathsf{U}},i}\mathbf{V}_{m,\ell_{\mathsf{U}}})^2+\sum_{m\in\mathcal{I}\setminus\{i\}}H_{m,i}^{\mathcal{B}}\left(\sum_{j_{\mathsf{D}}\in\mathcal{D}}(\mathbf{V}_{m,j_{\mathsf{D}}})^2\right)(H_{m,i}^{\mathcal{B}})^H+\sigma_{\mathsf{U}}^2 I_{N_2} \tag{5.11}$$

and *SI covariance mapping*

$$\bar{\Psi}_i^{SI}(\mathbf{V}_{\mathsf{D}}) \triangleq \sigma_{SI}^2 \sum_{\ell_{\mathsf{D}} \in \mathcal{D}} ||\mathbf{V}_{i,\ell_{\mathsf{D}}}||^2 I_{N_2}. \tag{5.12}$$

We consider the design problem

$$\max_{\mathbf{V}_{\mathsf{D}},\mathbf{V}_{\mathsf{U}},\boldsymbol{\alpha}} \mathcal{P}_1(\mathbf{V}_{\mathsf{D}},\mathbf{V}_{\mathsf{U}},\boldsymbol{\alpha}) \triangleq \sum_{(i,j_{\mathsf{D}})\in\mathcal{S}_1} f_{i,j_{\mathsf{D}}}(\mathbf{V}_{\mathsf{D}},\mathbf{V}_{\mathsf{U}},\boldsymbol{\alpha}_{i,j_{\mathsf{D}}}) + \sum_{i\in\mathcal{I}} f_i(\mathbf{V}_{\mathsf{D}},\mathbf{V}_{\mathsf{U}}) \quad \text{s.t.} \tag{5.13a}$$

$$0 < \boldsymbol{\alpha}_{i,j_{\mathsf{D}}} < 1, (i,j_{\mathsf{D}}) \in \mathcal{S}_1, \tag{5.13b}$$

$$\sum_{(i,j_{\mathsf{D}})\in\mathcal{S}_1} ||\mathbf{V}_{i,j_{\mathsf{D}}}||^2 + \sum_{(i,j_{\mathsf{U}})\in\mathcal{S}_2} ||\mathbf{V}_{i,j_{\mathsf{U}}}||^2 \leq P, \tag{5.13c}$$

$$\sum_{j_{\mathsf{D}}\in\mathcal{D}} ||\mathbf{V}_{i,j_{\mathsf{D}}}||^2 \leq P_i, \forall i \in \mathcal{I}, \tag{5.13d}$$

$$||\mathbf{V}_{i,j_{\mathsf{U}}}||^2 \leq P_{i,j_{\mathsf{U}}}, \forall (i,j_{\mathsf{U}}) \in \mathcal{S}_2, \tag{5.13e}$$

$$\langle \Phi_{i,j_{\mathsf{D}}}(\mathbf{V}_{\mathsf{D}},\mathbf{V}_{\mathsf{U}}) \rangle \geq e_{i,j_{\mathsf{D}}}^{\min}/\zeta_{i,j_{\mathsf{D}}}(1-\boldsymbol{\alpha}_{i,j_{\mathsf{D}}}), \forall (i,j_{\mathsf{D}}) \in \mathcal{S}_1, \tag{5.13f}$$

$$f_i(\mathbf{V}_{\mathsf{D}},\mathbf{V}_{\mathsf{U}}) \geq r_i^{\mathsf{U},\min}, \forall i \in \mathcal{I} \tag{5.13g}$$

$$f_{i,j_{\mathsf{D}}}(\mathbf{V}_{\mathsf{D}},\mathbf{V}_{\mathsf{U}},\boldsymbol{\alpha}_{i,j_{\mathsf{D}}}) \geq r_{i,j_{\mathsf{D}}}^{\mathsf{D},\min}, \forall (i,j_{\mathsf{D}}) \in \mathcal{S}_1. \tag{5.13h}$$

The convex constraints (5.13d) and (5.13e) specify the maximum transmit power available at the BSs and the ULUs whereas (5.13c) limits the total transmit power of the whole network. The nonconvex constraints (5.13f), (5.13g) and (5.13h) represent QoS guarantee, where $e_{i,j_{\mathsf{D}}}^{\min}, r_i^{\mathsf{U},\min}$ and $r_{i,j_{\mathsf{D}}}^{\mathsf{D},\min}$ are the minimum harvested energy required by DLU (i,j_{D}), the minimum data throughput required by BS i and the minimum data throughput required by DLU (i,j_{D}). In comparison to (4.7) in Chapter 4 for FD non-EH-enable networks, the UL throughput function $f_i(\mathbf{V}_{\mathsf{D}},\mathbf{V}_{\mathsf{U}})$ in (5.9) is the same, where the DL throughput function $f_{i,j_{\mathsf{D}}}(\mathbf{V}_{\mathsf{D}},\mathbf{V}_{\mathsf{U}},\boldsymbol{\alpha}_{i,j_{\mathsf{D}}})$ is now additionally dependent on the SP variable $\boldsymbol{\alpha}_{i,j_{\mathsf{D}}}$, is decoupled in (5.5) and thus does not add more difficulty as we will show now. We also show that the nonconvex EH constraints (5.13f) can easily be innerly approximated.

Under the definitions,

$$\mathcal{M}_{i,j_{\mathsf{D}}}(\mathbf{V}_{\mathsf{D}},\mathbf{V}_{\mathsf{U}},\boldsymbol{\alpha}_{i,j_{\mathsf{D}}}) \triangleq (\mathcal{L}_{i,j_{\mathsf{D}}}(\mathbf{V}_{i,j_{\mathsf{D}}}))^2 + \Psi_{i,j_{\mathsf{D}}}(\mathbf{V}_{\mathsf{D}},\mathbf{V}_{\mathsf{U}},\boldsymbol{\alpha}_{i,j_{\mathsf{D}}}) \tag{5.14}$$

$$\succeq \Psi_{i,j_{\mathsf{D}}}(\mathbf{V}_{\mathsf{D}},\mathbf{V}_{\mathsf{U}},\boldsymbol{\alpha}_{i,j_{\mathsf{D}}}), \tag{5.15}$$

$$\mathcal{M}_{i}(\mathbf{V}_{\mathsf{D}},\mathbf{V}_{\mathsf{U}}) \triangleq (\mathcal{L}_{i}(\mathbf{V}_{\mathsf{U}i}))^2 + \Psi_{i}(\mathbf{V}_{\mathsf{D}},\mathbf{V}_{\mathsf{U}}) \tag{5.16}$$

$$\succeq \Psi_{i}(\mathbf{V}_{\mathsf{D}},\mathbf{V}_{\mathsf{U}}), \tag{5.17}$$

by applying Theorem 5.1, we obtain the following concave quadratic minorants of throughput functions $f_{i,j_{\mathsf{D}}}(\mathbf{V}_{\mathsf{D}},\mathbf{V}_{\mathsf{U}},\boldsymbol{\alpha}_{i,j_{\mathsf{D}}})$ and $f_i(\mathbf{V}_{\mathsf{D}}^{(\kappa)},\mathbf{V}_{\mathsf{U}}^{(\kappa)})$ at $(V_{\mathsf{D}}^{(\kappa)},V_{\mathsf{U}}^{(\kappa)},\alpha^{(\kappa)}) \triangleq ([V_{i,j_{\mathsf{D}}}^{(\kappa)}]_{(i,j_{\mathsf{D}})\in\mathcal{S}_1},\,[V_{i,\ell_{\mathsf{U}}}^{(\kappa)}]_{(i,\ell_{\mathsf{U}})\in\mathcal{S}_2},[\alpha_{i,j_{\mathsf{D}}}^{(\kappa)}]_{(i,j_{\mathsf{D}})\in\mathcal{S}_1})$:

$$\Theta_{i,j_{\mathsf{D}}}^{(\kappa)}(\mathbf{V}_{\mathsf{D}},\mathbf{V}_{\mathsf{U}},\boldsymbol{\alpha}_{i,j_{\mathsf{D}}}) \triangleq a_{i,j_{\mathsf{D}}}^{(\kappa)} + 2\,\mathrm{Re}\left\{\langle \mathcal{A}_{i,j_{\mathsf{D}}}^{(\kappa)}, \mathcal{L}_{i,j_{\mathsf{D}}}(\mathbf{V}_{i,j_{\mathsf{D}}})\rangle\right\} - \langle \mathcal{B}_{i,j_{\mathsf{D}}}^{(\kappa)}, \mathcal{M}_{i,j_{\mathsf{D}}}(\mathbf{V}_{\mathsf{D}},\mathbf{V}_{\mathsf{U}},\boldsymbol{\alpha}_{i,j_{\mathsf{D}}})\rangle \tag{5.18}$$

and

$$\Theta_{i}^{(\kappa)}(\mathbf{V}_{\mathsf{D}},\mathbf{V}_{\mathsf{U}}) \triangleq a_{i}^{(\kappa)} + 2\,\mathrm{Re}\left\{\langle \mathcal{A}_{i}^{(\kappa)}, \mathcal{L}_{i}(\mathbf{V}_{\mathsf{U}_i})\rangle\right\} - \langle \mathcal{B}_{i}^{(\kappa)}, \mathcal{M}_{i}(\mathbf{V}_{\mathsf{D}},\mathbf{V}_{\mathsf{U}})\rangle, \tag{5.19}$$

where

$$\begin{aligned} 0 > a_{i,j_{\mathsf{D}}}^{(\kappa)} &= f_{i,j_{\mathsf{D}}}(V_{\mathsf{D}}^{(\kappa)},V_{\mathsf{U}}^{(\kappa)},\alpha_{i,j_{\mathsf{D}}}^{(\kappa)}) - \mathrm{Re}\left\{\langle \Psi_{i,j_{\mathsf{D}}}^{-1}(V_{\mathsf{D}}^{(\kappa)},V_{\mathsf{U}}^{(\kappa)})\mathcal{L}_{i,j_{\mathsf{D}}}(V_{i,j_{\mathsf{D}}}^{(\kappa)}), \mathcal{L}_{i,j_{\mathsf{D}}}(V_{i,j_{\mathsf{D}}}^{(\kappa)})\rangle\right\},\\ \mathcal{A}_{i,j_{\mathsf{D}}}^{(\kappa)} &= \Psi_{i,j_{\mathsf{D}}}^{-1}(V_{\mathsf{D}}^{(\kappa)},V_{\mathsf{U}}^{(\kappa)},\alpha_{i,j_{\mathsf{D}}}^{(\kappa)})\mathcal{L}_{i,j_{\mathsf{D}}}(V_{i,j_{\mathsf{D}}}^{(\kappa)}),\\ 0 \preceq \mathcal{B}_{i,j_{\mathsf{D}}}^{(\kappa)} &= \Psi_{i,j_{\mathsf{D}}}^{-1}(V_{\mathsf{D}}^{(\kappa)},V_{\mathsf{U}}^{(\kappa)},\alpha_{i,j_{\mathsf{D}}}^{(\kappa)}) - \mathcal{M}_{i,j_{\mathsf{D}}}^{-1}(V_{\mathsf{D}}^{(\kappa)},V_{\mathsf{U}}^{(\kappa)},\alpha_{i,j_{\mathsf{D}}}^{(\kappa)}), \end{aligned} \tag{5.20}$$

and

$$\begin{aligned} 0 > a_{i}^{(\kappa)} &= f_{i}(V_{\mathsf{D}}^{(\kappa)},V_{\mathsf{U}}^{(\kappa)}) - \mathrm{Re}\left\{\langle \Psi_{i}^{-1}(V_{\mathsf{D}}^{(\kappa)},V_{\mathsf{U}}^{(\kappa)})\mathcal{L}_{i}(V_{i}^{(\kappa)}), \mathcal{L}_{i}(V_{i}^{(\kappa)})\rangle\right\},\\ \mathcal{A}_{i}^{(\kappa)} &= \Psi_{i}^{-1}(V_{\mathsf{D}}^{(\kappa)},V_{\mathsf{U}}^{(\kappa)})\mathcal{L}_{i}(V_{\mathsf{U}_i}^{(\kappa)}),\\ 0 \preceq \mathcal{B}_{i}^{(\kappa)} &= \Psi_{i}^{-1}(V_{\mathsf{D}}^{(\kappa)},V_{\mathsf{U}}^{(\kappa)}) - \mathcal{M}_{i}^{-1}(V_{\mathsf{D}}^{(\kappa)},V_{\mathsf{U}}^{(\kappa)}). \end{aligned} \tag{5.21}$$

To handle the nonconvex EH constraints (5.13f), we define an affine function $\phi_{i,j_{\mathsf{D}}}^{(\kappa)}(\mathbf{V}_{\mathsf{D}},\mathbf{V}_{\mathsf{U}})$ as the first-order approximation of the convex function $\langle \Phi_{i,j_{\mathsf{D}}}(\mathbf{V}_{\mathsf{D}},\mathbf{V}_{\mathsf{U}})\rangle$ at $(V_{\mathsf{D}}^{(\kappa)},V_{\mathsf{U}}^{(\kappa)})$:

$$\begin{aligned} \phi_{i,j_{\mathsf{D}}}^{(\kappa)}(\mathbf{V}_{\mathsf{D}},\mathbf{V}_{\mathsf{U}}) \triangleq &-\langle \Phi_{i,j_{\mathsf{D}}}(V_{\mathsf{D}}^{(\kappa)},V_{\mathsf{U}}^{(\kappa)})\rangle + 2\,\mathrm{Re}\{\sum_{(m,\ell_{\mathsf{D}})\in\mathcal{S}_1}\langle H_{m,i,j_{\mathsf{D}}}V_{m,\ell_{\mathsf{D}}}^{(\kappa)}\mathbf{V}_{m,\ell_{\mathsf{D}}}H_{m,i,j_{\mathsf{D}}}^{H}\rangle\}\\ &+2\,\mathrm{Re}\{\textstyle\sum_{\ell_{\mathsf{U}}\in\mathcal{U}}\langle H_{i,i_{\mathsf{D}},\ell_{\mathsf{U}}}V_{i,\ell_{\mathsf{U}}}^{(\kappa)}\mathbf{V}_{i,\ell_{\mathsf{U}}}^{H}H_{i,i_{\mathsf{D}},\ell_{\mathsf{U}}}^{H}\rangle\} + 2\sigma_{\mathsf{D}}^2N_r, \end{aligned} \tag{5.22}$$

which is an minorant of $\langle \Phi_{i,j_{\mathsf{D}}}(\mathbf{V}_{\mathsf{D}}, \mathbf{V}_{\mathsf{U}}) \rangle$ at $(V_{\mathsf{D}}^{(\kappa)}, V_{\mathsf{U}}^{(\kappa)})$ [Tuy, 1998].

We now address the nonconvex problem (5.13) by successively solving its following inner approximation:

$$\max_{\mathbf{V}_{\mathsf{D}}, \mathbf{V}_{\mathsf{U}}, \boldsymbol{\alpha}} \sum_{(i,j_{\mathsf{D}}) \in \mathcal{S}_1} \mathcal{P}_1^{(\kappa)}(\mathbf{V}_{\mathsf{D}}, \mathbf{V}_{\mathsf{U}}, \boldsymbol{\alpha}) \triangleq \Theta_{i,j_{\mathsf{D}}}^{(\kappa)}(\mathbf{V}_{\mathsf{D}}, \mathbf{V}_{\mathsf{U}}, \boldsymbol{\alpha}_{i,j_{\mathsf{D}}}) + \sum_{i \in \mathcal{I}} \Theta_i^{(\kappa)}(\mathbf{V}_{\mathsf{D}}, \mathbf{V}_{\mathsf{U}}) \quad (5.23a)$$

$$\text{s.t.} \quad (5.13b) - (5.13e) \quad (5.23b)$$

$$\phi_{i,j_{\mathsf{D}}}^{(\kappa)}(\mathbf{V}_{\mathsf{D}}, \mathbf{V}_{\mathsf{U}}) \geq e_{i,j_{\mathsf{D}}}^{\min} / \zeta_{i,j_{\mathsf{D}}}(1 - \boldsymbol{\alpha}_{i,j_{\mathsf{D}}}), \forall (i, j_{\mathsf{D}}) \in \mathcal{S}_1, \quad (5.23c)$$

$$\Theta_i^{(\kappa)}(\mathbf{V}_{\mathsf{D}}, \mathbf{V}_{\mathsf{U}}) \geq r_i^{\mathsf{U},\min}, \forall i \in \mathcal{I} \quad (5.23d)$$

$$\Theta_{i,j_{\mathsf{D}}}^{(\kappa)}(\mathbf{V}_{\mathsf{D}}, \mathbf{V}_{\mathsf{U}}, \boldsymbol{\alpha}_{i,j_{\mathsf{D}}}) \geq r_{i,j_{\mathsf{D}}}^{\mathsf{D},\min}, \forall (i, j_{\mathsf{D}}) \in \mathcal{S}_1. \quad (5.23e)$$

Initializing from $(V_{\mathsf{D}}^{(\kappa)}, V_{\mathsf{U}}^{(\kappa)}, \alpha^{(\kappa)})$ being feasible point to (5.13), the optimal solution $(V_{\mathsf{D}}^{(\kappa+1)}, V_{\mathsf{U}}^{(\kappa+1)}, \alpha^{(\kappa+1)})$ of convex program (5.23) is feasible to the nonconvex program (5.13) and it is better than $(V_{\mathsf{D}}^{(\kappa)}, V_{\mathsf{U}}^{(\kappa)}, \alpha^{(\kappa)})$:

$$\begin{aligned} \mathcal{P}_1(V_{\mathsf{D}}^{(\kappa+1)}, V_{\mathsf{U}}^{(\kappa+1)}, \alpha^{(\kappa+1)}) &\geq \mathcal{P}_1^{(\kappa)}(V_{\mathsf{D}}^{(\kappa+1)}, V_{\mathsf{U}}^{(\kappa+1)}, \alpha^{(\kappa+1)}) && (5.24) \\ &\geq \mathcal{P}_1^{(\kappa)}(V_{\mathsf{D}}^{(\kappa)}, V_{\mathsf{U}}^{(\kappa)}, \alpha^{(\kappa)}) && (5.25) \\ &= \mathcal{P}_1(V_{\mathsf{D}}^{(\kappa)}, V_{\mathsf{U}}^{(\kappa)}, \alpha^{(\kappa)}), && (5.26) \end{aligned}$$

where the inequality (5.24) and the equality (5.26) follow from the fact that $\mathcal{P}_1^{(\kappa)}$ is a minorant of $\mathcal{P}_1$ while the inequality (5.25) follows from the fact that $(V_{\mathsf{D}}^{(\kappa+1)}, V_{\mathsf{U}}^{(\kappa+1)}, \alpha^{(\kappa+1)})$ and $(V_{\mathsf{D}}^{(\kappa)}, V_{\mathsf{U}}^{(\kappa)}, \alpha^{(\kappa)})$ are the optimal solution and feasible point of (5.23), respectively. This generates a sequence $\{(V_{\mathsf{D}}^{(\kappa)}, V_{\mathsf{U}}^{(\kappa)}, \alpha^{(\kappa)})\}$ of feasible and improved points which converge to a local optimum of (5.13) after finitely many iterations.

Algorithm 6 Path-following algorithm for PS sum throughput maximization (5.13)

Initialization: Set $\kappa := 0$, and choose a feasible point $(V_{\mathsf{D}}^{(0)}, V_{\mathsf{U}}^{(0)}, \alpha^{(0)})$ that satisfies (5.13b)-(5.13h).

κ-th iteration: Solve (5.23) for an optimal solution $(V_{\mathsf{D}}^{*}, V_{\mathsf{U}}^{*}, \alpha^{*})$ and set $\kappa := \kappa + 1$, $(V_{\mathsf{D}}^{(\kappa)}, V_{\mathsf{U}}^{(\kappa)}, \alpha^{(\kappa)}) := (V_{\mathsf{D}}^{*}, V_{\mathsf{U}}^{*}, \alpha^{*})$ and calculate $\mathcal{P}_1(V_{\mathsf{D}}^{(\kappa)}, V_{\mathsf{U}}^{(\kappa)}, \alpha^{(\kappa)})$. Stop if $\left| \left(\mathcal{P}_1(V_{\mathsf{D}}^{(\kappa)}, V_{\mathsf{U}}^{(\kappa)}, \alpha^{(\kappa)}) - \mathcal{P}_1(V_{\mathsf{D}}^{(\kappa-1)}, V_{\mathsf{U}}^{(\kappa-1)}, \alpha^{(\kappa-1)}) \right) / \mathcal{P}_1(V_{\mathsf{D}}^{(\kappa-1)}, V_{\mathsf{U}}^{(\kappa-1)}, \alpha^{(\kappa-1)}) \right| \leq \epsilon$.

The proposed path-following procedure that solves problem (5.13) is summarized in Algorithm 6. To find a feasible initial point $(V_{\mathsf{D}}^{(0)}, V_{\mathsf{U}}^{(0)}, \alpha^{(0)})$ meeting the nonconvex constraints (5.13f)-(5.13h) we consider the following problem:

$$\begin{aligned}\max_{\mathbf{V}_{\mathsf{D}},\mathbf{V}_{\mathsf{U}},\boldsymbol{\alpha}} \mathcal{P}_{1,f}(\mathbf{V}_{\mathsf{D}},\mathbf{V}_{\mathsf{U}},\boldsymbol{\alpha}) \triangleq \min_{(i,j_{\mathsf{D}})\in\mathcal{S}_1} \Big\{ & f_{i,j_{\mathsf{D}}}(\mathbf{V}_{\mathsf{D}},\mathbf{V}_{\mathsf{U}},\boldsymbol{\alpha}) - r_{i,i_{\mathsf{D}}}^{\min}, \\ \Phi_{i,j_{\mathsf{D}}}(\mathbf{V}_{\mathsf{D}},\mathbf{V}_{\mathsf{U}}) - \tfrac{e_{i,j_{\mathsf{D}}}^{\min}}{\zeta_{i,j_{\mathsf{D}}}(1-\boldsymbol{\alpha}_{i,j_{\mathsf{D}}})}, & f_i(\mathbf{V}_{\mathsf{D}},\mathbf{V}_{\mathsf{U}}) - r_i^{\min}, \Big\} \quad \text{s.t.} \quad (5.13\text{b}) - (5.13\text{e}).\end{aligned} \tag{5.27}$$

Initialized by a $(V_{\mathsf{D}}^{(0)}, V_{\mathsf{U}}^{(0)}, \alpha^{(0)})$ feasible to the convex constraints (5.13b)-(5.13e), an iterative point $(V_{\mathsf{D}}^{(\kappa+1)}, V_{\mathsf{U}}^{(\kappa+1)}, \alpha^{(\kappa+1)})$ for $\kappa = 0, 1, \ldots,$ is generated as the optimal solution of the following convex maximin program:

$$\begin{aligned}\max_{\mathbf{V}_{\mathsf{D}},\mathbf{V}_{\mathsf{U}},\boldsymbol{\alpha}} \mathcal{P}_{1,f}^{(\kappa)}(\mathbf{V}_{\mathsf{D}},\mathbf{V}_{\mathsf{U}},\boldsymbol{\alpha}) \triangleq \min_{(i,j_{\mathsf{D}})\in\mathcal{S}_1} \Big\{ & \langle \Theta_{i,j_{\mathsf{D}}}^{(\kappa)}(\mathbf{V}_{\mathsf{D}},\mathbf{V}_{\mathsf{U}},\boldsymbol{\alpha}) - r_{i,i_{\mathsf{D}}}^{\min}, \\ \Theta_i^{(\kappa)}(\mathbf{V}_{\mathsf{D}},\mathbf{V}_{\mathsf{U}}) - r_i^{\min}, & \phi_{i,j_{\mathsf{D}}}^{(\kappa)}(\mathbf{V}_{\mathsf{D}},\mathbf{V}_{\mathsf{U}}) - \tfrac{e_{i,j_{\mathsf{D}}}^{\min}}{\zeta_{i,j_{\mathsf{D}}}(1-\boldsymbol{\alpha}_{i,j_{\mathsf{D}}})} \Big\} \quad \text{s.t} \quad (5.13\text{b}) - (5.13\text{e}).\end{aligned} \tag{5.28}$$

which terminates upon reaching

$$\begin{aligned} & f_{i,j_{\mathsf{D}}}(V_{\mathsf{D}}^{(\kappa)}, V_{\mathsf{U}}^{(\kappa)}, \alpha^{(\kappa)}) \geq r_{i,i_{\mathsf{D}}}^{\min}, f_i(V_{\mathsf{D}}^{(\kappa)}, V_{\mathsf{U}}^{(\kappa)}) \geq r_i^{\min}, \\ & \langle \Phi_{i,j_{\mathsf{D}}}(V_{\mathsf{D}}^{(\kappa)}, V_{\mathsf{U}}^{(\kappa)}) \rangle \geq \frac{e_{i,j_{\mathsf{D}}}^{\min}}{\zeta_{i,j_{\mathsf{D}}}(1-\boldsymbol{\alpha}_{i,j_{\mathsf{D}}})}, \ \forall (i,j_{\mathsf{D}}) \in \mathcal{S}_1 \end{aligned}$$

to satisfy (5.13b)-(5.13h).

In parallel, we consider the following transmission strategy to configure FD BSs to operate in the HD mode. Here, all antennas $N = N_1 + N_2$ at each BS are used to serve all the DLUs in the downlink and all the ULUs in the uplink using half time slots, where DLUs are allowed to harvest energy from ULUs. The problem can be formulated as

$$\max_{\mathbf{V}_{\mathsf{D}},\mathbf{V}_{\mathsf{U}},\boldsymbol{\alpha}} \frac{1}{2}\left[\sum_{(i,j_{\mathsf{D}})\in\mathcal{S}_1} f_{i,j_{\mathsf{D}}}(\mathbf{V}_{\mathsf{D}}, 0_{\mathsf{U}}, \boldsymbol{\alpha}_{i,j_{\mathsf{D}}}) + \sum_{i\in\mathcal{I}} f_i(0_{\mathsf{D}}, \mathbf{V}_{\mathsf{U}})\right] \quad \text{s.t.} \tag{5.29a}$$

$$(5.13\text{b}), (5.13\text{c}), (5.13\text{d}), (5.13\text{e}),$$

$$\frac{1}{2}(E_{i,j_{\mathsf{D}}}(\mathbf{V}_{\mathsf{D}}, 0_{\mathsf{U}}, \boldsymbol{\alpha}_{i,j_{\mathsf{D}}}) + E_{i,j_{\mathsf{D}}}(0_{\mathsf{D}}, \mathbf{V}_{\mathsf{U}}, 0)) \geq e_{i,j_{\mathsf{D}}}^{\min}, \forall (i,j_{\mathsf{D}}) \in \mathcal{S}_1, \tag{5.29b}$$

$$\frac{1}{2} f_i(0_{\mathsf{D}}, \mathbf{V}_{\mathsf{U}}) \geq r_i^{\mathsf{U},\min}, \forall i \in \mathcal{I} \tag{5.29c}$$

$$\frac{1}{2} f_{i,j_{\mathsf{D}}}(\mathbf{V}_{\mathsf{D}}, 0_{\mathsf{U}}, \boldsymbol{\alpha}_{i,j_{\mathsf{D}}}) \geq r_{i,j_{\mathsf{D}}}^{\mathsf{D},\min}, \forall (i,j_{\mathsf{D}}) \in \mathcal{S}_1, \tag{5.29d}$$

where 0_{D} and 0_{U} are zero quantity of the same dimension with $\mathbf{V}_{\mathsf{D}}$ and $\mathbf{V}_{\mathsf{U}}$. In (5.29), DLU (i, j_{D}) uses $(1-\boldsymbol{\alpha}_{i,j_{\mathsf{D}}})$ of the received signal during DL transmission and the whole received signal during UL transmission for EH as formulated in (5.29b). The main difference between (5.13) and (5.29) is in (5.29b) where the harvested energy from UL transmission at DLU (i, j_{D}) does not multiply with $\boldsymbol{\alpha}_{i,j_{\mathsf{D}}}$. The constraint (5.29b) can be recast as

$$\langle \Phi_{i,j_{\mathsf{D}}}(\mathbf{V}_{\mathsf{D}}, 0_{\mathsf{U}})\rangle + \frac{\langle \Phi_{i,j_{\mathsf{D}}}(0_{\mathsf{D}}, \mathbf{V}_{\mathsf{U}})\rangle}{(1-\boldsymbol{\alpha}_{i,j_{\mathsf{D}}})} \geq \frac{2e^{\min}_{i,j_{\mathsf{D}}}}{\zeta_{i,j_{\mathsf{D}}}(1-\boldsymbol{\alpha}_{i,j_{\mathsf{D}}})}.$$

Define the following convex function:

$$\Lambda_{i,j_{\mathsf{D}}}(\mathbf{V}_{\mathsf{U}}, \boldsymbol{\alpha}_{i,j_{\mathsf{D}}}) \triangleq \frac{\langle \Phi_{i,j_{\mathsf{D}}}(0_{\mathsf{D}}, \mathbf{V}_{\mathsf{U}})\rangle}{(1-\boldsymbol{\alpha}_{i,j_{\mathsf{D}}})} = \frac{\langle \sum_{\ell_{\mathsf{U}}\in\mathcal{U}}(H_{i,i_{\mathsf{D}},\ell_{\mathsf{U}}}\mathbf{V}_{i,\ell_{\mathsf{U}}})^2 + \sigma^2_{\mathsf{D}} I_{N_r}\rangle}{1-\boldsymbol{\alpha}_{i,j_{\mathsf{D}}}}, \tag{5.30}$$

with its first-order approximation

$$\begin{aligned}\Lambda^{(\kappa)}_{i,j_{\mathsf{D}}}(\mathbf{V}_{\mathsf{U}}, 1-\boldsymbol{\alpha}_{i,j_{\mathsf{D}}}) \;\triangleq\; & \frac{2\,\mathrm{Re}\{\langle \sum_{\ell_{\mathsf{U}}\in\mathcal{U}}(H_{i,i_{\mathsf{D}},\ell_{\mathsf{U}}}\mathbf{V}_{i,\ell_{\mathsf{U}}})(H_{i,i_{\mathsf{D}},\ell_{\mathsf{U}}}V^{(\kappa)}_{i,\ell_{\mathsf{U}}})^H\rangle\}}{1-\alpha^{(\kappa)}_{i,j_{\mathsf{D}}}} \\ & - \frac{\langle \sum_{\ell_{\mathsf{U}}\in\mathcal{U}}(H_{i,i_{\mathsf{D}},\ell_{\mathsf{U}}}V^{(\kappa)}_{i,\ell_{\mathsf{U}}})^2 + \sigma^2_{\mathsf{D}} I_{N_r}\rangle}{(1-\alpha^{(\kappa)}_{i,j_{\mathsf{D}}})^2}(1-\boldsymbol{\alpha}_{i,j_{\mathsf{D}}})\end{aligned} \tag{5.31}$$

which is its minorant at $(V^{(\kappa)}_{\mathsf{D}}, V^{(\kappa)}_{\mathsf{U}}, \alpha^{(\kappa)})$.

Algorithm 6 can be used with the following convex program solved for κ-iteration:

$$\max_{\mathbf{V}_{\mathsf{D}},\mathbf{V}_{\mathsf{U}},\boldsymbol{\alpha}} \frac{1}{2}\left[\sum_{(i,j_{\mathsf{D}})\in\mathcal{S}_1}\Theta^{(\kappa)}_{i,j_{\mathsf{D}}}(\mathbf{V}_{\mathsf{D}}, 0_{\mathsf{U}}, \boldsymbol{\alpha}_{i,j_{\mathsf{D}}}) + \sum_{i\in\mathcal{I}}\Theta^{(\kappa)}_{i}(0_{\mathsf{D}}, \mathbf{V}_{\mathsf{U}}, 0)\right] \tag{5.32a}$$

$$\text{s.t. (5.13b), (5.13c), (5.13d), (5.13e),}$$

$$\phi^{(\kappa)}_{i,j_{\mathsf{D}}}(\mathbf{V}_{\mathsf{D}}, 0_{\mathsf{U}}) + \Lambda^{(\kappa)}_{i,j_{\mathsf{D}}}(\mathbf{V}_{\mathsf{U}}, 1-\boldsymbol{\alpha}_{i,j_{\mathsf{D}}}) \geq 2e^{\min}_{i,j_{\mathsf{D}}}/\zeta_{i,j_{\mathsf{D}}}(1-\boldsymbol{\alpha}_{i,j_{\mathsf{D}}}), \forall (i,j_{\mathsf{D}})\in\mathcal{S}_1, \tag{5.32b}$$

$$\frac{1}{2}\Theta^{(\kappa)}_{i}(0_{\mathsf{D}}, \mathbf{V}_{\mathsf{U}}) \geq r^{\mathsf{U},\min}_{i}, \forall i\in\mathcal{I} \tag{5.32c}$$

$$\frac{1}{2}\Theta^{(\kappa)}_{i,j_{\mathsf{D}}}(\mathbf{V}_{\mathsf{D}}, 0_{\mathsf{U}}, \boldsymbol{\alpha}_{i,j_{\mathsf{D}}}) \geq r^{\mathsf{D},\min}_{i,j_{\mathsf{D}}}, \forall (i,j_{\mathsf{D}})\in\mathcal{S}_1, \tag{5.32d}$$

where $\phi^{(\kappa)}_{i,j_{\mathsf{D}}}(\mathbf{V}_{\mathsf{D}}, 0_{\mathsf{U}})$ and $\Theta^{(\kappa)}_{i,j_{\mathsf{D}}}(\mathbf{V}_{\mathsf{D}}, 0_{\mathsf{U}}, \boldsymbol{\alpha}_{i,j_{\mathsf{D}}})$ are defined by (5.22) and (5.18) with both $\mathbf{V}_{\mathsf{U}}$ and $V^{(\kappa)}_{\mathsf{U}}$ replaced by 0_{U}, while $\Theta^{(\kappa)}_{i}(0_{\mathsf{D}}, \mathbf{V}_{\mathsf{U}})$ is defined by (5.19) with both $\mathbf{V}_{\mathsf{D}}$ and $V^{(\kappa)}_{\mathsf{D}}$ replaced by 0_{D}.

5.3 EH-enabled FD MU-MIMO by Time Switching

A much easier implementation is time splitting $0 < \boldsymbol{\alpha} < 1$ in downlink transmission where $(1-\boldsymbol{\alpha})$ time is used for DL energy transfer and $\boldsymbol{\alpha}$ time is used for DL information transmission. In this section, we define $\mathbf{V}_{\mathsf{D}}^{I} \triangleq [\mathbf{V}_{i,j_{\mathsf{D}}}^{I}]_{(i,j_{\mathsf{D}})\in\mathcal{S}_1}$, $\mathbf{V}_{\mathsf{D}}^{E} \triangleq [\mathbf{V}_{i,j_{\mathsf{D}}}^{E}]_{(i,j_{\mathsf{D}})\in\mathcal{S}_1}$ and redefine the notation $\mathbf{V}_{\mathsf{D}} \triangleq [\mathbf{V}_{\mathsf{D}}^{I}, \mathbf{V}_{\mathsf{D}}^{E}]$ where $\mathbf{V}_{i,j_{\mathsf{D}}}^{I}$ and $\mathbf{V}_{i,j_{\mathsf{D}}}^{E}$ are the information precoding matrix for ID and energy precoding matrix for EH, respectively. The received signal at DLU (i, j_{D}) for EH is

$$y_{i,j_{\mathsf{D}}}^{E} \triangleq \sum_{(m,\ell_{\mathsf{D}})\in\mathcal{S}_1} H_{m,i,j_{\mathsf{D}}} \mathbf{V}_{m,\ell_{\mathsf{D}}}^{E} s_{m,\ell_{\mathsf{D}}}^{E} + \underbrace{\sum_{\ell_{\mathsf{U}}\in\mathcal{U}} H_{i,i_{\mathsf{D}},\ell_{\mathsf{U}}} \mathbf{V}_{i,\ell_{\mathsf{U}}} s_{i,\ell_{\mathsf{U}}}}_{\text{UL intracell interference}} + n_{j_{\mathsf{D}}}, \tag{5.33}$$

where $s_{m,\ell_{\mathsf{D}}}^{E}$ is the energy signal sent for $(1-\boldsymbol{\alpha})$ time. With the definition (5.6), the harvested energy is

$$E_{i,j_{\mathsf{D}}}(\mathbf{V}_{\mathsf{D}}^{E}, \mathbf{V}_{\mathsf{U}}, \boldsymbol{\alpha}) = \zeta_{i,j_{\mathsf{D}}}(1-\boldsymbol{\alpha})\langle \Phi_{i,j_{\mathsf{D}}}(\mathbf{V}_{\mathsf{D}}^{E}, \mathbf{V}_{\mathsf{U}})\rangle,$$

where the downlink signal covariance mapping $\Phi_{i,j_{\mathsf{D}}}(.,.)$ is defined from (5.7).
Similarly to (5.1), the signal received at DLU (i, j_{D}) during the information transmission in time fraction $\boldsymbol{\alpha}$ is

$$y_{i,j_{\mathsf{D}}}^{I} \triangleq \underbrace{H_{i,i,j_{\mathsf{D}}} \mathbf{V}_{i,j_{\mathsf{D}}} s_{i,j_{\mathsf{D}}}^{I}}_{\text{desired signal}} + \underbrace{\sum_{(m,\ell_{\mathsf{D}})\in\mathcal{S}_1\setminus(i,j_{\mathsf{D}})} H_{m,i,j_{\mathsf{D}}} \mathbf{V}_{m,\ell_{\mathsf{D}}} s_{m,\ell_{\mathsf{D}}}^{I}}_{\text{DL interference}} + \underbrace{\sum_{\ell_{\mathsf{U}}\in\mathcal{U}} H_{i,j_{\mathsf{D}},\ell_{\mathsf{U}}} \mathbf{V}_{i,\ell_{\mathsf{U}}} s_{i,\ell_{\mathsf{U}}}}_{\text{UL intracell interference}} + n_{i,j_{\mathsf{D}}}, \tag{5.34}$$

where $s_{m,\ell_{\mathsf{D}}}^{I}$ is the information signal intended for DLU (m, ℓ_{D}). The ID throughput at DLU (i, j_{D}) is then given as $\boldsymbol{\alpha} f_{i,j_{\mathsf{D}}}(\mathbf{V})$, where

$$f_{i,j_{\mathsf{D}}}(\mathbf{V}_{\mathsf{D}}^{I}, \mathbf{V}_{\mathsf{U}}) = \ln\left|I_{N_r} + (\mathcal{L}_{i,j_{\mathsf{D}}}(\mathbf{V}_{i,j_{\mathsf{D}}}^{I}))^2 \bar{\Psi}_{i,j_{\mathsf{D}}}^{-1}(\mathbf{V}_{\mathsf{D}}^{I}, \mathbf{V}_{\mathsf{U}})\right|, \tag{5.35}$$

with the downlink interference covariance mapping $\bar{\Psi}(.,.)$ defined from (5.5).
The uplink throughput at the BS is

$$f_i(\mathbf{V}_{\mathsf{D}}, \mathbf{V}_{\mathsf{U}}, \boldsymbol{\alpha}) \triangleq \ln\left|I_{N_2} + (\mathcal{L}_i(\mathbf{V}_{\mathsf{U}_i}))^2 \Psi_i^{-1}(\mathbf{V}_{\mathsf{D}}, \mathbf{V}_{\mathsf{U}}, \boldsymbol{\alpha})\right|, \tag{5.36}$$

where $\mathcal{L}_i(\mathbf{V}_{\mathsf{U}_i})$ is already defined from (5.9) but

$$\Psi_i(\mathbf{V}_{\mathsf{D}}, \mathbf{V}_{\mathsf{U}}, \boldsymbol{\alpha}) \triangleq \bar{\Psi}_i^U(\mathbf{V}_{\mathsf{U}}) + \bar{\Psi}_i^{TSI}(\mathbf{V}_{\mathsf{D}}, \boldsymbol{\alpha}) \tag{5.37}$$

with the uplink interference covariance mapping $\bar{\Psi}_i^U(.)$ defined by (5.11) and the time-splitting SI covariance mapping

$$\bar{\Psi}_i^{TSI}(\mathbf{V}_{\mathsf{D}}, \boldsymbol{\alpha}) \triangleq \sigma_{SI}^2 \sum_{j_{\mathsf{D}} \in \mathcal{D}} \Big((1-\boldsymbol{\alpha}) ||\mathbf{V}_{i,j_{\mathsf{D}}}^E||^2 + \boldsymbol{\alpha} ||\mathbf{V}_{i,j_{\mathsf{D}}}^I||^2 \Big) I_{N_2}. \tag{5.38}$$

The problem of maximizing the network total throughput under throughput QoS and EH constraints is the following:

$$\max_{\mathbf{V}_{\mathsf{D}}, \mathbf{V}_{\mathsf{U}}, \boldsymbol{\alpha}} \ \mathcal{P}_2(\mathbf{V}_{\mathsf{D}}, \mathbf{V}_{\mathsf{U}}, \boldsymbol{\alpha}) \triangleq \sum_{(i,j_{\mathsf{D}}) \in \mathcal{S}_1} \Big(\boldsymbol{\alpha} f_{i,j_{\mathsf{D}}}(\mathbf{V}_{\mathsf{D}}^I, \mathbf{V}_{\mathsf{U}}) + f_i(\mathbf{V}_{\mathsf{D}}, \mathbf{V}_{\mathsf{U}}, \boldsymbol{\alpha}) \Big) \quad \text{s.t.} \tag{5.39a}$$

$$0 < \boldsymbol{\alpha} < 1, \tag{5.39b}$$

$$||\mathbf{V}_{i,j_{\mathsf{U}}}||^2 \leq P_{i,j_{\mathsf{U}}}, \forall (i, j_{\mathsf{U}}) \in \mathcal{S}_2, \tag{5.39c}$$

$$\sum_{(i,j_{\mathsf{D}}) \in \mathcal{S}_1} \Big((1-\boldsymbol{\alpha}) ||\mathbf{V}_{i,j_{\mathsf{D}}}^E||^2 + \boldsymbol{\alpha} ||\mathbf{V}_{i,j_{\mathsf{D}}}^I||^2 \Big) + \sum_{(i,j_{\mathsf{U}}) \in \mathcal{S}_2} ||\mathbf{V}_{i,j_{\mathsf{U}}}||^2 \leq P, \tag{5.39d}$$

$$\sum_{j_{\mathsf{D}} \in \mathcal{D}} \Big((1-\boldsymbol{\alpha}) ||\mathbf{V}_{i,j_{\mathsf{D}}}^E||^2 + \boldsymbol{\alpha} ||\mathbf{V}_{i,j_{\mathsf{D}}}^I||^2 \Big) \leq P_i, \forall i \in \mathcal{I}, \tag{5.39e}$$

$$f_i(\mathbf{V}_{\mathsf{D}}, \mathbf{V}_{\mathsf{U}}, \boldsymbol{\alpha}) \geq r_i^{\mathsf{U},\min}, \forall i \in \mathcal{I}, \tag{5.39f}$$

$$\boldsymbol{\alpha} f_{i,j_{\mathsf{D}}}(\mathbf{V}_{\mathsf{D}}^I, \mathbf{V}_{\mathsf{U}}) \geq r_{i,j_{\mathsf{D}}}^{\mathsf{D},\min}, \forall (i, j_{\mathsf{D}}) \in \mathcal{S}_1, \tag{5.39g}$$

$$E_{i,j_{\mathsf{D}}}(\mathbf{V}_{\mathsf{D}}^E, \mathbf{V}_{\mathsf{U}}, \boldsymbol{\alpha}) \geq e_{i,j_{\mathsf{D}}}^{\min}, \forall (i, j_{\mathsf{D}}) \in \mathcal{S}_1. \tag{5.39h}$$

Constraints (5.39c), (5.39d) and (5.39e) limits the transmit power of each ULU, the whole network and each BS, respectively. Constraints (5.39h) ensures that each DLUs harvest more than a threshold whereas constraints (5.39f) and (5.39g) guarantee the throughput QoS at BSs and DLUs, respectively. The key difficulty in problem (5.39) is to handle the time splitting factor $\boldsymbol{\alpha}$ that is coupled with the objective functions and other variables. Using the variable change $\boldsymbol{\rho} = 1/\boldsymbol{\alpha}$, which satisfies the convex constraint

$$\boldsymbol{\rho} > 1, \tag{5.40}$$

problem (5.39) is equivalent to

$$\max_{\mathbf{V}_{\mathsf{D}},\mathbf{V}_{\mathsf{U}},\boldsymbol{\rho}>0} \mathcal{P}_2(\mathbf{V}_{\mathsf{D}},\mathbf{V}_{\mathsf{U}},\boldsymbol{\rho}) \triangleq \sum_{(i,j_{\mathsf{D}})\in\mathcal{S}_1} f_{i,j_{\mathsf{D}}}(\mathbf{V}_{\mathsf{D}}^I,\mathbf{V}_{\mathsf{U}})/\boldsymbol{\rho} + \sum_{i\in\mathcal{I}} f_i(\mathbf{V}_{\mathsf{D}},\mathbf{V}_{\mathsf{U}},1/\boldsymbol{\rho}) \quad (5.41a)$$

$$\text{s.t. } (5.40),(5.39c),$$

$$\sum_{(i,j_{\mathsf{D}})\in\mathcal{S}_1} \left(||\mathbf{V}_{i,j_{\mathsf{D}}}^E||^2 + ||\mathbf{V}_{i,j_{\mathsf{D}}}^I||^2/\boldsymbol{\rho}\right) + \sum_{(i,j_{\mathsf{U}})\in\mathcal{S}_2} ||\mathbf{V}_{i,j_{\mathsf{U}}}||^2 \leq P + \sum_{(i,j_{\mathsf{D}})\in\mathcal{S}_1} ||\mathbf{V}_{i,j_{\mathsf{D}}}^E||^2/\boldsymbol{\rho}, \quad (5.41b)$$

$$\sum_{j_{\mathsf{D}}\in\mathcal{D}} \left(||\mathbf{V}_{i,j_{\mathsf{D}}}^E||^2 + ||\mathbf{V}_{i,j_{\mathsf{D}}}^I||^2/\boldsymbol{\rho}\right) \leq P_i + \sum_{j_{\mathsf{D}}\in\mathcal{D}} ||\mathbf{V}_{i,j_{\mathsf{D}}}^E||^2/\boldsymbol{\rho},\ \forall i\in\mathcal{I}, \quad (5.41c)$$

$$E_{i,j_{\mathsf{D}}}(\mathbf{V}_{\mathsf{D}}^E,\mathbf{V}_{\mathsf{U}},1/\boldsymbol{\rho}) \geq e_{i,j_{\mathsf{D}}}^{\min}, \forall (i,j_{\mathsf{D}})\in\mathcal{S}_1, \quad (5.41d)$$

$$f_i(\mathbf{V}_{\mathsf{D}},\mathbf{V}_{\mathsf{U}},1/\boldsymbol{\rho}) \geq r_i^{\mathsf{U},\min}, \forall i\in\mathcal{I}, \quad (5.41e)$$

$$f_{i,j_{\mathsf{D}}}(\mathbf{V}_{\mathsf{D}}^I,\mathbf{V}_{\mathsf{U}})/\boldsymbol{\rho} \geq r_{i,j_{\mathsf{D}}}^{\mathsf{D},\min}, \forall (i,j_{\mathsf{D}})\in\mathcal{S}_1. \quad (5.41f)$$

Problem (5.41) is much more difficult computationally than (5.13). Firstly, the DL throughput is now the multiplication of data throughput and the portion of time $1/\boldsymbol{\rho}$. Secondly, the SI in UL throughput is also coupled with $1/\boldsymbol{\rho}$. Finally, the power constraints (5.41b), (5.41c) are also coupled with $1/\boldsymbol{\rho}$. Therefore, the objective function (5.41a) and constraints (5.41b)-(5.41f) are all nonconvex and cannot be addressed as in (5.13). In the following, we will develop the new minorants of the DL throughput function and UL throughput function.

Firstly, we address a lower approximation for each $f_{i,j_{\mathsf{D}}}(\mathbf{V}_{\mathsf{D}}^I,\mathbf{V}_{\mathsf{U}})/\boldsymbol{\rho}$ in (5.41a) and (5.41f). Recalling the definition (5.35) of $f_{i,j_{\mathsf{D}}}(\mathbf{V}_{\mathsf{D}}^I,\mathbf{V}_{\mathsf{U}})$ we introduce

$$\mathcal{M}_{i,j_{\mathsf{D}}}(\mathbf{V}_{\mathsf{D}}^I,\mathbf{V}_{\mathsf{U}}) \triangleq (\mathcal{L}_{i,j_{\mathsf{D}}}(\mathbf{V}_{i,j_{\mathsf{D}}}))^2 + \bar{\Psi}_{i,j_{\mathsf{D}}}(\mathbf{V}_{\mathsf{D}},\mathbf{V}_{\mathsf{U}}),$$

to have its following minorant at $(V_{\mathsf{D}}^{(\kappa)},V_{\mathsf{U}}^{(\kappa)})$:

$$\Theta_{i,j_{\mathsf{D}}}^{(\kappa)}(\mathbf{V}_{\mathsf{D}}^I,\mathbf{V}_{\mathsf{U}}) \triangleq a_{i,j_{\mathsf{D}}}^{(\kappa)} + 2\,\mathrm{Re}\left\{\langle \mathcal{A}_{i,j_{\mathsf{D}}}^{(\kappa)}, \mathcal{L}_{i,j_{\mathsf{D}}}(\mathbf{V}_{i,j_{\mathsf{D}}}^I)\rangle\right\} - \langle \mathcal{B}_{i,j_{\mathsf{D}}}^{(\kappa)}, \mathcal{M}_{i,j_{\mathsf{D}}}(\mathbf{V}_{\mathsf{D}}^I,\mathbf{V}_{\mathsf{U}})\rangle, \quad (5.42)$$

where similarly to (5.20)

$$\begin{aligned} 0 > a_{i,j_{\mathsf{D}}}^{(\kappa)} &= f_{i,j_{\mathsf{D}}}(V_{\mathsf{D}}^{(\kappa)}, V_{\mathsf{U}}^{(\kappa)}) - \mathrm{Re}\left\{\langle \bar{\Psi}_{i,j_{\mathsf{D}}}^{-1}(V_{\mathsf{D}}^{(\kappa)}, V_{\mathsf{U}}^{(\kappa)}) \mathcal{L}_{i,j_{\mathsf{D}}}(V_{i,j_{\mathsf{D}}}^{(\kappa)}), \mathcal{L}_{i,j_{\mathsf{D}}}(V_{i,j_{\mathsf{D}}}^{(\kappa)})\rangle\right\}, \\ \mathcal{A}_{i,j_{\mathsf{D}}}^{(\kappa)} &= \bar{\Psi}_{i,j_{\mathsf{D}}}^{-1}(V_{\mathsf{D}}^{(\kappa)}, V_{\mathsf{U}}^{(\kappa)}) \mathcal{L}_{i,j_{\mathsf{D}}}(V_{i,j_{\mathsf{D}}}^{(\kappa)}), \\ 0 \preceq \mathcal{B}_{i,j_{\mathsf{D}}}^{(\kappa)} &= \bar{\Psi}_{i,j_{\mathsf{D}}}^{-1}(V_{\mathsf{D}}^{(\kappa)}, V_{\mathsf{U}}^{(\kappa)}) - \mathcal{M}_{i,j_{\mathsf{D}}}^{-1}(V_{\mathsf{D}}^{(\kappa)}, V_{\mathsf{U}}^{(\kappa)}). \end{aligned} \tag{5.43}$$

A minorant of $f_{i,j_{\mathsf{D}}}(\mathbf{V}_{\mathsf{D}}^I, \mathbf{V}_{\mathsf{U}})/\boldsymbol{\rho}$ is $\Theta_{i,j_{\mathsf{D}}}^{(\kappa)}(\mathbf{V}_{\mathsf{D}}^I, \mathbf{V}_{\mathsf{U}})/\boldsymbol{\rho}$ but it is still not concave. As $f_{i,j_{\mathsf{D}}}(\mathbf{V}_{\mathsf{D}}^I, \mathbf{V}_{\mathsf{U}}) > 0$ it is obvious that its lower bound $\Theta_{i,j_{\mathsf{D}}}^{(\kappa)}(\mathbf{V}_{\mathsf{D}}^I, \mathbf{V}_{\mathsf{U}})$ is meaningful for $(\mathbf{V}_{\mathsf{D}}^I, \mathbf{V}_{\mathsf{U}})$ such that

$$\Theta_{i,j_{\mathsf{D}}}^{(\kappa)}(\mathbf{V}_{\mathsf{D}}^I, \mathbf{V}_{\mathsf{U}}) \geq 0,\ (i, j_{\mathsf{D}}) \in \mathcal{S}_1 \tag{5.44}$$

which particularly implies

$$\mathrm{Re}\left\{\left\langle (\mathcal{A}_{i,j_{\mathsf{D}}}^{(\kappa)}, \mathcal{L}_{i,j_{\mathsf{D}}}(\mathbf{V}_{i,j_{\mathsf{D}}}^I)\right\rangle\right\} \geq 0,\ (i, j_{\mathsf{D}}) \in \mathcal{S}_1. \tag{5.45}$$

Under (5.45), we have

$$\frac{\mathrm{Re}\left\{\langle \mathcal{A}_{i,j_{\mathsf{D}}}^{(\kappa)}, \mathcal{L}_{i,j_{\mathsf{D}}}(\mathbf{V}_{i,j_{\mathsf{D}}}^I)\rangle\right\}}{\boldsymbol{\rho}} \geq 2b_{i,j_{\mathsf{D}}}^{(\kappa)} \sqrt{\mathrm{Re}\left\{\langle \mathcal{A}_{i,j_{\mathsf{D}}}^{(\kappa)}, \mathcal{L}_{i,j_{\mathsf{D}}}(\mathbf{V}_{i,j_{\mathsf{D}}}^I)\rangle\right\}} - c_{i,j_{\mathsf{D}}}^{(\kappa)} \boldsymbol{\rho} \tag{5.46}$$

for

$$0 < b_{i,j_{\mathsf{D}}}^{(\kappa)} = \frac{\sqrt{\langle \mathcal{A}_{i,j_{\mathsf{D}}}^{(\kappa)}, \mathcal{L}_{i,j_{\mathsf{D}}}(V_{i,j_{\mathsf{D}}}^{I,(\kappa)})\rangle}}{\rho^{(\kappa)}},\ 0 < c_{i,j_{\mathsf{D}}}^{(\kappa)} = (b_{i,j_{\mathsf{D}}}^{(\kappa)})^2. \tag{5.47}$$

Therefore, the following concave function

$$\begin{aligned} g_{i,j_{\mathsf{D}}}^{(\kappa)}(\mathbf{V}_{\mathsf{D}}^I, \mathbf{V}_{\mathsf{U}}, \boldsymbol{\rho}) \ \triangleq\ & \frac{a_{i,j_{\mathsf{D}}}^{(\kappa)}}{\boldsymbol{\rho}} + 4b_{i,j_{\mathsf{D}}}^{(\kappa)} \sqrt{\mathrm{Re}\left\{\langle \mathcal{A}_{i,j_{\mathsf{D}}}^{(\kappa)}, \mathcal{L}_{i,j_{\mathsf{D}}}(\mathbf{V}_{i,j_{\mathsf{D}}}^I)\rangle\right\}} - 2c_{i,j_{\mathsf{D}}}^{(\kappa)} \boldsymbol{\rho} \\ & - \frac{\langle \mathcal{B}^{(\kappa)}, \mathcal{M}_{i,j_{\mathsf{D}}}(\mathbf{V}_{\mathsf{D}}^I, \mathbf{V}_{\mathsf{U}})\rangle}{\boldsymbol{\rho}} \end{aligned} \tag{5.48}$$

is a minorant of $f_{i,j_{\mathsf{D}}}(\mathbf{V}_{\mathsf{D}}^I, \mathbf{V}_{\mathsf{U}})/\boldsymbol{\rho}$ at $(V_{\mathsf{D}}^{I,(\kappa)}, V_{\mathsf{U}}^{(\kappa)}, \rho^{(\kappa)})$.

Next, we address a lower approximation of $f_i(\mathbf{V}_{\mathsf{D}}, \mathbf{V}_{\mathsf{U}}, 1/\boldsymbol{\rho})$ in (5.41a), (5.41e). Recalling the definition (5.36) of $f_i(\mathbf{V}_{\mathsf{D}}, \mathbf{V}_{\mathsf{U}}, 1/\boldsymbol{\rho})$ we introduce

$$\mathcal{M}_i(\mathbf{V}_{\mathsf{D}}, \mathbf{V}_{\mathsf{U}}, \boldsymbol{\rho}) \triangleq (\mathcal{L}_i(\mathbf{V}_{\mathsf{U}i}))^2 + \bar{\Psi}_i^U(\mathbf{V}_{\mathsf{U}}) + \bar{\Psi}_i^{TSI}(\mathbf{V}_{\mathsf{D}}, 1/\boldsymbol{\rho}),$$

for $\bar{\Psi}_i^{TSI}(\mathbf{V}_\mathsf{D}, 1/\boldsymbol{\rho})$ defined from (5.38) as

$$\bar{\Psi}_i^{TSI}(\mathbf{V}_\mathsf{D}, 1/\boldsymbol{\rho}) = \sigma_{SI}^2 \sum_{j_\mathsf{D}\in\mathcal{D}} \Big(||\mathbf{V}_{i,j_\mathsf{D}}^E||^2 + \frac{1}{\boldsymbol{\rho}}||\mathbf{V}_{i,j_\mathsf{D}}^I||^2 - \frac{1}{\boldsymbol{\rho}}||\mathbf{V}_{i,j_\mathsf{D}}^E||^2 \Big) I_{N_2}, \tag{5.49}$$

to have its following minorant at $(V_\mathsf{D}^{(\kappa)}, V_\mathsf{U}^{(\kappa)}, \rho^{(\kappa)})$:

$$\Theta_i^{(\kappa)}(\mathbf{V}_\mathsf{D}, \mathbf{V}_\mathsf{U}, \boldsymbol{\rho}) \triangleq a_i^{(\kappa)} + 2\,\mathrm{Re}\Big\{ \langle \mathcal{A}_i^{(\kappa)}, \mathcal{L}_i(\mathbf{V}_{\mathsf{U}_i}) \rangle \Big\} - \langle \mathcal{B}_i^{(\kappa)}, \mathcal{M}_i(\mathbf{V}_\mathsf{D}, \mathbf{V}_\mathsf{U}, \boldsymbol{\rho}) \rangle, \tag{5.50}$$

where similarly to (5.21)

$$\begin{aligned} 0 > a_i^{(\kappa)} &= f_i(V_\mathsf{D}^{(\kappa)}, V_\mathsf{U}^{(\kappa)}) - \mathrm{Re}\Big\{ \langle \Psi_i^{-1}(V_\mathsf{D}^{(\kappa)}, V_\mathsf{U}^{(\kappa)}) \mathcal{L}_i(V_i^{(\kappa)}), \mathcal{L}_i(V_i^{(\kappa)}) \rangle \Big\}, \\ \mathcal{A}_i^{(\kappa)} &= \Psi_i^{-1}(V_\mathsf{D}^{(\kappa)}, V_\mathsf{U}^{(\kappa)}) \mathcal{L}_i(V_{\mathsf{U}_i}^{(\kappa)}), \\ 0 \preceq \mathcal{B}_i^{(\kappa)} &= \Psi_i^{-1}(V_\mathsf{D}^{(\kappa)}, V_\mathsf{U}^{(\kappa)}) - \mathcal{M}_i^{-1}(V_\mathsf{D}^{(\kappa)}, V_\mathsf{U}^{(\kappa)}). \end{aligned} \tag{5.51}$$

Function $\Theta_i^{(\kappa)}(\mathbf{V}_\mathsf{D}, \mathbf{V}_\mathsf{U}, \boldsymbol{\rho})$ is not concave due to the term $\bar{\Psi}_i^{TSI}(\mathbf{V}_\mathsf{D}, 1/\boldsymbol{\rho})$ defined by (5.49). However, the following *matrix inequality* holds true:

$$\frac{1}{\boldsymbol{\rho}}||\mathbf{V}_{i,j_\mathsf{D}}^E||^2 I_{N_2} \succeq \Big(\frac{2}{\rho^{(\kappa)}} \mathrm{Re}\{ \langle V_{j_\mathsf{D}}^{E,(\kappa)}, \mathbf{V}_{j_\mathsf{D}}^E \rangle \} - \frac{||V_{j_\mathsf{D}}^{E,(\kappa)}||^2}{(\rho^{(\kappa)})^2} \boldsymbol{\rho} \Big) I_{N_2}, \tag{5.52}$$

which yields the matrix inequality

$$\begin{aligned} \mathcal{M}_i(\mathbf{V}_\mathsf{D}, \mathbf{V}_\mathsf{U}, \boldsymbol{\rho}) &\succeq \mathcal{M}_i^{(\kappa)}(\mathbf{V}_\mathsf{D}, \mathbf{V}_\mathsf{U}, \boldsymbol{\rho}) \\ &\triangleq (\mathcal{L}_i(\mathbf{V}_{\mathsf{U}i}))^2 + \bar{\Psi}_i^U(\mathbf{V}_\mathsf{U}) + \sigma_{SI}^2 \Bigg(||\mathbf{V}_{i,j_\mathsf{D}}^E||^2 + \frac{1}{\boldsymbol{\rho}}||\mathbf{V}_{i,j_\mathsf{D}}^I||^2 \\ &\quad - \frac{2}{\rho^{(\kappa)}} \mathrm{Re}\{ \langle V_{j_\mathsf{D}}^{E,(\kappa)}, \mathbf{V}_{j_\mathsf{D}}^E \rangle \} + \frac{||V_{j_\mathsf{D}}^{E,(\kappa)}||^2}{(\rho^{(\kappa)})^2} \boldsymbol{\rho} \Bigg) I_{N_2}. \end{aligned}$$

As $\mathcal{B}_i^{(\kappa)} \succeq 0$ by (5.51), we then have

$$\langle \mathcal{B}_i^{(\kappa)}, \mathcal{M}_i(\mathbf{V}_\mathsf{D}, \mathbf{V}_\mathsf{U}, \boldsymbol{\rho}) \rangle \geq \langle \mathcal{B}_i^{(\kappa)}, \mathcal{M}_i^{(\kappa)}(\mathbf{V}_\mathsf{D}, \mathbf{V}_\mathsf{U}, \boldsymbol{\rho}) \rangle$$

so a concave minorant of both $f_i(\mathbf{V}_\mathsf{D}, \mathbf{V}_\mathsf{U}, 1/\boldsymbol{\rho})$ and $\Theta^{(\kappa)}(\mathbf{V}_\mathsf{D}, \mathbf{V}_\mathsf{U}, \boldsymbol{\rho})$ is

$$\tilde{\Theta}_i^{(\kappa)}(\mathbf{V}_\mathsf{D}, \mathbf{V}_\mathsf{U}, \boldsymbol{\rho}) \triangleq a_i^{(\kappa)} + 2\,\mathrm{Re}\Big\{ \langle \mathcal{A}_i^{(\kappa)}, \mathcal{L}_i(\mathbf{V}_{\mathsf{U}_i}) \rangle \Big\} - \langle \mathcal{B}_i^{(\kappa)}, \mathcal{M}_i^{(\kappa)}(\mathbf{V}_\mathsf{D}, \mathbf{V}_\mathsf{U}, \boldsymbol{\rho}) \rangle. \tag{5.53}$$

Concerned with $||\mathbf{V}_{i,j_\mathsf{D}}^E||^2/\boldsymbol{\rho}$ in the right hand side (RHS) of (5.41b) and (5.41c), it follows from (5.52) that

$$\begin{aligned} ||\mathbf{V}_{i,j_\mathsf{D}}^E||^2/\boldsymbol{\rho} &\geq \gamma_{i,j_\mathsf{D}}^{(\kappa)}(\mathbf{V}_{i,j_\mathsf{D}}^E, \boldsymbol{\rho}) \\ &\triangleq 2\,\mathrm{Re}\{ \langle V_{i,j_\mathsf{D}}^{E,(\kappa)}, \mathbf{V}_{i,j_\mathsf{D}}^E \rangle \}/\rho^{(\kappa)} - \boldsymbol{\rho}||V_{i,j_\mathsf{D}}^{E,(\kappa)}||^2/(\rho^{(\kappa)})^2. \end{aligned}$$

We also have $\phi_{i,j_\mathsf{D}}^{(\kappa)}(\mathbf{V}_\mathsf{D}^E, \mathbf{V}_\mathsf{U})$ defined in (5.22) as a minorant of $\langle \Phi_{i,j_\mathsf{D}}(\mathbf{V}_\mathsf{D}^E, \mathbf{V}_\mathsf{U})\rangle$. We now address the nonconvex problem (5.41) by successively solving its following innerly approximated convex program at κ-iteration:

$$\max_{\mathbf{V}_\mathsf{D},\mathbf{V}_\mathsf{U},\boldsymbol{\rho}>0} \mathcal{P}_2^{(\kappa)}(\mathbf{V}_\mathsf{D}, \mathbf{V}_\mathsf{U}, \boldsymbol{\rho}) \triangleq \sum_{(i,j_\mathsf{D})\in\mathcal{S}_1} g_{i,j_\mathsf{D}}^{(\kappa)}(\mathbf{V}_\mathsf{D}^I, \mathbf{V}_\mathsf{U}, \boldsymbol{\rho}) + \sum_{i\in\mathcal{I}} \tilde{\Theta}_i^{(\kappa)}(\mathbf{V}_\mathsf{D}, \mathbf{V}_\mathsf{U}, \boldsymbol{\rho}) \quad (5.54a)$$

$$\text{s.t. } (5.40), (5.39c), \quad (5.54b)$$

$$\sum_{(i,j_\mathsf{D})\in\mathcal{S}_1} \left(||\mathbf{V}_{i,j_\mathsf{D}}^E||^2 + \frac{1}{\boldsymbol{\rho}}||\mathbf{V}_{i,j_\mathsf{D}}^I||^2\right) + \sum_{(i,j_\mathsf{U})\in\mathcal{S}_2} ||\mathbf{V}_{i,j_\mathsf{U}}||^2 \leq P + \sum_{(i,j_\mathsf{D})\in\mathcal{S}_1} \gamma_{i,j_\mathsf{D}}^{(\kappa)}(\mathbf{V}_{i,j_\mathsf{D}}^E, \boldsymbol{\rho}), \quad (5.54c)$$

$$\sum_{j_\mathsf{D}\in\mathcal{D}} \left(||\mathbf{V}_{i,j_\mathsf{D}}^E||^2 + \frac{1}{\boldsymbol{\rho}}||\mathbf{V}_{i,j_\mathsf{D}}^I||^2\right) \leq P_i + \sum_{j_\mathsf{D}\in\mathcal{D}} \gamma_{i,j_\mathsf{D}}^{(\kappa)}(\mathbf{V}_{i,j_\mathsf{D}}^E, \boldsymbol{\rho}), \forall i \in \mathcal{I}, \quad (5.54d)$$

$$\phi_{i,j_\mathsf{D}}^{(\kappa)}(\mathbf{V}_\mathsf{D}^E, \mathbf{V}_\mathsf{U}) \geq e_{i,j_\mathsf{D}}^{\min}(1 + \frac{1}{\boldsymbol{\rho}-1})/\zeta_{i,j_\mathsf{D}}, \forall (i,j_\mathsf{D}) \in \mathcal{S}_1, \quad (5.54e)$$

$$\tilde{\Theta}_i^{(\kappa)}(\mathbf{V}_\mathsf{D}, \mathbf{V}_\mathsf{U}, \boldsymbol{\rho}) \geq r_i^{\mathsf{U},\min}, \forall i \in \mathcal{I}, \quad (5.54f)$$

$$g_{i,j_\mathsf{D}}^{(\kappa)}(\mathbf{V}_\mathsf{D}^I, \mathbf{V}_\mathsf{U}, \boldsymbol{\rho}) \geq r_{i,j_\mathsf{D}}^{\mathsf{D},\min}. \forall (i,j_\mathsf{D}) \in \mathcal{S}_1. \quad (5.54g)$$

A path-following procedure similar to Algorithm 6 can be applied to solve (5.41) as summarized in Algorithm 7. Thanks to the following relation, which is similar to (5.26):

$$\mathcal{P}_2(V_\mathsf{D}^{(\kappa+1)}, V_\mathsf{U}^{(\kappa+1)}, \rho^{(\kappa+1)}) \geq \mathcal{P}_2(V_\mathsf{D}^{(\kappa)}, V_\mathsf{U}^{(\kappa)}, \rho^{(\kappa)}), \quad (5.55)$$

Algorithm 7 improves feasible point at each iteration and then brings a local optimum after finitely many iterations.

Algorithm 7 Path-following algorithm for TS optimization problem (5.41)

Initialization: Set $\kappa := 0$, and choose a feasible point $(V_\mathsf{D}^{(0)}, V_\mathsf{U}^{(0)}, \alpha^{(0)})$ that satisfies (5.39b)-(5.39g). Set $\rho^{(0)} := 1/\alpha^{(0)}$.

κ-th iteration: Solve (5.54) for an optimal solution $(V_\mathsf{D}^*, V_\mathsf{U}^*, \rho^*)$ and set $\kappa := \kappa + 1$, $(V_\mathsf{D}^{(\kappa)}, V_\mathsf{U}^{(\kappa)}, \rho^{(\kappa)}) := (V_\mathsf{D}^*, V_\mathsf{U}^*, \rho^*)$ and calculate $\mathcal{P}_2(V_\mathsf{D}^{(\kappa)}, V_\mathsf{U}^{(\kappa)}, 1/\rho^{(\kappa)})$. Stop if $\left|\left(\mathcal{P}_2(V_\mathsf{D}^{(\kappa)}, V_\mathsf{U}^{(\kappa)}, 1/\rho^{(\kappa)}) - \mathcal{P}_2(V_\mathsf{D}^{(\kappa-1)}, V_\mathsf{U}^{(\kappa-1)}, 1/\rho^{(\kappa-1)})\right)/\mathcal{P}_2(V_\mathsf{D}^{(\kappa-1)}, V_\mathsf{U}^{(\kappa-1)}, 1/\rho^{(\kappa-1)})\right| \leq \epsilon$.

To find an initial feasible point for Algorithm 7, we consider the following problem:

$$\begin{aligned}\max_{\mathbf{V}_\mathsf{D},\mathbf{V}_\mathsf{U},\boldsymbol{\rho}} \min_{(i,j_\mathsf{D})\in\mathcal{S}_1} \Big\{ & f_{i,j_\mathsf{D}}(\mathbf{V}_\mathsf{D}^I,\mathbf{V}_\mathsf{U})/\boldsymbol{\rho} - r_{i,i_\mathsf{D}}^{\min}, \\ & f_i(\mathbf{V}_\mathsf{D},\mathbf{V}_\mathsf{U},1/\boldsymbol{\rho}) - r_i^{\min}, E_{i,j_\mathsf{D}}(\mathbf{V}_\mathsf{D}^E,\mathbf{V}_\mathsf{U},1/\boldsymbol{\rho}) - e_{i,j_\mathsf{D}}^{\min} \Big\} : \ (5.41\text{b}) - (5.41\text{c})\end{aligned} \tag{5.56}$$

which can be addressed by successively solving the following convex maximin program:

$$\begin{aligned}\max_{\mathbf{V}_\mathsf{D},\mathbf{V}_\mathsf{U},\boldsymbol{\rho}} \min_{(i,j_\mathsf{D})\in\mathcal{S}_1} \Big\{ & g_{i,j_\mathsf{D}}^{(\kappa)}(\mathbf{V}_\mathsf{D}^I,\mathbf{V}_\mathsf{U},\boldsymbol{\rho}) - r_{i,i_\mathsf{D}}^{\min}, \tilde{\Theta}_i^{(\kappa)}(\mathbf{V}_\mathsf{D},\mathbf{V}_\mathsf{U},\boldsymbol{\rho}) - r_i^{\min}, \\ & \phi_{i,j_\mathsf{D}}^{(\kappa)}(\mathbf{V}_\mathsf{D}^E,\mathbf{V}_\mathsf{U}) - e_{i,j_\mathsf{D}}^{\min}(1+\frac{1}{\boldsymbol{\rho}-1})/\zeta_{i,j_\mathsf{D}} \Big\} : (5.54\text{b}) - (5.54\text{d}),\end{aligned} \tag{5.57}$$

upon reaching

$$\begin{aligned}f_{i,j_\mathsf{D}}(V_\mathsf{D}^{I,(\kappa)},V_\mathsf{U}^{(\kappa)},\alpha^{(\kappa)}) \geq r_{i,i_\mathsf{D}}^{\min}, f_i(V_\mathsf{D}^{(\kappa)},V_\mathsf{U}^{(\kappa)},\alpha^{(\kappa)}) \geq r_i^{\min}, \\ E_{i,j_\mathsf{D}}(V_\mathsf{D}^{E,(\kappa)},V_\mathsf{U}^{(\kappa)},1/\rho^{(\kappa)}) \geq e_{i,j_\mathsf{D}}^{\min}, \forall (i,j_\mathsf{D}) \in \mathcal{S}_1.\end{aligned} \tag{5.58}$$

For the system operating in HD mode, we apply the same transmission strategy as in Section 5.2. Specifically, we consider the following problem:

$$\max_{\mathbf{V}_\mathsf{D},\mathbf{V}_\mathsf{U},\boldsymbol{\rho}} \ \frac{1}{2}[\sum_{(i,j_\mathsf{D})\in\mathcal{S}_1} \frac{1}{\boldsymbol{\rho}} f_{i,j_\mathsf{D}}(\mathbf{V}_\mathsf{D},0_\mathsf{U}) + \sum_{i\in\mathcal{I}} f_i(0_\mathsf{D},\mathbf{V}_\mathsf{U},1)] \tag{5.59a}$$

$$\text{s.t.} \quad (5.39\text{b}) - (5.39\text{e})$$

$$\frac{1}{2}(E_{i,j_\mathsf{D}}(\mathbf{V}_\mathsf{D},0_\mathsf{U},1/\boldsymbol{\rho}) + E_{i,j_\mathsf{D}}(0_\mathsf{D},\mathbf{V}_\mathsf{U},1)) \geq e_{i,j_\mathsf{D}}^{\min}, \ (i,j_\mathsf{D}) \in \mathcal{S}_1, \tag{5.59b}$$

$$\frac{1}{2\boldsymbol{\rho}} f_{i,j_\mathsf{D}}(\mathbf{V}_\mathsf{D},0_\mathsf{U}) \geq r_{i,j_\mathsf{D}}^{\mathsf{D},\min}, \forall (i,j_\mathsf{D}) \in \mathcal{S}_1, \tag{5.59c}$$

$$\frac{1}{2} f_i(0_\mathsf{D},\mathbf{V}_\mathsf{U},1) \geq r_i^{\mathsf{U},\min}, \forall i \in \mathcal{I}. \tag{5.59d}$$

In (5.59), DLUs harvest energy for $(1-\boldsymbol{\alpha})$ of 1/2 time slot during DL transmission and for the whole 1/2 time slot during UL transmission as formulated in (5.59b). The constraint (5.59b) can be written by

$$\Xi_{i,j_\mathsf{D}}(\mathbf{V}_\mathsf{D},\mathbf{V}_\mathsf{U},\boldsymbol{\rho}) \geq \frac{2e_{i,j_\mathsf{D}}^{\min}}{\zeta_{i,j_\mathsf{D}}}(1+\frac{1}{\boldsymbol{\rho}-1}), \tag{5.60}$$

for

$$\Xi_{i,j_\mathsf{D}}(\mathbf{V}_\mathsf{D},\mathbf{V}_\mathsf{U},\boldsymbol{\rho}) \triangleq \langle \Phi_{i,j_\mathsf{D}}(\mathbf{V}_\mathsf{D},0_\mathsf{U}) \rangle + \langle \Phi_{i,j_\mathsf{D}}(0_\mathsf{D},\mathbf{V}_\mathsf{U}) \rangle + \frac{\langle \Phi_{i,j_\mathsf{D}}(0_\mathsf{D},\mathbf{V}_\mathsf{U}) \rangle}{\boldsymbol{\rho}-1}.$$

As Ξ_{i,j_D} is convex, its minorant is its first-order approximation at $(V_\mathsf{D}^{(\kappa)}, V_\mathsf{U}^{(\kappa)}, \rho^{(\kappa)})$:

$$\Xi_{i,j_\mathsf{D}}^{(\kappa)}(\mathbf{V}_\mathsf{D}, \mathbf{V}_\mathsf{U}, \boldsymbol{\rho}) = \phi_{i,j_\mathsf{D}}^{(\kappa)}(\mathbf{V}_\mathsf{D}, 0_\mathsf{U}) + \phi_{i,j_\mathsf{D}}^{(\kappa)}(0_\mathsf{D}, \mathbf{V}_\mathsf{U}) + \Lambda_{i,j_\mathsf{D}}^{(\kappa)}(\mathbf{V}_\mathsf{U}, \boldsymbol{\rho} - 1),$$

for $\Lambda_{i,j_\mathsf{D}}^{(\kappa)}(.,.)$ defined by (5.31) and $\phi_{i,j_\mathsf{D}}^{(\kappa)}(0_\mathsf{D}, \mathbf{V}_\mathsf{U})$ defined from (5.22) with both $\mathbf{V}_\mathsf{U}$ and $V_\mathsf{U}^{(\kappa)}$ replaced by 0_U.

The problem (5.39) thus can be addressed via a path-following procedure similar to Algorithm 7 where the following convex program is solved for κ-iteration:

$$\max_{\mathbf{V}_\mathsf{D}, \mathbf{V}_\mathsf{U}, \boldsymbol{\rho}} \ \frac{1}{2}[\sum_{(i,j_\mathsf{D}) \in \mathcal{S}_1} g_{i,j_\mathsf{D}}^{(\kappa)}(\mathbf{V}_\mathsf{D}^I, 0_\mathsf{U}, \boldsymbol{\rho}) + \sum_{i \in \mathcal{I}} \tilde{\Theta}_i^{(\kappa)}(0_\mathsf{D}, \mathbf{V}_\mathsf{U}, 1)] \tag{5.61a}$$

$$\text{s.t.} \quad (5.39\text{b}) - (5.39\text{e})$$

$$\Xi_{i,j_\mathsf{D}}^{(\kappa)}(\mathbf{V}_\mathsf{D}, \mathbf{V}_\mathsf{U}, \boldsymbol{\rho}) \geq \frac{2e_{i,j_\mathsf{D}}^{\min}}{\zeta_{i,j_\mathsf{D}}}(1 + \frac{1}{\boldsymbol{\rho} - 1}), \ (i, j_\mathsf{D}) \in \mathcal{S}_1, \tag{5.61b}$$

$$\frac{1}{2} g_{i,j_\mathsf{D}}^{(\kappa)}(\mathbf{V}_\mathsf{D}, 0_\mathsf{U}, \boldsymbol{\rho}) \geq r_{i,j_\mathsf{D}}^{\mathsf{D},\min}, \forall (i, j_\mathsf{D}) \in \mathcal{S}_1, \tag{5.61c}$$

$$\frac{1}{2} \tilde{\Theta}_i^{(\kappa)}(0_\mathsf{D}, \mathbf{V}_\mathsf{U}, 1) \geq r_i^{\mathsf{U},\min}, \forall i \in \mathcal{I}, \tag{5.61d}$$

where $g_{i,j_\mathsf{D}}^{(\kappa)}(\mathbf{V}_\mathsf{D}^I, 0_\mathsf{U}, \boldsymbol{\rho})$ is defined by (5.48) with both $\mathbf{V}_\mathsf{U}$ and $V_\mathsf{U}^{(\kappa)}$ replaced by 0_U, while $\tilde{\Theta}_i^{(\kappa)}(0_\mathsf{D}, \mathbf{V}_\mathsf{U}, 0)$ is defined by (5.53) with both $\mathbf{V}_\mathsf{D}$ and $V_\mathsf{D}^{(\kappa)}$ replaced by 0_D and both $\boldsymbol{\rho}$ and $\rho^{(\kappa)}$ replaced by 1.

5.4 Throughput QoS Constrained Energy-Harvesting Optimization

We will justify numerically that TS is not only easier implemented but performs better than PS for FD EH-enabled MU MIMO networks. This motivates us to consider the following EH optimization with TS, which has not been previously considered at all:

$$\max_{\mathbf{V}_\mathsf{D}, \mathbf{V}_\mathsf{U}, \boldsymbol{\alpha}} \mathcal{P}_3(\mathbf{V}, \boldsymbol{\alpha}) \triangleq \sum_{(i,j_\mathsf{D}) \in \mathcal{S}_1} E_{i,j_\mathsf{D}}(\mathbf{V}_\mathsf{D}^E, \mathbf{V}_\mathsf{U}, \boldsymbol{\alpha}) \quad \text{s.t.} \quad (5.39\text{b}) - (5.39\text{g}). \tag{5.62}$$

By defining $\boldsymbol{\rho} = 1/\boldsymbol{\alpha}$, we firstly recast $E_{i,j_\mathsf{D}}(\mathbf{V}_\mathsf{D}^E, \mathbf{V}_\mathsf{U}, 1/\boldsymbol{\rho})$ as

$$E_{i,j_\mathsf{D}}(\mathbf{V}_\mathsf{D}^E, \mathbf{V}_\mathsf{U}, 1/\boldsymbol{\rho}) = \zeta_{i,j_\mathsf{D}} \Big(\langle \Phi_{i,j_\mathsf{D}}(\mathbf{V}_\mathsf{D}^E, \mathbf{V}_\mathsf{U}) \rangle - Q_{i,j_\mathsf{D}}(\mathbf{V}_\mathsf{D}^E, \mathbf{V}_\mathsf{U}, \boldsymbol{\rho}) \Big), \tag{5.63}$$

where $Q_{i,j_\mathsf{D}}(\mathbf{V}_\mathsf{D}^E, \mathbf{V}_\mathsf{U}, \boldsymbol{\rho}) \triangleq \frac{1}{\boldsymbol{\rho}}\langle \Phi_{i,j_\mathsf{D}}(\mathbf{V}_\mathsf{D}^E, \mathbf{V}_\mathsf{U})\rangle$ is a convex function. Recalling that $\phi_{i,j_\mathsf{D}}^{(\kappa)}(\mathbf{V}_\mathsf{D}^E, \mathbf{V}_\mathsf{U})$ defined in (5.22) is a minorant of $\langle \Phi_{i,j_\mathsf{D}}(\mathbf{V}_\mathsf{D}^E, \mathbf{V}_\mathsf{U})\rangle$, we can now address the nonconvex problem (5.62) by successively solving the following convex program at κ-iteration:

$$\begin{aligned} \max_{\mathbf{V},\boldsymbol{\rho}} \; & \sum_{(i,j_\mathsf{D})\in\mathcal{S}_1} \zeta_{i,j_\mathsf{D}} \Big(\phi_{i,j_\mathsf{D}}^{(\kappa)}(\mathbf{V}_\mathsf{D}^E, \mathbf{V}_\mathsf{U}) - Q_{i,j_\mathsf{D}}(\mathbf{V}_\mathsf{D}^E, \mathbf{V}_\mathsf{U}, \boldsymbol{\rho}) \Big) \\ \text{s.t.} \; & \text{(5.39b)}, \text{(5.39c)}, \text{(5.54c)}, \text{(5.54d)}, \text{(5.54f)}, \text{(5.54g)}. \end{aligned} \tag{5.64}$$

A path-following procedure similar to Algorithm 7 can be applied to solve (5.62).

For the system operating in HD mode, the same transmission strategy as in Section 5.2 is applied. Specifically, we consider the following problem:

$$\begin{aligned} \max_{\mathbf{V},\boldsymbol{\rho}} \; & \sum_{(i,j_\mathsf{D})\in\mathcal{S}_1} \frac{1}{2}(E_{i,j_\mathsf{D}}(\mathbf{V}_\mathsf{D}^E, 0_\mathsf{U}, 1/\boldsymbol{\rho}) + E_{i,j_\mathsf{D}}(0_\mathsf{D}, \mathbf{V}_\mathsf{U}, 0)) \\ \text{s.t.} \; & (5.39b), (5.39c), (5.39d), (5.39e), (5.59c), (5.59d). \end{aligned} \tag{5.65}$$

The problem (5.65) can be addressed via a path-following procedure similar to Algorithm 7 where the following convex program is solved for κ-iteration:

$$\begin{aligned} \max_{\mathbf{V},\boldsymbol{\rho}} \; & \sum_{(i,j_\mathsf{D})\in\mathcal{S}_1} \frac{\zeta_{i,j_\mathsf{D}}}{2} \Big(\phi_{i,j_\mathsf{D}}^{(\kappa)}(\mathbf{V}_\mathsf{D}^E, 0_\mathsf{U}) - Q_{i,j_\mathsf{D}}(\mathbf{V}_\mathsf{D}^E, 0_\mathsf{U}, \boldsymbol{\rho}) + \phi_{i,j_\mathsf{D}}^{(\kappa)}(0_\mathsf{D}, \mathbf{V}_\mathsf{U}) \Big) \\ \text{s.t.} \; & (5.39b), (5.39c), (5.39d), (5.39e), (5.61c), (5.61d), \end{aligned} \tag{5.66}$$

where $\phi_{i,j_\mathsf{D}}^{(\kappa)}(\mathbf{V}_\mathsf{D}^E, 0_\mathsf{U})$ ($\phi_{i,j_\mathsf{D}}^{(\kappa)}(0_\mathsf{D}, \mathbf{V}_\mathsf{U})$, resp.) is defined by (5.22) with both $\mathbf{V}_\mathsf{U}$ and $V_\mathsf{U}^{(\kappa)}$ (both $\mathbf{V}_\mathsf{D}$ and $V_\mathsf{D}^{(\kappa)}$, resp.) replaced by 0_U (0_D, resp.).

5.5 Numerical Results

In this simulation study, we use the example network in Fig. 5.2 to study the total network throughput in the presence of SI. The HD system is also implemented as a base line for both time splitting mechanism and power splitting mechanism. DLUs are randomly located on the circles with radius of $r_1 = 20$ m centered at their serving BSs whereas ULUs are uniformly distributed within the cell of their serving BSs whose

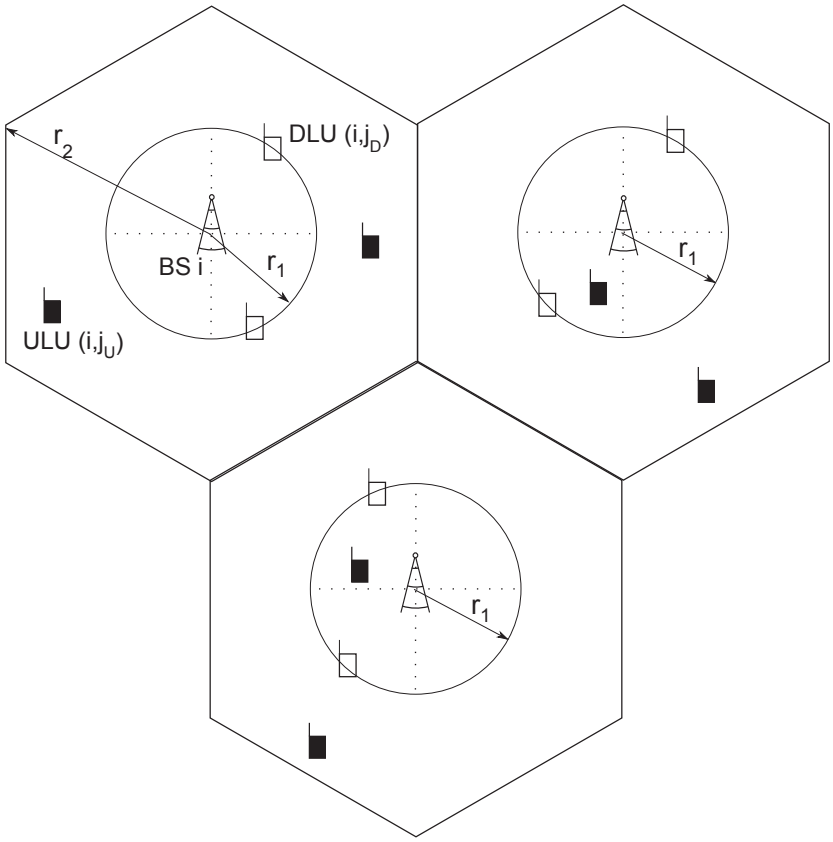

Figure 5.2: A three-cell network with 3 DLUs and 3 ULUs. DLUs are randomly located on the circles with radius of r_1 centered at their serving BS. ULUs are uniformly distributed within the cell of their serving BS.

radius are $r_2 = 40$ m. There are two DLUs and two ULUs within each cell. We set the path loss exponent $\beta = 4$. For small-scale fading, we generate the channel matrices $H_{m,i,j_{\mathsf{D}}}$ from BS m to UE (i, j_{D}), matrices $H_{i,j_{\mathsf{D}},\ell_{\mathsf{U}}}$ from ULU (i, ℓ_{U}) to DLU (i, j_{D}), matrices $H_{m,\ell_{\mathsf{U}},i}$ from ULU (m, ℓ_{U}) to BS i and matrices $H^{\mathcal{B}}_{m,i}$ from BS m to BS i using the Rician fading model as follows:

$$H = \sqrt{\frac{K_R}{1+K_R}} H^{LOS} + \sqrt{\frac{1}{1+K_R}} H^{NLOS}, \tag{5.67}$$

where $K_R = 10$ dB is the Rician factor, H^{LOS} is the line-of-sight (LOS) deterministic component and each element of Rayleigh fading component H^{NLOS} is the circularly-symmetric complex Gaussian random variable $\mathcal{CN}(0, 1)$. Here, we use the far-field

uniform linear antenna array model [Cho et al., 2010] with

$$H^{LOS} = [1, e^{j\theta_r}, e^{j2\theta_r}, \ldots, e^{j(N_r-1)\theta_r}] \times [1, e^{j\theta_t}, e^{j2\theta_t}, \ldots, e^{j(N_1-1)\theta_t}]^H, \tag{5.68}$$

for $\theta_r = \frac{2\pi d \sin(\phi_r)}{\lambda}$, $\theta_t = \frac{2\pi d \sin(\phi_t)}{\lambda}$, where $d = \lambda/2$ is the antenna spacing, λ is the carrier wavelength and ϕ_r, ϕ_t is the angle-of-arrival, the angle-of-departure, respectively. In our simulations, ϕ_r and ϕ_t are randomly generated between 0 and 2π. Unless stated otherwise, the number of transmit antennas and the number of receive antennas at a BS are set as $N_1 = N_2 = 4$. The numbers of concurrent downlink data streams and the numbers of concurrent uplink data streams are equal and $d_1 = d_2 = N_r$. To arrive at the final figures, we run each simulation 100 times and average out the result. In all simulations, we set $P = 23$ dBW, $P_i = 16$ dBW $\forall i \in \mathcal{I}$, $P_{i,j_{\mathsf{U}}} = 10$ dBW $\forall (i, j_{\mathsf{U}}) \in \mathcal{S}_2$, $\forall i \in \mathcal{I}$,$\zeta = 0.5$, $\sigma_c^2 = -90$ dBW, $\sigma^2 = -90$ dBW, $r_{i,j_{\mathsf{D}}}^{\min} = r^{\mathsf{D}} = 1$ bps/Hz and $r_i^{\min} = r^{\mathsf{U}} = Ur^{\mathsf{D}}$ bps/Hz. We further assume that the required harvested energy of all DLUs are the same and $e_{i,j_{\mathsf{D}}}^{\min} = e^{\min}$, $\forall (i, j_{\mathsf{D}})$. Unless stated otherwise, we set $e^{\min} = -20$ dBm. The SI level σ_{SI}^2 is choosen within the range of $[-150, -90]$ dB [1] as in [Nguyen et al., 2013, 2014; Tam et al., 2016] where $\sigma_{SI}^2 = -150$ dB represents the almost perfect SI cancellation.

5.5.1 Single Cell Network

Firstly, we consider the sum throughput maximization problem and the total harvested energy in the single cell networks. This will facilitate the analysis of the impact of SI to the network performance since there is no intercell interference. The network setting in Fig. 5.2 is used but only one cell is considered.

Fig. 5.3 illustrates the comparison of total network throughput between the power splitting mechanism and the time splitting mechanism in both FD and HD systems. Though FD provides a substantial improvement in comparison to HD in both power

[1] At $\sigma_{SI}^2 = -90$ dB, if a BS transmits at full power (i.e. 16 dBW), the SI power is 16 dB stronger than the background AWGN.

splitting mechanism (25.8%) and time splitting mechanism (26.1%) for $N_r = 2$ at $\sigma_{SI}^2 = -150$ dB. Note that we cannot expect a FD system to achieve twice the throughput of that is achieved by a HD system. This is because even when the SI cancellation is perfect, DLUs in FD are still vulnerable to the intracell interference from the ULUs of the same cell. Moreover, DLUs and ULUs in HD are served with more BS's antennas, resulting in a larger spatial diversity. Consequently, FD cannot double HD's throughput even with the almost perfect SI cancellation.

When we reduce the number of antennas at UEs from $N_r = 2$ to $N_r = 1$, the total network throughput of FD is significantly reduced by 42% for the time splitting mechanism and by 41% for the power splitting mechanism at $\sigma_{SI}^2 = -150$ dB. Notably, since UEs in FD are exposed to more sources of interference than UEs in HD, reducing the number of antennas of UEs degrades the performance of FD more than the counterpart of HD. Consequently, the improvement of FD in comparison to HD reduces to 16% at $\sigma_{SI}^2 = -150$ dB for both time splitting mechanism and power splitting mechanism.

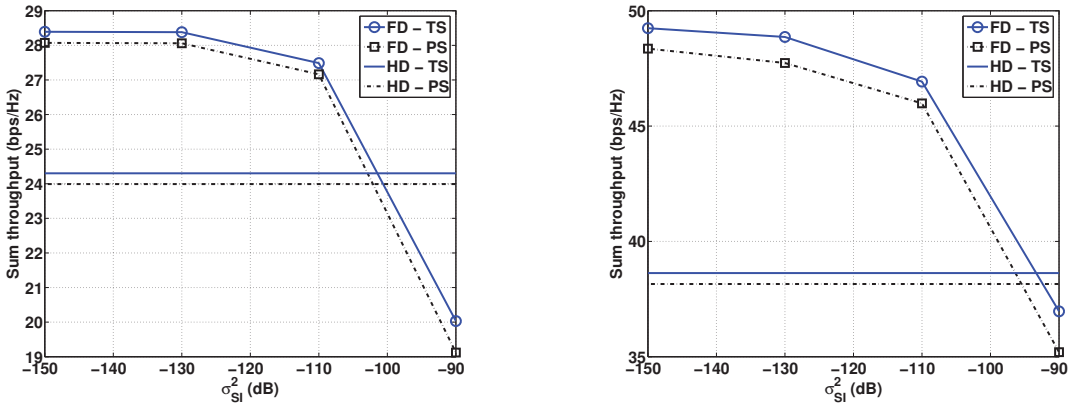

(a) $N_r = 1$ (b) $N_r = 2$

Figure 5.3: Effect of SI on the sum throughput performance in the single-cell networks.

Fig. 5.4 further illustrates how the total throughput is distributed into the downlink and uplink channels in the time splitting mechanism. The behaviour of the power splitting mechanism is similar and omitted here for brevity. With the increase of σ_{SI}^2, the UL throughput consistently decreases. Moreover, since the UL transmission

becomes less efficient, ULUs reduce their transmission power to reduce the interference toward DLUs. Consequently, a slight increase in FD DL throughput is observed as σ_{SI}^2 increases. Another note is that since the distance between ULU-DLU in small cell can be quite small due to the random deployment of ULUs and DLUs, DLUs' throughput can be severely degraded by the interference from ULUs. In fact, the FD DL throughput is 60% less than the counterpart of HD at $N_r = 1, \sigma_{SI}^2 = -150$ dB. By implementing multiple antenna at UEs (i.e. $N_r = 2$), DLUs in FD can handle the interference better and the FD DL throughput at $\sigma_{SI}^2 = -150$ dB is only 10% less than the counterpart of HD.

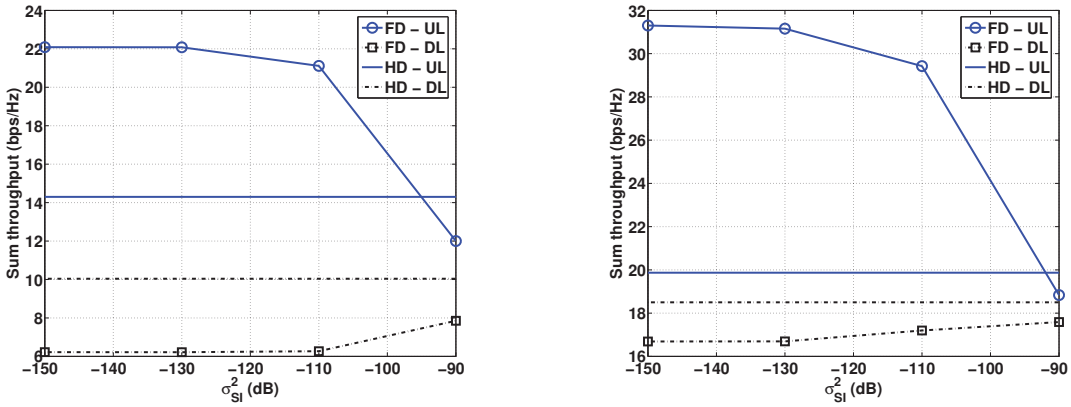

(a) $N_r = 1$ (b) $N_r = 2$

Figure 5.4: Effect of SI on the UL/DL throughput performance in the single-cell networks.

To analyze the effect of energy harvesting constraint, we fix $N_r = 2, \sigma_{SI}^2 = -110$ dB and vary $e^{\min}$. Fig. 5.5 illustrates a consistent decreasing trend of all schemes as $e^{\min}$ increases. The time splitting scheme outperforms the power splitting scheme in the considered range of $e^{\min}$ for both FD and HD. A similar conclusion can be drawn from Fig. 5.3. By using two different precoder matrices $\mathbf{V}^I$ and $\mathbf{V}^E$ for data transmission and energy transferring, the time splitting scheme can exploit the spatial diversity better than the power splitting scheme which only uses one type of precoder matrix for both purposes. Thus, the time splitting scheme is more efficient than the power splitting scheme in term of performance.

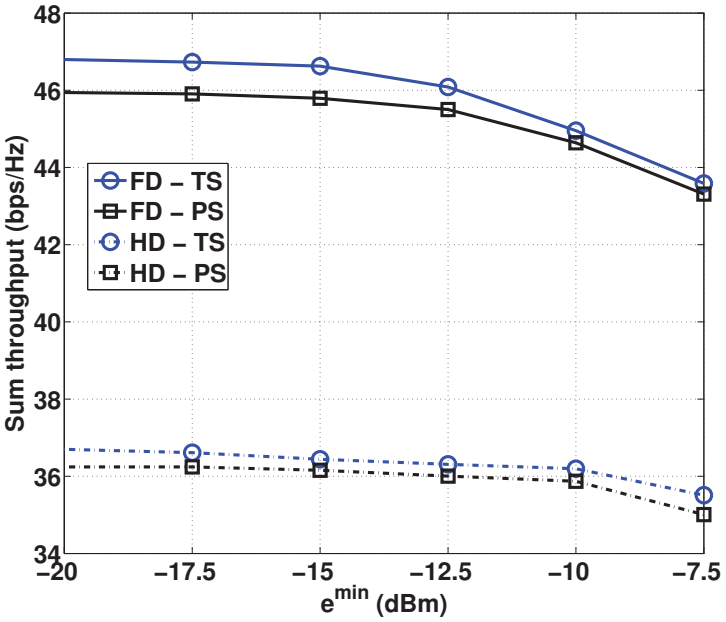

Figure 5.5: Effect of energy harvesting constraints on the total harvested energy performance in the single-cell networks.

The comparison of maximum harvested energy of time splitting scheme in both FD and HD systems is studied in Fig. 5.6. Interestingly, in case of $N_r = 1$, FD roughly harvests as much as HD. The reason of this is two folds. Firstly, it has been reported in [Nguyen et al., 2014; Mohammadi et al., 2015; Tam et al., 2016] that FD not always harnesses performance gain over HD if the distance between ULUs and DLUs are not large enough. Since we consider small cell networks with randomly deployed ULUs and DLUs, the ULU-DLU distance can be very small, which creates significant interference to DLUs. Secondly, with $N_r = 1$, DLUs can not exploit the spatial diversity to mitigate the interference from ULUs. Consequently, ULUs must reduce its transmit power to ensure the QoS at the DLUs, which lowers the amount of harvested energy at DLUs. In contrast, the results show that FD harvests more energy than HD given that $\sigma_{SI}^2 \leq -90$ dB for $N_r = 2$. All this implies that having multiple antennas at UEs is important to combat with extra interferences in FD.

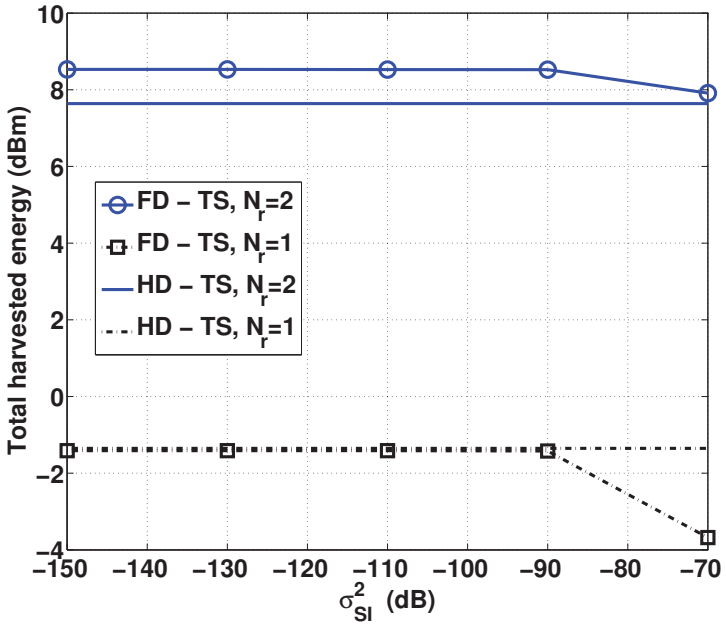

Figure 5.6: Effect of SI on the total harvested energy performance in the single-cell networks.

5.5.2 Three-cell Network

Now, we consider the sum throughput maximization problem and the total harvested energy in the three-cell networks as depicted in Fig. 5.2. In this scenario, DLUs and BSs are exposed to additional intercell interferences. According to Fig. 5.7, FD now only provides a marginal improvement regarding HD in both power splitting scheme (11.7%) and time splitting scheme (11.8%) for $N_r = 2, \sigma_{SI}^2 = -150$ dB. For $N_r = 1, \sigma_{SI}^2 = -150$ dB, the improvement is even lower with 4.1% in case of the power splitting scheme and 4.4% in case of time splitting scheme. Therefore, FD can give marginal gains compared to HD in the multi-cell networks with high level of interference.

The effect of energy harvesting constraint to the network sum throughput is also investigated in Fig. 5.8 for the three-cell networks with $N_r = 2, \sigma_{SI}^2 = -110$ dB. As in Fig. 5.5, a consistent decreasing trend of all schemes is observed as $e^{\min}$ increases. Since DLUs can also harvest energy from the signals arriving from other BSs in multicell

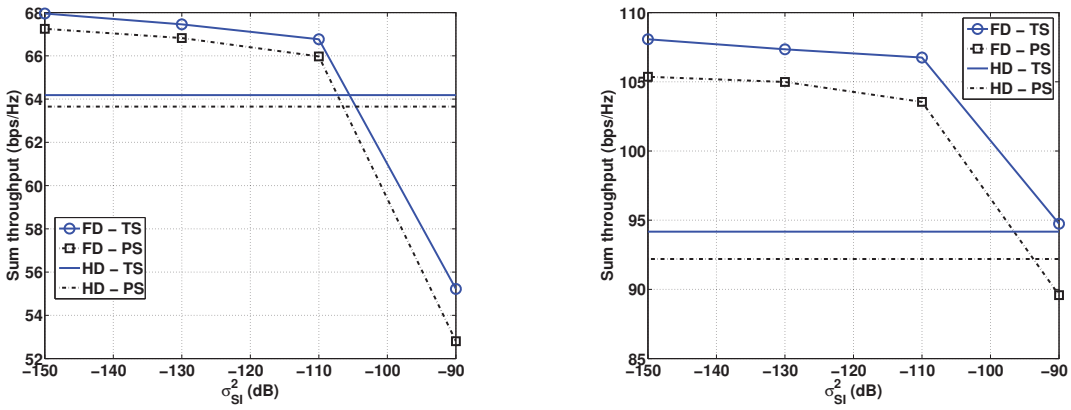

(a) $N_r = 1$ (b) $N_r = 2$

Figure 5.7: Effect of SI on the sum throughput performance in the three-cell networks.

networks, the FD network throughput only decreases by about 3% for both harvesting scheme when $e^{\min}$ increases from -20 dBm to -7.5 dBm. The counterpart throughput decrease in single-cell scenarios was about 8%.

Fig. 5.9 also illustrates the comparison of total harvested energy per cell of the EH maximization problem in both FD and HD systems in three-cell network. For $N_r = 1$, FD even harvests lesser amount of energy than HD given $\sigma^2_{SI} > -150$ dB due to the increasing level of interference when compared to a single-cell network. Similar to the single-cell network, FD outperforms HD for $\sigma^2_{SI} \leq -90$ dB if more antennas are equipped at UEs (i.e. $N_r = 2$). This observation again emphasizes the importance of having multiple antenna at UEs in FD to mitigate interference. Another note is that given $N_r = 2$ the amount of energy harvested per cell in three-cell networks (i.e. 10.09 dBm at $\sigma^2_{SI} = -150$ dB) is much higher than the harvested energy of single cell in Fig. 5.6 (i.e. 8.5 dBm at $\sigma^2_{SI} = -150$ dB), thanks to the extra energy harvested from the intercell interference.

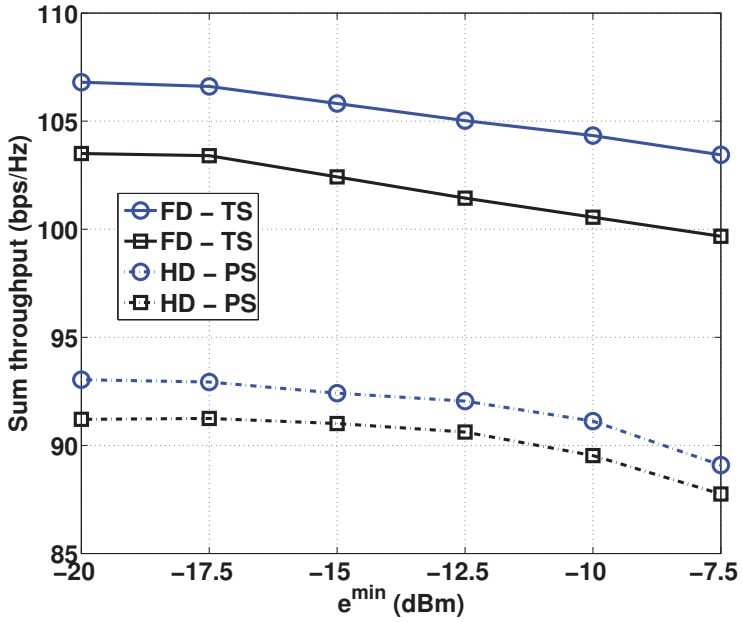

Figure 5.8: Effect of energy harvesting constraints on the total harvested energy performance in the three-cell networks.

5.5.3 Convergence Behavior

Finally, the convergence behavior of the proposed Algorithm 6 is illustrated in Fig. 5.10. For brevity, we only present the case of the three-cell network at $\sigma_{SI}^2 = -110$ dB and $N_r = 2$. Fig. 5.10(a) plots the convergence of the objective functions of the sum throughput maximization problem for the time splitting scheme and the power splitting scheme, whereas Fig. 5.10(b) plots the convergence of the objective function of the EH maximization problem. As can be seen, the sum throughput maximization problem achieve 90% of its final optimal value within 40 iterations whereas the EH maximization problem needs 10 iterations. Table 5.1 shows the average number of iterations required to solve each program. Note that each iteration of all programs only involves with a convex problem with polynomial complexity which can be solved efficiently by any available convex solvers such as CVX [Grant and Boyd, 2014].

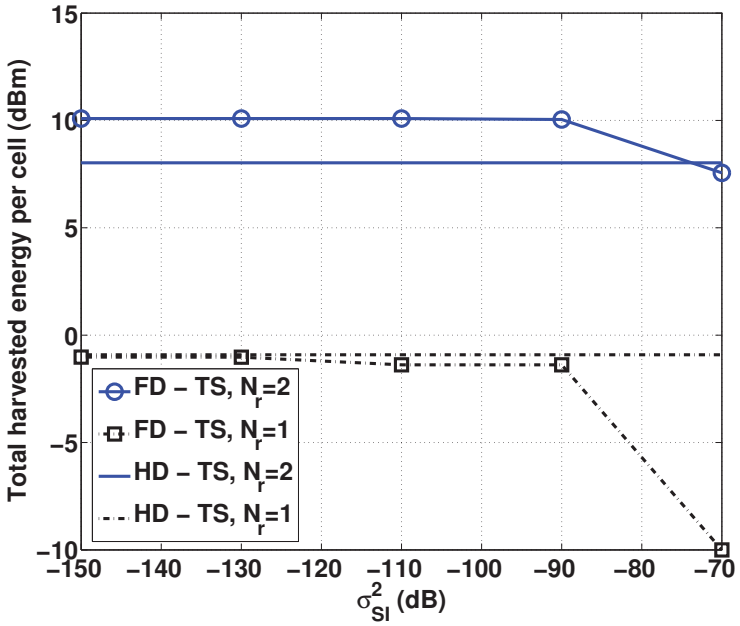

Figure 5.9: Effect of SI on the total harvested energy performance in the three-cell networks.

Table 5.1: The average number of iterations required by Algorithm 6

Programs	Throughput max., TS	Throughput max., PS	EH max.
FD	74	65.4	24.1
HD	67.5	50.6	20.2

5.6 Conclusion

In this chapter, we have proposed new optimal precoding matrix designs for EH-enabled FD multicell MU-MIMO networks. Specifically, the sum throughput maximization under throughput QoS constraints and energy harvesting (EH) constraints for energy-constrained devices under either TS or PS have been considered. The FD EH maximization problem under throughput QoS constraints in TS has also been addressed. Toward this end, we develop new path-following algorithms for their solution, which require a convex quadratic program for each iteration and is guaranteed to monotonically converge to at least a local optimum. In the end, we show the merits of our proposed

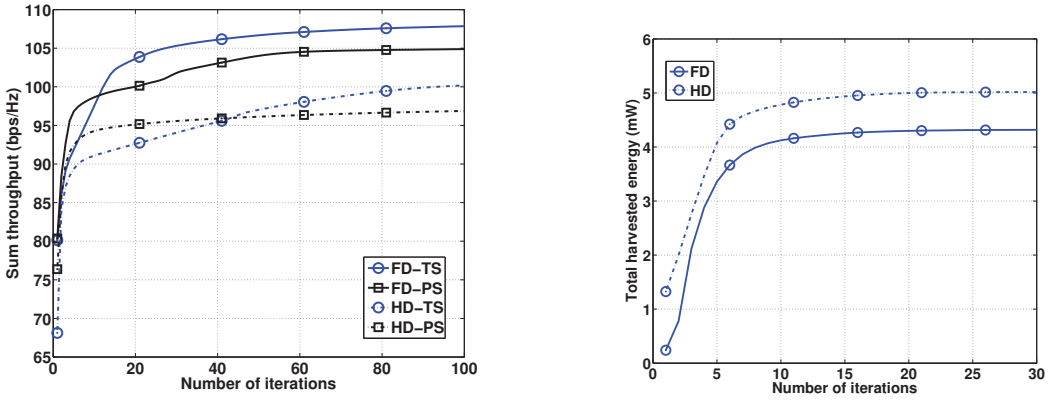

(a) Sum throughput maximization

(b) EH maximization

Figure 5.10: Convergence of Algorithm 6 for $\epsilon = 10^{-4}$.

algorithms through extensive simulations.

Chapter 6

Conclusions

6.1 Summary

To realize the ever increasing demand for high data throughput, massive user connectivity and extended device battery life, this dissertation considers three disruptive technologies in the 5G cellular network. Firstly, by densely deploying BSs of various sizes and types, HetNet provides better coverage and services for a large number of UEs in comparison to traditional cellular networks. Secondly, FD radio technology enables devices to simultaneously transmit and receive signals on the same frequency band, resulting in the potential of doubling the throughput. Thirdly, the new EH technology allows BSs to transmit both information and energy toward devices on the same channel, which potentially prolongs the battery life or even eliminates the need for a battery via wireless charging. However, the major obstacle preventing the successful implementation of these technologies is that they introduce even more sources of interference into the traditional network where the interference management has already been complicated. Managing interference under these technologies raises an inevitable demand for new resource allocation schemes (i.e., power allocation policy, BS-UE association policy and precoding matrix designs) to maximize the network performance while meeting the QoS requirements.

Since all the considered interference management problems are challenging nonconvex optimization problems, this dissertation has provided novel minorants/majorants of the nonconvex functions which are then used for the successive convex approximation framework. Consequently, the original optimization problems can be addressed via successively solving a low-complexity convex problem at each iteration. In **Chapter 3**, the joint design of BS-UE associations and transmit power control to maximize network total throughput or fairness among UEs in the downlink of a HetNet has been proposed. The nonconvex backhaul constraints are considered to represent the practical low-cost backhaul solutions of small cells. The considered problems belong to the class of mixed integer nonconvex optimization and have been addressed by the proposed iterative algorithms based on alternating descent and successive convex programming. Numerical results have illustrated the effect of backhaul capacity on the BS-UE associations and power control policy.

In **Chapter 4**, we firstly considered the joint design of UL and DL linear precoders in an FD MU-MIMO multicell network to maximize the total network throughput or the UE's fairness. The effect of the two new additional sources of interference in an FD network (i.e. SI and the cross interference of UL and DL transmission) on the network throughput was also analyzed. To prevent either side of the transmission from shutting down due to the excessive incurring interference, the throughput constraints that have not been efficiently handled before were applied. The considered problem is nonconvex and has been addressed by the proposed successive convex quadratic programming. Extensive numerical results demonstrated the advantages of the proposed algorithms over existing solutions. The FD system also has been verified to provide better spectral efficiency than the HD system.

The proposed framework can then be extended for the optimal precoding matrices design in an HD MU-MIMO multicell network with the H-K transmission strategy. The transmitted data information of users in this strategy is split into two parts: a private message to be decoded at the intended receiver and a common message that can

be decoded at both intended receiver and shared receiver. Under this strategy, the throughput maximization problem is nonconvex since the throughput function is nonsmooth and nonconvex. The optimal precoder matrices under H-K strategy are found via a successive convex quadratic programming algorithm that generates a sequence of improved points. As expected, the H-K strategy offers higher performance in comparison to the conventional approach where the intercell interference is treated as noise, especially in the medium to strong interference channels.

In **Chapter 5**, the efficient design of precoding matrices for the network sum throughput maximization with QoS constraints in an FD EH-enabled multicell MU-MIMO network has been proposed. EH constraints were considered to guarantee a reliable wireless charging. The considered problem with either PS or TS is challenging computationally due to nonconcave objective function and nonconvex constraints. By adapting the algorithms for the FD problem in Chapter 4, the problem with PS has been efficiently addressed. On the other hand, it is nontrivial to extend the same algorithm to solve the problem with TS due to the coupling of the TS variable with both the DL throughput function and the SI in the UL throughput function. A new inner approximation of the original problem has been proposed to solve the problem iteratively in a successive convex programming framework. Finally, the FD EH maximization problem with throughput QoS constraints with TS has also been addressed by applying an approach similar to that proposed for the TS problem.

6.2 Future Research Directions

All the results presented in this PhD dissertation have illustrated that the considered technologies in 5G provide the enhancement of network performance in terms of total network throughput or UE's fairness in comparison to traditional networks. However, we have assumed here that all the control information is delivered to a central processing unit (CPU) to do all the computation. This design creates a central point of failure.

In addition, since all the control information is gathered at the CPU, the capacity of backhaul links connected to the CPU must be sufficiently high. Otherwise, there will be delay/jitter in the service. It is of great interest to investigate algorithms that allow BS to decide their resource allocation strategy based on just local information or with minimum information exchange among the BSs. In addition, considering imperfect CSI is also an important future research direction.

In Chapter 3, we have assumed that all BSs and UEs are equipped with single antenna only. It would be more efficient to consider multiple antennas at BSs and UEs. In fact, MIMO setting will help to combat interference better with optimal precoding matrix designs. Thanks to spatial multiplexing gain, more UEs can be simultaneously served on the same channel. Although it is interesting to consider such MIMO HetNets, the throughput function is involved with the determinant operation, rendering the whole problem even more challenging. Another potential extension is to allow some small cells to temporally turn off if they serve no UEs to reduce the interference. In this case, since the throughput offered by a BS is divided by a number of UEs served by that BS, a new expression of throughput function is required to accommodate the deactivation of a BS. The structure of this new function might be very complicated to deal with compared to that considered in this dissertation.

Finally, the power consumption problem in the future cellular network design is receiving significant attention from both industry and academia [Li et al., 2011; Han et al., 2016; Zarakovitis et al., 2016]. Since the total energy consumed by the worldwide cellular networks and wireline communications is more than 3% of global electric energy consumption [Fettweis and Zimmermann, 2008], improving the efficiency of the energy usage reduces both the energy expense for the operators and the carbon footprint toward the environment. The energy efficiency utility which is a fraction of total throughput over total consumed energy has been proposed so that maximizing this utility will improve both the spectral efficiency and the energy usage [Wang et al., 2013; Zarakovitis et al., 2016]. The optimization problem involved with such a complicated fractional

function as the energy efficiency utility is a challenging and interesting problem for future research.

Appendix A

Proof of Proposition 3.2

Firstly, notice that functions

$$f_{nk}(\mathbf{x}_{nk}, \mathbf{y}_k) \triangleq \frac{r_{nk}(p)\boldsymbol{x}_{nk}^2}{\mathbf{y}_k},\ k = 1, \ldots, K$$

are jointly convex in $\mathbf{x}_{nk}$ and $\mathbf{y}_k$. Therefore, $f_{nk}(\mathbf{x}_{nk}, \mathbf{y}_k)$ admits its first order approximation at $(x_{nk}^{(\kappa)}, y_k^{(\kappa)})$ as a lower bound [Tuy, 1998] as follows

$$f_{nk}(\mathbf{x}_{nk}, \mathbf{y}_k) \geq f_{nk}(x_{nk}^{(\kappa)}, y_k^{(\kappa)}) + \frac{2r_{nk}(p)x_{nk}^{(\kappa)}\left(\mathbf{x}_{nk} - x_{nk}^{(\kappa)}\right)}{y_k^{(\kappa)}} - \frac{r_{nk}(p)(x_{nk}^{(\kappa)})^2}{(y_k^{(\kappa)})^2}\left(\mathbf{y}_k - y_k^{(\kappa)}\right).$$

By replacing $\mathbf{y}_k := \langle \mathbf{x}_k^2 \rangle > 0,\ \forall k = 1, \ldots, K$, we have

$$f_{nk}(\mathbf{x}_{nk}, [\langle \mathbf{x}_k^2 \rangle]_{k=1,\ldots,K}) = \frac{r_{nk}(p)\boldsymbol{x}_{nk}^2}{\langle \boldsymbol{x}_k^2 \rangle} \geq \alpha_{nk}^{(\kappa)}(\mathbf{x}, p).$$

Secondly, since $\mathbf{x}_{nk}^2 - \mathbf{x}_{nk}$ is a convex quadratic function, it also admits its first order approximation at $x^{(\kappa)}$ as a lower bound as

$$\mathbf{x}_{nk}^2 - \mathbf{x}_{nk} \geq (x_{nk}^{(\kappa)})^2 - x_{nk}^{(\kappa)} + \left(2x_{nk}^{(\kappa)} - 1\right)\left(\mathbf{x}_{nk} - x_{nk}^{(\kappa)}\right) = \gamma_{nk}^{(\kappa)}(\mathbf{x}).$$

Therefore, we have

$$\mathcal{P}_1(\mathbf{x}, p) \geq \tilde{\mathcal{P}}_1^{(\kappa)}(\mathbf{x}, p)$$

at a point $(x^{(\kappa)}, p)$. This completes the proof.

Appendix B

Proof of Proposition 3.3

To prove Proposition 3.3, we need some preliminary results first. Let us define

$$g_n(x_1, \ldots, x_n) \triangleq \left(\sum_{i=1}^{n} x_i^{-1} \right)^{-1}. \tag{2.1}$$

Theorem B.1. *For $x_1 > 0$, $x_2 > 0$, $g_2(x_1, x_2)$ is a concave and monotonically increasing function in (x_1, x_2).*

Proof. One has

$$g_2(x_1, x_2) = x_1 - x_1^2/(x_1 + x_2)$$

which is concave in $x_1 > 0$, $x_2 > 0$. Moreover, as $x_1^{-1} + x_2^{-1}$ is monotonically decreasing in $x_1 > 0$, $x_2 > 0$, $g_2(x_1, x_2) = 1/(x_1^{-1} + x_2^{-1})$ is monotonically increasing in $x_1 > 0$, $x_2 > 0$. ■

Theorem B.2. *The function $g_n(x_1, \ldots, x_n) = \left(\sum_{i=1}^{n} x_i^{-1}\right)^{-1}$ is concave in $x_i > 0,\ i = 1, \ldots, n$, $\forall n \geq 1$.*

Proof. In Theorem B.1, we have proved that $g_2(x_1, x_2)$ is concave in $x_1 > 0$, $x_2 > 0$. Assuming that $g_{n-1}(x_1, \ldots, x_{n-1})$ is concave in $x_i > 0,\ i = 1, \ldots, n-1$ for some n, we

now show that $g_n(x_1, \ldots, x_n)$ is also concave. Firstly, one has

$$\begin{aligned} g_n(x_1, \ldots, x_n) &= \left(\sum_{i=1}^{n} x_i^{-1} \right)^{-1} \\ &= x_n - x_n^2 \left(x_n + g_{n-1}(x_1, \ldots, x_{n-1}) \right)^{-1} \\ &= g_2 \left(x_n, g_{n-1}(x_1, \ldots, x_{n-1}) \right). \end{aligned}$$

Since $g_2(x, y)$ is a concave and monotonically increasing function in (x, y) and $g_{n-1}(x_1, \ldots, x_{n-1})$ is assumed to be concave, we have

$$\begin{aligned} & g_n(\alpha(x_1, \ldots, x_n) + \beta(y_1, \ldots, y_n)) \\ & = g_2 \left(\alpha x_n + \beta y_n, g_{n-1}(\alpha(x_1, \ldots, x_{n-1}) + \beta(y_1, \ldots, y_{n-1})) \right) \\ & \geq g_2 \left(\alpha x_n + \beta y_n, \alpha g_{n-1}(x_1, \ldots, x_{n-1}) + \beta g_{n-1}(y_1, \ldots, y_{n-1}) \right) \\ & \geq \alpha g_2(x_n, g_{n-1}(x_1, \ldots, x_{n-1})) + \beta g_2(y_n, g_{n-1}(y_1, \ldots, y_{n-1})) \\ & = \alpha g_n(x_1, \ldots, x_n) + \beta g_n(y_1, \ldots, y_n) \end{aligned}$$

for $\alpha \geq 0, \beta \geq 0, \alpha + \beta = 1$ and $\forall x_i > 0, y_i > 0, i = 1, \ldots, n > 0$. Thus, $g_n(x_1, \ldots, x_n)$ is also concave in $x_i > 0,\ i = 1, \ldots, n,\ \forall n \geq 2$. ■

Theorem B.3. *The function* $\ln \left(\sum_{i=1}^{n} x_i^{-1} \right)$ *is convex in* $x_i > 0,\ i = 1, \ldots, n,\ \forall n \geq 1$.

Proof. Let us define $f(x) \triangleq \ln(x)$. Then $\ln \left(\sum_{i=1}^{n} x_i^{-1} \right) = -f(g_n(x_1, \ldots, x_n))$. Since $g_n(x_1, \ldots, x_n)$ is a concave function in $x_i > 0, i = 1, \ldots, n$, according to Theorem B.2 we have

$$g_n(\alpha(x_1, \ldots, x_n) + \beta(y_1, \ldots, y_n)) \geq \alpha g_n(x_1, \ldots, x_n) + \beta g_n(y_1, \ldots, y_n),$$

with $\alpha \geq 0, \beta \geq 0, \alpha + \beta = 1$ and $\forall x_i > 0, y_i > 0, i = 1, \ldots, n > 0$. Moreover, since $f(x)$ is a concave and monotonically increasing function, we have

$$\begin{aligned} & f(g_n(\alpha(x_1, \ldots, x_n) + \beta(y_1, \ldots, y_n))) \\ & \geq f(\alpha g_n(x_1, \ldots, x_n) + \beta g_n(y_1, \ldots, y_n)) \\ & \geq \alpha f(g_n(x_1, \ldots, x_n)) + \beta f(g_n(y_1, \ldots, y_n)). \end{aligned}$$

This shows the concavity of $f(g_n(x_1,\ldots,x_n))$. Therefore, $-f(g_n(x_1,\ldots,x_n))$ is a convex function. ■

We are now ready to prove Proposition 3.3. One can write

$$r_{nk}(\mathbf{p}) \triangleq \ln\left(\sum_{j=1}^{K} g_{nj}\mathbf{p}_j + \sigma^2\right) - \ln\left(\sum_{j\neq k, j=1}^{K} g_{nj}\mathbf{p}_j + \sigma^2\right).$$

Since $\ln(x)$ is a concave function with $x > 0$, it is true that

$$\ln\left(\sum_{j=1}^{K} g_{nj}\mathbf{p}_j + \sigma^2\right) \leq \ln\left(\sum_{j=1}^{K} g_{nj}p_j^{(\kappa)} + \sigma^2\right) + \frac{\sum_{j=1}^{K} g_{nj}(\mathbf{p}_j - p_j^{(\kappa)})}{\sum_{j=1}^{K} g_{nj}p_j^{(\kappa)} + \sigma^2}, \tag{2.2}$$

at some point $p^{(\kappa)}$.

In addition, upon defining $f(x) \triangleq \ln\left(\sum_{i=1}^{n} x_i^{-1}\right)$ with $x = [x_1,\ldots,x_n],\ x_i > 0,\ \forall i$, one has

$$f(x) \geq \ln\left(\sum_{i=1}^{n}(x_i^{(\kappa)})^{-1}\right) - \frac{1}{\sum_{i=1}^{n}(x_i^{(\kappa)})^{-1}} \sum_{i=1}^{n}\left(\frac{x_i - x_i^{(\kappa)}}{(x_i^{(\kappa)})^2}\right)$$

at some $x^{(\kappa)}$, due to the convexity of $f(x)$ by Theorem B.3. Thus, one also has the following bound

$$\ln\left(\sum_{i=1}^{n} x_i\right) \geq \ln\left(\sum_{i=1}^{n} x_i^{(\kappa)}\right) - \frac{1}{\sum_{i=1}^{n} x_i^{(\kappa)}} \sum_{i=1}^{n}(x_i^{(\kappa)})^2\left(\frac{1}{x_i} - \frac{1}{x_i^{(\kappa)}}\right).$$

It follows that

$$\ln\left(\sum_{j\neq k, j=1}^{K} g_{nj}\mathbf{p}_j + \sigma^2\right) \leq \ln\left(\sum_{j\neq k, j=1}^{K} g_{nj}p_j^{(\kappa)} + \sigma^2\right) - \frac{1}{\sum_{j\neq k, j=1}^{K} g_{nj}p_j^{(\kappa)} + \sigma^2} \sum_{j\neq k, j=1}^{K}\left(g_{nj}p_j^{(\kappa)}\right)^2\left(\frac{1}{g_{nj}\mathbf{p}_j} - \frac{1}{g_{nj}p_j^{(\kappa)}}\right). \tag{2.3}$$

By combining (2.2) and (2.3), (3.20) follows. Similarly, (3.21) can be proved with minor modifications to (2.2) and (2.3).

Appendix C

Quadratic Forms

From (4.5) and (4.10), it is straightforward to see that

$$\mathcal{M}_{i,j_{\mathsf{D}}}(\mathbf{V}) \triangleq \sum_{(m,\ell_{\mathsf{D}})\in\mathcal{S}_1} H_{m,i,j_{\mathsf{D}}}\mathbf{V}_{m,\ell_{\mathsf{D}}}\mathbf{V}_{m,\ell_{\mathsf{D}}}^H H_{m,i,j_{\mathsf{D}}}^H + \sum_{\ell_{\mathsf{U}}\in\mathcal{U}} H_{i,j_{\mathsf{D}},\ell_{\mathsf{U}}}\mathbf{V}_{i,\ell_{\mathsf{U}}}\mathbf{V}_{i,\ell_{\mathsf{U}}}^H H_{i,j_{\mathsf{D}},\ell_{\mathsf{U}}}^H + \sigma_{\mathsf{D}}^2 I_{N_r}, \tag{3.1}$$

$$\begin{aligned}\mathcal{M}_i(\mathbf{V}) = &\sum_{(m,\ell_{\mathsf{U}})\in\mathcal{S}_2} H_{m,\ell_{\mathsf{U}},i}\mathbf{V}_{m,\ell_{\mathsf{U}}}\mathbf{V}_{m,\ell_{\mathsf{U}}}^H H_{m,\ell_{\mathsf{U}},i}^H + \sigma_{SI}^2 H_i^{\mathcal{SI}}\left(\sum_{\ell_{\mathsf{D}}\in\mathcal{D}}\mathbf{V}_{i,\ell_{\mathsf{D}}}\mathbf{V}_{i,\ell_{\mathsf{D}}}^H\right)(H_i^{\mathcal{SI}})^H \\ &+ \sum_{m\in\mathcal{I}\setminus\{i\}} H_{m,i}^{\mathcal{B}}\left(\sum_{j_{\mathsf{D}}\in\mathcal{D}}\mathbf{V}_{m,j_{\mathsf{D}}}\mathbf{V}_{m,j_{\mathsf{D}}}^H\right)(H_{m,i}^{\mathcal{B}})^H + \sigma_{\mathsf{U}}^2 I_{N_2}.\end{aligned} \tag{3.2}$$

Then,

$$\begin{aligned}\Theta_{i,j_{\mathsf{D}}}^{(\kappa)}(\mathbf{V}) = &f_{i,j_{\mathsf{D}}}(V^{(\kappa)}) + 2\,\mathrm{Re}\left\{\langle(\tilde{\mathcal{A}}_{i,j_{\mathsf{D}}}^{(\kappa)})^H, \mathbf{V}_{i,j_{\mathsf{D}}} - V_{i,j_{\mathsf{D}}}^{(\kappa)}\rangle\right\} \\ &- \sum_{(m,\ell_{\mathsf{D}})\in\mathcal{S}_1}(\langle(\mathbf{V}_{m,\ell_{\mathsf{D}}})^H\tilde{\mathcal{B}}_{i,j_{\mathsf{D}}}^{(\kappa)}(m)\mathbf{V}_{m,\ell_{\mathsf{D}}}\rangle - \langle(V_{m,\ell_{\mathsf{D}}}^{(\kappa)})^H\tilde{\mathcal{B}}_{i,j_{\mathsf{D}}}^{(\kappa)}(m)V_{m,\ell_{\mathsf{D}}}^{(\kappa)}\rangle) \\ &- \sum_{\ell_{\mathsf{U}}\in\mathcal{U}}(\langle(\mathbf{V}_{i,\ell_{\mathsf{U}}})^H\tilde{\mathcal{C}}_{i,j_{\mathsf{D}}}^{(\kappa)}(\ell_{\mathsf{U}})\mathbf{V}_{i,\ell_{\mathsf{U}}}\rangle - \langle(V_{i,\ell_{\mathsf{U}}}^{(\kappa)})^H\tilde{\mathcal{C}}_{i,j_{\mathsf{D}}}^{(\kappa)}(\ell_{\mathsf{U}})V_{i,\ell_{\mathsf{U}}}^{(\kappa)}\rangle),\end{aligned} \tag{3.3}$$

with

$$\tilde{\mathcal{A}}_{i,j_{\mathsf{D}}}^{(\kappa)} \triangleq (V_{i,j_{\mathsf{D}}}^{(\kappa)})^H H_{i,i,j_{\mathsf{D}}}^H \Psi_{i,j_{\mathsf{D}}}^{-1}(V^{(\kappa)})H_{i,i,j_{\mathsf{D}}}, \tag{3.4a}$$

$$\tilde{\mathcal{D}}_i^{(\kappa)}(\ell_{\mathsf{U}}) \triangleq (V_{i,\ell_{\mathsf{U}}}^{(\kappa)})^H H_{i,\ell_{\mathsf{U}}}^H \Psi_i^{-1}(V^{(\kappa)})H_{i,\ell_{\mathsf{U}}},\ \ell_{\mathsf{U}}\in\mathcal{U}, \tag{3.4b}$$

and

$$\tilde{\mathcal{B}}_{i,j_{\mathsf{D}}}^{(\kappa)}(m) \triangleq H_{m,i,j_{\mathsf{D}}}^{H}\left[\Psi_{i,j_{\mathsf{D}}}^{-1}(V^{(\kappa)}) - \mathcal{M}_{i,j_{\mathsf{D}}}^{-1}(V^{(\kappa)})\right] H_{m,i,j_{\mathsf{D}}} \succeq 0, \tag{3.5a}$$

$$\tilde{\mathcal{C}}_{i,j_{\mathsf{D}}}^{(\kappa)}(\ell_{\mathsf{U}}) \triangleq H_{i,j_{\mathsf{D}},\ell_{\mathsf{U}}}^{H}\left[\Psi_{i,j_{\mathsf{D}}}^{-1}(V^{(\kappa)}) - \mathcal{M}_{i,j_{\mathsf{D}}}^{-1}(V^{(\kappa)})\right] H_{i,j_{\mathsf{D}},\ell_{\mathsf{U}}} \succeq 0,\ \ell_U \in \mathcal{U}. \tag{3.5b}$$

Also,

$$\begin{aligned}\Theta_i^{(\kappa)}(\mathbf{V}) =& f_i(V^{(\kappa)}) + 2\sum_{\ell_{\mathsf{U}}\in\mathcal{U}} \mathrm{Re}\left\{\langle(\tilde{\mathcal{D}}_i^{(\kappa)}(\ell_{\mathsf{U}}))^H, \mathbf{V}_{i,\ell_{\mathsf{U}}} - V_{i,\ell_{\mathsf{U}}}^{(\kappa)}\rangle\right\} \\ &- \sum_{(m,\ell_{\mathsf{U}})\in\mathcal{S}_2} (\langle(\mathbf{V}_{m,\ell_{\mathsf{U}}})^H \tilde{\mathcal{E}}_i^{(\kappa)}(m,\ell_{\mathsf{U}})\mathbf{V}_{m,\ell_{\mathsf{U}}}\rangle - \langle(V_{m,\ell_{\mathsf{U}}}^{(\kappa)})^H \tilde{\mathcal{E}}_i^{(\kappa)}(m,\ell_{\mathsf{U}})V_{m,\ell_{\mathsf{U}}}^{(\kappa)}\rangle) \\ &- \sigma_{SI}^2 \sum_{\ell_{\mathsf{D}}\in\mathcal{D}} (\langle(\mathbf{V}_{i,\ell_{\mathsf{D}}})^H \tilde{\mathcal{F}}_i^{(\kappa)}\mathbf{V}_{i,\ell_{\mathsf{D}}}\rangle - \langle(V_{i,\ell_{\mathsf{D}}}^{(\kappa)})^H \tilde{\mathcal{F}}_i^{(\kappa)}V_{i,\ell_{\mathsf{D}}}^{(\kappa)}\rangle) \\ &- \sum_{m\in\mathcal{I}\setminus\{i\}} \sum_{j_{\mathsf{D}}\in\mathcal{D}} (\langle(\mathbf{V}_{m,j_{\mathsf{D}}})^H \tilde{\mathcal{G}}_i^{(\kappa)}(m)\mathbf{V}_{m,j_{\mathsf{D}}}\rangle - \langle(V_{m,j_{\mathsf{D}}}^{(\kappa)})^H \tilde{\mathcal{G}}_i^{(\kappa)}(m)V_{m,j_{\mathsf{D}}}^{(\kappa)}\rangle)\end{aligned} \tag{3.6}$$

with

$$\tilde{\mathcal{E}}_i^{(\kappa)}(m,\ell_{\mathsf{U}}) \triangleq H_{m,\ell_{\mathsf{U}},i}^{H}\left[\Psi_i^{-1}(V^{(\kappa)}) - \mathcal{M}_i^{-1}(V^{(\kappa)})\right] H_{m,\ell_{\mathsf{U}},i} \succeq 0,\ (m,\ell_{\mathsf{U}}) \in \mathcal{S}_2, \tag{3.7a}$$

$$\tilde{\mathcal{F}}_i^{(\kappa)} \triangleq (H_i^{\mathcal{SI}})^H\left[\Psi_i^{-1}(V^{(\kappa)}) - \mathcal{M}_i^{-1}(V^{(\kappa)})\right] H_i^{\mathcal{SI}} \succeq 0, \tag{3.7b}$$

$$\tilde{\mathcal{G}}_i^{(\kappa)}(m) \triangleq (H_{m,i}^{\mathcal{B}})^H\left[\Psi_i^{-1}(V^{(\kappa)}) - \mathcal{M}_i^{-1}(V^{(\kappa)})\right] H_{m,i}^{\mathcal{B}} \succeq 0,\ m \in \mathcal{I}\setminus\{i\}. \tag{3.7c}$$

Appendix D

Proof of Theorem 4.1

Let $\mathcal{L}(\mathbf{V})$ be a linear mapping in the form (4.4) or (4.8). Now introduce the intermediate matrix variable $\mathbf{Y}$, which satisfies the following matrix inequality:

$$\mathbf{Y} \succ \mathcal{L}(\mathbf{V})\mathcal{L}^H(\mathbf{V}). \tag{4.1}$$

Let us define

$$g(\mathbf{V}, \mathbf{Y}) \triangleq \ln \left| I_{N_2} - \mathcal{L}(\mathbf{V})\mathcal{L}^H(\mathbf{V})\mathbf{Y}^{-1} \right|, \tag{4.2}$$

which is well-posed in the domain (4.1).

To prove Theorem 4.1, the following theorem is needed.

Theorem D.1. *In the domain constrained by (4.1), function $g(\mathbf{V}, \mathbf{Y})$ is jointly concave in $(\mathbf{V}, \mathbf{Y})$ with its differential at point $(V^{(\kappa)}, Y^{(\kappa)})$ (which is also its super-differentials Tuy [1998]) given by*

$$\begin{aligned} \langle \nabla g(V^{(\kappa)}, Y^{(\kappa)}), (\mathbf{V}, \mathbf{Y}) - (V^{(\kappa)}, Y^{(\kappa)}) \rangle \quad &= \\ -2 \operatorname{Re} \left\{ \langle \left(Y^{(\kappa)} - \mathcal{L}(V^{(\kappa)})\mathcal{L}^H(V^{(\kappa)}) \right)^{-1} \mathcal{L}(V^{(\kappa)}), \mathcal{L}(\mathbf{V}) - \mathcal{L}(V^{(\kappa)}) \rangle \right\} & \\ + \langle \left(Y^{(\kappa)} - \mathcal{L}(V^{(\kappa)})\mathcal{L}^H(V^{(\kappa)}) \right)^{-1} - (Y^{(\kappa)})^{-1}, \mathbf{Y} - Y^{(\kappa)} \rangle. & \end{aligned} \tag{4.3}$$

In particular, the following global upper bound holds on the domain constrained by (4.1):

$$g(\mathbf{V}, \mathbf{Y}) \leq g(V^{(\kappa)}, Y^{(\kappa)}) + \langle \nabla g(V^{(\kappa)}, Y^{(\kappa)}), (\mathbf{V}, \mathbf{Y}) - (V^{(\kappa)}, Y^{(\kappa)}) \rangle. \tag{4.4}$$

To prove Theorem D.1, the following auxiliary lemmas are needed.

Lemma D.1 (Convex matrix inequality Rashid et al. [2014])**.** *For the matrix-valued mapping*

$$h\left(\mathbf{V},\mathbf{Y}\right)\triangleq\mathcal{L}(\mathbf{V})\mathbf{Y}^{-1}\mathcal{L}^{H}(\mathbf{V}),\tag{4.5}$$

the following matrix inequality holds for all $\mathbf{V}^{(1)}$*,* $\mathbf{V}^{(2)}$ *and* $\mathbf{Y}^{(1)}\succ 0,\ \mathbf{Y}^{(2)}\succ 0$ *and* $\lambda\in[0,1]$*:*

$$h\left(\lambda(\mathbf{V}^{(1)},\mathbf{Y}^{(1)})+(1-\lambda)(\mathbf{V}^{(2)},\mathbf{Y}^{(2)})\right)\preceq\lambda h(\mathbf{V}^{(1)},\mathbf{Y}^{(1)})+(1-\lambda)h(\mathbf{V}^{(2)},\mathbf{Y}^{(2)}).\tag{4.6}$$

Lemma D.2. *On the domain* $0\preceq\mathbf{S}\prec I_d$*, the function*

$$\varphi(\mathbf{S})\triangleq\ln|I_d-\mathbf{S}|$$

is concave and monotonically decreasing in the sense that

$$\varphi(\mathbf{S}_1)\leq\varphi(\mathbf{S}_2),\quad\forall\, I_d\succ\mathbf{S}_2\succeq\mathbf{S}_1\succeq 0.\tag{4.7}$$

Proof of Lemma D.2 The fact that φ is concave is well known. Also (4.7) follows from $I_d-\mathbf{S}_2\succeq I_d-\mathbf{S}_1\succeq 0$ that yields $|I_d-\mathbf{S}_2|\geq|I_d-\mathbf{S}_1|$. ■

With the above lemmas, we prove Theorem D.1 as follows. *Proof of Theorem D.1* Note that $g(\mathbf{V},\mathbf{Y})=\varphi(h(\mathbf{V},\mathbf{Y}))$. Therefore, whenever $\lambda\in[0,1]$, it is true that

$$\begin{aligned}
g(\lambda(\mathbf{V}^{(1)},\mathbf{Y}^{(1)})+(1-\lambda)(\mathbf{V}^{(2)},\mathbf{Y}^{(2)})) &= \varphi(h(\lambda(\mathbf{V}^{(1)},\mathbf{Y}^{(1)})+(1-\lambda)(\mathbf{V}^{(2)},\mathbf{Y}^{(2)})))\\
&\geq \varphi(\lambda h(\mathbf{V}^{(1)},\mathbf{Y}^{(1)})+(1-\lambda)h(\mathbf{V}^{(2)},\mathbf{Y}^{(2)}))\\
&\geq \lambda\varphi(h(\mathbf{V}^{(1)},\mathbf{Y}^{(1)}))+(1-\lambda)\varphi(h(\mathbf{V}^{(2)},\mathbf{Y}^{(2)}))\\
&= \lambda g(\mathbf{V}^{(1)},\mathbf{Y}^{(1)})+(1-\lambda)g(\mathbf{V}^{(2)},\mathbf{Y}^{(2)}),
\end{aligned}$$

which shows the concavity of $g(\cdot)$. To show (4.3), rewrite $g(\cdot)$ as

$$g(\mathbf{V},\mathbf{Y})=\ln\left|\mathbf{Y}-\mathcal{L}(\mathbf{V})\mathcal{L}^{H}(\mathbf{V})\right|-\ln|\mathbf{Y}|\tag{4.8}$$

and apply the standard differential rule for each natural logarithmic functions. Finally, (4.4) follows from the concavity of g Tuy [1998]. ■

Proof of Theorem 4.1. Upon substituting

$$\begin{gathered}\mathcal{L}(\mathbf{V}) \in \{\mathcal{L}_{i,j_{\mathsf{D}}}(\mathbf{V}_{i,j_{\mathsf{D}}}), \mathcal{L}_i(\mathbf{V}_{\mathsf{U}i})\}, \mathbf{Y} \in \{\mathcal{M}_{i,j_{\mathsf{D}}}(\mathbf{V}), \mathcal{M}_i(\mathbf{V})\}, \\ Y^{(\kappa)} \in \{\mathcal{M}_{i,j_{\mathsf{D}}}(V^{(\kappa)}), \mathcal{M}_i(V^{(\kappa)})\}\end{gathered} \tag{4.9}$$

into (4.4), (4.23) and (4.24) follow with the notice that

$$f_{i,j_{\mathsf{D}}}(\mathbf{V}) \equiv -g(\mathbf{V}_{i,j_{\mathsf{D}}}, \mathbf{Y}) \quad \text{or} \quad f_i(\mathbf{V}) \equiv -g(\mathbf{V}_{\mathsf{U}i}, \mathbf{Y})$$

under the substitution (4.9). ■

Appendix E

Proof of Proposition 4.1

Due to (4.23) and (4.24), any $\mathbf{V}$ feasible to (4.25) is also feasible to the nonconvex program (4.11). Moreover, (4.25) is a minorant maximization of (4.11). As $V^{(\kappa)}$ is feasible to (4.25), it follows that

$$\mathcal{P}_1(V^{(\kappa+1)}) \geq \mathcal{P}_1^{(\kappa)}(V^{(\kappa+1)}) > \mathcal{P}_1^{(\kappa)}(V^{(\kappa)}) = \mathcal{P}_1(V^{(\kappa)})$$

as far as $V^{(\kappa+1)} \neq V^{(\kappa)}$. Hence, (4.26) is shown.

Furthermore, the sequence $\{V^{(\kappa)}\}$ is bounded by constraint (4.11b). By Cauchy theorem, there is a convergent subsequence $\{V^{(\kappa_\nu)}\}$, so $\lim_{\nu\to+\infty} \left[\mathcal{P}_1(V^{(\kappa_{\nu+1})}) - \mathcal{P}_1(V^{(\kappa_\nu)})\right] = 0$. For every κ, there is ν such that $\kappa_\nu \leq \kappa$ and $\kappa + 1 \leq \kappa_{\nu+1}$. By (4.26), it is true that

$$0 \leq \lim_{\kappa\to+\infty} [\mathcal{P}_1(V^{(\kappa+1)}) - \mathcal{P}_1(V^{(\kappa)})] \leq \lim_{\nu\to+\infty} [\mathcal{P}_1(V^{(\kappa_{\nu+1})}) - \mathcal{P}_1(V^{(\kappa_\nu)})] = 0, \tag{5.1}$$

which shows that $\lim_{\kappa\to+\infty} \left[\mathcal{P}_1(V^{(\kappa+1)}) - \mathcal{P}_1(V^{(\kappa)})\right] = 0$. Therefore, for a given tolerance $\epsilon > 0$, the QPI will terminate after finitely many iterations under the stopping criterion

$$\left|\left(\mathcal{P}_1(V^{(\kappa+1)}) - \mathcal{P}_1(V^{(\kappa)})\right) / \mathcal{P}_1(V^{(\kappa)})\right| \leq \epsilon. \tag{5.2}$$

Each accumulation point $\bar{V}$ of the sequence $\{V^{(\kappa)}\}$ obviously satisfies the minimum principle necessary condition for optimality Marks and Wright [1978].

Appendix F

Proof of Corollary 4.1

We only provide an outline of this proof since it is based on Appendix D. The equality in (4.41) is obvious because $r_{i,j}^{x}(\mathbf{V}^{(\kappa)}) = r_{i,j}^{x,(\kappa)}(\mathbf{V}^{(\kappa)})$ for $x \in \{c, a, p\}$. To prove the inequality in (4.41), it suffices to show that

$$r_{i,j}^{x}(\mathbf{V}) \geq r_{i,j}^{x,(\kappa)}(\mathbf{V}) \; \forall \; \mathbf{V}, x \in \{c, a, p\}. \tag{6.1}$$

We will prove (6.1) for $x = c$ only, as the proof for $x = a$ and $x = p$ is similar. Rewrite $r_{i,j}^{c}(\mathbf{V})$ as $-g(\mathbf{V}_{i,j}^{c}, \mathbf{M}_{i,j}(\mathbf{V}))$ for $g(\mathbf{V}_{i,j}^{c}, \mathbf{M}) \triangleq \ln|\mathbf{I}_L - h(\mathbf{V}_{i,j}^{c}, \mathbf{M})|$ and $h(\mathbf{V}_{i,j}^{c}, \mathbf{M}) \triangleq (\mathbf{V}_{i,j}^{c})^H \mathbf{H}_{i,i,j}^H \mathbf{M}^{-1} \mathbf{H}_{i,i,j} \mathbf{V}_{i,j}^{c}$ in the domain

$$\mathcal{U} \triangleq \{(\mathbf{V}_{i,j}^{c}, \mathbf{M}) \; : \mathbf{M} \succ \mathbf{H}_{i,i,j} \mathbf{V}_{i,j}^{c} (\mathbf{V}_{i,j}^{c})^H \mathbf{H}_{i,i,j}^H\}.$$

By [Rashid et al., 2014, Appendix C], $h(.,.)$ is convex-valued in $\mathcal{U}$, i.e.,

$$\begin{aligned} &\alpha h(\mathbf{V}_{i,j}^{c}, \mathbf{M}) + \beta h(\mathbf{V}_{i,j}^{c,(\kappa)}, \mathbf{M}^{(\kappa)}) \\ &\succeq h(\alpha(\mathbf{V}_{i,j}^{c}, \mathbf{M}) + \beta(\mathbf{V}_{i,j}^{c,(\kappa)}, \mathbf{M}^{(\kappa)})), \end{aligned}$$

for all $\alpha \geq 0, \beta \geq 0, \alpha + \beta = 1$. It follows that

$$\begin{aligned} &g(\alpha(\mathbf{V}_{i,j}^{c}, \mathbf{M}) + \beta(\mathbf{V}_{i,j}^{c,(\kappa)}, \mathbf{M}^{(\kappa)})) \\ &\geq \ln|\mathbf{I}_{N_r} - \alpha h(\mathbf{V}_{i,j}^{c}, \mathbf{M}) - \beta h(\mathbf{V}_{i,j}^{c,(\kappa)}, \mathbf{M}^{(\kappa)})| \\ &\geq \alpha \ln|\mathbf{I}_{N_r} - h(\mathbf{V}_{i,j}^{c}, \mathbf{M})| + \beta \ln|\mathbf{I}_{N_r} - h(\mathbf{V}_{i,j}^{c,(\kappa)}, \mathbf{M}^{(\kappa)})| \\ &= \alpha g(\mathbf{V}_{i,j}^{c}, \mathbf{M}) + \beta g(\mathbf{V}_{i,j}^{c,(\kappa)}, \mathbf{M}^{(\kappa)}), \end{aligned}$$

i.e. $g(.,.)$ is concave in $\mathcal{U}$. And therefore, we have [Tuy, 1998]

$$\begin{aligned}
& g(\mathbf{V}_{i,j}^{c}, \mathbf{M}) - g(\mathbf{V}_{i,j}^{c,(\kappa)}, \mathbf{M}^{(\kappa)}) \\
& \leq \langle \nabla g(\mathbf{V}_{i,j}^{c,(\kappa)}, \mathbf{M}^{(\kappa)}), (\mathbf{V}_{i,j}^{c}, \mathbf{M}) - (\mathbf{V}_{i,j}^{c,(\kappa)}, \mathbf{M}^{(\kappa)}) \rangle \\
& = -2\,\mathrm{Re}\{\langle \mathbf{H}_{i,i,j}^{H} (\mathbf{M}^{(\kappa)})^{-1} \mathbf{V}_{i,j}^{c,(\kappa)} \mathbf{H}_{i,i,j}, \mathbf{V}_{i,j} - \mathbf{V}_{i,j}^{c,(\kappa)} \rangle\} \\
& + \langle (\mathbf{M}^{(\kappa)} - \mathbf{H}_{i,i,j} \mathbf{V}_{i,j}^{c,(\kappa)} (\mathbf{V}_{i,j}^{c,(\kappa)})^{H} \mathbf{H}_{i,i,j}^{H})^{-1} \\
& - (\mathbf{M}^{(\kappa)})^{-1}, \mathbf{M} - \mathbf{M}^{(\kappa)} \rangle,
\end{aligned}$$

which is (6.1) for $\mathbf{M} = \mathbf{M}_{i,j}(\mathbf{V})$ and $\mathbf{M}^{(\kappa)} = \mathbf{M}_{i,j}(\mathbf{V}^{(\kappa)})$.

Bibliography

3GPP [2010], Summary of the description of candidate eICIC solutions, 3GPP Std, Technical report, R1-104968, Madrid, Spain.

3GPP TS 36.814 V9.0.0 [2010], '3GPP technical specification group radio access network, evolved universal terrestrial radio access (E-UTRA): Further advancements for E-UTRA physical layer aspects (Release 9)'.

Alexiou, A. [2013], 'Visions for the wireless future - wireless world 2020 workshops', *Outlook* (8).
URL: *http://www.wwrf.ch/files/wwrf/content/files/publications/outlook/Outlook8.pdf*

Alizadeh, F. and Goldfarb, D. [2001], 'Second-order cone programming', *Mathematical programming* **95**, 3–51.

Andrews, J. [2013], 'Seven ways that HetNets are a cellular paradigm shift', *IEEE Commun. Mag.* **51**(3), 136–144.

Andrews, J. G., Buzzi, S., Choi, W., Hanly, S. V., Lozano, A., Soong, A. C. K. and Zhang, J. C. [2014], 'What will 5G be?', *IEEE J. Sel. Areas Commun.* **32**(6), 1065–1082.

Andrews, J., Singh, S., Ye, Q., Lin, X. and Dhillon, H. [2014], 'An overview of load balancing in HetNets: old myths and open problems', *IEEE Wireless Commun. Mag.* **21**(2), 18–25.

Annapureddy, V. and Veeravalli, V. [2011], 'Sum capacity of MIMO interference channels in the low interference regime', *IEEE Trans. Inf. Theory* **57**(5), 2565–2581.

Anttila et al, L. [2014], Modeling and efficient cancelation of nonlinear self-interference in MIMO full-duplex transceivers, *in* 'Proc. of Globecom', pp. 777–783.

Benjebbour, A., Li, A., Saito, K., Saito, Y., Kishiyama, Y. and Nakamura, T. [2015], NOMA: From concept to standardization, *in* 'Proc. of IEEE Conference on Standards for Communications and Networking (CSCN)', pp. 18–23.

Bertsekas, D. P. [1999], *Nonlinear Programming, 2nd*, Athena Scientific.

Beyranvand, H., Lim, W., Maier, M., Verikoukis, C. and Salehi, J. [2015], 'Backhaul-aware user association in FiWi enhanced LTE-A heterogeneous networks', *IEEE Trans. Wireless Commun.* **14**(6), 2992–3003.

Blum, R. [2003], 'MIMO capacity with interference', *IEEE J. Select. Areas in Commun.* **21**(5), 793–801.

Bonnans, J. F., Gilbert, J. C., Lemarechal, C. and Sagastizabal, C. [2006], *Numerical Optimization Theoretical and Practical Aspects*, 2nd edn, Springer.

Boostanimehr, H. and Bhargava, V. [2015], 'Unified and distributed QoS-driven cell association algorithms in heterogeneous networks', *IEEE Trans. Wireless Commun.* **14**(3), 1650–1662.

Boyd, S. and Vandenberghe, L. [2004], *Convex Optimization*, Cambridge University Press, New York, NY, USA.

Buzzi, S., I, C. L., Klein, T. E., Poor, H. V., Yang, C. and Zappone, A. [2016], 'A survey of energy-efficient techniques for 5G networks and challenges ahead', *IEEE J. Sel. Areas Commun.* **34**(4), 697–709.

Cai, D., Quek, T., Tan, C. W. and Low, S. [2012], 'Max-min SINR coordinated multi-point downlink transmission - Duality and algorithms', *IEEE Trans. Signal Process.* **60**(10), 5384–5395.

Caire, G. and Shamai, S. [2003], 'On the achievable throughput of a multiantenna gaussian broadcast channel', *IEEE Trans. Inf. Theory.* **49**(7), 1691 – 1706.

Chandrasekhar, V., Andrews, J. G. and Gatherer, A. [2008], 'Femtocell networks: a survey', *IEEE Commun. Mag.* **46**(9), 59–67.

Che, E. and Tuan, H. [2013*a*], Interference mitigation by jointly splitting rates and beamforming for multi-cell multi-user networks, *in* 'Proc. of 13th ISCIT', pp. 41–45.

Che, E. and Tuan, H. [2014], 'Sum-rate based coordinated beamforming in multicell multi-antenna wireless networks', *IEEE Commun. Lett.* **18**(6), 1019–1022.

Che, E. and Tuan, H. D. [2013*b*], Optimized coordinated precoding in multicell MIMO wireless systems, *in* 'Proc. of Communications and Information Technologies (ISCIT)', pp. 188–191.

Che, E., Tuan, H. D. and Nguyen, H. [2014], 'Joint optimization of cooperative beamforming and relay assignment in multi-user wireless relay networks', *IEEE Trans. Wireless Commun.* **13**(10), 5481–5495.

Che, E., Tuan, H. D., Tam, H. H. M. and Nguyen, H. [2015], 'Successive interference mitigation in multiuser MIMO channels', *IEEE Trans. Commun.* **63**(6), 2185–2199.

Chitti, K., Kuang, Q. and Speidel, J. [2013], Joint base station association and power allocation for uplink sum-rate maximization, *in* 'Proc. IEEE Workshop on Signal Process. Advances in Wireless Commun. (SPAWC)', pp. 6–10.

Cho, Y. S., Kim, J., Yang, W. Y. and Kang, C. G. [2010], *MIMO-OFDM Wireless Communications with MATLAB*, John Wiley & Sons, Ltd.

Choi, Y.-S. and Shirani-Mehr, H. [2013], 'Simultaneous transmission and reception: Algorithm, design and system level performance', *IEEE Trans. Wireless Commun.* **12**(12), 5992–6010.

Christensen, S., Agarwal, R., Carvalho, E. and Cioffi, J. [2008], 'Weighted sum-rate maximization using weighted MMSE for MIMO-BC beamforming design', *IEEE Trans. Wireless Commun.* **7**(12), 4792–4799.

Chuah, C.-N., Tse, D. N. C., Kahn, J. M. and Valenzuela, R. A. [2002], 'Capacity scaling in mimo wireless systems under correlated fading', *IEEE Trans. Inf. Theory* **48**(3), 637–650.

Cisco [2016], Visual networking index, Technical report.
URL: *http://www.cisco.com/c/en/us/solutions/collateral/service-provider/visual-networking-index-vni/mobile-white-paper-c11-520862.html*

Corroy, S., Falconetti, L. and Mathar, R. [2012], Cell association in small heterogeneous networks: Downlink sum rate and min rate maximization, *in* 'Proc. IEEE Wireless Commun. and Netw. Conf. (WCNC)', pp. 888–892.

Corroy, S. and Mathar, R. [2012], Semidefinite relaxation and randomization for dynamic cell association in heterogeneous networks, *in* 'Proc. IEEE Global Commun. Conf. (GLOBECOM)', pp. 2373–2378.

Costa, M. [1983], 'Writing on dirty paper', *IEEE Trans. Inf. Theory* **29**(3), 439–441.

Dahrouj, H. and Yu, W. [2011], 'Multicell interference mitigation with joint beamforming and common message decoding', *IEEE Trans. Commun.* **59**(8), 2264 –2273.

Damnjanovic, A., Montojo, J., Wei, Y., Ji, T., Luo, T., Vajapeyam, M., Yoo, T., Song, O. and Malladi, D. [2011], 'A survey on 3GPP heterogeneous networks', *IEEE Wireless Commun. Mag.* **18**(3), 10–21.

Day, B., Margetts, A., Bliss, D. and Schniter, P. [2012], 'Full-duplex bidirectional MIMO: Achievable rates under limited dynamic range', *IEEE Trans. Signal Process.* **60**(7), 3702–3713.

Dhillon, H. S., Ganti, R. K., Baccelli, F. and Andrews, J. G. [2012], 'Modeling and analysis of K-tier downlink heterogeneous cellular networks', *IEEE J. Sel. Areas Commun.* **30**(3), 550–560.

Ding, Z., Yang, Z., Fan, P. and Poor, H. V. [2014], 'On the performance of non-orthogonal multiple access in 5G systems with randomly deployed users', *IEEE Signal Process. Lett.* **21**(12), 1501–1505.

Ding, Z., Zhong, C., Ng, D. W. K., Peng, M., Suraweera, H. A., Schober, R. and Poor, H. V. [2015], 'Application of smart antenna technologies in simultaneous wireless information and power transfer', *IEEE Commun. Mag.* **53**(4), 86–93.

Duarte, M., Dick, C. and Sabharwal, A. [2012], 'Experiment-driven characterization of full-duplex wireless systems', *IEEE Trans. Wireless Commun.* **11**(12), 4296–4307.

Duarte, M., Sabharwal, A., Aggarwal, V., Jana, R., Ramakrishnan, K., Rice, C. and Shankaranarayanan, N. [2014], 'Design and characterization of a full-duplex multi-antenna system for WiFi networks', *IEEE Trans. Veh. Technol.* **63**(3), 1160–1177.

DUPLO project [2015], 'System scenarios and technical requirements for full-duplex concept', *Deliverable D1.1* .
URL: *at http://www.fp7-duplo.eu/index.php/deliverables.*

Erez, U. and ten Brink, S. [2005], 'A close-to-capacity dirty paper coding scheme', *IEEE Trans. Inf. Theory* **51**(10), 3417–3432.

Etkin, R., Tse, D. and Wang, H. [2008], 'Gaussian interference channel capacity to within one bit', *IEEE Trans. Inf. Theory* **54**(12), 5534–5562.

Everett, E., Sahai, A. and Sabharwal, A. [2014], 'Passive self-interference suppression for full-duplex infrastructure nodes', *IEEE Trans. Wireless Commun.* **13**(2), 680–694.

Fettweis, G. P. and Zimmermann, E. [2008], ICT energy consumption - trends and challenges, *in* 'Proc. Intl. Symp. on Wireless Personal Multimedia Commun. (WPMC)', Lapland, Finland, pp. 1–6.

Fooladivanda, D. and Rosenberg, C. [2013], 'Joint resource allocation and user association for heterogeneous wireless cellular networks', *IEEE Trans. Wireless Commun.* **12**(1), 248–257.

Foschini, G. J. [1996], 'Layered space-time architecture for wireless communication in a fading environment when using multi-element antennas', *Bell Labs Technical Journal* **1**(2), 41–59.

Gao, D. Y. and Sherali, H. D. [2009], *Advances in Applied Mathematics and Global Optimization: Dedicated to Gilbert Strang on the Occasion of His 70th Birthday*, Advances in Mechanics and Mathematics, Springer, Dordrecht.
URL: *https://cds.cern.ch/record/1315344*

Gesbert, D., Hanly, S., Huang, H., Shamai Shitz, S., Simeone, O. and Yu, W. [2010], 'Multi-cell MIMO cooperative networks: A new look at interference', *IEEE J. Sel. Areas Commun.* **28**(9), 1380–1408.

Ghimire, J. and Rosenberg, C. [2015], 'Revisiting scheduling in heterogeneous networks when the backhaul is limited', *IEEE J. Sel. Areas Commun.* **33**(10), 2039–2051.

Goldsmith, A. [2005], *Wireless Communications*, Cambridge University Press. Cambridge Books Online.
URL: *http://dx.doi.org/10.1017/CBO9780511841224*

Grant, M. and Boyd, S. [2014], 'CVX: Matlab software for disciplined convex programming, version 2.1', `http://cvxr.com/cvx`.

Grover, L. K. [1997], 'Quantum mechanics helps in searching for a needle in a haystack', *Phys. Rev. Lett.* **79**, 325–328.

Ha, V. N. and Le, L. B. [2014], 'Distributed base station association and power control for heterogeneous cellular networks', *IEEE Trans. Veh. Technol.* **63**(1), 282–296.

Han, T. S. and Kobayashi, K. [1981], 'A new achievable region for the interference channel', *IEEE Trans. Inf. Theory.* **33**, 49–60.

Han, W., Zhang, Y., Wang, X., Sheng, M., Li, J. and Ma, X. [2016], 'Orthogonal power division multiple access: A green communication perspective', *IEEE J. Sel. Areas Commun.* **PP**(99), 1–1.

Heino et al, M. [2015], 'Recent advances in antenna design and interference cancelllation algorithms for in-band full duplex relays', *IEEE Commun. Magazine* **53**(5), 91–101.

Hong, M. and Garcia, A. [2012], 'Mechanism design for base station association and resource allocation in downlink OFDMA network', *IEEE J. Sel. Areas Commun.* **30**(11), 2238–2250.

Hong, S., Brand, J., Choi, J. I., Jain, M., Mehlman, J., Katti, S. and Levis, P. [2014], 'Applications of self-interference cancellation in 5G and beyond', *IEEE Commun. Mag.* **52**(2), 114–121.

Horst, R. and Tuy, H. [1996], *Global Optimization: Deterministic Approaches*, Springer.

Hossain, E., Rasti, M., Tabassum, H. and Abdelnasser, A. [2014], 'Evolution toward 5G multi-tier cellular wireless networks: An interference management perspective', *IEEE Wireless Commun. Mag.* **21**(3), 118–127.

Huang, K. and Lau, V. K. N. [2014], 'Enabling wireless power transfer in cellular networks: Architecture, modeling and deployment', *IEEE Trans. Wireless Commun.* **13**(2), 902–912.

Huang, Y., Tan, C. W. and Rao, B. [2013], 'Joint beamforming and power control in coordinated multicell: Max-min duality, effective network and large system transition', *IEEE Trans. Wireless Commun.* **12**(6), 2730–2742.

Huberman, S. and Le-Ngoc, T. [2015], 'MIMO full-duplex precoding: A joint beamforming and self-interference cancellation structure', *IEEE Trans. Wireless Commun.* **14**(4), 2205–2217.

ITU [2015], ICT facts & figures 2015, Technical report.
URL: *http://www.itu.int/en/ITU-D/Statistics/Documents/facts/ICTFactsFigures2015.pdf*

Jafari, A. H., López-Pérez, D., Song, H., Claussen, H., Ho, L. and Zhang, J. [2015], 'Small cell backhaul: challenges and prospective solutions', *EURASIP Journal on Wireless Communications and Networking* **2015**(1), 1–18.
URL: *http://dx.doi.org/10.1186/s13638-015-0426-y*

Jo, H.-S., Sang, Y. J., Xia, P. and Andrews, J. [2012], 'Heterogeneous cellular networks with flexible cell association: A comprehensive downlink SINR analysis', *IEEE Trans. Wireless Commun.* **11**(10), 3484–3495.

Karmakar, S. and Varanasi, M. [2013], 'The capacity region of the MIMO interference channel and its reciprocity to within a constant gap', *IEEE Trans. Inf. Theory* **59**(8), 4781–4797.

Kha, H. H., Tuan, H. D. and Nguyen, H. H. [2012], 'Fast global optimal power allocation in wireless networks by local d.c. programming', *IEEE Trans. Wireless Commun.* **11**(2), 510–515.

Kim, S.-J. and Giannakis, G. [2011], 'Optimal resource allocation for MIMO ad hoc cognitive radio networks', *IEEE Trans. Inf. Theory* **57**(5), 3117–3131.

Korpi et al, D. [2014], 'Full-duplex transceiver system calculations: analysis of adc and linearity challenges', *IEEE Trans. Wireless Commun.* **13**(7), 3821–3836.

Kuang, Q., Speidel, J. and Droste, H. [2012], Joint base-station association, channel assignment, beamforming and power control in heterogeneous networks, *in* 'Proc. IEEE Veh. Technol. Conf. (VTC Spring)', pp. 1–5.

Larsson, E. G., Edfors, O., Tufvesson, F. and Marzetta, T. L. [2014], 'Massive MIMO for next generation wireless systems', *IEEE Commun. Mag.* **52**(2), 186–195.

Lee, J., Kim, Y., Lee, H., Ng, B. L., Mazzarese, D., Liu, J., Xiao, W. and Zhou, Y. [2012], 'Coordinated multipoint transmission and reception in LTE-Advanced systems', *IEEE Commun. Mag.* **50**(11), 44–50.

Lee, S., Son, K., Gong, H. and Yi, Y. [2012], 'Base station association in wireless cellular networks: An emulation based approach', *IEEE Trans. Wireless Commun.* **11**(8), 2720–2729.

Li, G. Y., Xu, Z., Xiong, C., Yang, C., Zhang, S., Chen, Y. and Xu, S. [2011], 'Energy-efficient wireless communications: Tutorial, survey, and open issues', *IEEE Wireless Communications* **18**(6), 28–35.

Li, Q., Niu, H., Papathanassiou, A. and Wu, G. [2014], '5G network capacity: Key elements and technologies', *IEEE Veh. Technol. Mag.* **9**(1), 71–78.

Liu, D., Wang, L., Chen, Y., Elkashlan, M., Wong, K. K., Schober, R. and Hanzo, L. [2016], 'User association in 5G networks: A survey and an outlook', *IEEE Communications Surveys and Tuts.* **18**(2), 1018–1044.

Liu, L., Chen, R., Geirhofer, S., Sayana, K., Shi, Z. and Zhou, Y. [2012], 'Downlink MIMO in LTE-advanced: SU-MIMO vs. MU-MIMO', *IEEE Commun. Mag.* **50**(2), 140–147.

Liu, W., Zhou, X., Durrani, S. and Popovski, P. [2016], SWIPT with practical modulation and RF energy harvesting sensitivity, *in* 'In Proc. of IEEE International Conference on Communications (ICC 2016)', pp. 1–7.

Lopez-Perez, D., Guvenc, I., de la Roche, G., Kountouris, M., Quek, T. Q. S. and Zhang, J. [2011], 'Enhanced intercell interference coordination challenges in heterogeneous networks', *IEEE Wireless Commun.* **18**(3), 22–30.

Lopez-Perez, D., Valcarce, A., de la Roche, G. and Zhang, J. [2009], 'OFDMA femtocells: A roadmap on interference avoidance', *IEEE Commun. Mag.* **47**(9), 41–48.

Low, S. H. and Lapsley, D. E. [1999], 'Optimization flow control. I. Basic algorithm and convergence', *IEEE/ACM Trans. Netw.* **7**(6), 861–874.

Lu, X., Niyato, D., Wang, P. and Kim, D. I. [2015], 'Wireless charger networking for mobile devices: fundamentals, standards, and applications', *IEEE Wireless Commun. Mag.* **22**(2), 126–135.

Lu, X., Wang, P., Niyato, D. and Han, Z. [2015], 'Resource allocation in wireless networks with RF energy harvesting and transfer', *IEEE Network* **29**(6), 68–75.

Lu, X., Wang, P., Niyato, D., Kim, D. I. and Han, Z. [2016], 'Wireless charging technologies: Fundamentals, standards, and network applications', *IEEE Communications Surveys Tutorials* **18**(2), 1413–1452.

Madan, R., Borran, J., Sampath, A., Bhushan, N., Khandekar, A. and Ji, T. [2010], 'Cell association and interference coordination in heterogeneous LTE-A cellular networks', *IEEE J. Sel. Areas Commun.* **28**(9), 1479–1489.

Marks, B. R. and Wright, G. P. [1978], 'A general inner approximation algorithm for nonconvex mathematical programms', *Operations Research* **26**(4), 681–683.

Metis [2013], Scenarios, requirements and KPIs for 5G mobile and wireless system, Technical report, ICT-317669 METIS project.

Mohammadi, M., Suraweera, H. A., Cao, Y., Krikidis, I. and Tellambura, C. [2015], 'Full-duplex radio for uplink/downlink wireless access with spatially random nodes', *IEEE Trans. Commun.* **63**(12), 5250–5266.

Nasir, A. A., Ngo, D. T., Tuan, H. D. and Durrani, S. [2015], Iterative optimization for max-min SINR in dense small-cell multiuser MISO SWIPT system, *in* 'Proc. IEEE Global Conference on Signal Processing (GlobalSIP)'.

Nasir, A. A., Tuan, H. D., Ngo, D. T., Durrani, S. and Kim, D. I. [2016], 'Path-following algorithms for beamforming and signal splitting in RF energy harvesting networks', *IEEE Communications Letters* **20**(8), 1687–1690.

Nemirovski, A. [2004], 'Interior point polynomial time methods in convex programming'.
URL: *http://www2.isye.gatech.edu/ nemirovs/Lect_IPM.pdf*

Ng, C. and Huang, H. [2010], 'Linear precoding in cooperative MIMO cellular networks with limited coordination clusters', *IEEE J. Sel. Areas Commun.* **28**(9), 1446 –1454.

Nguyen, D., Tran, L.-N., Pirinen, P. and Latva-aho, M. [2013], 'Precoding for full duplex multiuser MIMO systems: Spectral and energy efficiency maximization', *IEEE Trans. Signal Process.* **61**(16), 4038 –4050.

Nguyen, D., Tran, L.-N., Pirinen, P. and Latva-aho, M. [2014], 'On the spectral efficiency of full-duplex small cell wireless systems', *IEEE Trans. Wireless Commun.* **13**(9), 4896–4910.

Olmos, J., Ferrus, R. and Galeana-Zapien, H. [2013], 'Analytical modeling and performance evaluation of cell selection algorithms for mobile networks with backhaul capacity constraints', *IEEE Trans. Wireless Commun.* **12**(12), 6011–6023.

Park, J. and Clerckx, B. [2014], 'Joint wireless information and energy transfer in a K-user MIMO interference channel', *IEEE Trans. Wireless Commun.* **13**(10), 5781–5796.

Park, J. and Clerckx, B. [2015], 'Joint wireless information and energy transfer with reduced feedback in MIMO interference channels', *IEEE J. Sel. Areas Commun.* **33**(8), 1563–1577.

Phan, A. H., Tuan, H. D., Kha, H. H. and Ngo, D. T. [2012], 'Nonsmooth optimization for efficient beamforming in cognitive radio multicast transmission', *IEEE Trans. Signal Process.* **60**, 2941–2951.

Qian, Yang, C. and Molisch, A. [2013], 'Downlink base station cooperative transmission under limited-capacity backhaul', *IEEE Trans. Wireless Commun.* **12**(8), 3746–3759.

Rappaport, T. S., Sun, S., Mayzus, R., Zhao, H., Azar, Y., Wang, K., Wong, G. N., Schulz, J. K., Samimi, M. and Gutierrez, F. [2013], 'Millimeter wave mobile communications for 5G cellular: It will work!', *IEEE Access* **1**, 335–349.

Rashid, U., Tuan, H. D., Kha, H. H. and Nguyen, H. H. [2014], 'Joint optimization of source precoding and relay beamforming in wireless MIMO relay networks', *IEEE Trans. Commun.* **62**(2), 488–499.

Rusek, F., Persson, D., Lau, B. K., Larsson, E. G., Marzetta, T. L., Edfors, O. and Tufvesson, F. [2013], 'Scaling up MIMO: Opportunities and challenges with very large arrays', *IEEE Signal Process Magazine* **30**(1), 40–60.

Sabharwal et al, A. [2014], 'In-band full-duplex wireless: challenges and opportunities', *IEEE J. Selected Areas in Commun.* **32**(9), 1637–1652.

Sanayei, S. and Nosratinia, A. [2004], 'Antenna selection in MIMO systems', *IEEE Communications Magazine* **42**(10), 68–73.

Sezer, S., Scott-Hayward, S., Chouhan, P. K., Fraser, B., Lake, D., Finnegan, J., Viljoen, N., Miller, M. and Rao, N. [2013], 'Are we ready for SDN? Implementation challenges for software-defined networks', *IEEE Commun. Mag.* **51**(7), 36–43.

Shang, X., Chen, B. and Gans, M. [2006], 'On the achievable sum rate for MIMO interference channels', *IEEE Trans. Inf. Theory* **52**(9), 4313–4320.

Shang, X. and Poor, H. V. [2013], 'Noisy-interference sum-rate capacity for vector Gaussian interference channels', *IEEE Trans. Inf. Theory* **59**(1), 132–153.

Shen, C., Li, W. C. and Chang, T. H. [2014], 'Wireless information and energy transfer in multi-antenna interference channel', *IEEE Trans. Signal Process.* **62**(23), 6249–6264.

Shen, K. and Yu, W. [2014], 'Distributed pricing-based user association for downlink heterogeneous cellular networks', *IEEE J. Sel. Areas Commun.* **32**(6), 1100–1113.

Shi, Q., Razaviyayn, M., Luo, Z.-Q. and He, C. [2011], 'An iteratively weighted MMSE approach to distributed sum-utility maximization for a MIMO interfering broadcast channel', *IEEE Trans. Wireless Commun.* **59**(9), 4331–4340.

Shi, Q., Xu, W., Chang, T. H., Wang, Y. and Song, E. [2014], 'Joint beamforming and power splitting for MISO interference channel with swipt: An SOCP relaxation and decentralized algorithm', *IEEE Trans. Signal Process.* **62**(23), 6194–6208.

Singh, S. and Andrews, J. G. [2014], 'Joint resource partitioning and offloading in heterogeneous cellular networks', *IEEE Trans. Wireless Commun.* **13**(2), 888–901.

Song, B., Cruz, R. and Rao, B. [2007], 'Network duality for multiuser MIMO beamforming networks and applications', *IEEE Trans. Commun.* **55**(3), 618–630.

Spencer, Q. H., Swindlehurst, A. L. and Haardt, M. [2004], 'Zero-forcing methods for downlink spatial multiplexing in multiuser mimo channels', *IEEE Trans. Signal Process.* **52**(2), 461–471.

Sun, R., Hong, M. and Luo, Z.-Q. [2015], 'Joint downlink base station association and power control for max-min fairness: Computation and complexity', *IEEE J. Sel. Areas Commun.* **33**(6), 1040–1054.

Tam, H. H. M., Che, E. and Tuan, H. D. [2013], Optimized linear precoder in MIMO interference channel using D.C. programming, *in* 'Proc. of 7th Signal Processing and Communication Systems (ICSPCS)', pp. 1–5.

Tam, H. H. M., Tuan, H. D. and Ngo, D. T. [2016], 'Successive convex quadratic programming for quality-of-service management in full-duplex MU-MIMO multicell networks', *IEEE Trans. Commun.* **64**(6), 2340–2353.

Telatar, E. [1999], 'Capacity of multi-antenna Gaussian channels', *European Transactions on Telecommunications* **10**(6), 585–595.
URL: *http://dx.doi.org/10.1002/ett.4460100604*

Timotheou, S., Krikidis, I., Zheng, G. and Ottersten, B. [2014], 'Beamforming for MISO interference channels with QoS and RF energy transfer', *IEEE Trans. Wireless Commun.* **13**(5), 2646–2658.

Tipmongkolsilp, O., Zaghloul, S. and Jukan, A. [2011], 'The evolution of cellular backhaul technologies: Current issues and future trends', *IEEE Commun. Surveys and Tutorials* **13**(1), 97–113.

Tse, D. and Viswanath, P. [2005], *Fundamentals of Wireless Communication*, Cambridge University Press, New York, NY, USA.

Tuy, H. [1998], *Convex Analysis and Global Optimization*, Kluwer Academic.

Varshney, L. R. [2008], Transporting information and energy simultaneously, *in* 'Proc. of IEEE International Symposium on Information Theory', pp. 1612–1616.

Wang, K., Wang, X., Xu, W. and Zhang, X. [2012], 'Coordinated linear precoding in downlink multicell MIMO-OFDMA networks', *IEEE Trans. Signal Process.* **60**(8), 4264–4277.

Wang, S., Ge, M. and Zhao, W. [2013], 'Energy-efficient resource allocation for OFDM-based cognitive radio networks', *IEEE Trans. Commun.* **61**(8), 3181–3191.

Wiesel, A., Eldar, Y. and Shamai, S. [2006], 'Linear precoding via conic optimization for fixed MIMO receivers', *IEEE Trans. Signal Process.* **54**(1), 161 – 176.

Winters, J. [1987], 'On the capacity of radio communication systems with diversity in a Rayleigh fading environment', *IEEE J. Sel. Areas Commun.* **5**(5), 871–878.

Xu, W. and Wang, X. [2012], 'Pricing-based distributed downlink beamforming in multi-cell OFDMA networks', *IEEE J. Sel. Areas Commun.* **30**(9), 1605–1613.

Ye, Q., Rong, B., Chen, Y., Al-Shalash, M., Caramanis, C. and Andrews, J. [2013], 'User association for load balancing in heterogeneous cellular networks', *IEEE Trans. Wireless Commun.* **12**(6), 2706–2716.

Yu, J., Wang, Y., Lin, X. and Zhang, Q. [2014], Power allocation for CoMP system with backhaul limitation, *in* 'Proc. IEEE Intl. Conf. Commun. (ICC)', pp. 4759–4764.

Yu, W. and Cioffi, J. [2004], 'Sum capacity of Gaussian vector broadcast channels', *IEEE Trans. Inf. Theory* **50**(9), 1875–1892.

Zarakovitis, C. C., Ni, Q. and Spiliotis, J. [2016], 'Energy efficient green wireless communication systems with imperfect CSI and data outage', *IEEE J. Sel. Areas Commun.* **PP**(99), 1–1.

Zhang, G., Quek, T. Q. S., Kountouris, M., Huang, A. and Shan, H. [2016], 'Fundamentals of heterogeneous backhaul design - Analysis and optimization', *IEEE Trans. Commun.* (2), 876–889.

Zhang, R. and Ho, C. K. [2013], 'MIMO broadcasting for simultaneous wireless information and power transfer', *IEEE Trans. Wireless Commun.* **12**(5), 1989–2001.

Zheng, L. and Tse, D. N. C. [2003], 'Diversity and multiplexing: A fundamental tradeoff in multiple-antenna channels', *IEEE Trans. Inf. Theory* **49**(5), 1073–1096.

Zong, Z., Feng, H., Yu, F. R., Zhao, N., Yang, T. and Hu, B. [2016], 'Optimal transceiver design for SWIPT in K-user MIMO interference channels', *IEEE Trans. Wireless Commun.* **15**(1), 430–445.